Modification of polymer surfaces to enhance enzyme activity and stability

Hoffmann, Christian

Publication date:
2017

Document Version
Publisher's PDF, also known as Version of record

Modification of polymer surfaces to enhance enzyme activity and stability

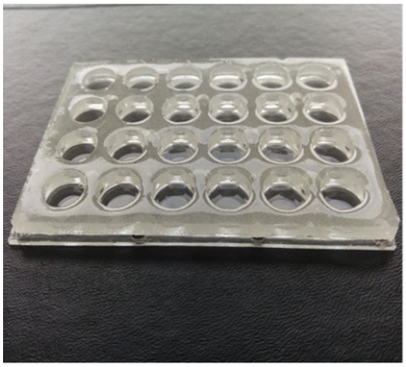

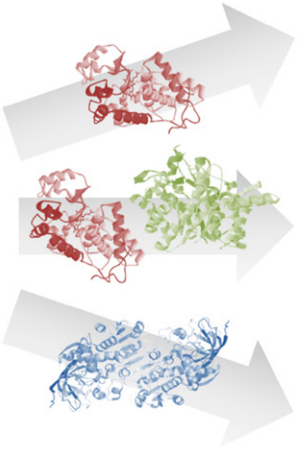

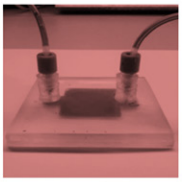

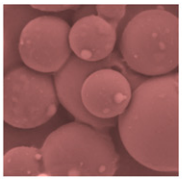

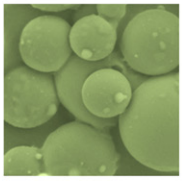

Christian Hoffmann

PhD Thesis

July 2017

DTU Chemical Engineering
Department of Chemical and Biochemical Engineering

Modification of polymer surfaces to enhance enzyme activity and stability

Christian Hoffmann

Supervisor:
Assoc. Prof. Anders E. Daugaard

Co-supervisors:
Prof. John M. Woodley
Assoc. Prof. Manuel Pinelo

PhD thesis
July 2017

DTU Chemical Engineering
Department of Chemical and Biochemical Engineering

Preface

This thesis is the result of my Ph.D. project conducted at the Danish Polymer Centre (DPC), Department of Chemical and Biochemical Engineering, Technical University of Denmark, from 2014 until 2017. The project was financed in part by DTU and the Aage and Johanne Louis-Hansen Foundation.

First and foremost, I would like to thank my supervisor Associate Professor Anders Egede Daugaard for giving me the possibility of working on this exciting and multifaceted project. I am very grateful for your constant support, your ideas and positive mindset throughout the entire time. I really appreciated our open discussions and that you gave me space to implement my own thoughts, which let me grow personally and scientifically. I believe both of us would have liked a more homogeneous distribution of our "tasting sessions" throughout this time, but a high concentration in the end is also not to be scoffed at.

Additionally, I would like to thank my co-supervisors Professor John M. Woodley and Associate Professor Manuel Pinelo for their outstanding contributions with their extensive expertise in biocatalysis and membrane technology. Furthermore, your constant availability and constructive feedback made me and my work feel very valued. John, I would like to thank you for establishing the contact to Professor Patrick Adlercreutz at Lund University for my external research stay.

At Lund University, I would like to thank Professor Patrick Adlercreutz for allowing me to join his group and being part of a research environment with a biotechnological focus, which was a new experience for me. This time broadened my horizon by discussing new approaches, which I appreciated a lot. Furthermore, I am very grateful to Carl Grey for your openness to all my questions about enzymes and their analysis.

A big thank you goes also to the current and former members of the Danish Polymer Centre for creating such a welcoming and positive environment. I enjoyed all the nice moments from scientific conversations to any social activities. It is a pleasure to be part of that community.

Finally; I would like to thank my family, especially my parents for letting me pursue my way into the large field of chemistry, even though you were not familiar with Chemistry at all. A special thank you goes to my girlfriend Susan for your love, never-ending support and your help to make bubbleland so awesome.

Christian Hoffmann
July 2017
Kgs. Lyngby, Denmark

Abstract

Enzyme immobilization is an important concept for the development of improved biocatalytic processes, primarily through facilitated separation procedures. However, enzyme immobilization usually comes at a price of reduced biocatalytic activity. For this reason, different immobilization methods have already been developed, combining the same goal to improve enzyme activity, stability and selectivity. Polymer materials have shown, due to their easy processibility and versatile properties, high potential as enzyme support. However, in order to achieve improved enzyme performance, the combination of different factors, such as the nature of the enzyme, the properties of the support, the type of immobilization and the interaction between enzyme and support, has to be taken into consideration. In this thesis, these factors are pursued and addressed by exploiting various types of polymers with focus on their tailored surface modification in order to obtain improved enzyme-support systems.

Firstly, an off-stoichiometric thiol-ene (OSTE) thermosetting material was used for the development of a screening platform allowing the investigation of micro-environmental effects and their impact on the **activity** of immobilized enzymes. Micro-environmental changes were generated through the introduction of tailored surface functionalities via thiol-ene chemistry (TEC) and surface chain transfer free radical polymerization (SCT-FRP), which demonstrated a significant influence on the activity of immobilized horseradish peroxidase (HRP). Thereby, this versatile screening substantiated the identification of suitable support surfaces for the immobilization of enzymes.

Secondly, in order to facilitate the **application** of previously identified enzyme-support combinations, OSTE particles as enzyme carriers were prepared. Here, a novel fabrication process via suspension polymerization in glycerol was applied resulting in microparticles with high control over particle size, which were further surface functionalized through TEC and SCT-FRP. In this case, epoxide functional particles were applied for the covalent immobilization of HRP and thus, demonstrated their potential as enzyme carrier in a continuous biocatalytically active plug-flow reactor.

Thirdly, OSTE particles with different surface functionalities were further used for the immobilization of β-glucosidase. The aim of this study was primarily to improve enzymatic **selectivity** through tailored changes of the micro-environment between enzyme and surface, which was achieved by introducing different surface chemistries onto the particles. The resulting selectivity between trans-glycosylation and hydrolysis of p-nitrophenyl glucopyranoside (pNPG) catalyzed by immobilized β-glucosidase was significantly improved and showed a direct correlation to the surface chemistry.

Furthermore, enzyme **effectiveness** is another important factor for the development of biocatalytic processes, which was addressed by immobilizing HRP in microfluidic devices based on OSTE+ materials. In this approach, area selective surface functionalization allowed the immobilization of HRP in various surface patterns and consequently, the effect of spatial enzyme distribution was determined towards the overall reactor performance. Two checkerboard patterns were identified to exploit enzymes more efficiently compared to an even distribution on the surface.

Finally, improvements in enzyme **stability** was the focus of applying tailored surface functionalization and polymer grafting of polysulfone (PSf) membranes and their subsequent application as biocatalytic membrane reactors (BMRs). Immobilization of alcohol dehydrogenase (ADH) onto poly(1-vinyl imidazole) (pVim) grafted membranes demonstrated

increased biocatalytic activity and stability compared to pristine membranes and thus, showed improved enzyme performance through tailored micro-environment by polymer grafting.

Resumé

Enzym immobilisering er et vigtigt element i udviklingen af forbedrede biokatalytiske processer, hvor specielt forbedring af separationsprocesser er en drivende faktor. Imidlertid resulterer enzymimmobilisering normalt i en reduceret biokatalytisk aktivitet. Derfor arbejdes der på nuværende tidspunkt på udvikling af forskellige nye immobiliseringsmetoder, der resulterer i forbedret enzymaktivitet, stabilitet såvel som selektivitet. Polymermaterialer har på grund af deres enkle forarbejdning og alsidige egenskaber et stort potentiale som bærematerialer til enzymer. For at opnå en forbedret enzymydelse skal der imidlertid tages hensyn til kombinationen af forskellige faktorer, såsom enzymets egenskaber, egenskaberne af bærematerialet, typen af immobilisering og vekselvirkningerne imellem enzym og overfladen af bærematerialet. I denne afhandling forsøges disse faktorer håndteret ved overflademodificering af polymerer med fokus på at skræddersy overfladeegenskaberne og dermed at opnå en synergi imellem bærematerialet og det immobiliserede enzym.

Indledningsvist blev en off-støkiometrisk thiol-ene (OSTE) hærdeplast anvendt til udvikling af en screeningsplatform, der muliggør undersøgelse af mikromiljøeffekter og deres indvirkning på aktiviteten af immobiliserede enzymer. Ændringer i mikromiljøet blev opnået ved overflademodifikation via thiol-en-kemi (TEC) og ved overfladeterminerede fri radikalpolymerisationer (SCT-FRP), hvilket resulterede i en signifikant forbedring af aktiviteten af immobiliseret peberrodsperoxidase (HRP). Dermed blev screeningsplatformen anvendt til identifikation af egnede overfladekemier til immobilisering af enzymer.

For det andet blev en ny fremstillingsmetode af OSTE-partikler til anvendelse som bærematerialer for enzymer udviklet, for at lette overførslen af identificerede overfladekemier til et kommercielt relevant bærematerialе. Ved suspensionspolymerisation i glycerol var det muligt at fremstille mikropartikler med en kontrolleret partikelstørrelse, som efterfølgende blev overfladefunktionaliseret ved TEC og SCT-FRP. Som eksempel blev epoxidfunktionelle partikler anvendt til kovalent immobilisering af HRP, hvorved partiklernes potentiale som enzymbærere i en kontinuerlig biokatalytisk aktiv plug-flow reaktor blev demonstreret.

For det tredje blev OSTE-partikler med forskellige overfladefunktionaliteter også anvendt til immobilisering af β-glucosidase. Formålet med denne undersøgelse var primært at forbedre den enzymatiske selektivitet ved ændring af interaktionen mellem enzym og overflade, hvilket blev opnået ved at indføre forskellige overfladekemier på partiklerne. Den resulterende selektivitet mellem transglycosylering og hydrolyse af p-nitrophenylglucopyranosid (pNPG) katalyseret ved immobiliseret β-glucosidase blev signifikant forbedret og viste en direkte korrelation med overfladekemien på partiklerne.

Endvidere blev enzymeffektivitet, en anden vigtig faktor for udviklingen af biokatalytiske processer, adresseret ved immobilisering af HRP i mikrofluide systemer baseret på OSTE+ materialer. Her var det muligt, områdeselektivt, at modificere overfladen i de mikrofluide reaktorer med HRP. Dermed kunne virkningen af enzymdistributionen i forhold til den samlede reaktorydelse bestemmes. To skakternsmønste blev identificeret som de mest effektive mønstre, sammenlignet med en tilsvarende jævn fordeling af enzymer på overfladen i den mikrofluide reaktor.

Slutteligt blev effekten af overflademodicering af bærematerialer på enzymstabiliteten, undersøgt ved modificering af polysulfon (PSf) membraner, der efterfølgende blev testet som biokatalytiske membranreaktorer (BMR'er). Immobilisering af alkohol dehydrogenase (ADH) på poly(1-vinylimidazol) (pVim) modificerede membraner viste øget biokatalytisk aktivitet og

stabilitet i forhold til umodificerede membraner og viste således forbedret enzymydelse som et resultat af overflademodificeringen.

Contents

List of Abbreviations

AA	allyl alcohol
AAc	acrylic acid
AAm	acyl amide
Aam hc	allyl amine hydrochloride
ABTS	2,2′-azino-bis(3-ethylbenzothiazoline-6-sulfonic acid) diammonium salt
ADH	alcohol dehydrogenase
AGE	allyl glycidyl ether
AMA	allyl malonic acid
APFB	allyl pentafluorobenzene
ATFA	allyl trifluoroacetate
ATR	attenuated total reflectance
BADGE	bisphenol A diglycidyl ether
BMR	biocatalytic membrane reactor
CALB	*candida antarctica* lipase B
CFD	computational fluid dynamics
CuAAC	Cu(I)-catalyzed alkyne azide cycloaddition
DLS	dynamic light scattering
DMPA	2,2-dimethoxy-2-phenylacetophenone
FI	fluorescence intensity
FT	fourier transform
GA	glutaraldehyde
GMA	glycidyl methacrylate
HEMA	2-hydroxyethyl methacrylate
HCOH	formaldehyde
HIPE	high internal phase emulsion
HRP	horseradish peroxidase
IR	infrared
MPEGMA	methoxy poly(ethylene glycol) methacrylate
MWCO	molecular weight cut-off
n-BuLi	n-butyllithium
NaAsc	sodium ascorbate
NAD	β-nicotinamide adenine dinucleotide
NADH	β-nicotinamide adenine dinucleotide reduced form
OFPA	2,2,3,3,4,4,5,5 octafluoropentyl acrylate
OSTE	off-stoichiometric thiol-ene
PAN	polyacrylonitrile
PBS	phosphate buffered saline
PDMS	polydimethylsiloxane
PEG	poly(ethylene glycol)
PEGMA	poly(ethylene glycol)methacrylate
PEI	polyethylenimine
PETMP	pentaerythritol tetrakis(3-mercaptopropionate)

PGA	penicillin G acylase
PMDETA	N,N,N′,N″,N″-pentamethyldiethylenetriamine
PMMA	poly(methyl methacrylate)
pNP	para-nitrophenol
pNPG	para-nitrophenyl glucopyranoside
propyl-G	propyl-glycoside
PSf	polysulfone
PVA	poly(vinyl alcohol)
Rho-HRP	rhodamine labeled horseradish peroxidase
SAM	self-assembled monolayer
SBMA	sulfobetaine methacrylate [2-(methacryloyloxy)ethyl]dimethyl-(3-sulfopropyl)ammonium hydroxide
SCT-FRP	surface chain transfer free radical polymerization
SDBA	sodium dodecyl benzene sulfate
SDS	sodium dodecyl sulfate
SEC	size exclusion chromatography
SI-ATRP	surface initiated atom transfer free radical polymerization
STE	stoichiometric thiol-ene
TATATO	1,3,5-triallyl-1,3,5-triazine-2,4,6(1H,3H,5H)-trione
TEC	thiol-ene chemistry
TFAA	trifluoro acetic anhydride
THF	tetrahydrofuran
UV	ultra-violet
Vim	1-vinylimidazole
WCA	water contact angle
XPS	x-ray photoelectron spectroscopy

1 Objectives and Outline

Enzymes are proteins occurring naturally in living organisms, where they have important catalytic functions. Depending on their structure enzymes possess the ability to catalyze complex reactions with high selectivity and substrate specificity under mild reaction conditions and thus, are crucial for metabolic processes. These beneficial features make them very attractive as biocatalysts for the industrial synthesis of chemical compounds, such as pharmaceuticals and fine chemicals. In these processes, enzymes are used under conditions, which differ significantly from their natural environment and thus, result in a substantial loss in enzyme performance. However, high activity and stability are necessary for economically and technically feasible processes, which also require the re-use of biocatalysts with maintained high activity and stability for numerous reaction cycles. Immobilization of enzymes has been demonstrated to be an important concept in order to fixate the biocatalysts and thereby facilitating their separation and reusability. Despite these advantages of improved biocatalyst recovery, immobilization of enzymes comes generally at a cost of reduced activity. Therefore, different immobilization strategies, such as cross-linking of enzymes or their attachment to a solid support are under constant development in order to improve their biocatalytic performance. Due to their simplified processability and wide range of properties, different types of polymers have already shown their suitability as support material. Various examples have already demonstrated improvements in enzyme stability upon immobilization. However, the structure of each individual enzyme is unique, which results in specific, intrinsic properties and functions. Therefore, successful immobilization of enzymes cannot be generalized and depends on the specific factors, being the nature of the enzyme, the type of immobilization, the properties of the support, micro-environmental effects as well as the applied reaction conditions.

Therefore, the aim of this project was the chemical surface modification of various polymer materials and their exploitation for the immobilization of enzymes in order to achieve enzyme-support constructs with improved biocatalytic performance and applicability (see Figure 1-1). More specifically, the objective of this study was (1), the preparation and application of different polymer materials, (2), their tailored surface functionalization and (3), the investigation how the introduction of different surface chemistries and thus, micro-environmental changes, affect the activity, selectivity and stability of immobilized enzymes. Additionally to this strategy, the use of polymers as support materials in different configurations as well as various enzymes was intended to explore a wide range of application possibilities.

The importance of biocatalysis, enzyme immobilization, and a brief introduction on thiol-ene chemistry (TEC), which is widely used in this work, are described in *Chapter 2*, followed by different methodologies in order to develop promising polymer carriers for enzyme immobilization.
In the first approach, TEC has been used for the development of a screening platform focusing on micro-environmental effects, which are caused by various surfaces chemistries, and their impact on the **activity** of immobilized enzymes, as described in *Chapter 3*.
The broad **application** of suitable enzyme-surface candidates, identified through the first screening was the focus in *Chapter 4*, where a new preparation method for functional polymer particles and their application as enzyme support is described.

The importance of micro-environmental effects, not only for the activity of immobilized enzymes, but also for their **selectivity** was subsequently investigated by applying surface functional particles as support for the immobilization of β-glucosidase (see *Chapter 5*).
Additionally, the **effective** exploitation of immobilized enzymes in a biocatalytic process is crucial and was studied by selective surface modification via TEC and immobilization of horseradish peroxidase in a microfluidic device, as presented in *Chapter 6*.
Finally, in *Chapter 7*, the beneficial influence in terms of activity and **stability** of a suitable micro-environment through tailored surface modification was demonstrated on immobilized alcohol dehydrogenase (ADH) in a biocatalytically active membrane.
An overall Conclusion and Future perspectives can be found thereafter in *Chapter 8* and *9*, whereas experimental procedures of unpublished results are the content of *Chapter 10*.

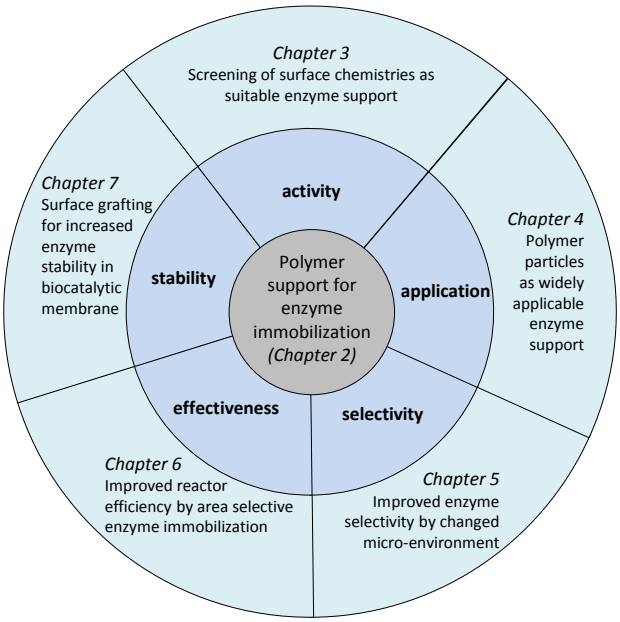

Figure 1-1 Important parameters when developing new polymer carriers for the immobilization of enzymes and their discussion in the different chapters of the thesis

This dissertation is based on the following publications/manuscripts:

Publication 1 (see Appendix 1.1, supporting information in Appendix 1.2)
Hoffmann, C.; Pinelo, M.; Woodley J. M.; Daugaard, A. E. Development of a thiol-ene based screening platform for enzyme immobilization demonstrated using horseradish peroxidase *Biotechnology Progress*, 2017, DOI: 10.1002/btpr.2526

Manuscript 2 (see Appendix 2.1, supporting information in Appendix 2.2)
Hoffmann, C.; Chiaula, V.; Pinelo, M.; Woodley J. M.; Daugaard, A. E. Simple preparation of thiol-ene particles from glycerol and surface functionalization by thiol-ene chemistry (TEC) and surface chain transfer free radical polymerization (SCT-FRP) *Macromol Rapid Comm*, in review

Manuscript 3 (see Appendix 3.1, supporting information in Appendix 3.2)
Hoffmann, C.; Grey, C.; Pinelo, M.; Woodley J. M.; Daugaard, A. E., Adlercreutz, P. Improved alkyl glycoside synthesis by trans-glycosylation through tailored micro-environment of immobilized β-glucosidase, manuscript draft, submission after successful publication of *manuscript 2*

Manuscript 4 (see Appendix 4.1, supporting information in Appendix 4.2)
Hoffmann, C.; Rosinha Grundtvig, I. P.; Thrane, J.; Garg, N.; Gernaey, K.; Pinelo, M.; Woodley J. M.; Krühne, U.; Daugaard, A. E. Experimental and computational evaluation of area selectively immobilized horseradish peroxidase in a microfluidic device *Chemical Engineering Journal*, in review

Additionally to the published articles, the described work has been presented at different international conferences, which are listed below:

a) Hoffmann, C.; Pinelo, M.; Woodley J. M.; Daugaard, A. E., Modification of polymer surfaces to enhance enzyme activity and stability, *Annual Polymer Day*, Kgs. Lyngby, Denmark, November 2014 (talk)

b) Hoffmann, C.; Pinelo, M.; Woodley J. M.; Daugaard, A. E., Tailored Functionalization of polymeric membranes by the application of surface grafting techniques, *7th EPF Summer School*, Gargnano, Italy, May 2015 (poster)

c) Hoffmann, C.; Pinelo, M.; Woodley J. M.; Daugaard, A. E., Tailoring polymeric membranes by surface grafting, *Nordic Polymer Days*, Copenhagen, Denmark, June 2015 (talk)

d) Hoffmann, C.; Pinelo, M.; Woodley J. M.; Daugaard, A. E., Tailored surfaces for enzyme immobilization by surface functionalization of polymeric materials, *Annual Polymer Day*, Kgs. Lyngby, Denmark, November 2015 (talk)

e) Hoffmann, C.; Rosinha Grundtvig, I. P.; Thrane, J.; Garg, N.; Gernaey, K.; Pinelo, M.; Woodley J. M.; Krühne, U.; Daugaard, A. E., OSTE+ microreactors and their surface modification for directed enzyme immobilization, *DTU Kemiteknik – Research Day*, Kgs. Lyngby, Denmark, May 2016 (talk)

f) Hoffmann, C.; Pinelo, M.; Woodley J. M.; Daugaard, A. E., Thiol-ene based material as a promising biocatalysis platform, *Nordic Polymer Days*, Helsinki, Finland, June 2016 (talk)

g) Hoffmann, C.; Rosinha Grundtvig, I. P.; Thrane, J.; Garg, N.; Gernaey, K.; Pinelo, M.; Woodley J. M.; Krühne, U.; Daugaard, A. E., Area Selective Surface Functionalization and Enzyme Immobilization in Thiol-ene-epoxy Microfluidic Devices, *Biocat 2016 - 8th International Congress on Biocatalysis*, Hamburg, Germany, August 2016 (talk)

h) Hoffmann, C.; Pinelo, M.; Woodley J. M.; Daugaard, A. E., Activity of enzymes immobilized on OSTE surfaces as a function of surface functionality, *5th International Symposium Frontiers in Polymer Science*, Seville, Spain, May 2017 (poster)

2 Background

Application of enzymes in biocatalysis

Enzymes are natural molecules, precisely proteins, which are produced in living cells and developed by natural evolution in order to catalyze essential reactions for the metabolism of organisms. Their discovery, isolation and application outside living organisms as biocatalysts in chemical reactions, was and still is very intriguing to scientists.[1] In biocatalysis, enzymes are used for synthesis of chemical compounds by conversion of natural or synthetic substrates. Thus, they substitute or supplement existing chemical catalysts, or provide completely new routes for particular reaction steps or the entire synthesis of chemical molecules. Nowadays, enzymes, either isolated or in whole cells, are already applied as biocatalysts for the production of pharmaceuticals, fine chemicals, or in the food industry.[2] In these cases, enzymes are used under a broader range of conditions, which include new substrates, large ranges in pH and temperature, high substrate and product concentrations, as well as organic solvents. Even though these conditions differ significantly from their natural environment, active, substrate specific and selective enzymes are require for the economic, sustainable and technical feasibility of a biocatalytic process. Additionally, high biocatalytic activity over a long operational time is necessary. In order to meet these requirements the discovery and isolation of different variants from known enzymes and evolving methods in protein engineering are playing a crucial role.[3] Alternatively, immobilization of enzymes has already in the 1960s been identified as a promising method in order to improve enzyme stability and reusability.[4] These beneficial features combined with advantages with respect to downstream processing increased the relevance of enzyme immobilization for industrial processes tremendously.[5–7]

Immobilization of enzymes

The recovery and reusability of the biocatalyst for industrially relevant processes is of significant importance. Simple separation of the enzymes and their repeated application over extended periods of time are essential for the realization of economical, technical and sustainable processes. Enzyme immobilization, which describes the fixation of enzymes and thus, limits their mobility, is therefore an excellent and probably the most important concept enabling enzyme recovery and reusability.[8] Furthermore, enzymes are considered to be relatively instable, especially under the conditions used for biocatalytic applications. Immobilization has already been demonstrated to improve enzyme stability and in some cases their activity. Thus, enzyme immobilization combines simplification in downstream processing, ideally combined with improvements in enzyme performance, which makes it a crucial concept in biocatalysis and related fields.

In this context, enzyme performance is used as a general term including activity, stability, selectivity and effectiveness. Enzyme activity describes the amount of converted substrate per unit time and is often related to the amount of used enzyme. Thus, the “international unit” (IU) or simply “unit” (U) defines the activity as the conversion of 1 micro mole substrate per minute.[9] More relevant, however, is the specific and volumetric activity relating the activity to the amount of enzyme, either by mass or volume. For immobilized enzymes, the activity can additionally be expressed relative to the amount of support. Enzyme stability is a measure for the deactivation of an enzyme, which can be divided into storage and operational stability. Thus, stability describes the enzyme performance, under different conditions and can be expressed as activity relative to the initial activity. Storage or in other words resting stability describes the

deactivation of the enzyme with time as the only parameter. In order to measure storage stability, external influences such as temperature and pH have to be constant.[10] Operational stability, however, considers the influence of the catalyzed reaction towards the enzyme performance. Therefore, using immobilized enzymes in batch processes the operational stability is a measure related to the reusability. Selectivity can be divided into enantio-, regio- and chemoselectivity, which are all important measures depending on the biocatalytic reaction. In this thesis, selectivity is mainly related to chemoselectivity, which means the preference for a specific reaction over one or more plausible reactions. Additionally, enzyme effectiveness is another term, which is discussed in this thesis and refers to the exploitation of a given amount of immobilized enzymes and their contribution to the performance of the biocatalytic reactor. All these parameters are significant measures for the use of enzymes in their free or immobilized conformation as biocatalysts.

During the past decades, different strategies for enzyme immobilization and their influence on enzyme activity, stability and selectivity have been thoroughly reviewed.[11–18] Generally, many different methods have been utilized in order to achieve immobilized enzyme systems, always with the goal to obtain improvements in terms of (bio-) catalytic performance for a selected application (see Figure 2-1).

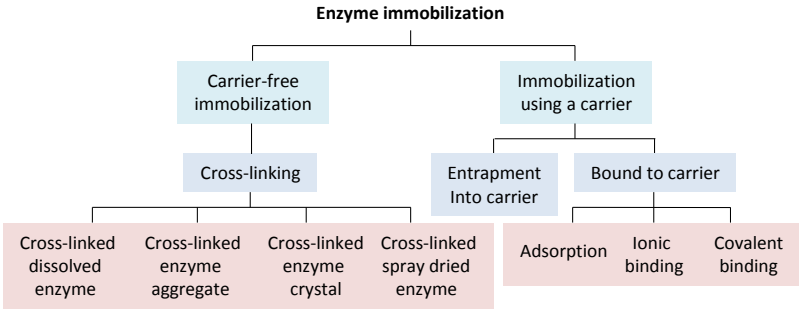

Figure 2-1 Overview of different approaches for enzyme immobilization based on the use of a carrier

These methods can be divided into two main groups, depending on whether the immobilization is achieved by means of a carrier as a support or not. Carrier-free immobilization mainly includes cross-linking by using molecules (cross-linking agents), which can react multiple times with the enzymes and thus, forming an enzyme aggregate.[19] Depending on the cross-linking strategy various methods are available. Glutaraldehyde (GA), being a bifunctional aldehyde, which can react covalently with enzymes is the most common and widely used one. However, also physical cross-linking is possible. Conversely, using a carrier for immobilization, enzymes can either be entrapped into the carrier matrix, for instance into gels or microcapsules, or alternatively bound to the carrier surface.[16] The latter option can be realized by means of physical adsorption, ionic or covalent bond formation. For this approach, different support materials, such as glass, metals, nanomaterials and polymers have already been investigated.[4] It has been emphasized that for successful implementation of carrier immobilized enzyme processes the type of support, immobilization strategy, used enzyme and reaction conditions play a crucial role and their effects overlap each other. Therefore, all of these factors have to be taken into consideration and finally balanced in order to establish a feasible process.

Carrier-bound enzyme immobilization

As mentioned, physical adsorption is one of the oldest and easiest methods for enzyme immobilization on solid supports. Due to its advantages, being fast, simple and reversible, this method has been studied extensively with various supports. Physical adsorption onto carriers often results in highly active biocatalytic systems, since no chemical modification of the enzyme is required, contrary to covalent immobilization. However, a drawback of adsorbed systems is a potential enzyme leakage due to relatively weak interactions with the support. In order to overcome this issue, further approaches by combining different methods, such as adsorption-cross-linking or adsorption-covalent bonding, were developed.[20]
Covalent immobilization is generally an important alternative to adsorption, offering a tightly bound enzyme-support system, which is consequently less prone to exhibit enzyme leakage.[21] However, the stronger interactions between immobilized enzymes and the support, as a result of covalent bond formation, can affect the enzyme structure significantly, which can have positive as well as negative consequences. Conventionally, covalent immobilization is achieved by the chemical reaction between specific functional groups from the support (as exemplified in Figure 2-2A) with reactive groups situated in the enzyme (Figure 2-2B).

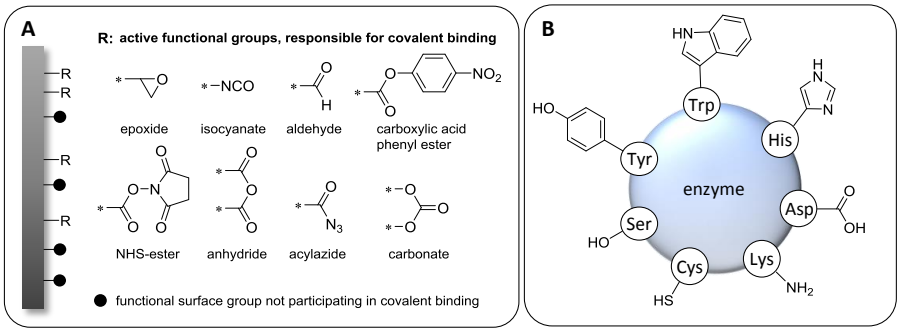

Figure 2-2 A) Representation of carriers with reactive functionalities that are selective towards enzyme immobilization as well as functionalities, which are not able to form covalent bonds with enzymes, but contribute to non-covalent surface-enzyme interactions; B) reactive enzyme functionalities originating from amino acids, which can react with carrier functionalities

The latter ones originate from amino acids, which are present at the surface of the enzyme. In order to achieve a stable covalent bond between the enzyme and the support, many carrier-bound functional groups have been investigated. Noteworthy is also the presence of carrier-bound functional groups, which do not participate in the covalent immobilization (see Figure 2-2A). The nature of these functionalities contributes significantly to physical interactions between the carrier and the enzyme and thus the biocatalytic performance.
In general, various factors for stabilization and destabilization have been identified for the attachment of enzymes to solid surfaces, which have already been broadly reviewed.[13,17,22] Enzyme activity and stability are strongly related to the obtained protein structure (conformation) and its preservation in a biocatalytic process. Interactions of any kind between the enzyme and the support can directly affect the enzyme structure and thus the resulting performance, as illustrated in Table 2-1. For this reason different approaches have been investigated in order to achieve surface modifications, which lead to improved biocatalytic activity of immobilized enzymes. In order to prevent deactivation, the properties of the surface

have to match structural and compositional characteristics of a particular enzyme and provide a favorable local environment for the immobilized enzyme.[23] Interactions based on surfaces containing charged[24,25], hydrophilic[26] or hydrophobic[27] moieties can affect the enzyme structure substantially. Whether, these interactions are beneficial or not, depend in any case on the match between surface and enzyme. For instance, hydrophobic interactions are usually considered to affect the enzyme activity negatively due to unfolding of the hydrophobic enzyme structure.[22] Lipases, however, contain a characteristic hydrophobic peptide chain (called "lid") covering the active center of the lipase, which opens up due to hydrophobic interactions with the carrier. Consequently, their active center shows improved accessibility for substrate molecules and thus, demonstrates increased activity when immobilized on hydrophobic supports.[13]

Direct attachment to the surface via covalent binding, for instance by multibond attachment, leads to structurally confined and rigid immobilized enzymes with strong interactions between the surface and the enzyme (see Table 2-1).[22] This rigidification leads commonly to improvements in stability due to conformational restrictions of the enzyme.[13] In some specific cases, this strong attachment of enzymes to a surface can also have a beneficial effect on the activity. On the other hand, strong rigidification might cause unfavorable conformation changes, which could be overcome by the introduction of spacer molecules between the surface and the enzyme. Polymers grafted to or from a surface[28–30] as well as surface bound tethers[12,31] can act as spacers, which offers higher mobility of the enzyme. This may result in an improved enzyme activity, but could also negatively impact the stability due to higher mobility and reduced rigidity.

Moreover, the choice of carrier can also indirectly influence the enzyme behavior without directly affecting its structure. Surface hydrophilicity/hydrophobicity might impact the partition of deactivating reagents (solvent, surfactants, dissolved gases etc.) in a favorable way on the surface.[13] Thus, deactivating reagents exhibit a reduced effect on immobilized enzymes. However, as discussed, each enzyme has a unique structure and consequently, the final result on activity and stability is a balance between several effects, which should preferably be identified for each specific enzyme. Predictions and generalizations about stabilization effects on specific surfaces are therefore not universally applicable.

Furthermore, the immobilization on porous materials offers the advantages of creating a protected environment, and form due to diffusion limitations substrate, product and pH gradients, which can be beneficial under specific circumstances.[13,32] Additionally to favorable properties of protective pH, substrate and product gradients, diffusion limitations impact mass-transport processes, which are playing a significant role for the implementation of biocatalytic processes.[5] Mass-transport limitations can substantially affect the overall activity of immobilized enzyme. Additionally to the catalytic step, several other rate limiting parameters can contribute to the alteration of the apparent enzyme activity. In general it can be distinguished between external and internal diffusion of both, substrate and product. External diffusion, also called film diffusion, considers mass-transport through a boundary layer directly on the support surface. Internal or pore diffusion is related to the diffusion between the support surface and the catalytic active site. A comprehensive determination including the mathematical description of diffusion and mass-transfer in biocatalysis has been widely discussed in literature.[10,33] However, in order to evaluate and optimize the immobilized enzyme, it is important to determine the rate limiting step being either the intrinsic enzyme activity or diffusion related. In practice, various methods have been identified to determine possible mass-transfer limitations, including the increase of stirrer-speed in stirred batch reactors or the flow

Table 2-1 Overview of immobilization characteristics on solid supports and their features and influence on enzyme performance

Support properties	Resulting effect	Influence on enzyme activity, stability, selectivity	Influence type	Ref.
Polar / charged support surface	Electrostatic interaction (repulsion or attraction) or hydrogen bonds	Possible conformational changes of the enzyme (or even distortion), changes in enzyme orientation, which can have both, positive or negative effect on enzyme performance (depending on enzyme-surface)	ES	[24,25]
Hydrophilicity or hydrophobicity of support surface	Hydrophobic and hydrophilic interactions with enzyme	Hydrophobic interactions may lead to structural distortion, however, beneficial for lipases	ES	[26,27]
		Hydrophilic surfaces lead generally to high enzyme conformation retention	ES	[22]
	Alteration of medium partition	Possible improvement of enzyme environment and thus activity by alteration of partition of compounds, like deactivating agents towards and away from enzyme	P	[13]
Functional groups for multi-point bonding	Rigidification of the protein structure	Improved stability by retention of enzyme structure under drastic conditions, like high temperatures, in the presence of distorting agents, mechanical stress	ES	[22,15]
		Decrease in mobility and unbeneficial changes of enzyme structure might lead to activity reduction	ES	[13]
		Prevention of enzyme inhibition, due to inhibition site blocking	ES	[34]
Functional groups for multi-subunit bonding	Rigidification of the protein structure	Reduction of subunit dissociation, which results often in increased activity	ES	[35]
Attached spacer for covalent immobilization	Effect on mobility	Increased enzyme mobility and thus possibly improved activity	ES	[28–30]
		Increased mobility, nature of spacer and enzyme binding to spacer might affect the biocatalytic stability either positively or negatively	ES	[21]
	Effect on micro-environment	Micro-environmental changes through the spacer beneficially affect the biocatalytic activity	ES	[21]
Porous support	Alteration of substrate and product partition	Change in substrate and product concentration in proximity to enzyme, which can improve biocatalytic activity under specific circumstances	P	[13]
	Influence on enzyme alteration by harsh reaction conditions	Limiting access of deactivating agents, like gas bubbles, organic solvent	P	[11]
		Reduced negative influence of strong stirring (mechanical stabilization)	P/ES	[13]
	Diffusion effects	Possible positive effect on enzyme stability due to gradients in substrate concentration and pH	P	[36]

ES: enzyme structure, P: process related

rate in plug-flow reactors, in order to reduce internal diffusion. Furthermore, reduction in particle (support) size and increase of pore size are possible parameters. Consequently, increased reaction rates indicate diffusion limitations of the process.[36]
In summary, successful immobilization of enzymes depends on many different factors, related to the nature of the enzyme, type of immobilization, environment and process related limitations. All of these parameters play a significant role for the implementation of successful enzyme immobilization.[35]

Polymer materials as enzyme carriers

As already discussed, the selection of a suitable carrier for enzyme immobilization, including its material, design, chemical nature, mechanical properties, density and porosity, is strongly dependent on the biocatalytic reaction, the nature of the enzyme and the process conditions. Polymer materials with a broad range in chemical structure have demonstrated simple processibility, fabrication, and possibilities for post-fabrication functionalization. Their large variety of possible material geometries, such as coatings, films, particles, membranes, monoliths and many more, provide an enormous application spectrum. Thus, due to their large variations of inherent properties, polymers can be tailor-made for specific purposes and have shown their suitability as enzyme support.[6,37] Industrially, many resins, which are fabricated to porous or non-porous particles of different polymers, have evolved to be attractive for enzyme immobilization. Industrially relevant synthetic polymers are polyacrylates, poly(methacrylate)s, polystyrene and polypropylene, containing different functionalities enabling various types of adsorption (non-specific, specific, hydrophobic), ionic interactions or covalent binding of enzymes. Hydrophilic Eupergit® C is a widely used copolymer consisting of methacrylamide, glycidyl methacrylate and allyl glycidyl ether, which is cross-linked by N,N'-methylene-bis(methacrylamide). Its porous particles have been applied for covalent immobilization of various different enzymes, such as glucose oxidase, phosphodiesterase, and penicillin G acylase (PGA).[38] On the other hand, hydrophobic supports, like macroporous Amberlite XAD-7 being an acrylic polymer, have served for the adsorption of enzymes, as exemplified for immobilized lipase B from *Candita antarctica* (CALB), which is commercially available as Novozyme 435.[16] Furthermore, natural polymers like cellulose, starch, agarose or chitosan and their particles have been successfully applied for the industrial immobilization of PGA, laccases, lipases and glucose isomerase.[22] These examples show that support properties for the immobilization of specific enzymes can be tailored by selecting different type of polymers or by changing the polymer bulk composition. Moreover, post-fabrication surface functionalization of a selected polymer material can be used for distinct modification of the material properties. For instance, hydrophilicity or hydrophobicity of the carrier can be modified and applied for specific applications, such as for the improvement in anti-fouling properties of membranes.[39]
Additionally to the type of polymer, different preparation methods allow variations in the appearance of these materials, such as coatings, gels, and porous structures. Consequently, this strategy can be used to tune the material according to their application. For instance, the use of polymer particles in general enables the application of immobilized enzymes in batch reactors as well as in continuous packed-bed reactors. Additionally, the preparation of polymer membranes and their application as biocatalytic membrane reactors (BMRs) has gained significant attention. α-Amylase, lipase, laccase and several other enzymes have already been immobilized onto polymer membranes made of polyacrylonitrile (PAN), polypropylene, polyamide and more specific modified polymers.[40] Other fields, in which enzyme

immobilization has also benefited from polymer support materials are medical applications, microfluidics and biosensors.

Thiol-ene chemistry in polymer materials

Recently, a few examples illustrated the immobilization of enzymes onto polymer supports based on thiol-ene chemistry (TEC).[41–43] TEC is well-known to be a versatile and efficient type of reaction and thus, has been exploited widely in material science.[44] TEC describes conventionally the radical mediated reaction between a thiol group and an electron rich carbon-carbon double bond, called ene, whereas, thiol-Michael addition refers to the reaction with electron deficient enes under alkaline conditions.[45] TEC accepts a wide range of possible thiol as well as ene substrates, which facilitates the formation of a vast amount of chemical structures. Due to its beneficial features, being a very rapid and nearly quantitative method, tolerating oxygen and water, being orthogonal to other organic reactions and its mild reaction conditions it has emerged to an attractive pathway for the synthesis and functionalization of polymers.[46–48] Especially the photochemically mediated TEC has been used for the synthesis of linear, dendritic, and cross-linked polymer scaffolds, which, depending on the reaction conditions, have been applied for preparation of hydrogels,[49,50] nano- and microparticles,[51] porous structures by emulsion templating,[52] and development of soft lithography.[53,54] The wide range of applicable monomers reflects the high modularity of thiol-ene (TE) networks, which can be used to tailor their mechanical properties.[55] Not only the type of monomers, but also their stoichiometry towards each other can be used to tune the mechanical and surface properties of the network.[56,57] Therefore, off-stoichiometric thiol-ene (OSTE) materials, in which a stoichiometric imbalance between thiol and ene functionality is used, have been increasingly applied for the fabrication of microfluidics and lab-on-chip technologies.[58–61] The applied stoichiometric imbalance, using either thiol or ene functionality in excess, results in unreacted functional groups in the bulk and on the surface, which have already been exploited for surface functionalization under photochemical TEC conditions. Thus, different chemistries have been introduced onto OSTE surfaces, such as hydrophilic poly(ethylene glycol) (PEG) groups, hydrophobic fluorinated groups[62] or biological affinity moieties, like biotin.[63] OSTE surfaces were also functionalized with more specific groups, such as maleic anhydride[43] and cysteamine[64], which have been applied for immobilization of enzymes.

This approach was further extended introducing these functionalities in micro-sized patterns by use of stencil masks in photochemical reactions. This type of surface functionalization can in principle be used on any alkene or thiol terminated surface, as demonstrated on thiol functional self-assembled-monolayers (SAM's)[65] and polydimethylsiloxane (PDMS)[66] as well as on alkene functional polymer brushes on silicon or glass wafers.[67] These advantageous features make TEC a powerful tool for preparation of polymer materials and for efficient surface functionalization. Therefore, it has been one of the primary techniques applied in this PhD study.

3 Thiol-ene (TE) based screening platform for enzyme immobilization

As initially described, one of the major requirements for immobilized enzymes as biocatalysts, is a high biocatalytic **activity**. Therefore, the objective of this PhD study was the versatile functionalization of polymer surfaces in order to investigate their impact on the biocatalytic performance of immobilized enzymes. Depending on the chemical nature of the support, a variety of different interactions between the surface and the enzyme can be formed. Thus, beneficial changes of the micro-environment, created by different surface chemistries, are intended to improve the enzymatic performance. Consequently, the objective of this chapter is the development of a method for fast screening of various surface functionalities and their impact on residual activity of immobilized horseradish peroxidase (HRP), as illustrated in Figure 3-1. The work has been published in *publication 1* (see Appendix 1).

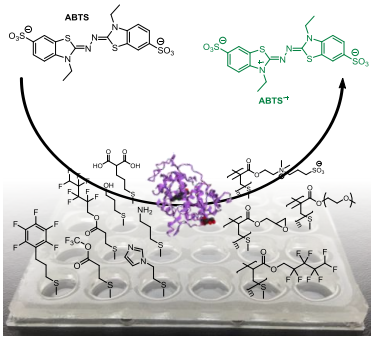

Figure 3-1 Illustration of a versatile screening platform for the investigation of different surface functionalities and their impact on the activity of immobilized HRP

Versatile TEC for material and surface development

The properties of a particular support are crucial for the successful immobilization of enzymes. Therefore, a vast number of different materials, like glass, metals and polymers have been tested. Especially polymers have extensively been used due to the easy processibility, adjustable mechanical properties, conductivity, and ease of post-functionalization.[37] However, in order to determine a suitable support for a specific enzyme, separate trial and error experiments of different materials with different characteristics have usually to be conducted. In order to improve this process, it would be desirable to use a single material, of which the properties can easily be modified and thus, tested for the immobilization with enzymes. As previously discussed, TEC, combining high efficiency and versatility in polymer synthesis and functionalization, would be well-suited for the preparation of such as a screening platform. Consequently, using this approach the preparation of a library would simplify the entire screening process and could allow predictions for new enzyme-support combinations.

The aforementioned development of stoichiometric thiol-ene (STE) and furthermore OSTE polymer thermosets with tunable mechanical and surface properties was recently reported.[53,56,58,68] Therefore, STE and OSTE based microfluidics,[57,69] particles[70], hydrogels[49] and high internal phase emulsions (HIPEs) were fabricated.[52] Further surface modification by TEC

allows the introduction of various chemistries on the surface and consequently surface properties, such as hydrophilicity can be tailored.[61–63] These beneficial features of photochemical TEC as a method for material preparation as well as post-preparation surface functionalization offer a large spectrum of possibilities in order to develop suitable supports for the immobilization of specific enzymes. This approach has been demonstrated in this Chapter through the fabrication of a microwell plate as tunable enzyme support.

Preparation of a TE based microwell plate

STE/OSTE microplates were prepared through a 2-step curing process via photoinitiated TEC using pentaerythritol tetrakis(3-mercaptopropionate) (PETMP) and 1,3,5-triallyl-1,3,5-triazine-2,4,6(1H,3H,5H)-trione (TATATO) as shown in Figure 3-2A.

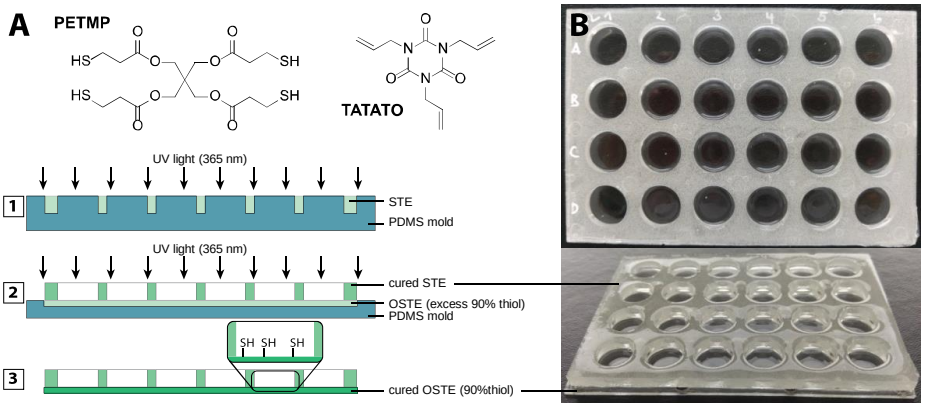

Figure 3-2 A) schematic representation of the microplate preparation using a 2-step curing process, (1) curing by irradiation with UV light of the top part prepared from a stoichiometric thiol-ene (STE) mixture of PETMP and TATATO in a PDMS mold, (2) the prepared top part is placed on a OSTE mixture (excess 90% thiol) of PETMP and TATATO, where a second curing step by irradiation with UV light leads to the final microplate, (3) which contain excess thiol groups in the bottom and STE on the well walls, B) Photographs of the final microwell plate.

In a first stage, the top part of the microplate in a STE mixture of PETMP and TATATO was photochemically cured in the presence of TPO-L in a polydimethylsiloxane (PDMS) mold, as shown in Figure 3-2A (1). The mold consisted of the outer geometries of the microplate (127.7 x 85.6 mm^2), pillars with the size of the round wells (diameter 15.1 mm) and a depth of 5 mm. A second mold with a depth of 1.5 mm and the outer diameters of the microtiter plate was then applied for the second curing step. Here, an OSTE composition of PETMP, TATATO and TPO-L using a 90 % excess of thiol was applied for the well bottom. The previously prepared STE top part was then placed on top of the uncured OSTE mixture and both parts were cured together (see Figure 3-2A (2)). This preparation process resulted in a fully sealed microplate consisting of 24 wells with a depth of 5 mm, shown in Figure 3-2A (3) and Figure 3-2B. Due to the used compositions, excess thiol groups remained on the bottom of each well. The side walls of the wells, based on a STE composition, did not contain any residual thiols, as determined using Ellman's reagent, which is commonly used for quantification of thiol groups either on surfaces or in solution (see Appendix 1.2, Figure S2).[71] From these results it could be seen that Ellman's reagent, which was added to a STE surface, exhibit a very low absorbance compared to the OSTE with 90 % excess of thiols. Therefore, it was deduced that the number of thiols on

the side walls was considered negligible and that modification of surface bound thiols occurred exclusively on the bottom surfaces. Furthermore, the transmittance of the OSTE material was measured in order to validate the possible application in colorimetric assays. The material demonstrated a strong absorbance in the UV range from 220 to 340 nm, as shown in Appendix 1.2, Figure S3. Between 340 and 410 nm, the transmittance increased up to 36 % (absorbance = 0.44) and at any wavelength above, the material was completely transparent (absorbance < 0.15). In general, the absorbance of the STE/OSTE microplate does not substantially differ from a commercial polystyrene microplate, as indicated in Appendix 1.2, Figure S3. Therefore, the STE/OSTE plate is well suited for any application in which absorbance measurements of solutions or surface modifications are performed.

Photochemical functionalization of microwell surfaces

Excess thiol groups on the bottom surface originating from the OSTE mixture allow controlled surface functionalization via TEC and surface chain transfer free radical polymerization (SCT-FRP). In this study, the surface modification using both methods has been conducted with a large range of monomers in order to introduce different types of functionalities as illustrated in Scheme 3-1.

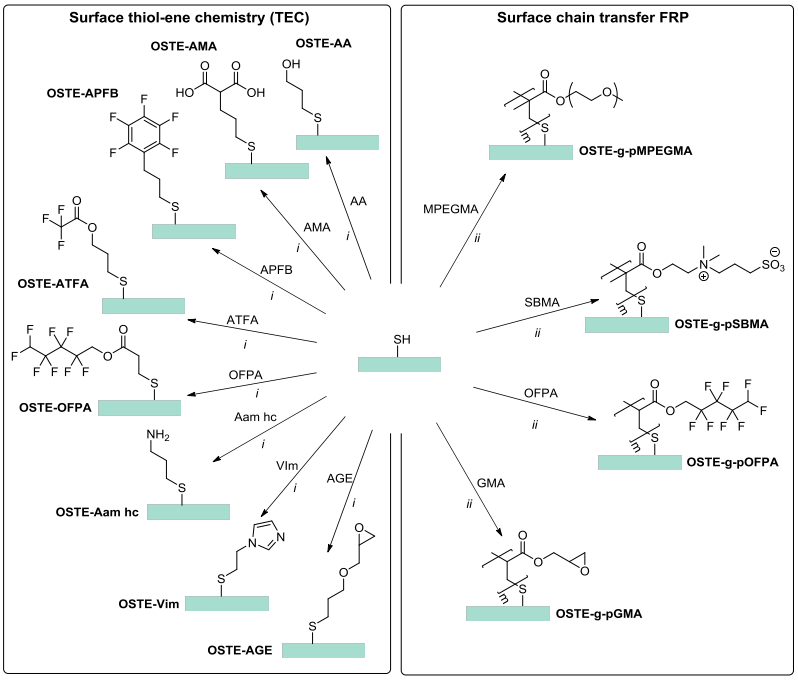

Scheme 3-1 Surface functionalization of thiols from OSTE microwell surfaces via two different routes; left: surface thiol-ene chemistry (TEC) with allyl alcohol (AA), allyl malonic acid (AMA), allyl pentafluorobenzene (APFB), allyl trifluoroacetate (ATFA), 2,2,3,3,4,4,5,5 octafluoropentyl acrylate (OFPA), allyl amine hydrochloride (Aam hc), 1-vinyl imidazole (Vim) and allyl glycidyl ether (AGE) at low concentration (0.3 M) leading to a functional monolayer on the surface; right: SCT-FRP with methoxy poly(ethylene glycol) methacrylate (MPEGMA), zwitterionic sulfobetaine methacrylate (SBMA, via [2-(methacryloyloxy)ethyl]dimethyl-(3-sulfopropyl)ammonium hydroxide), OFPA and glycidyl methacrylate (GMA) based monomers at high concentration (0.7 – 2.4 M), leading to a functional polymer grafted surface.

With the aim to develop a platform for enzyme immobilization, which enables screening of various surface functionalities and their impact on the activity of surface bound enzymes, a variety of functional monomers were utilized under TEC conditions. Based on different types of possible interactions and immobilization mechanisms various reactive moieties were selected. Hydroxyl functional groups (AA) were introduced as well as fluorine groups (APFB, ATFA and OFPA). pH responsive modifications, with either acidic groups (AMA) or basic functionalities, such as amine (Aam hc) and imidazole (Vim) were used as well. This range of introduced surface chemistries offered possible immobilization mechanisms including hydrophilic (with OSTE-AA, -AMA), hydrophobic (OSTE-APFB, -ATFA, -OFPA) and ionic interactions (OSTE-Vim and -AMA). Furthermore, epoxides were introduced (AGE) allowing bioconjugation through covalent enzyme binding with amine, thiol, imidazole or phenolic moieties from the enzyme.[72] The application of such a broad range of reagents demonstrates the great versatility of this process and can extensively be expanded, since TEC offers a vast range of surface chemistries by reaction of any allyl, vinyl or acrylic compound onto the screening platform. Photochemical surface TEC was performed with low monomer concentrations (0.3 M) in ethanol solutions in order to prevent polymerization reactions. The IR spectrum of the starting material (OSTE) contains typical alkane (C-H, 2968 cm^{-1}), carbonyl (C=O, 1729 cm^{-1}), alkene (C=C, 1683 cm^{-1}) and aliphatic ester (C-O-C, 1141 cm^{-1}) elements. Comparison with TEC grafted surfaces did not exhibit significant differences, as illustrated in Appendix 1.2, Figure S4. This could be explained by a low surface coverage due to a TE addition on the surface. Small structural changes as a result of monolayer formation can generally not be detected by attenuated total reflectance (ATR) FT-IR due to the domination of the bulk material in the spectrum, caused by the penetration depth of the IR signal. However, by using x-ray photoelectron spectroscopy (XPS) in combination with static water contact angle (WCA) measurements, the individual modifications were confirmed, as shown in Table 3-1 for the virgin (OSTE) and TEC modified surfaces.

The atom composition of the unreacted OSTE surface estimated by XPS was in agreement with the theoretical values and therefore used for further comparisons with modified surfaces.

Table 3-1 XPS data and static water contact angles (WCA) of virgin and functionalized OSTE surfaces via TEC with a variety of ene compounds

Surface type	C1s [atom%]	O1s [atom%]	N1s [atom%]	S2p [atom%]	F1s [atom%]	WCA [°]
OSTE	61.1±0.6 (60.6)	23.3±0.2 (24.9)	4.5±0.3 (4.1)	11.1±0.3 (10.4)		67.0±1.2
OSTE-APFB	58.8±2.8	27.2±2.0	2.7±0.0	9.9±0.5	1.4±0.3	62.4±2.1
OSTE-ATFA	55.3±0.0	28.6±0.1	5.2±0.2	8.1±0.2	2.8±0.1	41.1±2.4
OSTE-OFPA	53.4±0.4	26.9±0.1	4.5±0.3	8.1±0.0	7.1±0.6	77.7±4.1
OSTE-AA	60.4±0.2	27.6±0.7	4.5±0.5	7.6±0.4		35.0±1.5
OSTE-AMA	61.3±0.1	27.8±0.1	4.2±0.0	6.7±0.1		25.1±3.6
OSTE-Vim	63.3±1.5	22.6±0.8	7.3±0.2	6.8±0.5		38.5±3.6
OSTE-AGE	58.7±0.6	28.7±0.3	4.2±0.3	8.4±0.2		55.9±3.7
OSTE- Aam hc	59.3±0.2	26.5±0.1	5.5±0.1	8.7±0.1		55.4±4.7

In parenthesis, theoretical atom composition of the virgin surface (OSTE), results are based on three replicated measurements on the same surface (n=3)

Surface functionalization with fluorinated reagents such as APFB, ATFA and OFPA was confirmed by the presence of fluorine atoms (F1s) in the XPS spectra, which was not detected on the native OSTE surface. APFB modified OSTE exhibited with 1.4 atom% the lowest fluorine content, which suggested a low grafting efficiency. This could be improved by reaction with ATFA and OFPA (2.8 and 7.1 atom%). In contrast to the allylic reagents, OFPA being an acrylic monomer is prone to undergo polymerization under radical conditions. Here, the overall atom composition of OFPA modified surfaces under TEC conditions, showed additional to the increase in fluorine content a slight reduction in carbon, sulfur and nitrogen. This confirmed that under the applied low concentration TEC conditions, even for an acrylic monomer like OFPA, the addition reaction dominated, leading to the formation of a monolayer (polymerization could then be suppressed). The atom composition after surface TEC with AMA, AA and AGE did not differ significantly from the reference OSTE surface. This could be attributed to similar theoretical atom composition of these reagents and the OSTE base material. In contrast, surface functionalization via TEC of Vim and Aam hc could be clearly confirmed by a significant increase in nitrogen (N1s) content, from 4.5 (OSTE) to 7.3 and 5.5 atom%, respectively. Vim is a reactive monomer and known to polymerize under radical condition, which could explain the relatively strong increase in nitrogen content using Vim.[73] Consequently, the high reactivity of Vim could have led to the formation of short polymer grafts on the surface, even at low concentrations and short reaction times.

In addition to XPS analysis, the impact of the different surface modifications was also investigated by water contact angle (WCA) measurements. The WCA of APFB reacted surface (62.4°) changed slightly compared to the reference surface (OSTE, 67.0°), which was assumed to be the result of the low reactivity, as already seen from the XPS data. A similar trend was observed for OSTE-ATFA, where the WCA was reduced more significantly to 41.1° upon modification. This was attributed to the polar nature of ATFA. As expected, increased hydrophobicity of the surface was achieved via functionalization with OFPB, which was confirmed by a WCA of 77.0°. Reduced WCAs of 35.0° (OSTE-AA), 25.1° (OSTE-AMA) and 55.2° (OSTE-AGE) were observed due to the introduction of hydroxyl, carboxylic acid and epoxide groups via surface TEC with AMA, AA and AGE. Similarly, WCAs of 38.5° (OSTE-Vim) and 55.4° (OSTE-Aam hc) validated the functionalization with Vim and Aam hc. This illustrates the versatility of the system providing successful surface modification by TEC and that the surface properties of the microplate wells could be adjusted by the formation of a functional monolayer.

Additionally, thiol groups are known to serve as chain transfer agents in free radical polymerization reactions in order to reduce molecular weight of the polymers. Surface bound thiols can act in a similar way as reported earlier for other types of surfaces, where the surface could be grafted by termination of growing polymer chains.[74–76] In this study, we have expanded this SCT-FRP approach as an alternative method to TEC for controlled surface modification of OSTE materials. Different acrylic and methacrylic monomers containing PEG (via MPEGMA), a zwitterionic sulfobetaine (SBMA), fluorine (OFPA) and epoxide groups (GMA) were utilized. In this case, by running the photochemical reaction at a higher concentration, polymer grafting onto the well surfaces could be achieved by SCT-FRP in the presence of DMPA as radical photoinitiator, as shown in Scheme 3-1. Typically, the liquid monomers were used in a 1:2 volume ratio in ethanol, whereas SBMA, being a solid, was applied in a concentration of 2.4 M. In contrast to TEC, surface modification via SCT-FRP can be confirmed by IR spectroscopy, as illustrated in Figure 3-3.

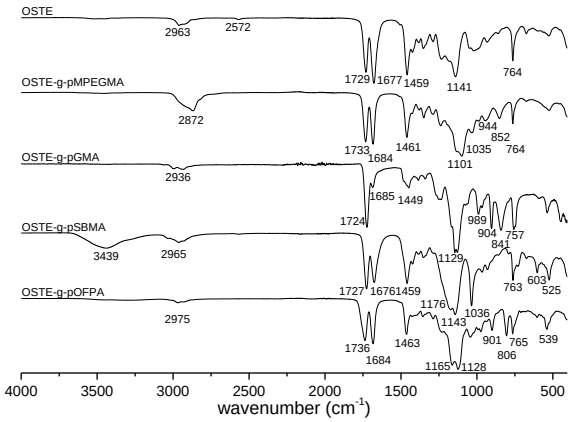

Figure 3-3 IR spectra of virgin OSTE surface and OSTE grafted via SCT FRP with various acrylate and methacrylate based polymer, such as MPEGMA, GMA, SBMA or OFPA

A clear indication of the formation of a thick surface layer by SCT-FRP is the complete disappearance of the S-H stretch band at 2572 cm^{-1} upon surface polymerization of each monomer. The spectrum of OSTE-g-pMPEGMA showed a strong absorption at 1100 cm^{-1}, which can be assigned to C-O-C stretch vibration originating from the PEG side chain. An additional band at 904 cm^{-1} for the OSTE-g-pGMA is observed, which is the epoxide ring vibration. In the IR spectrum of the OSTE surface upon grafting with pSBMA, a band at 3439 cm^{-1} indicates the ammonium N-H stretch vibration. Furthermore a broadening of the C-O-C stretch absorption at 1143 cm^{-1} as well as the strong band at 1036 cm^{-1} confirms the presence of pSBMA. Surface grafting with pOFPA led to the appearance of carbon-fluorine bands at 1163, 806 and 539 cm^{-1}. XPS and WCA analysis corroborated these results, which are presented in Table 3-2. XPS analysis of a pMPEGMA grafted surface (OSTE-g-pMPEGMA) showed significantly increased carbon and oxygen contents, which is consistent with the theoretical value of MPEGMA. Combination with the simultaneous decrease in sulfur and nitrogen confirms the polymer grafting of the OSTE-g-pMPEGMA surface. Similar XPS results were achieved by polymer grafting with pGMA, where the oxygen and carbon content increased approaching the theoretical value of the monomer. The amount of nitrogen and sulfur was even lower compared to OSTE-g-pMPEGMA, indicating an even thicker pGMA layer. The theoretical atom composition of SBMA is more similar to that of the OSTE background, which leads to only minor changes in the atom composition as a result of grafting. However, the content of the individual atoms from the OSTE-g-pSBMA surface approximated the theoretical values of the SBMA monomer, substantiating the success of the grafting reaction. Compared to the aforementioned surface modification via TEC with OFPA, polymerization conditions (higher concentration, longer reaction time) lead here to the appearance of a much higher fluorine content of 44.0 atom% compared to the 7.1 atom% by TEC. Additionally, the total atom composition of the OSTE-g-pOFPA surface was found to be in good agreement with that of the pure monomer, which confirms the formation of a polymer layer on the surface under SCT-FRP conditions. These presented changes in atom composition, upon polymer grafting with the individual monomers, were corroborated by the variation in WCAs of the reacted surfaces.

Table 3-2 XPS data and static water contact angles (WCA) of virgin and grafted OSTE surfaces via SCT FRP with a variety of acrylate and methacrylate based polymers[a]

Surface type	C1s [atom%]	O1s [atom%]	N1s [atom%]	S2p [atom%]	F1s [atom%]	WCA [°]
OSTE	61.1 (60.6)	23.3±0.2 (24.9)	4.5±0.3 (4.1)	11.1±0.3 (10.4)		67.0±1.2
OSTE-g-pMPEGMA	65.6±0.6 (67.6)	30.1±0.2 (32.4)	0.5±0.4 (0.0)	3.9±0.2 (0.0)		25.4±3.6
OSTE-g-pGMA	70.7±0.4 (70.0)	28.7±0.4 (30.0)	0.5±0.1 (0.0)			69.6±7.5
OSTE-g-pSBMA	62.9±0.0 (61.1)	25.2±0.0 (27.8)	4.7±0.1 (5.6)	7.2±0.1 (5.6)		20.4±4.8
OSTE-g-pOFPA	43.2±0.6 (44.4)	11.1±0.3 (11.1)	0.5±0.1 (0.0)	1.3±0.3 (0.0)	44.0±1.3 (44.4)	118.1±1.9

[a)]In parenthesis, theoretical atom composition of the virgin surface (OSTE) and monomers used for SCT FRP, results are based on three replicated measurements on the same surface (n=3)

Grafting with pMPEGMA increased the hydrophilic character, which was shown by a reduction in WCA from 67° (OSTE) to 25.4°. Similarly, a substantial hydrophilization was achieved by grafting with pSBMA (20.4°) confirming the surface reaction. The WCA increased slightly upon SCT-FRP using GMA (69.6°). OSTE-g-pOFPA exhibits a very high WCA of 118.1° and demonstrates the drastically increased hydrophobicity of the surface upon polymer grafting, which is significantly higher than the one obtained from TEC using the same monomer (77.0°). These results, together with the earlier discussed XPS and IR data, illustrate the potential for altering surface properties through selection of reaction conditions. Low concentrations and short reaction times lead to addition of the acrylate to the thiol groups based on TEC. Increased concentrations and longer reaction times favor polymerization, which undergoes chain transfer or termination with surface thiols leading to a thicker surface coating. The application of either surface modification method, TEC or SCT-FRP, demonstrated the versatility of these grafting reactions in order to achieve high control over the surface functionality and properties.

Immobilization of horseradish peroxidase (HRP) on functional surfaces

The functionalized well bottom surfaces were subsequently used for enzyme immobilization. For this purpose, a rhodamine labelled horseradish peroxidase (Rho-HRP) dissolved in PBS buffer (pH7.3) was used as a model enzyme. HRP (EC 1.11.1.7), belonging to the class of peroxidases, catalyzes the oxidation of electron donating substrates with hydrogen peroxidase (H_2O_2). The reaction mechanism has already been extensively discussed in literature.[77] Several isoenzymes of HRP exist, from which the C type is the most common one. It is an important and well-studied enzyme and is accepting a wide range of substrates, such as phenols, aromatic amines, indoles and sulfonates.[78] The oxidation of different chromogenic, fluorescent and chemiluminescent molecules by HRP is used in spectrophotometric applications like analytical diagnostics in biosensors for the detection of peroxidases. Moreover, due to the ability to oxidize phenols, HRP is also applied in wastewater treatment, and also for the polymerization of phenols, which makes it to a widely applicable enzyme.

Here, the presence of immobilized Rho-HRP was confirmed by fluorescence intensity (FI) measurements on all surfaces. In order to evaluate qualitatively the amount of immobilized

enzyme, FI measurements ($\lambda_{excitation}$ = 544 nm, $\lambda_{emission}$ = 595 nm) of the surfaces were conducted before (as reference) and after incubation with Rho-HRP. Figure 3-4 shows the reference corrected FI measurements of enzyme exposed TEC (A) and SCT-FRP modified surfaces (B).

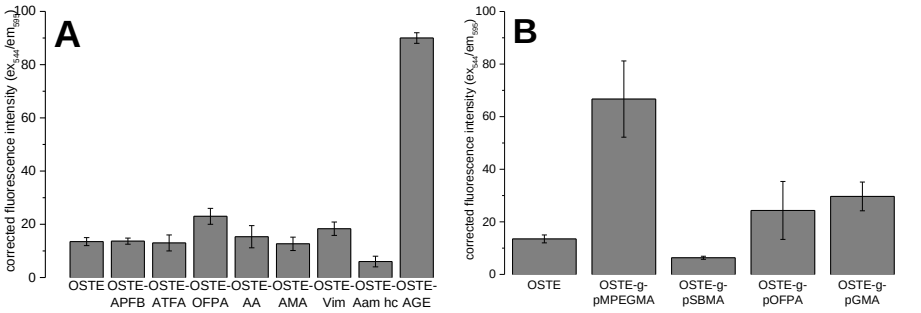

Figure 3-4 Reference corrected fluorescence intensity of virgin (OSTE) and functionalized surfaces via TEC (A) and SCT FRP (B) after immobilization of rhodamine labeled horseradish peroxidase (Rho-HRP), excitation at 544 nm and emission at 595 nm

It can be seen that the native OSTE surface exhibited a substantial FI upon exposure to Rho-HRP (Figure 3-4A, OSTE), which relates to significant loading of labeled enzyme on the surface. TEC functionalized surfaces, such as APFB, ATFA, AA, AMA and Vim provided similar FI results and consequently comparable adsorption of Rho-HRP. Higher FI results are the consequence of OFPA modifications, which is an indication for increased enzyme loading. Accordingly, the lower FI values of Aam hc compared to other functionalized surfaces suggest lower enzyme coverage. Compared to all aforementioned surfaces, surface functionalization with epoxide groups due to the reaction with AGE leads to a drastic increase in FI upon exposure to enzyme, which is more than 6-fold higher compared to that of the native OSTE surface. Amine groups from lysine or thiols from cysteine residues within the enzyme structure are expected to react covalently with epoxide groups on the surface and thus create a higher enzyme loading.[79] Similar measurements were performed with surfaces functionalized by SCT-FRP, as shown in Figure 3-4B. The highest FI was observed for pMPEGMA modified surfaces. This result was unexpected, since PEG surface grafts were reported in the literature to exhibit anti-fouling properties and therefore reduced unspecific protein adsorption.[80,81] In order to explain this discrepancy, FI of Rho-HRP was measured in solution in the presence of different MPEGMA concentrations, as presented in Appendix 1.2, Figure S5. These results show a direct correlation of FI with increasing amounts of MPEGMA. This effect of FI enhancement for Rho-HRP in the presence of MPEGMA could indicate an artificially high loading of enzyme on the OSTE-g-pMPEGMA surfaces. Good biocompatibility and anti-fouling properties have also been described for zwitterionic polymers, such as pSBMA.[82–84] Herein, pSBMA grafted surfaces with an increased hydrophilicity, show a very low FI after enzyme immobilization, which reinforces the hypothesis of low enzyme loading on these surfaces. Surface functionalization by pOFPA under SCT-FRP conditions shows slightly increased FI compared to the native OSTE surface, which is similar to that of TEC functionalized surface with OFPA (Figure 3-4A). Relatively similar enzyme loading based on comparable FI results were achieved by surface grafting with pGMA via SCT-FRP, even though the epoxide containing pGMA enables covalent immobilization. A significant advantage of this platform is that biocatalytic activity of

immobilized enzymes could be measured spectrophotometrically directly in a microplate reader by using a colorimetric assay. For immobilized Rho-HRP on the previously prepared surfaces by either TEC or SCT-FRP, 2,2′-azino-bis(3-ethylbenzothiazoline-6-sulfonic acid) diammonium salt (ABTS) was used as a colorimetric assay. In the presence of H_2O_2, HRP catalyzes a one-electron oxidation of ABTS to a radical cationic product ($ABTS^{\bullet+}$). The absorbance maximum of ABTS at 340 nm (ε_{340}=3.6 x 10^4 M^{-1} cm^{-1}) is shifted to 414 nm (ε_{414}=3.6 x 10^4 M^{-1} cm^{-1}) for its oxidized product $ABTS^{\bullet+}$, from which the activity of immobilized HRP can be determined.[85] The slope of absorbance at 414 nm, which correlated directly to the formed product, over time, was used to express the initial enzymatic activity of the particular surfaces, as shown in Figure 3-5A for TEC modified surfaces.

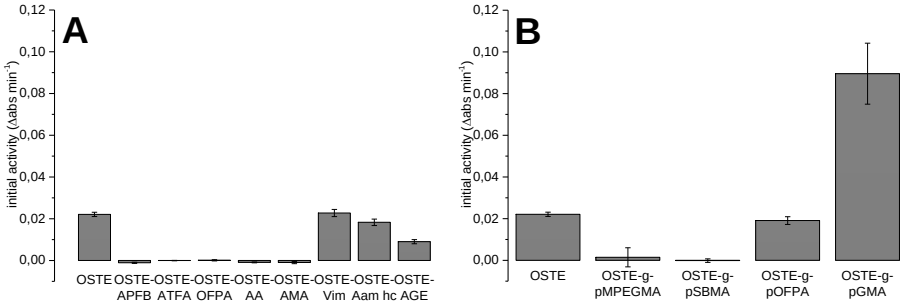

Figure 3-5 Initial enzyme activity of Rho-HRP immobilized on virgin (OSTE) and functionalized surfaces via TEC (A) with various ene compounds and SCT FRP (B) with various acrylate and methacrylate based polymers

From these results, a clear difference in Rho-HRP activity from the individual surface modification, upon enzyme immobilization, can be seen. In general, the displayed activities are caused by two factors, enzyme loading and biocatalytic activity, which both directly affected the overall activity. This directly reflects the influence of the individual surface chemistry. The native OSTE surface exhibited an activity of 0.022 Δabs min^{-1}. Even though TEC modified surfaces with fluorinated (APFB, ATFA and OFPA), hydroxyl (AA) and carboxylic acid containing compounds (AMA) expressed a substantial enzyme loading, these were not active at all (see Figure 3-5A), which suggested an unfavorable environment for the enzyme by these functional groups. On the contrary, imidazole (Vim) and amine (Aam hc) functional surfaces showed the highest initial activities for TEC modified surfaces of about 0.023 and 0.018 Δabs min^{-1}, respectively. These results indicate that amine, imidazole as well as thiol groups from the native OSTE surface provide a more beneficial local environment towards the enzyme and thus, activity was retained. FI indicated high enzyme coverage on surfaces, functionalized with epoxide groups (OSTE-AGE). However, the resulting initial activity was only 0.009 Δabs min^{-1}, which is significantly lower than that of OSTE, Vim and Aam hc surfaces. It was assumed that this is a result of unfavorable interaction of the surface with the enzyme, which is known to have a significant impact during the adsorption-covalent immobilization mechanism onto epoxy supports.[72] As a consequence, blocking of the active site or conformational changes of the enzyme could have resulted in the low activity.

Likewise, the initial enzyme activity was determined from surfaces grafted with polymer layers by SCT-FRP after Rho-HRP immobilization (see Figure 3-5B). Hydrophilic surfaces due to

grafting with pMPEGMA and pSBMA tend to be enzymatically inactive. The low activity of OSTE-g- pSBMA correlates directly with the low enzyme loading, which was determined by FI measurements. The low activity of pMPEGMA grafted OSTE surfaces relates well with the anti-fouling nature of PEG grafted surfaces. Their tendency to FI enhancement indicates an artificially high enzyme loading. Surfaces which were grafted with hydrophobic pOFPA by SCT-FRP, exhibit a similar activity (0.019 Δabs min^{-1}) compared to the original OSTE surface, which correlates well with the results from the FI measurements. The activity was found to be substantially higher than those of surfaces with OFPA monolayer functionalization via TEC, even though both surfaces show comparable enzyme loadings. Thus, increased hydrophobic interactions between the enzyme and the surface created by a thicker surface layer seems to have a positive effect on the enzyme activity A high HRP activity (0.07 Δabs min^{-1}) can be seen from OSTE-g-pGMA surfaces prepared by SCT-FRP. GMA based polymers, bearing epoxide groups, allow covalent attachment of HRP and has already been used in various studies for enzyme immobilization.[86,87] Compared to the epoxide functional monolayer formed from AGE by TEC, the pGMA surface layer shows a decreased enzyme loading, but substantial improvement of enzymatic activity.

Conclusions

In this chapter, a single, versatile platform for testing a broad variety of surface chemistries as support for enzyme immobilization is proposed. The main objective was to change the micro-environment generated by the support surface and hence, identify suitable surface/enzyme combinations with improved biocatalytic activity. This strategy indeed permits a faster, easier and broader surface–enzyme screening compared to the traditional “trial and error” method. The results showed that the STE/OSTE microplate is suitable for colorimetric measurements above 340 nm and the thiol functional wells can be functionalized through either TEC or SCT-FRP providing a broad selection of functional surfaces as a functional monolayer or thicker polymer layer. Thus, different surface functionalities, such as hydroxyl, carboxylic acid, amine, fluorine, imidazole, epoxide, PEG and zwitterionic groups could be introduced, which consequently changed the surface environment. Through immobilization of HRP as a model enzyme, the effects of surface/enzyme interactions were illustrated, showing clear correlations between surface functionalities and enzymatic activities. HRP displayed improved activities when attached directly to imidazole, thiol and amine functional surfaces, compared to hydroxyl, fluorinated, carboxylic acid or epoxide containing surfaces. Immobilization of HRP on pOFPA modified surfaces demonstrated a significant activity, which might be caused by increased hydrophobic interactions between enzyme and surface. Therefore, this platform showed how different surface chemistries and thus, micro-environments, affect significantly the biocatalytic activity of immobilized HRP. Thereby this screening platform demonstrated its potential to be used for other enzymes, facilitating the identification of suitable surfaces for immobilization. Furthermore, by use of such a platform it would be possible to determine the influence of other parameters, such as temperature, pH, and e.g. substrate concentration.

4 OSTE particles as enzyme support

The previously presented STE/OSTE platform demonstrated high suitability for initial screening of immobilized enzyme activity as a function of surface chemistry. However, a broad **applicability** of the immobilized enzymes is of high importance. In industrial processes, polymer particles are often applied as enzyme support, since particles offer a large surface area and allow simplified purification of the biocatalyst from the reaction. Therefore, the goal of this study was to extend the developments of the OSTE material by implementing a new and simple procedure for the preparation of OSTE microparticles. Particles with large variety of possible surface functionalities, which is illustrated in Figure 4-1, were intended to serve as support for the immobilization of enzymes, which is the content of *manuscript 2* (see Appendix 2).

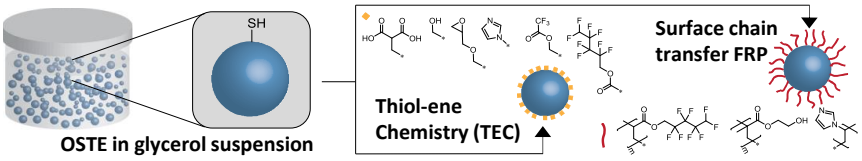

Figure 4-1 Illustration of prepared OSTE particles, which were subsequently surface functionalized by means of TEC and surface chain transfer free radical polymerization (SCT-FRP)

Polymer particles based on TEC

The high versatility and modularity of TEC has also resulted in the preparation of well-defined polymer particles with controlled attributes, such as surface functionality, particle size, and thermal and mechanical properties. Polymer particles are attractive due to their large application spectrum, such as drug-delivery, paints and coatings, chromatography and catalyst supports.[88,89] TE particles are typically prepared by heterogeneous techniques, such as suspension and emulsion polymerization processes. Initially, well-defined water immiscible monomer droplets, facilitated by the use of different stabilizers and co-solvents, are formed in an aqueous phase. Following polymerization, well-defined particles are obtained, as shown by Durham et al., who investigated the effect of different monomer combinations, stabilizers and stabilizer concentrations,[51,90,91] as well as the effects of different modes of initiation, such as photochemical, thermal and redox initiation and their influence on particle size.[92] Similarly, porous TE and thiol-alkyne particles were prepared using different porogens.[93,94] Jasinski et al. used photoinitiated TEC for the preparation of nanoparticles from linear polymers.[95] Likewise thiol-Michael addition has been used for the formation of monodisperse particles at the micrometer scale.[96,97] It has also been demonstrated that the surface of OSTE particles, containing excess thiol or ene groups, can be functionalized with fluorescent moieties by thiol-Michael reaction under alkaline conditions, photochemical TEC or by thiol-isocyanate reaction.[70,98,99]

However, surfactants as well as organic co-solvents are generally necessary for the formation of polymer particles via suspension polymerization. Therefore, the objective of this study was the development of a simple method for the controlled formation of OSTE particles without using surfactants or organic co-solvents by replacing water with glycerol as the dispersing medium and their subsequent application as enzyme supports.

Preparation of OSTE particles in glycerol

Here, in a surfactant and organic co-solvent free process, OSTE particles were prepared by suspension polymerization in glycerol, which is a byproduct of biodiesel production and therefore a cheap, green and environmentally friendly alternative to water.[100] OSTE particles (90% thiol excess) were prepared by one-pot mixing of the monomers PETMP and TATATO and the photoinitiator TPO-L in glycerol in a high speed mixer, as shown in Figure 4-2A.

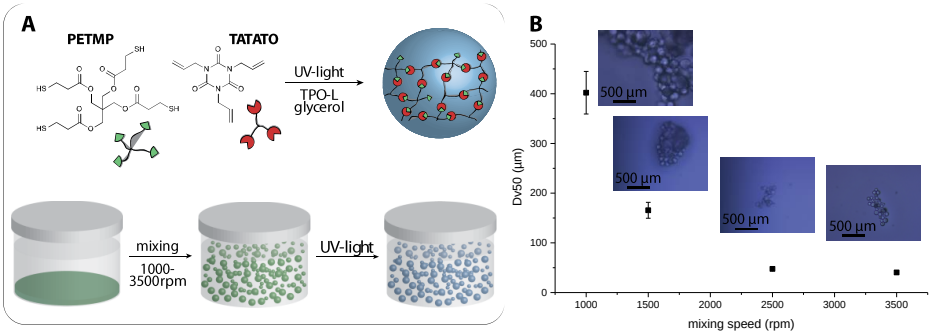

Figure 4-2 A) Preparation of OSTE microparticles via suspension in a speedmixer followed by subsequent photochemical cross-linking of PETMP and TATATO. B) Particle size (Dv50) as a function of mixing speed with optical microscopy images (50 x magnification) of the OSTE particles.

Mixing speeds in the range of 1000 to 3500 rpm were applied in order to obtain well-dispersed OSTE droplets in glycerol, followed by photochemical cross-linking. The resulting microparticles were characterized by dynamic light scattering (DLS) and optical microscopy. As illustrated in Figure 4-2B, the applied mixing speed could be used to control the particle size. The particle size, depicted here as median of the volume distribution (Dv50) obtained from DLS, decreased with increasing mixing speeds from 402 ± 43 µm to 40.4 ± 3.6 µm. Additionally, the size distributions (span) of the formed particles (between 1.1 and 2.4) was very similar to those obtained from traditional processes in water, in which sodium dodecyl sulfate (SDS) or sodium dodecyl benzene sulfate (SDBS) as surfactants and water as a dispersion phase were used.[90] Optical microscopy images (see Figure 4-2B) confirmed the spherical shape of the prepared particles as well as the decreasing size of particles as a function of mixing speed.

Two routes for surface functionalization of OSTE particles

Post-preparation surface functionalization was conducted by photoinitiated TEC using different vinyl, allyl or (meth-)acrylic monomers as well as by SCT-FRP, as a novel pathway for surface modification of OSTE particles. As previously shown on flat surfaces, these approaches demonstrated the capacity of excess surface thiols for versatile surface functionalization with control over different surface chemistries (see Figure 4-3).

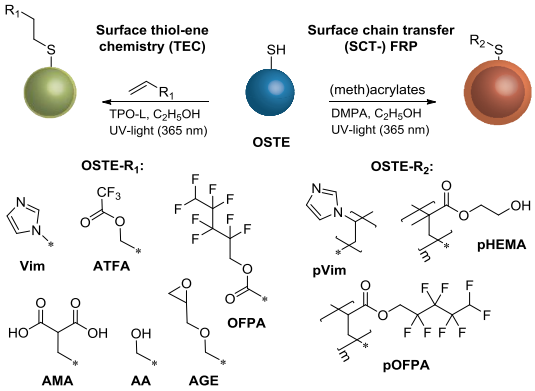

Figure 4-3 Surface functionalization of OSTE particles via two different routes, left: surface TEC with different reagents, such as 1-vinyl imidazole (Vim), allyl trifluoroacetate (ATFA), 2,2,3,3,4,4,5,5 octylfluoropentylacrylate (OFPA), allyl malonic acid (AMA), allyl alcohol (AA), and allyl glycidyl ether (AGE) at low concentration (0.3 M) leading to a functional monolayer on the surface; right: SCT-FRP with various monomers, such as Vim, 2-hydroxyethyl methacrylate (HEMA) and OFPA at high concentration (0.7 – 2.4 M), leading to a functional polymer grafted surface.

OSTE particles (prepared at a mixing speed of 1000 rpm) were surface functionalized via TEC introducing hydroxyl (AA), epoxide (AGE) and fluorinated groups (ATFA, OFPA). Additionally, pH responsive particle surfaces were achieved by grafting with Vim and AMA. Photochemical TEC was conducted at low monomer concentrations (0.3 M) in order to suppress potential polymerization reactions to occur. The IR spectrum of the virgin OSTE particles was characterized by alkane (2960 cm^{-1}, C-H), thiol (2569 cm^{-1}, S-H) carbonyl (1730 cm^{-1}, C=O), alkene (1678, C=C) and ester (1020 cm^{-1}, C-O-C) stretches. TEC surface functionalized particles did not show any significant changes in their IR spectra, as shown in Appendix 2.2, Figure S1. This was attributed to the penetration depth of the IR signal of several micrometers into the sample, which is known to result in very low intensity from thin surface layers.[101] Consequently, the OSTE background dominated the spectrum. However, analysis via surface sensitive x-ray photoelectron spectroscopy (XPS) confirmed the surface modification with the individual reagents (see Table 4-1).

The atom composition of the virgin OSTE particles determined by XPS was in good agreement with the theoretical values. Surface TEC with ATFA and OFPA showed fluorine (F1s) contents of 17.3 atom% and 9.0 atom%, which confirmed the functionalization, since fluorine was unique for these types of particles. Modification using Vim led to an increase in nitrogen content (4.4 N1s atom%) compared to the original OSTE surfaces (3.0 N1s atom%). The atom composition after surface modification with AGE, AA and AMA was identical to the reference OSTE particles, which is a result of similar theoretical atom compositions of these monomers and the OSTE material. Overall, short reaction times (5 min) and low monomer concentrations (0.3 M) limited the thiol-ene reaction to a surface reaction forming a functional monolayer. Conversely, by increasing the monomer concentration to classical polymerization conditions (1:2 v/v monomers to ethanol) and extending the reaction time to 30 min, it was possible to promote polymerization and termination on the surface by SCT-FRP in order to achieve a thick and dense polymer layer on the particle surface. In this way, it is possible to control the type of grafting reaction by tuning the reaction conditions, which was demonstrated by SCT-FRP with

Table 4-1 XPS data of pristine and surface functionalized OSTE particles

particle type	C1s [atom%]	O1s [atom%]	N1s [atom%]	S2p [atom%]	F1s [atom%]
OSTE	60.1 ± 1.4 (60.6)	26.6 ± 0.9 (24.9)	3.0 ± 0.6 (4.1)	10.3 ± 0.3 (10.4)	-
OSTE-Vim[a]	60.8 ± 0.5	24.2 ± 0.8	4.4 ± 0.3	10.6 ± 0.8	-
OSTE-ATFA[a]	52.8 ± 0.4	21.5 ± 0.5	2.4 ± 0.4	6.0 ± 0.4	17.3 ± 0.7
OSTE-OFPA[a]	55.5 ± 1.0	22.4 ± 0.7	4.1 ± 0.5	9.0 ± 0.5	9.0 ± 1.7
OSTE-AGE[a]	62.3 ± 0.3	24.1 ± 0.5	3.5 ± 0.5	10.1 ± 0.3	-
OSTE-AA[a]	62.2 ± 0.9	23.6 ± 0.7	3.5 ± 0.4	10.7 ± 0.2	-
OSTE-AMA[a]	61.7 ± 0.3	24.4 ± 0.5	3.7 ± 0.0	10.2 ± 0.5	-
OSTE-pVim[b]	63.8 ± 0.9	19.0 ± 0.3	9.0 ± 0.3	8.2 ± 0.8	-
OSTE-pOFPA[b]	42.6 ± 0.2	11.1 ± 0.5	0.6 ± 0.6	1.4 ± 0.2	44.4 ± 1.0
OSTE-pHEMA[b]	62.9 ± 0.7	28.3 ± 0.5	2.2 ± 0.1	6.6 ± 0.1	-

[a)]surface functionalization via TEC and [b)]via SCT-FRP

Vim, OFPA and HEMA. The monomers were polymerized in proximity to the particles and IR analysis confirmed a significant polymer grafting (see Appendix 2.2, Figure S2). The spectrum of OSTE-g-pVim exhibited a sharp alkene stretch at 662 cm^{-1}, which confirmed the introduced imidazole groups. The polymer grafting with pOFPA and pHEMA was confirmed through the presence of C-F stretches (806 cm^{-1}) typical for fluorinated compounds and hydroxyl stretches (3465 cm^{-1}, O-H), respectively. Additionally, increased intensity of the C-O band at 1129 and 1143 cm^{-1}, originating from the ester in the pendant group confirmed the polymer grafting. Furthermore, XPS analysis showed substantial changes in atom composition for SCT-FRP functionalized particles, which were significantly higher than the corresponding particles prepared by TEC (see Table 4-1). The substantial decrease in sulfur content (S1s) in each case (pVim, pOFPA, and pHEMA) illustrated the formation of a polymer surface layer. pHEMA grafted particles showed increased oxygen and carbon content, as well as a significant reduction in nitrogen content (2.2 atom% N1s), confirming the pHEMA grafting. Surface grafting with pVim and pOFPA resulted in significant increases in nitrogen (9.0 atom% N1s) and fluorine (44.4 atom% F1s) content, respectively, compared to the reference OSTE surface. These results confirmed that the grafting density can be controlled by selecting TEC conditions for monolayer formation or polymer grafting via SCT-FRP.

Furthermore, a swelling study of the pristine and functionalized particles was conducted in ethanol and water in order to determine the swelling behavior as a function of the surface chemistry (see Figure 4-4). The pristine OSTE particles displayed a very similar median size (Dv50) in both ethanol (353 µm) and water (408 µm). Statistical ANOVA analysis using a significance level ≤ 0.05 revealed a minor reduction in particle size in both, ethanol and water, upon TEC functionalization. Compared to the pristine OSTE, Vim, ATFA and OFPA functional particles could be considered similar when swollen in ethanol, whereas AMA, AGE and AA showed further decrease in size. This general tendency was statistically more pronounced in water, where all functionalized particles, besides OSTE-Vim, decreased significantly in size compared to the pristine one. This general size reduction in both ethanol and water was attributed to the newly introduced functional moieties that prevented the penetration of solvent into the particle core and thereby limited the swelling of the particles.

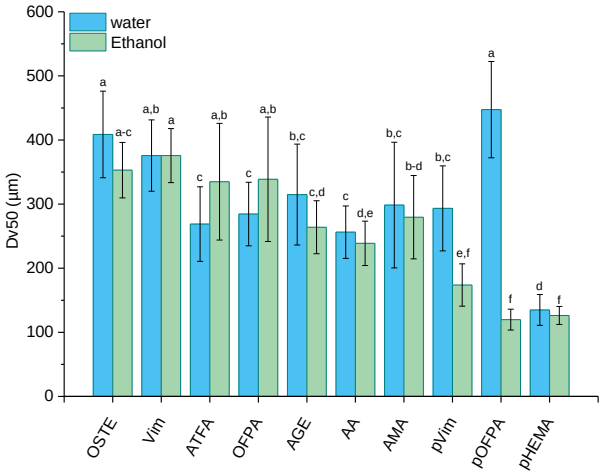

Figure 4-4 Swelling study of OSTE particles containing various surface functionalities grouped by ANOVA analysis (letters above bars, p=0.05) in ethanol and water individually.

Compared to functionalizations by TEC, SCT-FRP with Vim, OFPA or HEMA resulted in particles with a significant reduction in size when measured in ethanol (120 to 174 µm). A reference experiment without initiator and UV irradiation did not show any changes in particle size, which confirmed that the reduction in size was a result of functionalization and not abrasion from the agitator. The size of the particles was highly dependent on the type polymer graft, where pHEMA grafted particles had similar sizes in water and ethanol. In contrast, OSTE-pVim particles submerged in water exhibited a much higher degree of swelling (293 µm) compared to the swelling in ethanol (173 µm), which could be explained by protonation of imidazole moieties in water and the resultant repulsive interactions between the polymer grafts leading to an increased thickness of the grafting layer. Likewise pOFPA grafted particles were observed to exhibit significantly different sizes in water and ethanol with a particle size of 447 µm in water, almost 4-fold higher than the corresponding particle size in ethanol. The difference in size was attributed to a high degree of agglomeration as a result of the hydrophobic nature of the pOFPA, which was also observed visually.

Epoxide functional particles as support for HRP in a plug-flow reactor

In order to demonstrate their application potential, particles were used as a support for enzyme immobilization in a biocatalytic plug-flow reactor. Epoxide groups are known to covalently bind enzymes through direct reaction with amine and thiol groups, which are found in the lysine and cysteine residues on the surface of the protein structure.[41] In this study, OSTE particles, which were prepared at 1000 rpm mixing speed, were surface functionalized through TEC with AGE. These epoxide functional particles (OSTE-AGE) were incubated with HRP serving as a model enzyme, as illustrated in Figure 4-5A.

After filling the reactor with HRP immobilized particles and thorough rinsing with PBS buffer, the enzymatic activity was continuously tested using a solution containing ABTS (1 mM) and H_2O_2 (10 mM) in phosphate buffer (pH 5, 0.1 M) as a colorimetric assay. As previously discussed ABTS could be oxidized by HRP in the presence of H_2O_2 to $ABTS^{\bullet+}$, which showed

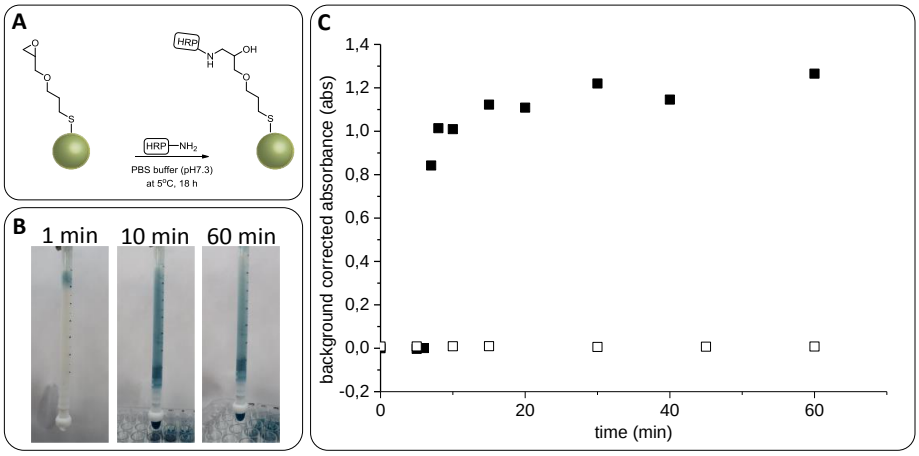

Figure 4-5 A) Immobilization of HRP on OSTE-AGE particles. B) Photographs of plug-flow reactor at 1 min, 10 min and 60 min of reaction time using a flow of 0.2 ml min-1 during a ABTS/H_2O_2 activity measurement of immobilized HRP on OSTE-AGE particles. C) Enzyme activity as background corrected absorbance at 412 nm over time of OSTE-AGE particles with immobilized enzyme (full squares) and a reference (without enzyme -empty squares)

a distinct absorbance maximum at 414 nm. Using a constant flowrate of 0.2 mL min^{-1} allowed sampling at regular time intervals. In Figure 4-5B, photographs of the reactor at 1, 10 and 60 minutes operation time are shown, where the substrate solution was continuously added at the top and samples were taken at the bottom. The green color, which is formed after 1 min only at the top and over the entire reactor at 10 and 60 min, corresponds to the formed product. The absorbance of the withdrawn samples corresponding to the formed $ABTS^{\bullet+}$ was determined and monitored over time, as shown in Figure 4-5C (full squares). Once the residence time within the plug-flow reactor of 6 min was reached, the absorbance from the product measured at the outlet increased significantly. After 15 minutes, steady state conditions were reached demonstrating stable enzymatic activity over the entire operation time. Reference particles (OSTE-AGE particles without HRP) were also tested, and are represented as empty squares in the Figure 4-5C, showing no enzymatic activity at any time. These results demonstrate the successful application of the prepared and surface functionalized OSTE particles in a biocatalytic application.

Conclusions

The scope of this study was the development of a widely applicable OSTE support suitable for the immobilization of enzymes, which has been achieved by implementing a novel, green and simple method for the preparation of OSTE particles in a controlled fashion. This approach demonstrated a high control over particle size and the possibility of post-preparation surface functionalization via surface TEC or SCT-FRP and thereby, the introduction of different surface chemistries. The functional monolayer, which formed via TEC, resulted in a minor decrease in particle size, when submerged in ethanol or water. Thicker polymer surface grafts as a result of SCT-FRP showed substantially reduced swelling in ethanol and increased swelling and agglomeration tendencies in water. However, the functional OSTE particles provided an excellent and broadly applicable support for the immobilization of enzymes as demonstrated

with HRP. Here, epoxide functional particles allowed the covalent attachment of HRP, which were subsequently utilized in a continuous biocatalytic reaction using a plug-flow reactor. The complementary nature of the simple particle preparation and the controlled surface functionalization opens up for a broad range of possibilities allowing the investigation of different surface chemistries on the immobilization of different enzymes under applied conditions. Hence, activity, stability or selectivity of immobilized enzymes depending on micro-environmental variations can be investigated, either in batch reactors or as shown in continuous plug-flow reactors.

5 Tailored enzyme selectivity of immobilized β-glucosidase

Additionally to activity and applicability, high **selectivity** is another crucial parameter for the application of immobilized enzymes in biocatalytic reactions. Therefore, improvements in enzyme selectivity through tailored surface functionalization and thus, micro-environmental changes were a further goal of this PhD project. As earlier discussed, tailored changes in surface chemistry of OSTE surfaces allowed distinct modifications of the micro-environment and thus, influenced the activity of immobilized HRP significantly. Here, the immobilization of β-glucosidase was investigated, which is an enzyme that catalyzes both, hydrolysis and trans-glycosylation of different glycoside substrates. The objective of this study was the synthesis of alkyl-glycosides by improving the **selectivity** of immobilized β-glucosidase through changing the surface chemistry of the OSTE support, as illustrated in Figure 5-1. This chapter is based on *manuscript 3*, which can be found in Appendix 3.

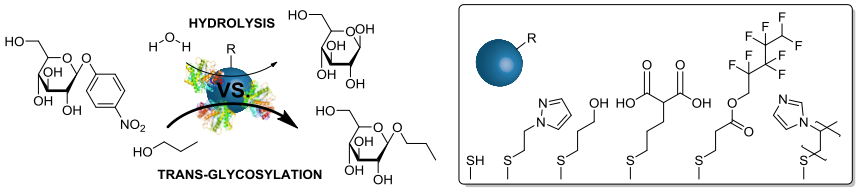

Figure 5-1 Illustration of β-glucosidase immobilization on functional OSTE particles and their use for enzymatic selectivity investigation

Importance of alkyl glycosides and their enzymatic synthesis

Alkyl glycosides are amphiphilic molecules, in which a hydrophilic sugar moiety is covalently linked through a glycosidic bond to a hydrophobic alkyl chain. Due to their structure, alkyl glycosides are industrially useful as non-ionic surfactants in detergents and cosmetics.[102,103] Compared to the traditional method of chemical preparation, enzymatically catalyzed synthesis of alkyl glycosides through glycosylation using glycoside hydrolases (EC 3.2.1) has lately received increased attention due to mild reaction conditions and high selectivity.[104,105] Enzymatic glycosylation involves the reaction of an alcohol directly with a monosaccharide in reverse hydrolysis (thermodynamic control), or with a glycoside as a donor undergoing a trans-glycosylation (kinetic control). The developments within this field have been the subject of a recent mini review, which summarized different approaches in order to increase the catalytic activity, selectivity and yields.[106] Especially the selectivity between synthesis (s) (in this case trans-glycosylation) and hydrolysis (h) is an important parameter that can be described as a ratio of the individual reaction rates r_s/r_h or as a selectivity S_c, taking the nucleophile concentrations (or activities) into account.[107,108] For the synthesis of alkyl glycosides, water-miscible[109] as well as water-immiscible alcohols, as glycoside acceptors have been studied. It has been shown that the enzyme activity and selectivity are highly dependent on the water activity[108,110–112] and the alcohol concentrations and can be exploited in 2-phase systems.[113,114] Protein engineering of β-glucosidases[115] as well as the choice of other glycoside hydrolases[116–118] were also considered in order to improve the selectivity and activity. In addition, immobilization of β-glucosidases on commercial resins was investigated for trans-glycosylation reactions, resulting in improved activity and selectivity at low water activities compared to freeze-dried enzymes.[119] Increased

stability and reusability was obtained from immobilization on zinc oxide (ZnO) as solid support.[120] In general, many different materials, such as chitosan, calcium alginate and polymer materials have already been applied for glycoside hydrolase immobilization.[121] Recently, OSTE materials have also been used as an enzyme support.[41,43,64] As previously demonstrated, the development of an OSTE microtiter plate allowed screening of a large range of surface chemistries as promising supports for the immobilization of enzymes.[122] Thus, fast and versatile investigation of micro-environmental effects on enzyme activity was possible, as verified by the use of HRP. Changes in the environmental properties at the interface between the enzyme and support surface have already been shown to be an important factor for the performance of immobilized enzymes.[23] For immobilized β-galactosidases and lipases for instance, it has been found that a favorable environment can improve both, the stability and activity.[15,123–126]
The objective of this study was to investigate micro-environmental influences towards the biocatalytic activity and more importantly selectivity of an immobilized β-glucosidase, with the goal to increase the trans-glycosylation over hydrolysis. Therefore, the versatility of functional OSTE particles offered an excellent opportunity for the investigation of the micro-environmental effects by changing the surface chemistry.

Surface functional OSTE particles as support for β-glucosidase

OSTE particles were prepared by suspension polymerization in accordance to the method described in Chapter 4. Similarly, by rapid mixing (1000 rpm), the monomers PETMP and TATATO as well as TPO-L as a photoinitiator, formed micrometer sized droplets in glycerol, followed by photochemical cross-linking. The off-stoichiometric ratio between the monomers (90% thiol in excess) resulted in thiol functional particles, which were subsequently subjected for further surface functionalization. Photochemical TEC and SCT-FRP were previously described to be efficient methods for the introduction of distinct functionalities as a functional monolayer or thicker polymer grafts (see Chapter 4). In this study, TEC was applied with AA, AMA, OFPA and Vim in order to introduce different functional groups on the particle surface, as illustrated in Scheme 5-1.

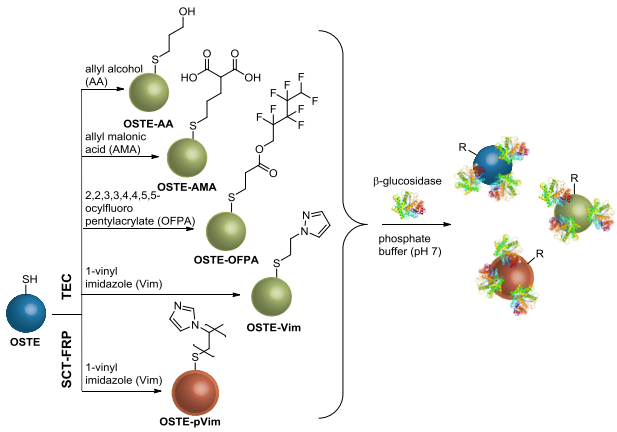

Scheme 5-1 Surface functionalization of OSTE particles via thiol-ene chemistry (TEC) using Vim, AA, AMA, and OFPA introducing a functional monolayer; and via surface chain transfer free radical polymerization (SCT-FRP) using Vim grafting the surface with a dense polymer layer (pVim) followed by immobilization of β-glucosidase on pristine and functional OSTE particles

Thus, hydroxyl, carboxylic acid, fluorine and imidazole functional particles were obtained. In contrast to this monolayer functionalization achieved by TEC, SCT-FRP was applied using Vim in order to create a functional pVim layer on top of the particle surface. The chemical changes on the surface after TEC and SCT-FRP were confirmed by FT- IR and XPS measurements, as described in Chapter 4. The different functionalities in this study were selected in order to create various surface environments for the immobilization of β-glucosidase, and thus impact the enzyme performance in terms of activity and selectivity. Hydroxyl or carboxylic acid functional particles were intended to form hydrophilic interactions or hydrogen bonds, whereas fluorinated particles have the potential of creating hydrophobic interactions between the surface and immobilized enzymes. Imidazole groups and their derivatives are known for their biological relevance and have already demonstrated beneficial effects for immobilized HRP.[122] Following the surface functionalization, β-glucosidase from *Thermotoga neapolitana* (EC 3.2.1.21) was immobilized onto the pristine (OSTE) and functionalized particles by submerging the particles into a phosphate buffer solution (0.1 M, pH 7.2) containing β-glucosidase (1.0 mg mL^{-1}). An aliquot of the supernatant was withdrawn before and after the incubation time and the protein content was estimated using the assay developed by Bradford.[127] The amount of immobilized enzyme per gram particle is illustrated in Figure 5-2 for the individual particle types. From these results a significant enzyme loading for OSTE-AMA, OSTE-OFPA and OSTE-pVim particles could be concluded. In contrast, low amounts of immobilized enzyme were found on pristine OSTE particles, OSTE-AA as well as OSTE-Vim particles. However, as a result of relatively large solution volumes compared to the amount of particles, and the reproducibility of the spectrophotometer, substantial uncertainties for the quantification were observed using the method by Bradford in this case. Therefore, the amount of immobilized β-glucosidase was not considered in the evaluation of activity and selectivity, which was solely based on the type of particles used.

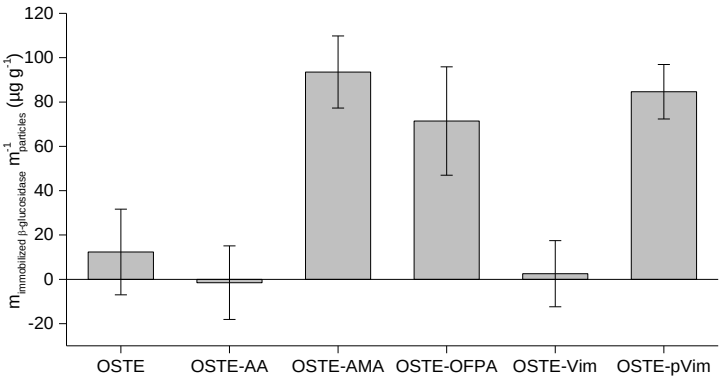

Figure 5-2 Quantification of immobilized β-glucosidase onto pristine and functional OSTE particles based on the Bradford assay

Activity of immobilized β-glucosidase on different surfaces

As a model system, the β-glucosidase catalyzed competition reaction between trans-glycosylation and hydrolysis of p-nitrophenyl glucopyranoside (pNPG) was selected, as illustrated in Scheme 5-2.

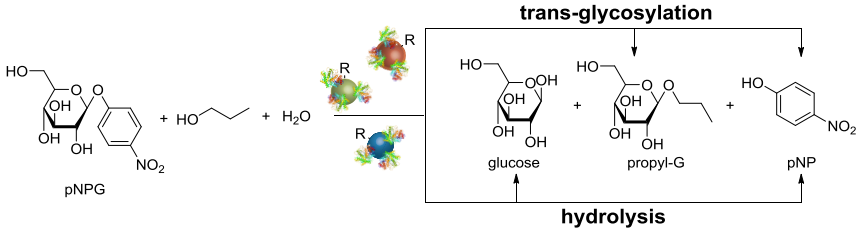

Scheme 5-2 Enzymatic conversion of p-nitrophenyl β-D-glucopyranoside (pNPG) catalyzed by β-glucosidase immobilized on pristine and functional OSTE particles, in order to determine the biocatalytic activity and selectivity between trans-glycosylation with 1-propanol forming propyl-glucoside (propyl-G) and p-nitrophenol (pNP) as products and hydrolysis with water forming glucose and pNP as products

1-Propanol was used as a water soluble glycosyl acceptor in order to obtain a one-phase reaction system with different volume ratios between alcohol and acetate buffer (0.1 M, pH 5.0). β-Glucosidase from *Thermotoga neapolitana*, which already demonstrated its potential as a catalyst for the trans-glycosylation of pNPG with 1-hexanol in a 2-phase system (r_s/r_h = 4.0),[113] was immobilized on pristine and functional OSTE particles (see Scheme 5-1). Initial experiments with free β-glucosidase, in which the 1-propanol content was varied from 75 to 5 vol%, demonstrated high preference of β-glucosidase for trans-glycosylation over hydrolysis at high water contents (see Appendix 3.2, Figure S1). Under these conditions, the ratio between trans-glycosylation and hydrolysis r_s/r_h ranged between 28.3 and 2.6 (see Appendix 3.2, Table S1). However, it is particularly interesting to improve the selectivity even further at lower alcohol contents. In order to study the effects of the micro-environment on the enzyme selectivity with high precision, a regime with significant reaction rates for both trans-glycosylation and hydrolysis was chosen, which was achieved using 1-propanol contents of 5, 2, and 1 vol% and 95, 98, 99 vol% acetate buffer, respectively. In these experiments, the pristine and functional OSTE particles with immobilized β-glucosidase (≈ 0.6 g particles) were submerged in acetate buffer/1-propanol solutions containing pNPG (28 mM) as the substrate. The resulting enzyme activity, as combined initial reaction rate of trans-glycosylation and hydrolysis was evaluated according to the particle functionality as well as the amount of 1-propanol, which is presented in Figure 5-3.

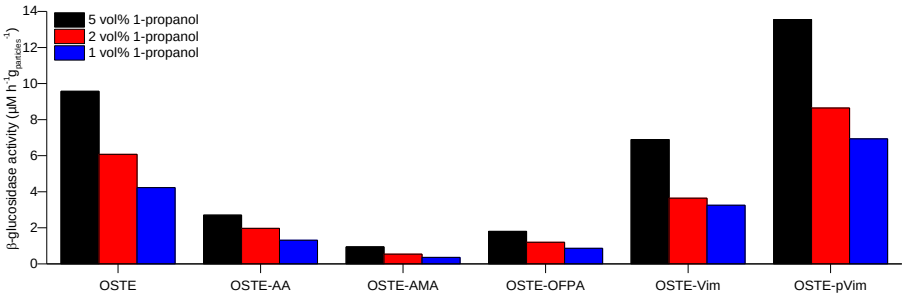

Figure 5-3 Activity (combined initial reaction rates of trans-glycosylation and hydrolysis) of β-glucosidase immobilized on pristine (OSTE) and functional OSTE particles in solutions with different 1-propanol contents, such as 5, 2 and 1 vol%

From these results a general increase in overall enzyme activity with increasing alcohol content was observed, indicating that the enzyme has a high preference for 1-propanol as acceptor substrate. Furthermore, the activity varied substantially between the individual functional particles due to micro-environmental differences around the enzyme. Depending on the amount of 1-propanol, the reference OSTE particles containing β-glucosidase showed a high activity of 4.2 to 9.7 µM h^{-1} $g_{particles}^{-1}$, whereas a considerably reduced activity by 3 to 12-fold was observed for hydroxyl (OSTE-AA), carboxylic acid (OSTE-AMA) and fluorine (OSTE-OFPA) functional particles. Immobilization of β-glucosidase on imidazole functional particles (OSTE-Vim) resulted in activities of about 3.2 to 6.9 µM h^{-1} $g_{particles}^{-1}$, which was even further increased by polymer grafting (OSTE-pVim) (6.9 - 13.6 µM h^{-1} $g_{particles}^{-1}$) corresponding to a factor of 1.4 compared to the pristine particles. Reactions ran in total for 23 hours and the conversion was monitored in time course plots as shown in Figure 5-4A-C. The reaction reached 100 % conversion for OSTE-pVim and OSTE-Vim particles as well as pristine OSTE particles after 23 hours at any alcohol concentration. For the remaining particle types OSTE-AA (84-52%), OSTE-AMA (43-26%) and OSTE-OFPA (75-40%) conversions below 100% were achieved.

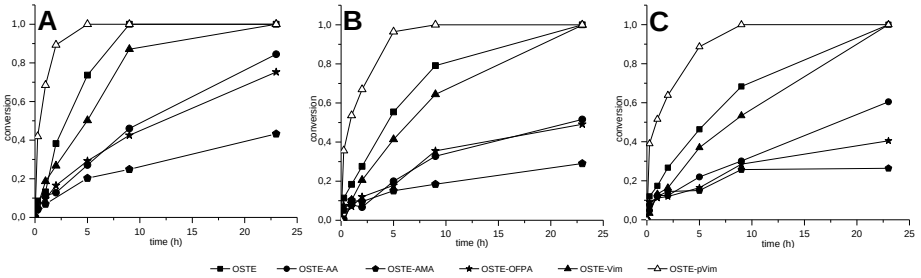

Figure 5-4 Time course of pNPG conversion catalyzed by β-glucosidase immobilized on pristine (OSTE) and functionalized OSTE particles OSTE-AA, OSTE-AMA, OSTE-OFPA, OSTE-Vim and OSTE-pVim in reaction solution, containing (A) 5 vol% , (B) 2 vol% and (C) 1 vol% 1-propanol

Trans-glycosylation vs. hydrolysis catalyzed by immobilized β-glucosidase

The previously obtained activities (initial reaction rates) from pNPG consumption were split into the individual rates for trans-glycosylation and hydrolysis (see Appendix 3.2, Table S2) in order to calculate the reactivity ratios r_s/r_h for the individual particles. The ratios r_s/r_h as a measure for the selectivity is presented in Figure 5-5 for the three different 1-propanol contents and the different particles.

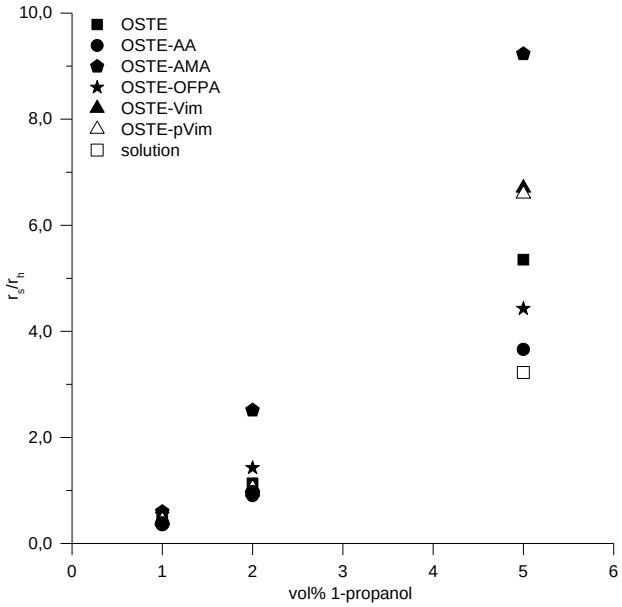

Figure 5-5 Selectivity (r_s/r_h) between trans-glycosylation (s) and hydrolysis (h) of pNPG catalyzed by β-glucosidase immobilized on pristine (OSTE) and functionalized OSTE particles OSTE-AA, OSTE-AMA, OSTE-OFPA, OSTE-Vim and OSTE-pVim at different 1-propanol contents

From these results, it could be seen that the selectivity (r_s/r_h) improved with increasing alcohol concentration. Furthermore, the results demonstrated that the immobilization has a considerable impact on selectivity at higher alcohol contents. Using 1 vol% of 1-propanol, r_s/r_h ratios below 1 (0.35 to 0.60) were obtained, implying substantial preference for the hydrolysis for all types of particles as well as in solution. An increase of 1-propanol content to 2 vol% resulted in similar trans-glycosylation and hydrolysis rates and therefore r_s/r_h values of about 1 were obtained for immobilized and free enzyme. An exception being OSTE-AMA particles consisting of carboxylic acid surface moieties, which generated a preference for trans-glycosylation (r_s/r_h = 2.3) already at this low alcohol content. This tendency was even more pronounced at higher alcohol concentration (5 vol%) with a r_s/r_h of 9.2. The high preference for trans-glycosylation of OSTE-AMA was also seen for Vim and pVim functional (6.6/6.7), pristine OSTE (5.4), OSTE-OFPA (4.4) and OSTE-AA (3.7) particles. At this 1-propanol content, immobilization of β-glucosidase improved in each case the formation of propyl-G compared to the reaction in solution (with r_s/r_h of 3.2). As assumed, the differences in selectivity were ascribed to the variations in surface chemistry and consequently in the generation of different enzyme-surface environments. Despite significant differences in overall activity, identical selectivity was achieved for OSTE-Vim and OSTE-pVim particles both containing imidazole functional groups underlining a high dependency of the selectivity on the surface chemistry and micro-environment.

Conclusions

In this study, OSTE particles containing various surface functionalities were exploited for the immobilization of β-glucosidase in order to improve the selectivity between trans-glycosylation and hydrolysis by changing the micro-environment of the enzyme. Therefore, OSTE particles were prepared by suspension polymerization in glycerol, as described in Chapter 4. Through subsequent surface functionalization via TEC and SCT-FRP various surface chemistries were introduced. The different nature of particles functionalized with hydroxyl (AA), carboxylic acid (AMA), fluorine-containing (OFPA) and imidazole (Vim and pVim) groups allowed changes in surface properties and consequently environmental variations. β-glucosidase from *Thermotoga neapolitana* was immobilized via physical adsorption and all particles exhibited significant activity for the reaction of pNPG depending on the surface functionality. Especially, pristine OSTE (containing surface thiols) as well as imidazole (OSTE-Vim and OSTE-pVim) functional particles demonstrated high activities between 6.9 and 13.6 μM h^{-1} $g_{particles}^{-1}$. Furthermore, in each case an increase in overall activity was observed with increased 1-propanol contents from 1 to 5 vol%. Similarly, the trans-glycosylation over hydrolysis ratio increased with increasing alcohol concentration. Compared to free β-glucosidase, trans-glycosylation could be further promoted by immobilization on OSTE particles. Especially at 5 vol% alcohol, the selectivity r_s/r_h increased almost 3 fold from 3.2 up to 9.2 for carboxylic acid functional particles (OSTE-AMA), which was attributed to the individual surface functionalities. These results demonstrated clearly that variations in surface chemistry and thus, changes in surface environment have a significant impact on the selectivity of immobilized enzymes and therefore can be used in order to tailor biocatalytic reactions as demonstrated with β-glucosidase in this case.

6 Spatial distribution of enzymes in a microfluidic reactor

The relevance of highly active, stable and selective immobilized enzymes for biocatalytic processes has already been comprehensively discussed. Nevertheless, enzymes are generally considered to be expensive biocatalysts and consequently, their most **effective** exploitation is of high importance for the design of efficient biocatalytic reactors. Here, the spatial distribution of immobilized enzymes in a biocatalytic reactor is considered to be a significant factor contributing to the effectiveness of the applied biocatalyst. Thus, the preparation and selective surface functionalization of a microfluidic device allowed the immobilization of HRP in different surface patterns and the investigation of local enzyme distribution and its influence towards the overall reactor efficacy (see Figure 6-1). The experimental results were compared with computational fluid dynamics simulations (CFD) in order to develop a methodology with the goal to predict and improve the performance of a biocatalytic reactor, which is the core of *manuscript 4* (see Appendix 4).

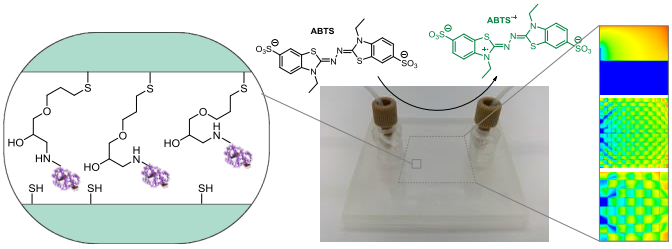

Figure 6-1 Illustration of fabricated microreactors including the area selective immobilization of horseradish peroxidase (HRP) and subsequent reactor performance tests using ABTS as a colorimetric assay

Microfluidics, OSTE+ materials and spatial distribution of catalyst

Recently, Schäpper et al. developed a theoretical topology optimization of immobilized yeast cells, which resulted in an 8-10 fold improvement in theoretical production rate.[128] Inspired by this approach and by applying enzymes instead of whole cells, computational fluid dynamic (CFD) simulations demonstrated that in a laminar flow field of a square reactor with a distributed flow pattern, the biocatalytic reactor efficacy considerably depends on the positioning of the immobilized enzyme.[129] By varying computationally the topology of immobilized enzymes inside the reactor, simulated reactor configurations with substantially improved productivities were obtained. In order to verify the computational results, an experimental setup is required in which the same conditions were applied.

Due to their small size, low consumption of reagents and limited reaction volumes as well as high throughput combined with a high degree of reproducibility, microfluidic devices have proven to be suitable to test the influence of such modifications in continuous flow systems.[130,131] Additionally, good heat and mass transfer in combination with laminar flow provide good control over reaction conditions.[132] Laminar flow restricts mixing to occur exclusively by diffusion, unless this is circumvented by specific microchannel configurations. Heterogeneous reactions take place solely on the surface of the catalyst or on the surface that the catalyst is bound to. In these systems, diffusion shows a great impact on the overall reaction, which is influenced by many different parameters, such as flow rate, concentration, dimensions of the reactor geometry and reaction rate.[133] Microfluidic systems are traditionally fabricated in

glass or polymeric materials such as poly(methyl methacrylate) (PMMA) or PDMS.[134–136] Especially PDMS has been used extensively for microfluidics due to the ease of fabrication and relatively low cost.[137] Mold casting enables the preparation of different reactor designs and has been applied for the development of biocatalytic microreactors. Hence, enzymes were immobilized on polymer microbeads[138,139] or onto the reactor walls.[140] Alternatively, the formation of a surface patterned phospholipid bi-layer or an adsorbed protein layer enabled the attachment of enzymes on the PDMS surfaces.[141]

Direct protein and enzyme immobilization onto polymer surfaces in microfluidic devices of OSTE material is an interesting alternative to the currently used PDMS systems. The OSTE approach has recently been updated in order to improve mechanical properties as well as surface bonding, which is essential for the fabrication of microfluidics. In this OSTE+ system, Bisphenol A diglycidyl ether (BADC) undergoes a thiol-epoxy reaction in an additional, orthogonal curing step. This enables covalent sealing between interfaces of the precured material in order to prevent leaking under operating conditions, which is a well-known challenge in microfluidics.[69,142] Further surface functionalization via photochemical TEC offers a possible pathway for surface modification in various patterns by application of a stencil.[143,144] So far, OSTE(+) thermosets have been rarely used for the immobilization of enzymes.

The objective of this proof-of-concept study was the methodological development of a biocatalytic reactor, which enabled experimental confirmation of the computationally investigated effect of immobilized enzymes and their local distribution towards the overall reactor efficacy. The correlation between experimental and computational results should demonstrate the potential of CFD simulations to predict the biocatalytic performance of such reactors, and would thus open up for the use of CFD for optimization of the microfluidic reactor configuration.

Preparation of OSTE+ microreactors

In Figure 6-2 the fabrication process of the thiol-ene-epoxy based microreactors is illustrated, including the used monomers (A), the photochemical (B) and the subsequent thermal (C) curing step. As base compounds PETMP, TATATO and BADC (see Figure 6-2A) were used in a ratio of 2.0:1.0:0.25.

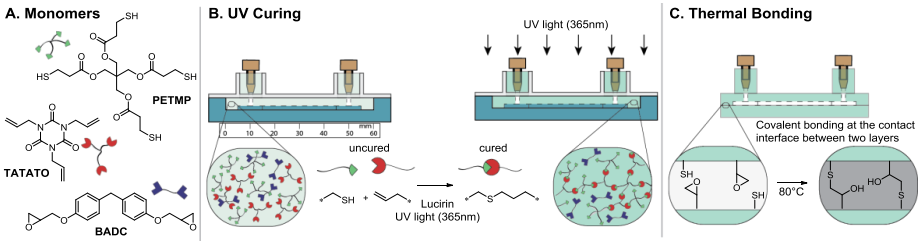

Figure 6-2 Schematic representation of the preparation of OSTE+ microchips with subsequent surface modification. A) Monomers for OSTE+ preparation tetra functional thiol PETMP, trifunctional allyl TATATO and bifunctional BADC, B) First UV curing of the OSTE+ mixture via thiol-ene reaction followed by C) a second curing that seals the system "leakage free"

The liquid mixture was cured in a PDMS mold using lucirin as a photoinitiator and UV light (λ=365 nm), as illustrated in Figure 6-2B. After crosslinking, the upper and lower part of the

microchip were assembled and residual epoxide and thiol groups were utilized in a thermal bonding reaction at the interface, which resulted in a stable and leakage-free microreactor (see Figure 6-2C). The geometry of the microreactor is based on a square shape with a length and width of 30 mm and a thickness of 0.25 mm with an inlet and outlet channel of 10 mm in length and width located at the two opposite ends of the reactor, as can be seen in Figure 6-3A.

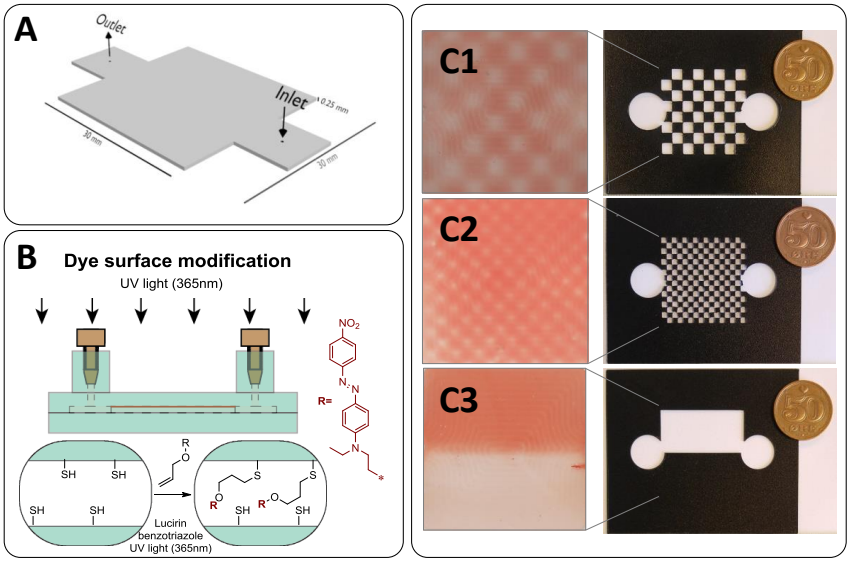

Figure 6-3 A) Microreactor geometry, B) Microreactor surface modification via TEC using allyl disperse red, C1-3) Images of surface functionalized microchips using allyl disperse red and different stencil masks: C1 – coarse checkerboard, C2 – fine checkerboard, C3 - half reacted surface

Area selective surface functionalization and HRP immobilization

The reactor was prepared using a thiol-ene mixture with excess of PETMP, which leads to residual unreacted thiol groups within the bulk material and on the reactor surface. These free thiol groups on the microreactor surface permit functionalization of the surface after assembly of the microfluidic system. Application of stencil masks combined with UV initiated surface grafting enabled preparation of various patterns in the reactor. In order to test the enzymatic activity of immobilized enzymes in various configurations, four different geometric patterns were selected. A full surface (30 x 30 mm^2), a half surface (15 x 30 mm^2) and two checkerboard patterns with either a fine (256 squares of 1.7 x 1.7 mm^2 each of which 128 were modified) or a coarse (64 squares of 3.55 x 3.55 mm^2 each of which 32 were modified) were prepared. In order to test and visualize the surface patterning, an allyl functional disperse red dye was used as shown schematically in Figure 6-3B. The high selectivity of the reaction permits direct and accurate replication of the applied stencils as shown in the photographs of the final surfaces in Figure 6-3C. Additionally, due to the use of benzotriazole as UV-absorber, significant reaction selectivity for the irradiated surface was obtained. In fact, by irradiation from the top, exclusively the upper surface of the reactor cavity was modified with the allyl disperse red leaving the bottom surface unreacted. An image of the upper and lower surface after photochemical reaction with the red dye can be found in Appendix 4.2, Figure S2. The surface

modification procedure offers a controlled area functionalization with high selectivity for the irradiated surface by UV initiated TEC. Replacement of the dye with allyl glycidyl ether undergoing the same TEC leads to surface patterned epoxides, which are known to covalently bind enzymes via ring-opening with free amine residues from the enzyme structure [41]. The reaction scheme from surface modification with allyl glycidyl ether and subsequent covalent immobilization of HRP (EC 1.11.1.7) can be seen in Figure 6-4.

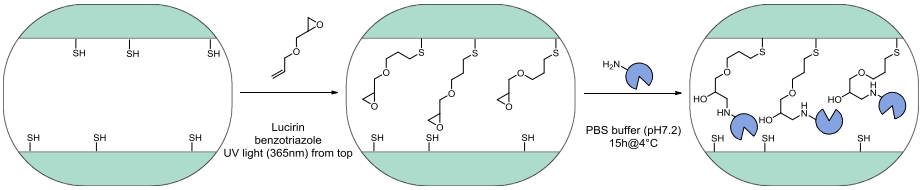

Figure 6-4 Microchip functionalization of remaining surface thiol groups using allyl glycidyl ether via UV initiated thiol-ene reaction and subsequent covalent HRP immobilization with introduced epoxide groups on the microreactor surface

HRP dissolved in PBS buffer was immobilized on the epoxy patterned reactors by overnight incubation. The quantification of the immobilized amount of HRP was attempted using the Bradford assay[145] and the bicinchoninic acid (BCA) assay, which were in both cases inconclusive due to the low concentration of enzyme and interference with residual thiol groups on the surface, respectively.[146] Quantification using fluorescently labeled enzymes on thiol-ene surfaces confirmed the presence of immobilized enzymes on the surface, but could not be used to determine the amount of attached enzyme due to background fluorescence from the material (see Appendix 4.2, Figure S3). Therefore, the exact quantification of the enzyme concentration on the surfaces was not possible.

Reactor performance depending on distribution of immobilized HRP

In the presence of H_2O_2, HRP catalyzes a one-electron oxidation of ABTS to a radical cationic product ($ABTS^{\bullet+}$). Kinetic parameters of immobilized HRP have been studied previously in a microfluidic packed bed reactor[139], monolith structures[147] or on planar surfaces.[148] It has been shown that apparent enzyme kinetics vary greatly depending on the applied configuration, flow rate and type of immobilization compared to that of enzymes free in solution. In this study, HRP was uniformly immobilized via covalent bonding on the same support, which resulted in the same individual activity for all immobilized enzymes. However, their contribution to the overall reactor activity is a function of many parameters, including flow rate mass transfer, diffusion but also the spatial distribution of the immobilized enzymes in the microreactor. The used concentrations of ABTS and H_2O_2 were significantly higher than required for the applied conditions in order to ensure large excess of substrates. The overall reactor performance of the individual configurations was constantly measured over time as shown in Appendix 4.2, Figure S4. An average of the absorbance measured under steady state conditions between 350 and 850 s, which was in agreement with CFD, correlated directly to the formed product at the outlet of the reactor, as presented in Figure 6-5.

A reference measurement was performed, in order to eliminate the potential contribution of adsorbed enzymes to the measured activities. The native surface, undergoing the same enzyme incubation procedure, did not show any activity (Figure 6-5, reference). Therefore, the absence

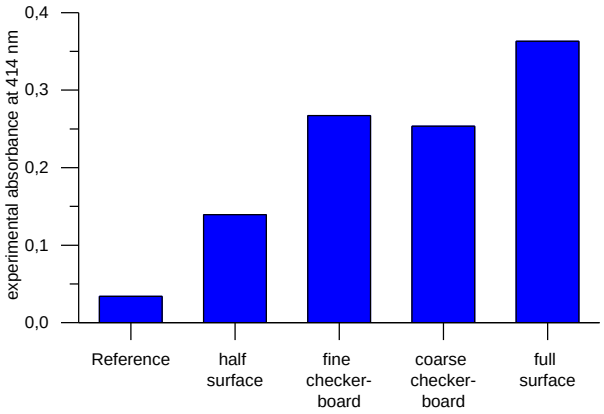

Figure 6-5 Overall reactor performance of the different reactor configurations illustrated as absorbance measurements at 414 nm corresponding to the formed product at the reactor outlet

of unspecific adsorption of HRP on the selected surfaces could be confirmed, which makes this surface well suited for immobilization of HRP. These results of the four different configurations show clearly that the fully modified microreactor, containing the largest activated surface and thus the highest amount of immobilized HRP, was the most active one. The two checkerboard structures had a reduced performance by 26 and 30 % of that of the fully immobilized surface. Furthermore, the overall reactor activity was reduced even further when only half of the reactor surface was modified.

The main focus of this study was the determination of the effect of enzyme distribution over the reactor surface and the specific system was therefore designed only to illustrate the impact of different surface patterns. Therefore, the product absorbance for the individual patterns is additionally shown relative to the respective modified surface area, which allows direct comparison of the reactor efficiency between the selected patterns (see Figure 6-6A). The areas of the individual activated surface patterns were calculated from the applied photomasks (see Appendix 4.2, Table S1).

Investigating the impact of different patterns demonstrated a slightly reduced absorbance per enzyme area (by 23%) for the microreactor with half of the area covered compared to the fully modified surface, which was not entirely plausible due to symmetry of the pattern, but was finally attributed to experimental inaccuracy. However, the fine and the coarse checkerboard structures exhibited an increased efficiency with 81 and 56 % higher absorbance per active area than the fully modified surface, which demonstrates a significant improvement in product concentration relative to the functionalized surface area or in other words, amount of immobilized enzyme. In fact, it is clearly demonstrated here that the enzyme distribution over the surface affects the overall activity of the microreactor. This improvement of the reactor productivity is influenced by a series of other factors such as flow conditions, substrate diffusion rates and local substrate concentrations. The flow within this reactor geometry is characterized by a gradient, in which the highest velocity is present in the center of the reactor and a reduced velocity at the sides. The difference in velocities across the reactor can consequently influence the mass transport and mixing of the fluid. Therefore, the accessibility of substrate for the enzyme near the surface depends on the position and the local conditions.

The selection of this particular reactor design was used in order to generate this complexity of overlapping phenomena.

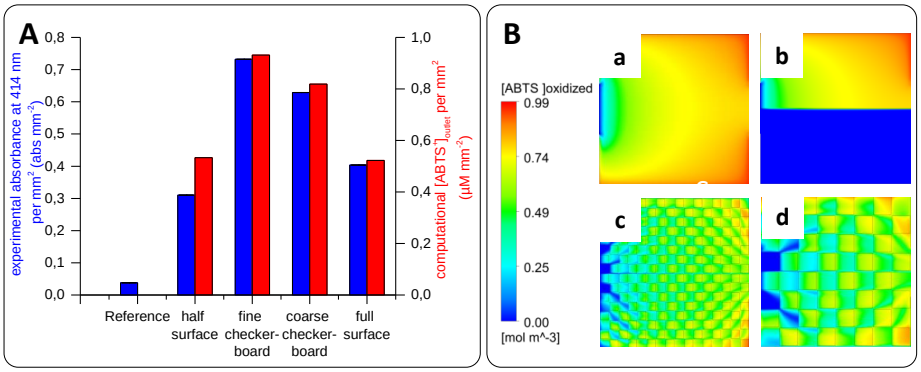

Figure 6-6 A) Comparison of experimentally determined $ABTS^{\bullet+}$ absorbance at 414 nm per mm^2 modified area at the reactor outlet in steady state condition (blue) and $ABTS^{\bullet+}$ outlet concentration obtained from CFD simulations in mM mm^{-2} (red) of various surface patterns, reference (HRP adsorption on non-modified surface, empty squares), half modified surface, coarse checkerboard, fine checkerboard, fully modified surface; and B) Illustration of product concentration on the top surface in the microreactor (in steady state simulations) dimensions using fully modified surface (a), half modified surface (b), fine checkerboard structure (c), coarse checkerboard structure (d), where red surfaces illustrate a high and blue surfaces a low product concentration.

CFD simulations were conducted in order to validate the experimentally determined performance of the microreactors as a function of the different enzyme immobilization patterns, the impact of the laminar flow conditions, geometry and material transport limitations (diffusion). The product concentrations at the outlet of the reactor for each modified surface area were determined, as presented in Figure 6-6A (red) and visualized in different patterns, as shown in Figure 6-6B. In the flow simulations under steady-state condition all parameters were selected to reflect the experimental setup, such as dimensions of the microreactor, outlet, inlet and immobilization patterns, flow rates, substrate concentrations and theoretical diffusivity. Therefore, it is not possible to compare the results from the experimental and the computational results directly, but merely the trends. Using the same surface patterns, the CFD simulations exhibit the same trend in terms of reactor efficiency as seen in the experimental setup (see Figure 6-6A, red). The simulation of the full and half modified surface show very similar product concentrations relative to the activated surface area. Similarly for the experimental results, the product concentration obtained from CFD simulations showed an increase of 78 and 57 % for the fine and the coarse checkerboard structure compared to the fully modified surface. The experimental results and computational findings correlate well and demonstrate a clear dependence of the overall product formation relative to the distribution pattern of enzymes on the modified surface area.

Conclusions

The most effective exploitation of expensive enzymes in a biocatalytic process is of crucial importance. The local position of immobilized enzymes in a bioreactor has been identified to be an important factor, which influences the contribution of the individual enzyme to the overall reactor efficacy. Therefore, this proof-of-concept study correlates experimental results of

fabricated microreactors containing immobilized enzymes in different surface patters with results from CFD simulations. Thereby, it demonstrated how the position of immobilized enzymes influences the biocatalytic efficacy of a reactor and thus, how reactor performance can be predicted and potentially optimized.

Initially, an experimental setup was prepared in which HRP could be selectively immobilized in specific patterns onto the surface of an OSTE+ microfluidic reactor. OSTE+ based microfluidic devices were surface modified with allyl disperse red, illustrating the effect of applied stencil masks, and with allyl glycidyl ether enabling the covalent immobilization of HRP. The performance of the microreactors was significantly influenced by patterning of the enzyme on the surface and two checkerboard structures. Fine and coarse patterns showed an efficiency increase by 81 and 56 % higher absorbance per active area compared to the fully covered surface, which demonstrates a significant improvement in effectiveness of the applied enzymes. These results correlated very well with CFD simulations of the same reactor designs, illustrating that the configuration pattern plays a significant role in explaining the outstanding performance of the two checkerboard structures.

7 Biocatalytic polysulfone (PSf) membranes

As demonstrated throughout the previous chapters, tailored surface modification of polymer materials is an excellent strategy in order to improve their application as new and versatile enzyme supports. Different surface chemistries create distinct changes in the micro-environment between surface and enzyme, which has been used for the preparation of immobilized enzymes with increased biocatalytic activity and selectivity. Generally, also the biocatalytic **stability** of enzymes can be improved through immobilization. Hence, surface functionalization of a polymer material, here a polysulfone (PSf) membrane was investigated in order to enhance the stability of immobilized alcohol dehydrogenase (ADH). These membranes were initially heterogeneously surface functionalized prior to polymer grafting with the goal to generate a beneficial environment for immobilized ADH maintaining high biocatalytic activity during continuous operation (see Figure 7-1). This work is based on unpublished results and the experimental data can be found in Chapter 10. Additional information, such as Figures and Tables are available in Appendix 5.

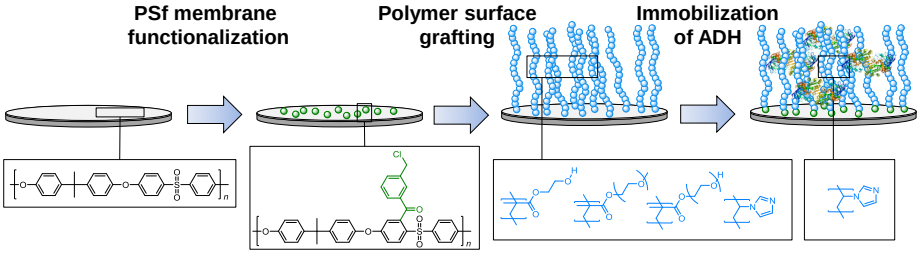

Figure 7-1 Schematic representation of surface functionalization of PSf membranes by a two-step process including lithiation and acylation, followed by polymer grafting, which allowed the immobilization of ADH

Modification and application of PSf membranes

Polysulfone (PSf) as a suitable material for polymer membranes has gained high importance throughout the past decades due to its outstanding properties, such as the acceptance of a wide pH range and organic media as well as a very good thermal and mechanical stability. Therefore, PSf membranes have been used in a broad range of applications including gas and liquid separation,[149] in fuel cells[150] and ion-exchange processes.[151] Furthermore, the development of PSf membranes as support for enzyme immobilization in biocatalytic membrane reactors (BMRs) has demonstrated increased relevance.[152] The significant advantage of BMRs is the direct combination of a biocatalytic reaction with a separation step. However, in order to achieve a high biocatalytic productivity, high enzymatic activity and stability are required, which is mainly a function of the type of immobilization, the generated environment as well as the process conditions.[11] So far, various approaches have been investigated including pressure-driven entrapment into pristine[153]or modified PSf membranes[154–156] as well as by cross-linking of entrapped enzymes.[157,158] Furthermore, immobilization by induced fouling into the skin layer and alternatively in the porous support layer were studied.[159–161]

Additionally to biocatalytic challenges, pressure-driven membranes generally require high permeability and thus, good anti-fouling properties. High membrane flux and low fouling are directly related and can be significantly improved by increasing the hydrophilicity of the membrane surface.[39] Membrane surface modification has been shown to be a successful

pathway in order to improve anti-fouling properties[162] as well to generate a beneficial environment for immobilized enzymes.[40] PSf membranes can generally be modified through coating with an additional surface layer, such as hydrophilic poly(ethylene glycol) (PEG) or poly(vinyl alcohol) (PVA) based polymers[163,164] or cross-linked hydrogels[165,166], which demonstrated significantly improved fouling resistance. For the preparation of biocatalytic membranes, polyethylenimine (PEI) was coated onto PSf allowing immobilization of β-galactosidase onto the attached polyelectrolyte layer.[167] The incorporation of PEG into a sodium alginate coatings increased simultaneously membrane flux as well as biocatalytic performance of entrapped ADH.[168] Surface modification by covalent grafting is a second possibility in order to improve anti-fouling and biocatalytic performance of BMRs, which can be achieved by plasma treatment, UV irradiation and by chemical means. Plasma treatment has been used in order to covalently link hydrophilic polymers, such as PEG and poly(acrylic acid) (polyAAc) onto PSf membranes.[169,170] Plasma was also applied for the grafting of amine functional polymers onto PSf, which allowed covalent enzyme immobilization.[171] Reduced membrane fouling was also achieved through UV initiated grafting of poly(ethylene glycol) methacrylate (PEGMA).[172] UV-polymerization of acrylic acid (AAc) and acrylamide (AAm) resulted in PSf membranes with improved water permeability and by activation of the carboxylic acid moieties catalase was covalently immobilized demonstrating improved biocatalytic activity.[173] Wet chemical methods were also used in order to introduce various functionalities onto PSf surfaces. For instance, Friedel-Crafts catalysts allowed chloromethylation, aminomethylation as well as functionalization with propylene oxide.[174–176] Heterogeneous lithiation with subsequent carboxylation using CO_2 and further modification resulted in PSf membranes with either carboxylic acid or acyl fluoride functionality.[177,178] These small molecular weight modifications have been extended by further polymer grafting, for instance through surface-initiated atom transfer free radical polymerization (SI-ATRP) of halogen functionalized PSf surfaces prepared by chloromethylation. This "grafting from" approach substantiated the introduction of hydrophilic polymers and thus, improved anti-fouling properties of the membrane.[83,179] Alternatively, the use of "Click Chemistry" as a "*grafting to*" technique permitted the introduction of a large range of different substituents or fully characterized polymers.[180] As such, the hydrophilicity of PSf membranes has been increased by Cu(I)-catalyzed alkyne azide cycloaddition (CuAAC) between azide functional PSf and terminal alkyne functional zwitterionic and PEG based polymers.[181,182]

This broad toolbox of functionalization methods opens up for tailor-made surface modifications of PSf membranes allowing distinct changes of membrane properties, which makes them suitable for different applications. In this study, the formation of a biocatalytic PSf membrane through immobilization of ADH by maintaining high membrane permeability was the focus.

Heterogeneous lithiation and acylation of PSf membranes

Functionalized PSf membranes were prepared by following an *in situ* two-step process. Firstly, commercially available PSf membranes were heterogeneously lithiated using n-butyllithium (n-BuLi) in diethyl ether, followed by acylation using various acid chlorides, as illustrated in Scheme 7-1.

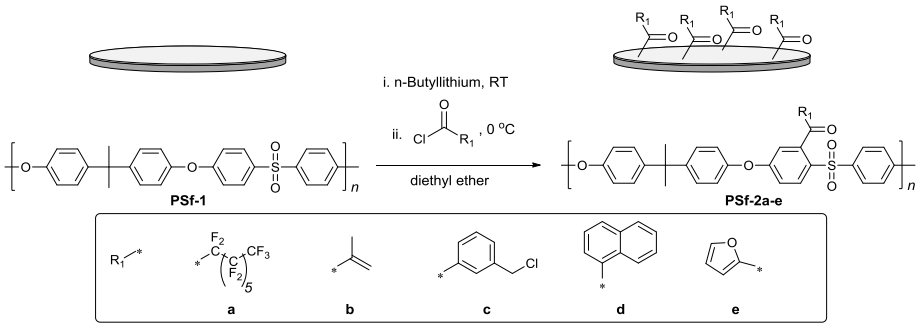

Scheme 7-1 PSf membranes (PSf-1) were lithiated with n-butyl lithium (n-BuLi), and subsequently acylated using pentadecafluorooctanoyl chloride (a), methacryloyl chloride (b), 3-(chloromethyl)benzoyl chloride (c), 1-naphthoyl chloride (d) and 2-furoyl chloride (e) in order to obtain small molecular weight functional PSf membranes PSf-2a-e.

Typically, lithiations are conducted under low temperatures (e.g. -78 °C) as a result of the reactivity of n-butyllithium and the potential degradation of commonly used solvents such as tetrahydrofuran.[183] A few examples in which heterogeneous lithiation was performed at ambient conditions have also been seen.[184] Therefore, reaction conditions were modified to accommodate the membrane in terms of solubility as well as mechanical performance, where diethyl ether was identified as the optimal solvent leading to maintained integrity of membrane and support layer after the reaction. Diethyl ether, compared to THF, also allowed the lithiation reaction to be conducted at higher temperatures due to the increased half-life time of diethyl ether compared to THF. Thus, the lithiation step was conducted at room temperature and the subsequent acylation at 0°C. By reacting the lithiated PSf membrane with pentadecafluorooctanoyl chloride, covalent functionalization of the membrane surface (PSf-2a) was confirmed by the appearance of carbonyl stretches at 1804 and 1750 cm^{-1} in the respective IR spectra (see Figure 7-2).

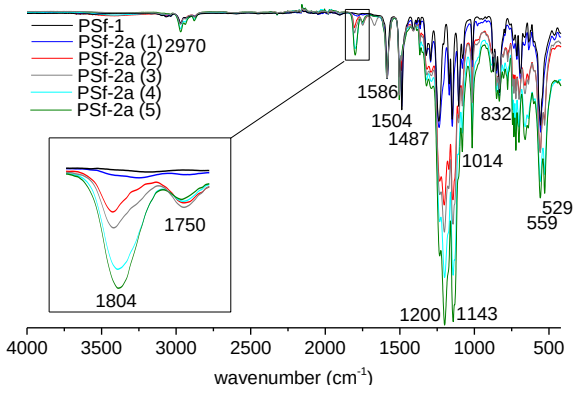

Figure 7-2 IR spectra of PSf membrane (PSf-1) and activated PSf membranes PSf-2a (1)-(5) with pentadecafluorooctanoyl chloride with increasing n-BuLi concentration from 1.16 $mmol_{n\text{-}BuLi}\ g_{membrane}^{-1}$ (PSf-2a (1)) until 39.8 $mmol_{n\text{-}BuLi}\ g_{membrane}^{-1}$ (PSf-2a (5)), magnification in the wavelength range of 1720 to 1860 cm^{-1}

The generation of two bands in the carbonyl range was explained by the introduction of a ketone group represented as the band at the lower wavenumber (here 1750 cm^{-1}), which has been

already reported for the homogeneous modification of PSf with n-BuLi and acid chlorides.[185] The membranes applied in this study were commercially available and thus, the exact composition – particularly the additives added after synthesis, which also influence the performance of the membrane – remained unknown. Therefore, the second carbonyl band at the higher wavenumber, here 1804 cm^{-1}, was assigned to a carbonyl group originating from acylation of hydrophilic residues in the membrane surface. They exhibited a weak reactivity towards surface active reagents such as TFAA (Appendix 5, Figure S1), which indicated that the surface itself has some hydroxyl groups as a result of processing. Thorough washing and Soxhlet extraction of the membranes with ethanol did not allow extraction of the introduced functionalities from the membrane (based on the IR spectra) and both modifications covalently bound to the membranes. The capability of the method was investigated by applying various n-BuLi concentrations, ranging from 1.2 to 39.8 mmol of n-BuLi per gram of membrane, followed by acylation using pentadecafluorooctanoyl chloride, leading to PSf-2a (1) to (5). The concentration dependent surface modification can be seen from the IR data presented in Figure 7-2. The respective IR spectra show an intensity increase in the ester carbonyl band in line with increasing n-BuLi concentration until 20.5 $mmol_{n\text{-}BuLi}\ g_{membrane}^{-1}$. In contrast, the band at 1750 cm^{-1} reaches already a steady intensity at 4.5 $mmol_{n\text{-}BuLi}\ g_{membrane}^{-1}$ (PSf-2a (2)), which could originate from saturation of the heterogeneous aromatic substitution reaction. However, the reaction forming the carbonyl band at 1804 cm^{-1} is still taking place with additional amounts of n-BuLi and acid chloride, respectively. These results were confirmed by XPS analyses showing an increasing fluorine atom content with increasing n-BuLi concentration (see Table 7-1).

Table 7-1 PSf membranes reacted with different concentrations of n-BuLi and subsequent acylation using pentadecafluorooctanoyl chloride (PSf-2a), dynamic water contact angles, and fluorine content by XPS

Entry	c ($mmol_{n\text{-}BuLi}\ g_{membrane}^{-1}$)	$\theta_{advancing}$ (°)	$\theta_{receding}$ (°)	F content (atom%)
PSf-1	0	88.1	48.7	-
PSf-2a (1)	1.16	81.9	40.2	8.0
PSf-2a (2)	4.49	99.3	54.0	29.8
PSf-2a (3)	10.0	109.0	58.0	30.6
PSf-2a (4)	20.5	110.0	72.9	36.1
PSf-2a (5)	39.8	119.1	64.4	42.5

The theoretical fluorine content, assuming each PSf repeating unit reacts once with n-BuLi followed by acid chloride, was calculated as being 27.9 atom%. A fluorine content of 29.8 atom% was already obtained at 4.5 mmol g^{-1} for PSf-2a (2). By increasing the n-BuLi concentration up to 39.8 $mmol_{n\text{-}BuLi}\ g_{membrane}^{-1}$, a fluorine content of up to 42.5 atom% was achieved, indicating that additional functionalization, besides the known PSf reaction, occurred. These results are in agreement with those obtained from the aforementioned IR spectroscopy, which exhibited a well-controlled surface reaction in terms of surface loading. Additionally, WCAs increased from 88.1 ° and 48.7 ° for the original surface up to 119.1° and 64.4°, respectively, clearly corroborate derivatization through an increase in hydrophobicity as a function of increased content of fluorine (see Table 7-1).

In order to emphasize the ease and the potential value of this heterogeneous modification technique, various organic acid chlorides were investigated, as shown in Scheme 7-1. In this way, methacryl (PSf-2b), 3-(chloromethyl)benzyl (PSf-2c), naphthyl (PSf-2d), and furyl (PSf-

2e) functionalities were introduced, thereby demonstrating the versatility of this activation procedure. For each of these modifications, a concentration of 5 $mmol_{n\text{-}BuLi}\ g_{membrane}^{-1}$, identified above as the optimal concentration for having a significant impact on surface functionalization, was utilized. Functionalization was confirmed by IR analysis and the appearance of the previously mentioned carbonyl stretch bands, as shown in Figure 7-3.

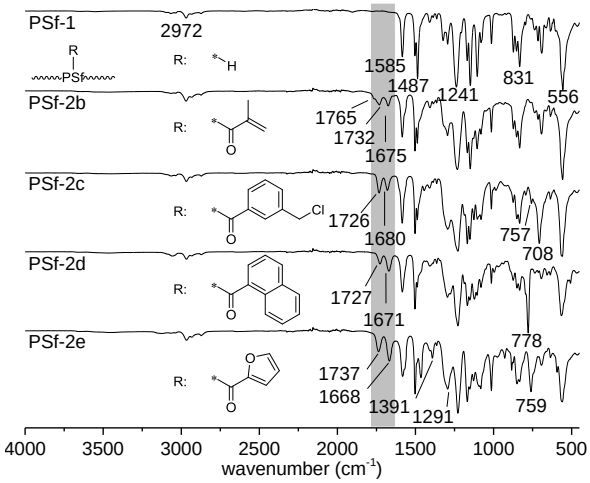

Figure 7-3 IR spectra of initial PSf membrane (PSf-1) and activated PSf membranes PSf-2 with various acid chlorides, PSf-2b: methacryloyl chloride, PSf-2c: 3-(chloromethyl)benzoyl chloride, PSf-2d: 1-naphthoyl chloride, PSf-2e: 2-furoyl chloride

Additionally, IR bands characteristic to the different functionalities illustrate modifications made to the membrane surface. The methacryloyl-functionalized PSf membranes (PSf-2b) showed the two carbonyl stretches at 1732 and 1675 cm^{-1}, with the latter one appearing within the range of a typical C=C stretch. The additional ester was confirmed with the additional carbonyl peak at 1765 cm^{-1}, which originates from the methacryloyl group. The spectrum of PSf-2c, shows in addition to the carbonyl bands (1726/1680 cm^{-1}) the introduction of a significant band at 708 and a small band at 757 cm^{-1} assigned to an aromatic out-of-plane deformation and a carbon-chloride vibration, respectively. The acylation using 1-naphthoyl chloride provided an IR spectrum showing a C-H out-of-plane deformation characteristic for naphthalenes at 778 cm^{-1} in addition to the respective carbonyl bands at 1727 and 1671 cm^{-1}. 2-furoyl functionalized PSf membranes offered similar results, with carbonyl stretches at 1737 and 1668 cm^{-1}, while bands at 1391 (furylic C=C stretch vibration) and 759 cm^{-1} (furylic C-H stretch vibration) confirmed the reaction. The introduction of the various functional groups opens up for further derivatization methodologies through, for example, methacryl groups by thiol-ene reactions[46,53,54] or Aza Michael additions[186], whereas furyl groups are known to react in Diels-Alder cycloaddition.[187,188]

Polymer modified PSf membranes via “*Grafting from*” and “*Grafting to*”

Chloride functional PSf membranes PSf-2c allowed further polymer grafting directly via SI-ATRP through a “*grafting from*” approach and after substitution of the chloride by an azide through CuAAC as a “*grafting to*” approach, as illustrated in Scheme 7-2.

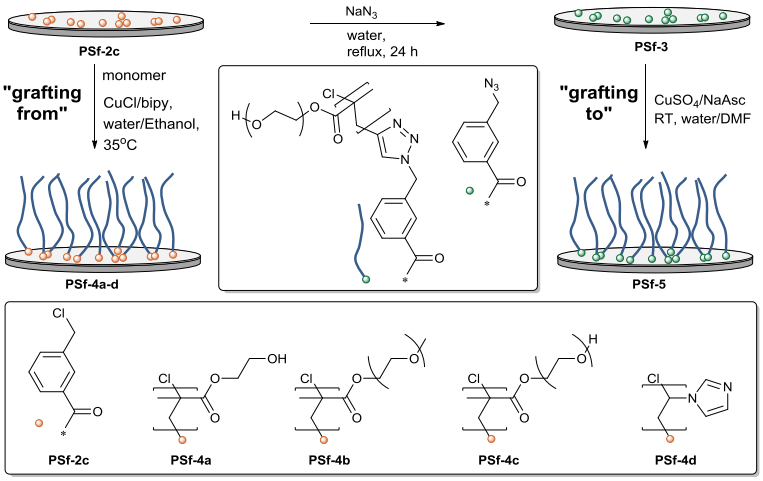

Scheme 7-2 Two surface grafting approaches: "Grafting from" by SI-ATRP of the chloride functionalized PSf membranes (PSf-2c) to provide PSf-4a-d; azidation of PSf-2c, leading to PSf-3, followed by "Grafting to" through CuAAC with alkyne functionalized polyPEGMA, resulting in PSf-5

Therefore, various hydrophilic monomers, such as 2-hydroxyl methacrylate (HEMA) (PSf-4a), methoxy poly(ethylene glycol) methacylate (MPEGMA) (PSf-4b), PEGMA (PSf-4c) and 1-vinyl imidazole (Vim) (PSf-4d) were reacted onto PSf-2c under SI-ATRP conditions. IR analysis confirmed the reaction by significantly increased intensity in the ester band at 1726 cm^{-1} compared to the ketone carbonyl band at 1680 cm^{-1} for the used methacrylates (see Appendix 5, Figure S2). Furthermore, the appearance of bands related to C-O-C ether at 1100 cm^{-1} (for PSf-4a, b, c) and hydroxyl groups at 3466 cm^{-1} (for PSf-2a) provided evidence for the "*grafting from*" method being efficient. Grafting of poly(1-vinyl imidazole) (pVim) could not conclusively be confirmed by IR. XPS analysis corroborated the polymer grafting via SI-ATRP, as shown in Table 7-2.

Table 7-2 XPS data of activated and polymer grafted PSf membranes

Membrane modification	C1s [atom%]	O1s [atom%]	N1s [atom%]	S2p [atom%]	Cl2p [atom%]
PSf-1	82.8 ± 0.2	13.1 ± 0.2	-	4.0 ± 0.0	-
PSf-2c	79.9 ± 1.2	12.2 ± 0.3	-	2.2 ± 0.1	5.7 ± 1.1
PSf-4a	72.0 ± 0.5	24.3 ± 0.9	-	1.4 ± 0.1	1.9 ± 0.2
PSf-4b	72.2 ± 0.8	24.9 ± 0.8	-	1.7 ± 0.2	1.0 ± 0.1
PSf-4c	77.4 ± 0.1	19.0 ± 0.3	-	2.6 ± 0.2	0.9 ± 0.2
PSf-4d	72.9 ± 3.4	14.5 ± 0.7	5.8 ± 0.2	2.3 ± 0.2	1.9 ± 0.7
PSf-3	78.3 ± 1.8	13.5 ± 0.8	3.4 ± 1.4	2.3 ± 0.1	2.4 ± 0.3
PSf-5	71.3 ± 0.9	25.4 ± 1.7	1.1 ± 0.4	0.9 ± 0.2	1.3 ± 0.2

Initially, the introduction of SI-ATRP initiating sites through activation with 3-(chloromethyl)benzyl groups (PSf-2c) was confirmed by the appearance of a significant chloride signal (5.7 atom%) compared to the pristine membrane (PSf-1). Polymer grafting using HEMA, MPEGMA and PEGMA (PSf-4a,b,c) demonstrated a substantial increase in oxygen

content and pVim grafting (PSf-4d) was confirmed through the presence of nitrogen (5.8 atom%). Furthermore, all polymer grafted surfaces PSf-4a-d, including pVim, showed significantly reduced WCAs confirming an increase in the hydrophilicity (see Appendix 5, Figure S3).

In an alternative strategy the chloride groups of PSf-2c were substituted by azides, thus allowing grafting through CuAAC with alkyne-terminated polymers (see Scheme 7-2). The azide functional PSf surface (PSf-3) showed an IR absorption band at around 2100 cm^{-1}, characteristic for the azide (-N=N=N) stretch (see Appendix 5, Figure S4). The appearance of a nitrogen N1s split peak and a decrease in the chloride Cl1s peak in the XPS spectrum corroborated the substitution reaction (see Table 7-2 and Appendix 5, Figure S5, S6). In order to undergo a CuAAC as a "*grafting to*" reaction, a hydrophilic alkyne-terminated polyPEGMA (alkyne-pPEGMA) was prepared by ATRP and reacted onto the functional PSf-3 surface in order to obtain PSf-5 (see Scheme 7-2). The increase in ester C=O stretch intensity at 1726 and the C-O ether band at 1096 cm^{-1} confirmed the grafting (see Appendix 5, Figure S4). The preservation of the azide vibration band at 2100 cm^{-1} showed that only surface functionalization took place and that the aqueous environment prevents penetration into the hydrophobic membrane, whereas the ATR FT-IR measurement penetrates several micrometres into the sample, thus identifying residual azide groups in the bulk. In contrast, XPS analysis penetrates the surface by up to 10 nanometres, and the PSf-5 spectrum in our study showed only a single nitrogen N1s peak (see Appendix 5, Figure S7 and S8). This change from a split to a single nitrogen peak is characteristic of the formation of a triazole group from an azide.[189] Compared to the precursor, azide functionalization (PSf-3) resulted in a slight decrease in WCAs. This minor increase in hydrophilicity was significantly intensified through CuAAC with the alkyne-pPEGMA resulting in substantial reduced WCAs (see Appendix 5, Figure S3), showing similar results compared to SI-ATRP grafted membranes.

Biocatalytic membrane through immobilization of ADH

Compared to the pristine PSf membranes (PSf-1),having a molecular weight cut-off (MWCO) of 20 kDa, the water permeability of chloride (PSf-2c) and azide functional (PSf-3) membranes decreased slightly. Polymer grafting through SI-ATRP and CuAAC, however, resulted in a significant permeability reduction of up to 89 % (see Appendix 5, Table S1) and thus, actual application of the membranes was not practical. Therefore, PSf membranes with a MWCO of 100 kDa, exhibiting a 10-fold higher permeability, were selected for surface grafting with pVim for the subsequent application as a biocatalytic support. Imidiazole groups showing biocompatible and antimicrobial features as well as being bioactive moieties due to their ability to bind to metal ions and form hydrogen bonds.[190] Additionally, Vim functional surfaces demonstrated recently beneficial results of immobilized of horseradish peroxidase and β-glucosidase as shown in Chapter 2 and 4.[122] In this study, ADH from *Saccharomyces cerevisiae* (EC 1.1.1.1), a zinc metalloenzyme belonging to the family of oxireductases, has been used.[191] ADH catalyzes the oxidation of alcohols to the corresponding aldehyde or ketone, by simultaneously reducing β-Nicotinamide adenine dinucleotide (NAD^+) to NADH as the cofactor. Therefore, ADH has a significant importance, including the enantioselective oxidation of alcohols. The ADH catalyzed reverse reaction of a carbonyl substrate to the corresponding alcohol using NADH is also possible, which can be used in fermentation applications, but also in the third step of sequential reduction of carbon dioxide to methanol.[192] However, the stability

of ADH is significantly limited and therefore, various immobilization approaches have already been investigated with the goal to improve the enzyme activity and stability.[193–195]
Here, PSf membranes (100 kDa MWCO), were functionalized with pVim using short grafting times (5 and 40 min) in order to retain high membrane permeability, which were subjected for the immobilization of ADH. Consequently, ADH (0.1 mg L^{-1}, 45 mL, in phosphate buffer, pH 7) was immobilized by pressure driven filtration into virgin (PSf-1) as well as pVim functionalized membranes (PSf-4d-100k-5min and PSf-4d-100k-40min). In an additional rinsing step, phosphate buffer (40 mL) was passed through the membranes in order to prevent any enzyme to remain in the retentate. Figure 7-4A demonstrates the permeability during the immobilization, from which a significant reduction in permeability of the two pVim grafted membranes compared to the virgin PSf-100k-1 was observed.

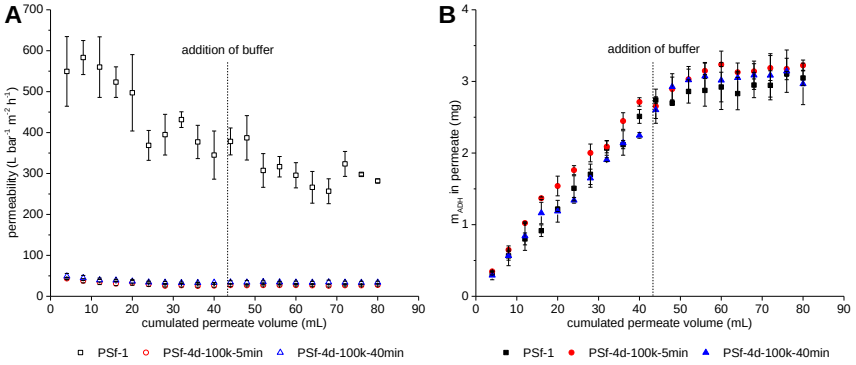

Figure 7-4 Comparison between permeability (A) and amount of enzyme collected in the permeate during ADH (B) immobilization on pristine PSf membrane (PSf-1) and pVim grafted PSf membranes for 5 and 40 min (PSf-4d-100k-5min and PSf-4d-100k-40min)

Furthermore, a permeability loss between 31 and 49 % was observed for both pVim functionalized membranes, as shown by initial and final permeability in Table 7-3. Even though, PSf-4d-100k-5min and PSf-4d-100k-40min exhibited significantly reduced permeabilities, their use as support for enzyme immobilization was still promising. The amount of ADH in the permeate throughout the immobilization process (see Figure 7-4B) showed initially a steady increase indicating enzymes passing through the membrane. The slope of permeated ADH over accumulated permeate volume was very similar for the virgin PSf-1 as well as the pVim modified membranes indicating that no significant pore size reduction occurred under the applied grafting conditions via SI-ATRP.
As soon as buffer was added the amount of enzyme in the permeate remained constant after 56 mL confirming that all possible ADH was flushed out of the membrane. Consequently, the difference between the applied ADH stock solution and the final amount in the permeate resulted in the final immobilization yield. Thus, the enzyme loading was calculated to be around 0.5 mg for the virgin membrane (PSf-1), which was further increased by a factor of 2 through pVim grafting (see Table 7-3).

Table 7-3 Membrane performance and enzyme loading during immobilization of ADH for virgin (PSf-100k-1) and pVim grafted PSf membranes (PSf-4d-100k-5min and PSf-4d-100k- 40min)

Entry	Initial membrane permeability ($L\ m^{-2}\ h^{-1}\ bar^{-1}$)	final membrane permeability ($L\ m^{-2}\ h^{-1}\ bar^{-1}$)	Enzyme loading (mg)	Enzyme loading ($mg\ cm^{-2}$)	Loading Efficiency (%)
PSf-100k-1	549 ± 85	282 ± 5	0.51 ± 0.04	0.038 ± 0.003	13.5 ± 0.8
PSf-4d-100k-5min	43.5 ± 2.5	27.6 ± 2.7	0.98 ± 0.06	0.073 ± 0.005	23.7 ± 0.4
PSf-4d-100k-40min	49.0 ± 6.9	33.7 ± 3.0	1.05 ± 0.03	0.079 ± 0.002	27.5 ± 2.6

In this study, ADH catalyzed the reduction of formaldehyde (HCOH) to methanol (CH_3OH) by simultaneous oxidation of β-nicotinamide adenine dinucleotide reduced form (NADH) to NAD^+, which was used for the evaluation of the biocatalytic activity and stability of immobilized ADH. During constant permeation of substrate no significant change in membrane permeability was observed for all three tested membranes (see Figure 7-5A).

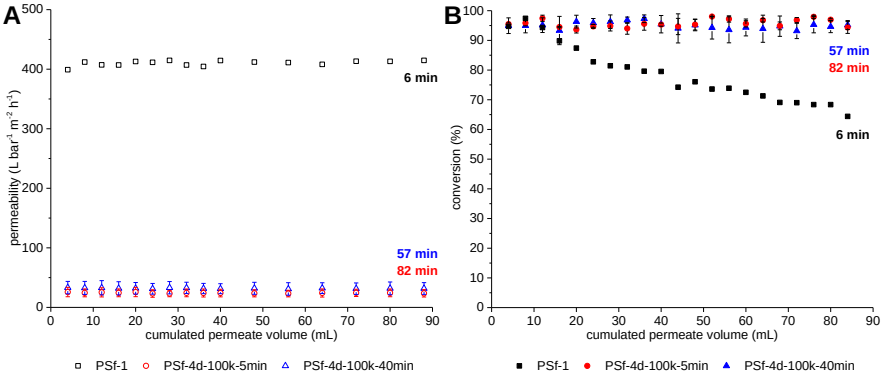

Figure 7-5 Permeability (A) and NADH conversion (B) during enzymatic reaction catalysed by immobilized ADH on pristine PSf membrane (PSf-1) and pVim grafted PSf membranes for 5 and 40 min

However, similarly to the immobilization procedure, the virgin PSf-100k-1 membrane exhibited a 10-fold increased permeability compared to the pVim grafted ones. The conversion was estimated spectrophotometrically through absorbance measurements of NADH at a wavelength of 340 nm and is presented in Figure 7-5B. For ADH immobilized in PSf-100k-1, a substantial decrease in conversion from around 94 % to 64 % within 88 mL of accumulated permeate in 6 min was observed, which indicated enzyme deactivation in the original porous PSf structure. Due to the reduced permeability of pVim (for 5 as well as 40 min) grafted membranes, 88 mL of permeate were collected after 82 and 57 min, respectively. Within this time, these membranes demonstrated a significant improved stability by remaining highly active (conversion > 94 %) during the entire procedure. This outstanding performance compared to the virgin membrane was ascribed to the generation of a beneficial environment supplied by pVim reducing enzyme deactivation within this period and thus improving the biocatalytic performance substantially.

Conclusions

In this study, a facile and easily conductible methodology has been applied in order to covalently surface modify commercially available PSf membranes. For this purpose, off-the-shelf PSf flat sheet membranes were heterogeneously lithiated prior to acylation, using various acid chlorides. Retaining membrane integrity by introducing target functionality onto the surface shows the versatility and importance of this method. Surface modifications with methacryloyl-, furoyl-, and halogen-containing functional groups open up a broad range of surface grafting reactions for tailoring the surface properties of the applied membranes. Chloride functionality to the membrane surface allowed polymer surface by SI-ATRP treatment of hydrophilic monomers such as HEMA, MPEGMA, PEGMA and Vim in a "*grafting from*" approach. Conversion of anchored chlorides into azide groups offered the possibility for surface functionalization via CuAAC with an alkyne-pPEGMA as a "*grafting to*" techniques. Both cases resulted in significantly improved membrane hydrophilicity. Immobilization of ADH onto pVim grafted PSf membranes with a MWCO of 100 kDa demonstrated a 2 fold increase in enzyme loading (loading of 23 – 27 %) compared to virgin PSf membranes. Furthermore, high enzyme activities (conversions > 94 %) and significantly improved enzyme stability were achieved using pVim grafted membranes. These outstanding performances by maintaining permeabilities in a good operational window demonstrated their potential as excellent support for ADH. This toolbox of simple surface activation followed by polymer grafting of commercially available PSf membranes opens up for the application of a broad variety of potential polymers and their possibility to serve as improved BMRs.

8 Conclusions

Biocatalytic processes require active, stable and selective biocatalysts in order to be economically and environmentally feasible. Due to its advantages in terms of improved purification procedures and promoting biocatalytic stability, enzyme immobilization is an important concept within biocatalysis. However, a suitable immobilization strategy depends on the nature of the enzyme and the support, type of immobilization, micro-environmental effects and applied process conditions. These factors play a significant role and have to be taken into consideration when developing immobilized enzyme systems, which require being highly active, selective, effective, stable and applicable.

In this dissertation, these requirements are addressed by exploiting polymer materials as enzyme supports. The versatile surface functionalization of different polymers permitted the introduction of tailored properties for distinct purposes within enzyme immobilization. Initially, a platform, based on STE/OSTE materials was developed allowing a broad screening of different surface chemistries and thus the influence of micro-environmental changes towards the biocatalytic **activity** of immobilized enzymes. It demonstrated the importance of a precise match between the surface functionality of the support and the enzyme in order to obtain a highly active system. For practical **application** of the identified candidates exhibiting excellent enzyme activities, OSTE particles containing highly versatile surface chemistries were prepared. These particles showed their high application potential as a suitable support for enzyme immobilization in continuous plug-flow or batch reactors. Furthermore, the influence of different surface functionalities towards the **selectivity** of enzymes was investigated by immobilization of β-glucosidase onto functional OSTE particles. Hereby, changes in the micro-environment around the immobilized enzyme improved the enzymes selectivity significantly, as demonstrated through the competitive reaction between trans-glycosylation and hydrolysis catalyzed by β-glucosidase. Additionally, the exploitation of enzymes in their most effective way is a fundamental goal for efficient reactor design. Therefore, the local distribution of enzymes immobilized on the surface of a microreactor was investigated towards their contribution to the overall reactor performance. In this way, specific surface patterns were identified, showing a significant increase in **effectiveness** of the applied enzymes. Finally, enzyme **stability**, being one of the most crucial parameters for the continuous application and the reusability of a biocatalyst, was addressed by the preparation of biocatalytically active PSf membranes. Here, surface grafting with specific polymers allowed enzyme immobilization with a significant improvement in terms of operational stability compared to unmodified membranes and shows the substantial impact of the generated micro-environment towards the enzyme stability.

As demonstrated in this thesis, different aspects are playing a crucial role for the development of immobilized enzymes in biocatalytic processes. The versatile application of polymers and their potential for broad surface functionalization allows detailed and distinct modifications of the support in order to achieve improved biocatalytic performance. Therefore, tailor-made materials and the understanding of their influence expand the possibilities for the preparation of excellent enzyme supports substantially.

9 Future Work

The investigation of enzyme immobilization onto functionalized polymer surfaces and their importance for the development of biocatalytic systems with improved performance was the core of this project. This concept has been demonstrated by focusing on the introduction of different surface chemistries and thus, creating micro-environmental changes, onto different polymers, which were used for the immobilization of different enzymes.

Initially, the impact of micro-environmental changes through tailor-made surface functionalization was shown through the developed screening platform, which offered the possibility for investigation and distinct selection of suitable surface-enzyme combinations. As a proof-of-concept, different candidates in terms of surface functionality as well as model enzymes were selected. This platform opens up for further investigation of a vast number of different influence factors, being (1) extended and more complex surface chemistries, (2) binding chemistries between surface and enzyme, like different covalent, ionic or physical attachment, (3) the type of enzyme and (4) process parameters, like pH, temperature, and substrate concentration. Thereby, optimal immobilization and process conditions for a particular enzyme could be identified in a fast and straight forward way. Consequently, the generation of a library would allow comparison and the identification of similarities between different enzymes, which could lead to predictions of new enzyme-surface candidates. However, the quantitative determination of immobilized enzyme in this setup would be of significant value. Precise quantification requires assays with increased sensitivity and reduced unspecific side reactions or alternative methods, such as quartz crystal micro balance.

Additionally to the identification of beneficial surface-enzyme combinations through changes in the micro-environment, the understanding of the individual effects between enzyme and support is crucial for specific design of immobilized enzyme. In order to generate this data, computational methods in combination with experimental investigations, could generate more structural evidence for the observed tendencies.

Furthermore, TEC has demonstrated its excellent features for the preparation of TE materials in different forms, such as a microplate, polymer particles and microfluidics. This versatility could be extended for the preparation of additional geometries. For instance, the fabrication of porous particles would be an obvious choice, due to their advantage of a significantly increased surface area. Thereby, an increased amount of enzymes could be immobilized, which would improve the sensitivity of quantification. Furthermore, through tailored pore functionalization, enzyme activity and stability could be positively influenced.

10 Experimental Section

Materials and methods

Materials

Polysulfone membranes GR61PP (PSf-1, 20kDa MWCO) were obtained from Alfa Laval. N-butyl lithium (n-BuLi, 2.5 M in hexane), pentadecafluorooctanoyl chloride (97%), 3-(chloromethyl)benzoyl chloride (98%), methacryloyl chloride (97%), 1-naphtoyl chloride (97%), 2-furoyl chloride (95%), sodium azide (99%), tetrahydrofuran (THF, ≥ 99%), copper(I)chloride (99%), 2,2' bipyridine (98%), copper(II)sulfate (99,9%), (+)-sodium L-ascorbate (NaAsc, 98%), propargyl 2-bromoisobutyrate (97%), 1-vinyl imidazole (Vim, ≥ 99 %), formaldehyde (HCOH, 37 wt% in water), N,N,N′,N″,N″-pentamethyldiethylenetriamine (PMDETA), alcohol dehydrogenase from *Saccharomyces cerevisiae* (ADH, ≥ 300 units/mg protein) and β-Nicotinamide adenine dinucleotide, reduced disodium salt hydrate (NADH, ≥ 97%) were purchased from Sigma Aldrich. Poly(ethylene glycol) methacrylate (PEGMA, 360 g mol^{-1}), poly(ethylene glycol)methylether metacrylate (MPEGMA, 300 g mol^{-1}), and 2-hydroxyethyl methacrylate (HEMA; 97%) were purchased from Sigma Aldrich and passed through a short plug-flow column containing aluminum oxide (Sigma-Aldrich, activated, basic, Brockmann I, standard grade) prior to using for SI-ATRP or regular ATRP. Diethyl ether (Sigma-Aldrich, 99.8%) was dried with molecular sieves (Sigma-Aldrich, 4 Å) prior to using for lithiation reactions. All other chemicals were acquired from Sigma Aldrich were used as received.

Characterization

NMR spectroscopy was carried out on a Bruker Avance 300 MHz spectrometer. Chemical shifts are given in ppm. Number average molecular weights of the alkyne-pPEGMA were determined by ^{1}H NMR experiments. Additionally, molecular weights and the polydispersity index of alkyne-pPEGMA was estimated by size exclusion chromatography (SEC), using a Viscotek GPCmax VE-2001 equipped with a Viscotek TriSEC Model 302 triple detector array (refractive index (RI) detector, viscometer detector, and laser light-scattering detector with a light wavelength of 670 nm and measuring angles of 90° and 7°) and a Knauer K-2501 UV detector using two PLgel mixed-D columns from Polymer Laboratories (PL). The samples were run in THF at 30°C (1 mL min^{-1}). Molecular weights were calculated using polystyrene (PS) standards from PL. Differential scanning calorimetry (DSC) was performed using a TA instruments Discovery DSC at a heating and cooling rate of 10°C min^{-1}. The melting temperatures (T_m) are reported as the peak temperatures of the endothermic melting peaks. Glass transition temperatures (T_g's) were measured at the inflection point. Fourier transform infrared (FT-IR) spectroscopy was carried out using a Nicolet iS50 FT-IR fitted with a diamond crystal attenuated total reflection accessory (ATR), which operated at a resolution of 4 cm^{-1} and 32 scans per measurement and was used to identify chemical modifications made by surface functionalization. XPS experiments were conducted on a Thermo Fisher Scientific K-Alpha (East Grinstead, UK). Large area surface analysis used a 400 μm spot of monochromatized aluminum Kα radiation, following which survey (pass energy 200 eV) and high-resolution (pass energy 50 eV) spectra for relevant elements were acquired. Data analyses of the obtained XPS spectra were performed using the Avantage software package as provided by the manufacturer. Advancing and receding water contact angles (WCAs) of the PSf membrane surfaces were

determined by using a Dataphysics Contact Angle System OCA20. Each surface was tested via the dynamic sessile drop method at 23°C, and the average value was determined from three different measurements. For Scanning Electron Microscopy, the membranes were submerged in liquid nitrogen and broken by bending with two precooled tweezers. Subsequently, the samples were dried at room temperature and mounted onto a sample holder and coated with a thin gold film using a sputter coater (Cressington, model 208HR). The cross-sectional scanning electron micrographs were recorded with a FEI Quanta 200 FEG microscope and the secondary electron signal was recorded at 5keV with an Everhart-Thornley detector.
Membrane permeability measurements were carried out in a stirred cell (Amicon 8050, Millipore, USA), using a fixed stirring speed at 100 rpm and an effective membrane surface area of 13.4 cm^2. The cells were filled with 40 mL of phosphate buffer (0.1M, pH 7). A constant nitrogen pressure of 2 bar was maintained while collecting permeate into a beaker until 13 to 25 mL of permeate was collected. Placing the beaker on an electronic balance allowed for monitoring the permeate flux and, consequently, permeability (permeate density was defined as 1 g mL^{-1}). The permeate flux was calculated according to the following equation:

$$Flux = \frac{V}{tS}$$

where V is the volume of permeate solution in mL; t is the time of the flux experiment in h and S is the effective membrane area in m^2.
Subsequently the permeability was calculated as followed:

$$Permeability = \frac{Flux}{P}$$

where P is the applied N_2 pressure to the membrane in bar. One-way ANOVA analysis in order to calculate the statistical significance of the various permeabilities was conducted in Origin (OriginLab Corporation). Statistical significance between the results was established at $p<0.05$.

Preparation of activated PSf membrane (PSf-2a)

In a general activation procedure, a piece of PSf-1 (2x2 cm^2, 0.216 g) was first submerged in ethanol for 2 h, then in diethyl ether for 0.5 h. Thereafter, it was transferred into a pre-dried schlenk tube under nitrogen atmosphere, which was then evacuated and back-filled with N_2 three times. Diethyl ether (20 mL) was added under stirring, and n-BuLi (0.1 mL, 0.25 mmol, 1.2 mmol $g^{-1}_{membrane}$) was added dropwise at room temperature. The reaction mixture was stirred for 2 h. The membrane surface changed colour from white to light yellow. Then, the reaction was cooled down to 0°C, and pentadecafluorooctanoyl chloride (0.08 mL, 0.31 mmol) was added slowly. After continuing stirring for another 60 min, the reaction was quenched by adding ethanol (appr. 20 mL). The reacted membrane was removed from the reaction flask and thoroughly rinsed with ethanol before drying in an oven *in vacuo* at room temperature.
PSf-2a (1) IR (cm^{-1}): 2971 (C-H), 1804 (C=O), 1750 (C=O), 1585 (C=C_{arom}), 1502 (C=C_{arom}), 1488 (C-H_{arom}), 1200 (C-F), 1143 (C-F), 1105, 1014 (C-O-C), 832 (C-H_{arom}), 659 (C-F), 559 (oop arom), 529 (C-F)

Synthesis of PSf-2b. Compound PSf-2b was synthesized in accordance with the general procedure in which PSf-1 (7x5 cm^2, 1.034 g), diethyl ether (100 mL), n-BuLi (2.0 mL, 5.0 mmol, 4.9 mmol $g^{-1}_{membrane}$), and methacryloyl chloride (0.65 mL, 6.5 mmol) were used.
PSf-2b IR (cm^{-1}): 2970 (C-H), 1731 (C=O), 1675 (C=O/C=C_{alkene}), 1585 (C=C_{arom}), 1503 (C=C_{arom}), 1295 (C-O), 1229 (C-O-C), 1149, 1014 (C-O-C), 558 (oop arom).

Synthesis of PSf-2c. Compound PSf-2c was synthesized in accordance with the general procedure in which PSf-1 (12 pieces à 5x5 cm^2, 5.3 g), diethyl ether (400 mL), n-BuLi (10.6 mL, 26.5 mmol, 5.0 mmol $g^{-1}_{membrane}$), and 3-(chloromethyl)benzoyl chloride (4.6 mL, 31.7 mmol) were used. An inert atmosphere was achieved in this case through bubbling with N_2 for 15 min, before adding n-BuLi.
PSf-2c IR (cm^{-1}): 2967 (C-H), 1732 (C=O), 1680 (C=O), 1585 (C=C_{arom}), 1502 (C=C_{arom}), 1488 (C-H_{arom}), 1294 (C-O), 1228 (C-O-C), 1168 (CO-C_{phenyl}), 1014 (C-O-C), 833 (C-H_{arom}), 757 (C-Cl), 707 (oop arom), 560 (oop arom).

Synthesis of PSf-2d. Compound PSf-2d was synthesized in accordance with the general procedure in which PSf-1 (2x2 cm^2, 0.254 g), diethyl ether (20 mL), n-BuLi (0.5 mL, 1.3 mmol, 4.9 mmol $g^{-1}_{membrane}$), and 1-naphthoyl chloride (0.25 mL, 1.6 mmol) were used.
PSf-2d IR (cm^{-1}): 2967 (C-H), 1726 (C=O), 1670 (C=O), 1584 (C=C_{arom}), 1504 (C=C_{arom}), 1296 (CO), 1228 (C-O-C), 1168 (CO-C_{phenyl}), 1123 (C-O-C), 1014 (C-O-C), 778 (C-H oop), 566 (oop arom).

Synthesis of PSf-2e. Compound PSf-2e was synthesized in accordance with the general procedure in which PSf-1 (2x2 cm^2, 0.244 g), diethyl ether (20 mL), n-BuLi (0.5 mL, 1.3 mmol, 5.1 mmol $g^{-1}_{membrane}$), and 2-furoyl chloride (0.18 mL, 1.7 mmol) were used.
PSf-2e IR (cm^{-1}): 2966 (C-H), 1735 (C=O), 1668 (C=O), 1582 (C=C_{arom}), 1503 (C=C_{arom}), 1463, 1391 (C=C furyl), 1291 (C-O), 1227 (C-O-C), 1168 (CO-C_{arom}), 1013 (C-O-C), 929 (C-H furyl), 759 (C-H furyl), 566 (oop arom).

Preparation of azide functionalized PSf membrane (PSf-3)

Into a round-bottom flask, NaN_3 (1.10 g, 16.8 mmol), H_2O (205 mL), and PSf membrane PSf-2c (four pieces at 5x5 cm^2, theor. 1.76 g) were added. This mixture was stirred under reflux for 22 h. The membrane was then removed from the reaction bath and thoroughly rinsed with H_2O before immersing in a H_2O/ethanol (50:50) bath until further use.
PSf-3 IR (cm^{-1}): 2968 (C-H), 2099 (N_3) 1734 (C=O), 1679 (C=O), 1585 (C=C_{arom}), 1503 (C=C_{arom}), 1294 (C-O), 1230 (C-O-C), 1168 (CO-C_{phenyl}), 1014 (C-O-C), 833 (C-H_{arom}), 707 (oop arom), 558 (oop arom).

Preparation of grafted PSf membrane via SI-ATRP (PSf-4a)

In a typical grafting experiment, CuCl (107 mg, 1.07 mmol) and 2,2' bipyridine (347 mg, 2.20 mmol) were introduced into a round-bottom flask. The flask was evacuated and backfilled with N_2 three times. Then, HEMA (8.15 mL, 8.75 g, 65.9 mmol), ethanol, and water (4 mL of each, bubbled with N_2 for 60 min prior to use) were introduced. After 50 min of purging with N_2, this mixture was transferred under N_2 into a schlenk tube equipped with a PSf membrane PSf-2c (5x5 cm^2, appr. 0.44 g) and kept in an inert atmosphere. The reaction flask was then heated up to 35°C, and the polymerization was allowed to proceed for 180 min before being stopped by

removing the membrane from the polymerization bath. The substrate was thoroughly rinsed with water and kept immersed in a H_2O/ethanol (50:50) bath until further use.
PSf-4a IR (cm^{-1}): 3443 (O-H), 2964 (C-H), 1726 (C=O), 1682 (C=O), 1585 (C=C_{arom}), 1503 (C=C_{arom}), 1234 (C-O-C), 1152 (C-O), 1079 (C-OH), 1014 (C-O-C), 832 (C-H_{arom}), 757 (C-Cl), 707 (oop arom), 567 (oop arom).

Synthesis of PSf-4b. Compound PSf-4b was synthesized in accordance with the general procedure in which PSf-2c (5x5 cm^2, appr. 0.44 g) was modified using CuCl (107 mg, 1.07 mmol), 2,2' bipyridine (347 mg, 2.20 mmol), MPEGMA (18.5 mL, 19.44 g, 60.5 mmol), ethanol, and water (9.5 mL of each, bubbled with N_2 for 60 min prior to use).
PSf-4b IR (cm^{-1}): 2966 (C-H), 1729 (C=O), 1680 (C=O), 1585 (C=C_{arom}), 1503 (C=C_{arom}), 1294, 1236 (C-O-C), 1150 (C-O), 1013 (C-O-C), 833 (C-H_{arom}), 707 (C-Cl), 559 (oop arom).

Synthesis of PSf-4c. Compound PSf-4b was synthesized in accordance with the general procedure in which PSf-2c (5x5 cm^2, appr. 0.44 g) was modified using CuCl (107 mg, 1.07 mmol), 2,2' bipyridine (347 mg, 2.20 mmol), PEGMA (20.8 mL, 23.01 g, 56.7 mmol), ethanol, and water (each 10.5 mL, bubbled with N_2 for 60 min prior to use).
PSf-4c IR (cm^{-1}): 3367 (O-H), 2965 (C-H), 1728 (C=O), 1678 (C=O), 1585 (C-C_{arom}), 1503 (C-C_{arom}), 1230 (C-O-C), 1152 (C-O), 1013 (C-O-C), 834 (C-H_{arom}), 757 (C-Cl), 707 (oop arom), 558 (oop arom).

Synthesis of PSf-4d. Compound PSf-4d was synthesized in accordance with the general procedure in which PSf-2c (5x5 cm^2, appr. 0.44 g) was modified using CuCl (107 mg, 1.07 mmol), 2,2' bipyridine (347 mg, 2.20 mmol), Vim (18.0 mL, 18.7 g, 199 mmol), ethanol, and water (each 12 mL, bubbled with N_2 for 60 min prior to use).
PSf-4d IR (cm^{-1}): 3384 (O-H), 2965 (C-H), 1728 (C=O), 1678 (C=O), 1585 (C-C_{arom}), 1503 (C-C_{arom}), 1235 (C-O-C), 1150 (C-O), 1013 (C-O-C), 832 (C-H_{arom}), 710 (oop arom), 558 (oop arom).

Synthesis of alkyne polyPEGMA

In a typical ATRP experiment, CuCl (20.2 mg, 0.200 mmol) was added into a schlenk tube equipped with a stirring bar and a rubber septum, which was evacuated and back-filled with N_2 three times. Subsequently, PEGMA (2.6 mL, 8.0 mmol), water (7.8 mL), and methanol (7.8 mL) were added and two freeze-pump-thaw cycles were performed. PMDETA (42 µL, 0.20 mmol) was added and an additional freeze-pump-thaw cycle was carried out. Then, propargyl-2-bromoisobutyrate (32 µL, 0.20 mmol) was added followed by a final freeze-pump-thaw cycle. Polymerization was run at 25°C for 90 min. Finally, the product was concentrated *in vacuo* and precipitated three times from THF into diethyl ether. Drying of the precipitate under vacuum conditions led to a light-blue, highly viscous oil as the targeted product (m =1.44 g, 49 % yield). T_g (°C): -49.2 (DSC); M_n (g mol^{-1}): 2500 (SEC), 1900 (^{1}H NMR); M_w/M_n: 1.06 (SEC); IR (cm^{-1}): 3464 (O-H), 2869 (C-H), 1726 (C=O), 1450 (C-H), 1247 (C-O), 1096 (C-O-C), 747 (C-Cl); ^{1}H-NMR (δ, ppm, 300 MHz, $CDCl_3$): 4.05 (br s, 10.5 H), 3.66 (br m, 106H), 2.22 (s, 1H), 1.13 (m, 19 H).

Preparation of grafted PSf membrane via CuAAC (PSf-5)

Alkyne-polyPEGMA (0.4131g, 0,217 mmol), H_2O (18 mL), aqueous $CuSO_4$ solution (0.890 mL, 0.1M, 0.089 mmol), and aqueous sodium ascorbate (1.78 mL, 0.1 M, 0.178 mmol) were

added under stirring into a reaction vial. After 30 minutes, the slightly milky reaction mixture turned yellow and the PSf membrane PSf-3 (5x5 cm^2) was introduced. After stirring for 14 h, the colour of the reaction mixture changed to brown and the reacted membrane was removed, thoroughly rinsed with water, and kept immersed in a H_2O/ethanol (50:50) bath until further use.

PSf-5 IR (cm^{-1}): 3453 (O-H), 2965 (C-H), 2100 (N_3), 1731 (C=O), 1679 (C=O), 1585 (C-C_{arom}), 1503 (C-C_{arom}), 1247 (C-O), 1228 (C-O-C), 1013 (C-O-C), 746 (C-Cl), 833 (C-H_{arom}), 707 (oop arom), 559 (oop arom).

Immobilization of alcohol dehydrogenase (ADH) in PSf membranes

The pristine membrane (PSf-1) was prior to alcohol dehydrogenase (ADH) immobilization submerged in ethanol for 2 h and subsequently rinsed with deionized water. Modified membranes were stored in ethanol/water (50:50 vol%) and rinsed with deionized water prior to immobilization. A round PSf membrane (r=2.25 cm) was placed in an Amicon 8050 stirred cell instrument and 45 ml of a phosphate buffer solution (0,1 M, pH=7.0) containing ADH (100 mg/L) was added. The pressure driven immobilization was conducted under a pressure of 1.5 bar and stirring at 100 rpm. After 44 ml of ADH solution were collected, 10 mL phosphate buffer was added. After collecting further 10 mL of permeate, a second portion (35mL) of phosphate buffer was flushed through the membrane until a final permeate volume of 88 mL was collected. The cumulated permeate was collected in a beaker and after each 4 ml, an aliquot of 100 µL was withdrawn for analysis. The concentration of ADH was measured as protein concentration at 280 nm in microtiter plates (96 wells, acrylic from CORNING) using a microtiter plate reader (POLARstar OMEGA from BMG Labtech equipped with an UV-VIS probe).

Enzymatic reaction of immobilized ADH

50 mL of a phosphate buffer solution (0,1 M, pH=7.0) containing NADH (100 µM) and HCOH (100 mM) was added to the membrane previously immobilized with ADH. A pressure of 1.5 bar and stirring of 100 rpm were used during the filtration. The cumulated permeate was collected in a beaker and after each 4 ml, an aliquot of 100 µL was withdrawn for analysis. The NADH concentration was determined through absorbance measurements at 340 nm in microtiter plates (96 wells, acrylic from CORNING) using a microtiter plate reader (POLARstar OMEGA from BMG Labtech equipped with an UV-VIS probe).

References

(1) Buchholz, K.; Kasche, V.; Bornsheuer, U. T. In *Biocatalysis and Enzyme Technology*; WILEY-VCH, 2012; pp 1–26.
(2) Bommarius, A. S.; Riebel, B. R. In *Biocatalysis*; WILEY-VCH, 2004; pp 1–18.
(3) Bornscheuer, U. T.; Huisman, G. W.; Kazlauskas, R. J.; Lutz, S.; Moore, J. C.; Robins, K. *Nature* **2012**, *485* (7397), 185–194.
(4) Cao, L. In *Carrier-bound Immobilized Enzymes: Principles, Application and Design*; WILEY-VCH, 2006; pp 1–52.
(5) Liese, A.; Hilterhaus, L. *Chem. Soc. Rev.* **2013**, *42* (15), 6236–6249.
(6) Cantone, S.; Ferrario, V.; Corici, L.; Ebert, C.; Fattor, D.; Spizzo, P.; Gardossi, L. *Chem. Soc. Rev.* **2013**, *42* (15), 6262–6276.
(7) DiCosimo, R.; McAuliffe, J.; Poulose, A. J.; Bohlmann, G. *Chem. Soc. Rev.* **2013**, *42* (15), 6437–6474.
(8) Cao, L. *Carrier-bound Immobilized Enzymes: Principles, Application and Design*; WILEY-VCH, 2006.
(9) Bommarius, A. S.; Riebel, B. R. In *Biocatalysis*; WILEY-VCH, 2004; pp 19–42.
(10) Bommarius, A. S.; Riebel, B. R. In *Biocatalysis*; WILEY-VCH, 2004; pp 91–134.
(11) Mateo, C.; Palomo, J. M.; Fernandez-Lorente, G.; Guisan, J. M.; Fernandez-Lafuente, R. *Enzyme Microb. Technol.* **2007**, *40* (6), 1451–1463.
(12) Mahoney, K. W.; Talbert, J. N.; Goddard, J. M. *J. Appl. Polym. Sci.* **2013**, *127* (2), 1203–1210.
(13) Rodrigues, R. C.; Ortiz, C.; Berenguer-Murcia, Á.; Torres, R.; Fernández-Lafuente, R. *Chem. Soc. Rev.* **2013**, *42* (15), 6290–6307.
(14) Secundo, F. *Chem. Soc. Rev.* **2013**, *42* (15), 6250–6261.
(15) Barbosa, O.; Torres, R.; Ortiz, C.; Berenguer-Murcia, Á.; Rodrigues, R. C.; Fernandez-Lafuente, R. *Biomacromolecules* **2013**, *14* (8), 2433–2462.
(16) Sheldon, R. A.; van Pelt, S. *Chem. Soc. Rev.* **2013**, *42* (15), 6223–6235.
(17) Balcão, V. M.; Vila, M. M. D. C. *Adv. Drug Deliv. Rev.* **2015**, *93*, 25–41.
(18) Hanefeld, U.; Gardossi, L.; Magner, E. *Chem. Soc. Rev.* **2009**, *38* (2), 453–468.
(19) Sheldon, R. A.; Schoevaart, R.; Van Langen, L. M. *Biocatal. Biotransformation* **2005**, *23* (3–4), 141–147.
(20) Cao, L. In *Carrier-bound Immobilized Enzymes: Principles, Application and Design*; WILEY-VCH, 2006; pp 53–168.
(21) Cao, L. In *Carrier-bound Immobilized Enzymes: Principles, Application and Design*; WILEY-VCH, 2006; pp 169–316.
(22) Talbert, J. N.; Goddard, J. M. *Colloids Surfaces B Biointerfaces* **2012**, *93*, 8–19.
(23) Santos, J. C. S. Dos; Barbosa, O.; Ortiz, C.; Berenguer-Murcia, A.; Rodrigues, R. C.; Fernandez-Lafuente, R. *ChemCatChem* **2015**, *7* (16), 2413–2432.
(24) Hamlin, R. E.; Daytong, T. L.; Johnson, L. E.; Johal, M. S. *Langmuir* **2007**, *23* (8), 4432–4437.
(25) Malinin, A. S.; Rakhnyanskaya, A. A.; Bacheva, A. V; Yaroslavov, A. A. *Polym. Sci. Ser. A* **2011**, *53* (1), 52–56.
(26) Cheng, Z.; Teoh, S.-H. *Biomaterials* **2004**, *25* (11), 1991–2001.
(27) Misson, M.; Dai, S.; Jin, B.; Chen, B. H.; Zhang, H. *J. Biotechnol.* **2016**, *222*, 56–64.
(28) Huang, J.; Li, X.; Zheng, Y.; Zhang, Y.; Zhao, R.; Gao, X.; Yan, H. *Macromol. Biosci.* **2008**, *8* (6), 508–515.
(29) Bayramoglu, G.; Karagoz, B.; Altintas, B.; Arica, M. Y.; Bicak, N. *Bioprocess Biosyst. Eng.* **2011**, *34* (6), 735–746.
(30) Chen, H.; Teramura, Y.; Iwata, H. *J. Control. Release* **2011**, *150* (2), 229–234.
(31) Manta, C.; Ferraz, N.; Betancor, L.; Antunes, G.; Batista-Viera, F.; Carlsson, J.; Caldwell, K. *Enzyme Microb. Technol.* **2003**, *33* (7), 890–898.
(32) Bolivar, J. M.; Eisl, I.; Nidetzky, B. *Catal. Today* **2016**, *259*, 66–80.

(33) Kasche, V. *Enzyme Microb. Technol.* **1983**, *5* (1), 2–13.
(34) Pessela, B. C. C.; Fernández-lafuente, R.; Fuentes, M.; Vián, A.; Garc, J. L.; Carrascosa, A. V; Mateo, C.; Guisán, J. M. *Enzyme Microb. Technol.* **2003**, *32*, 369–374.
(35) Illanes, A.; Altamirano, C. *Enzyme Biocatalysis*; 2008.
(36) Tischer, W.; Kasche, V. *Trends Biotechnol.* **1999**, *17* (8), 326–335.
(37) Goddard, J. M.; Hotchkiss, J. H. *Prog. Polym. Sci.* **2007**, *32* (7), 698–725.
(38) Katchalski-Katzir, E.; Kraemer, D. M. *J. Mol. Catal. B Enzym.* **2000**, *10* (1–3), 157–176.
(39) Rana, D.; Matsuura, T. *Chem. Rev.* **2010**, *110*, 2448–2471.
(40) Jochems, P.; Satyawali, Y.; Diels, L.; Dejonghe, W. *Green Chem.* **2011**, *13* (7), 1609.
(41) Cakmakci, E.; Danis, O.; Demir, S.; Mulazim, Y.; Kahraman, M. V. *J. Microbiol. Biotechnol.* **2013**, *23*, 205–210.
(42) Lafleur, J. P.; Senkbeil, S.; Novotny, J.; Nys, G.; Bøgelund, N.; Rand, K. D.; Foret, F.; Kutter, J. P. J. P. *Lab Chip* **2015**, *15* (10), 1381–1388.
(43) Çakmakçi, E.; Yuce-Dursun, B.; Demir, S. *React. Funct. Polym.* **2017**, *111*, 38–43.
(44) Hoyle, C. E.; Bowman, C. N. *Angew. Chemie* **2010**, *49* (9), 1540–1573.
(45) Nair, D. P.; Podgórski, M.; Chatani, S.; Gong, T.; Xi, W.; Fenoli, C. R.; Bowman, C. N. *Chem. Mater.* **2014**, *26* (1), 724–744.
(46) Lowe, A. B. *Polym. Chem.* **2010**, *1* (1), 17–36.
(47) Hoyle, C. E.; Lowe, A. B.; Bowman, C. N. *Chem. Soc. Rev.* **2010**, *39* (4), 1355–1387.
(48) Lowe, A. B. *Polym. Chem.* **2014**, *5* (17), 4820.
(49) Aimetti, A. A.; Machen, A. J.; Anseth, K. S. *Biomaterials* **2009**, *30* (30), 6048–6054.
(50) Yigit, S.; Sanyal, R.; Sanyal, A. *Chem. Asian J.* **2011**, *6* (10), 2648–2659.
(51) Durham, O. Z.; Krishnan, S.; Shipp, D. A. *ACS Macro Lett.* **2012**, *1* (9), 1134–1137.
(52) Lovelady, E.; Kimmins, S. D.; Wu, J.; Cameron, N. R. *Polym. Chem.* **2011**, *2* (3), 559–562.
(53) Campos, L. M.; Meinel, I.; Guino, R. G.; Schierhorn, M.; Gupta, N.; Stucky, G. D.; Hawker, C. J. *Adv. Mater.* **2008**, *20* (19), 3728–3733.
(54) Gupta, N.; Lin, B. F.; Campos, L. M.; Dimitriou, M. D.; Hikita, S. T.; Treat, N. D.; Tirrell, M. V; Clegg, D. O.; Kramer, E. J.; Hawker, C. J. *Nat. Chem.* **2010**, *2* (2), 138–145.
(55) Mongkhontreerat, S.; Öberg, K.; Erixon, L.; Löwenhielm, P.; Hult, A.; Malkoch, M. *J. Mater. Chem. A* **2013**, *1* (44), 13732.
(56) Khire, V. S.; Yi, Y.; Clark, N. A.; Bowman, C. N. *Adv. Mater.* **2008**, *20*, 3308–3313.
(57) Tähkä, S. M.; Bonabi, A.; Nordberg, M. E.; Kanerva, M.; Jokinen, V. P.; Sikanen, T. M. *J. Chromatogr. A* **2015**, *1426*, 233–240.
(58) Carlborg, C. F.; Haraldsson, T.; Öberg, K.; Malkoch, M.; van der Wijngaart, W. *Lab Chip* **2011**, *11* (18), 3136.
(59) Sikanen, T. M.; Lafleur, J. P.; Moilanen, M.-E.; Zhuang, G.; Jensen, T. G.; Kutter, J. P. *J. Micromechanics Microengineering* **2013**, *23* (3), 37002.
(60) Pardon, G.; Haraldsson, T.; Wijngaart, W. Van Der. In *Micro Electro Mechanical Systems*; 2014; pp 96–99.
(61) Pardon, G.; Saharil, F.; Karlsson, J. M.; Supekar, O.; Carlborg, C. F.; van der Wijngaart, W.; Haraldsson, T. *Microfluid. Nanofluidics* **2014**, *17* (4), 773–779.
(62) Carlborg, C. F.; Moraga, F.; Saharil, F.; van der Wijngaart, W.; Haraldsson, T. In *Proceedings Micro Total Analysis Systems*; 2012; pp 677–679.
(63) Feidenhans'l, N. A.; Lafleur, J. P.; Jensen, T. G.; Kutter, J. P. *Electrophoresis* **2014**, *35* (2–3), 282–288.
(64) Lafleur, J. P.; Senkbeil, S.; Novotny, J.; Nys, G.; Bøgelund, N.; Rand, K. D.; Foret, F.; Kutter, J. P. J. P. *Lab Chip* **2015**, *15* (10), 1–2.
(65) Han, X.; Wu, C.; Sun, S. *Appl. Surf. Sci.* **2012**, *258* (12), 5153–5156.
(66) Zhang, J.; Chen, Y.; Brook, M. A. *Langmuir* **2013**, *29* (40), 12432–12442.
(67) Tan, K. Y.; Ramstedt, M.; Colak, B.; Huck, W. T. S.; Gautrot, J. E. *Polym. Chem.* **2016**, *7* (4), 979–990.

(68) Mongkhontreerat, S.; Öberg, K.; Erixon, L.; Löwenhielm, P.; Hult, A.; Malkoch, M. *J. Mater. Chem. A* **2013**, *1* (44), 13732–13737.
(69) Mazurek, P.; Daugaard, A. E.; Skolimowski, M.; Hvilsted, S.; Skov, A. L. *RSC Adv.* **2015**, *5* (20), 15379–15386.
(70) Durham, O. Z.; Norton, H. R.; Shipp, D. A. *RSC Adv.* **2015**, *5* (82), 66757–66766.
(71) Hansson, S.; Antoni, P.; Bergenudd, H.; Malmström, E. *Polym. Chem.* **2011**, *2* (3), 556–558.
(72) Mateo, C.; Grazú, V.; Pessela, B. C. C.; Montes, T.; Paloma, J. M.; López-Gallego, F.; Fernández-Lafuente, R.; Guisán, J. M. *Biochem. Soc. Trans.* **2007**, *35* (6), 1593–1601.
(73) Fodor, C.; Bozi, J.; Blazsó, M.; Iván, B. *Macromolecules* **2012**, *45* (22), 8953–8960.
(74) Liu, S.; Zhou, F.; Di, D.; Jiang, S. *Colloids Surfaces A Physicochem. Eng. Asp.* **2004**, *244* (1–3), 87–93.
(75) Wang, S.; Zhou, Y.; Guan, W.; Ding, B. *Appl. Surf. Sci.* **2008**, *254* (16), 5170–5174.
(76) Bertin, A.; Schlaad, H. *Chem. Mater.* **2009**, *21* (24), 5698–5700.
(77) Veitch, N. C. *Phytochemistry* **2004**, *65* (3), 249–259.
(78) Azevedo, A. M.; Martins, V. C.; Prazeres, D. M. F.; Vojinovic, V.; Cabral, J. M. S.; Fonseca, L. P. *Biotechnol. Annu. Rev.* **2003**, *9* (3), 199–247.
(79) Jiang, H.; Xu, F.-J. *Chem. Soc. Rev.* **2013**, *42* (8), 3394–3426.
(80) Xu, F. J.; Neoh, K. G.; Kang, E. T. *Prog. Polym. Sci.* **2009**, *34* (8), 719–761.
(81) Xiu, K. M.; Cai, Q.; Li, J. S.; Yang, X. P.; Yang, W. T.; Xu, F. J. *Colloids Surf. B. Biointerfaces* **2012**, *90*, 177–183.
(82) Fristrup, C. J.; Jankova, K.; Hvilsted, S. *Soft Matter* **2009**, *5* (23), 4623.
(83) Yue, W.-W.; Li, H.-J.; Xiang, T.; Qin, H.; Sun, S.-D.; Zhao, C.-S. *J. Memb. Sci.* **2013**, *446*, 79–91.
(84) Xiang, T.; Zhang, L.-S.; Wang, R.; Xia, Y.; Su, B.-H.; Zhao, C.-S. *J. Colloid Interface Sci.* **2014**, *432*, 47–56.
(85) Childs, B. R. E.; Bardsley, W. G. *Biochem. J.* **1975**, *145*, 93–103.
(86) Xu, F. J.; Cai, Q. J.; Li, Y. L.; Kang, E. T.; Neoh, K. G. *Biomacromolecules* **2005**, *6* (2), 1012–1020.
(87) Shen, Y.; Guo, W.; Qi, L.; Qiao, J.; Wang, F.; Mao, L. *J. Mater. Chem. B* **2013**, *1* (17), 2260–2267.
(88) Kawaguchi, H. *Prog. Polym. Sci.* **2000**, *25* (8), 1171–1210.
(89) Champion, J. A.; Katare, Y. K.; Mitragotri, S. *J. Control. Release* **2007**, *121* (1–2), 3–9.
(90) Durham, O. Z.; Shipp, D. A. *Polymer* **2014**, *55* (7), 1674–1680.
(91) Durham, O. Z.; Shipp, D. A. *Colloid Polym. Sci.* **2015**, *293* (8), 2385–2394.
(92) Alimohammadi, F.; Wang, C.; Durham, O. Z.; Norton, H. R.; Bowman, C. N.; Shipp, D. A. *Polymer* **2016**, *105*, 180–186.
(93) Tan, J.; Li, C.; Zhou, J.; Yin, C.; Zhang, B.; Gu, J.; Zhang, Q. *Rsc Adv.* **2014**, *4*, 13334–13339.
(94) Cai, S.; Weng, Z.; Zheng, Y.; Zhao, B.; Gao, Z.; Gao, C. *Polym. Chem.* **2016**, *7* (48), 7400–7407.
(95) Jasinski, F.; Lobry, E.; Tarablsi, B.; Chemtob, A.; Croutxé-Barghorn, C.; Nouen, D. Le; Criqui, A. *ACS Macro Lett.* **2014**, *3* (9), 958–962.
(96) Wang, C.; Podgórski, M.; Bowman, C. N. *Mater. Horizons* **2014**, No. 1, 1173–1184.
(97) Wang, C.; Zhang, X.; Podgórski, M.; Xi, W.; Shah, P.; Stansbury, J.; Bowman, C. N. *Macromolecules* **2015**, *48* (23), 8461–8470.
(98) Amato, D. V.; Amato, D. N.; Flynt, A. S.; Patton, D. L. *Polym. Chem.* **2014**, *6*, 5625–5632.
(99) Amato, D. N.; Amato, D. V.; Narayanan, J.; Donovan, B. R.; Douglas, J. R.; Walley, S. E.; Flynt, A. S.; Patton, D. L. *Chem. Commun.* **2015**, *51* (54), 10910–10913.
(100) Quispe, C. A. G.; Coronado, C. J. R.; Carvalho Jr, J. A. *Renew. Sustain. Energy Rev.* **2013**, *27*, 475–493.
(101) Tang, C. Y.; Kwon, Y. N.; Leckie, J. O. *J. Memb. Sci.* **2007**, *287* (1), 146–156.

(102) Andree, H.; Hessel, J. F.; Krings, P.; Meine, G.; Middelhauve, B.; Schmid, K. In *Alkyl Polyglycosides: Technology, Properties, Applications*; Hill, K., von Rybinski, W., Stoll, G., Eds.; John Wiley & Sons, Inc., 2008; pp 99–130.
(103) Tesmann, H.; Kahre, J.; Hensen, H.; Salka, B. A. In *Alkyl Polyglycosides: Technology, Properties, Applications*; Hill, K., von Rybinski, W., Stoll, G., Eds.; John Wiley & Sons, Inc., 2008; pp 71–98.
(104) De Roode, B. M.; Franssen, M. C. R.; Van Der Padt, A.; Boom, R. M. *Biotechnol. Prog.* **2003**, *19* (5), 1391–1402.
(105) Rather, M.; Mishra, S. *Sustain. Chem. Process.* **2013**, *1* (1), 7.
(106) Adlercreutz, P. *Appl. Microbiol. Biotechnol.* **2017**, *101* (2), 513–519.
(107) Van Rantwijk, F.; Woudenberg-Van Oosterom, M.; Sheldon, R. A. *J. Mol. Catal. - B Enzym.* **1999**, *6* (6), 511–532.
(108) Hansson, T.; Andersson, M.; Wehtje, E.; Adlercreutz, P. *Enzyme Microb. Technol.* **2001**, *29* (8–9), 527–534.
(109) Parry, N. J.; Beever, D. E.; Owen, E.; Vandenberghe, I.; Van Beeumen, J.; Bhat, Mm. K. *Biochem. J.* **2001**, *353*, 117–127.
(110) Ljunger, G.; Adlercreutz, P.; Mattiasson, B. *Enzyme Microb. Technol.* **1994**, *16*, 751–755.
(111) Hansson, T.; Adlercreutz, P. *Biotechnol. Bioeng.* **2001**, *75* (6), 656–665.
(112) Mladenoska, I. *Food Technol. Biotechnol.* **2016**, *54* (2), 211–216.
(113) Turner, P.; Svensson, D.; Adlercreutz, P.; Karlsson, E. N. *J. Biotechnol.* **2007**, *130* (1), 67–74.
(114) Guo, D. H.; Xu, Y. S.; Kang, Y. J.; Han, S. Y.; Zheng, S. P. *Enzyme Microb. Technol.* **2016**, *85*, 90–97.
(115) Lundemo, P.; Adlercreutz, P.; Karlsson, E. N. *Appl. Environ. Microbiol.* **2013**, *79* (11), 3400–3405.
(116) Martearena, M. R.; Blanco, S.; Ellenrieder, G. *Bioresour. Technol.* **2003**, *90* (3), 297–303.
(117) Larsson, J.; Svensson, D.; Adlercreutz, P. *J. Mol. Catal. B Enzym.* **2005**, *37* (1–6), 84–87.
(118) Svensson, D.; Ulvenlund, S.; Adlercreutz, P. *Biotechnol. Bioeng.* **2009**, *104* (5), 854–861.
(119) Lundemo, P.; Karlsson, E. N.; Adlercreutz, P. *J. Mol. Catal. B Enzym.* **2014**, *108*, 1–6.
(120) Kumar, P.; Ryan, B.; Henehan, G. T. M. *Protein Expr. Purif.* **2017**, *132*, 164–170.
(121) Graebin, N. G.; Schöffer, J. D. N.; De Andrades, D.; Hertz, P. F.; Ayub, M. A. Z.; Rodrigues, R. C. *Molecules* **2016**, *21* (8), 1–38.
(122) Hoffmann, C.; Pinelo, M.; Woodley, J. M.; Daugaard, A. E. *Biotechnol. Prog.* **2017**.
(123) Giacomini, C.; Irazoqui, G.; Batista-Viera, F.; Brena, B. M. *J. Mol. Catal. B Enzym.* **2001**, *11* (4–6), 597–606.
(124) Irazoqui, G.; Villarino, A.; Batista-Viera, F.; Brena, B. M. *Biotechnol. Bioeng.* **2002**, *77* (4), 430–434.
(125) Liu, J.; Bai, S.; Jin, Q.; Zhong, H.; Li, C.; Yang, Q. *Langmuir* **2012**, *28* (25), 9788–9796.
(126) dos Santos, J. C. S.; Rueda, N.; Goncalves, L. R. B.; Fernandez-Lafuente, R. *Enzyme Microb. Technol.* **2015**, *77*, 1–7.
(127) Hammond, J. B.; Kruger, N. J. *Methods Mol. Biol.* **1988**, *3*, 25–32.
(128) Schäpper, D.; Lencastre Fernandes, R.; Lantz, A. E.; Okkels, F.; Bruus, H.; Gernaey, K. V. *Biotechnol. Bioeng.* **2011**, *108* (4), 786–796.
(129) Rosinha Grundtvig, I. P.; Woodley, J. M.; Gernaey, K. V.; Daugaard, A. E.; Krühne, U. Shape and topology optimization of enzymatic microreactors, Technical University of Denmark, 2015.
(130) Krenková, J.; Foret, F. *Electrophoresis* **2004**, *25* (21–22), 3550–3563.
(131) Yamaguchi, H.; Honda, T.; Miyazaki, M. *J. Flow Chem.* **2016**, 1–5.
(132) Jensen, K. F. *AIChE J.* **1999**, *45* (10), 2051–2054.

(133) Swarts, J. W.; Kolfschoten, R. C.; Jansen, M. C. A. A.; Janssen, A. E. M.; Boom, R. M. *Chem. Eng. J.* **2010**, *162* (1), 301–306.
(134) Zhang, W.; Lin, S.; Wang, C.; Hu, J.; Li, C.; Zhuang, Z.; Zhou, Y.; Mathies, R. A.; Yang, C. J. *Lab Chip* **2009**, *9* (21), 3088–3094.
(135) Lee, S. H.; Kang, D. H.; Kim, H. N.; Suh, K. Y. *Lab Chip* **2010**, *10* (23), 3300–3306.
(136) Farshchian, B.; Park, S.; Choi, J.; Amirsadeghi, A.; Lee, J.; Park, S. *Lab Chip* **2012**, *12* (2), 4764.
(137) McDonald, J. C.; Whitesides, G. M. *Acc. Chem. Res.* **2002**, *35* (7), 491–499.
(138) Seong, G. H.; Crooks, R. M. *J. Am. Chem. Soc.* **2002**, *124* (45), 13360–13361.
(139) Seong, G. H.; Heo, J.; Crooks, R. M. *Anal. Chem.* **2003**, *75* (13), 5206–5212.
(140) Mao, H.; Yang, T.; Cremer, P. S. *Anal. Chem.* **2002**, *74* (2), 379–385.
(141) Holden, M. A.; Jung, S. Y.; Cremer, P. S. *Anal. Chem.* **2004**, *76* (7), 1838–1843.
(142) Carlborg, C. F.; Vastesson, A.; Liu, Y.; van der Wijngaart, W.; Johansson, M.; Haraldsson, T. *J. Polym. Sci. Part A Polym. Chem.* **2014**, *52*, 2604–2615.
(143) Jonkheijm, P.; Weinrich, D.; Köhn, M.; Engelkamp, H.; Christianen, P. C. M.; Kuhlmann, J.; Maan, J. C.; Nüsse, D.; Schroeder, H.; Wacker, R.; Breinbauer, R.; Niemeyer, C. M.; Waldmann, H. *Angew. Chemie* **2008**, *120* (23), 4493–4496.
(144) Wasserberg, D.; Steentjes, T.; Stopel, M. H. W.; Huskens, J.; Blum, C.; Subramaniam, V.; Jonkheijm, P. *J. Mater. Chem.* **2012**, *22*, 16606–16610.
(145) Bradford, M. M. *Anal. Biochem.* **1976**, *72* (1–2), 248–254.
(146) Wiechelman, K. J.; Braun, R. D.; Fitzpatrick, J. D. *Anal. Biochem.* **1988**, *237*, 231–237.
(147) Logan, T. C.; Clark, D. S.; Stachowiak, T. B.; Svec, F.; Fréchet, J. M. J. *Anal. Chem.* **2007**, *79* (17), 6592–6598.
(148) Wang, Z.; King, T. L.; Branagan, S. P.; Bohn, P. W. *Analyst* **2009**, *134*, 851–859.
(149) Ulbricht, M. *Polymer* **2006**, *47* (7), 2217–2262.
(150) Jannasch, P. *Fuel Cells* **2005**, *5* (2), 248–260.
(151) Wang, G.; Weng, Y.; Chu, D.; Chen, R.; Xie, D. *J. Memb. Sci.* **2009**, *332* (1–2), 63–68.
(152) Rios, G. M.; Belleville, M. P.; Paolucci, D.; Sanchez, J. *J. Memb. Sci.* **2004**, *242* (1), 189–196.
(153) Mazzei, R.; Giorno, L.; Piacentini, E.; Mazzuca, S.; Drioli, E. *J. Memb. Sci.* **2009**, *339* (1–2), 215–223.
(154) Wang, Z. G.; Wang, J. Q.; Xu, Z. K. *J. Mol. Catal. B Enzym.* **2006**, *42* (1–2), 45–51.
(155) Cano, À.; Minguillón, C.; Palet, C. *J. Memb. Sci.* **2006**, *280* (1–2), 383–388.
(156) Łukowska, E.; Wojciechowsk, C.; Chwojnowski, A.; Dudziński, K.; Sabalińska, S.; Ciechanowska, A.; Czapiewska, G. *Biocybern. Biomed. Eng.* **2012**, *32* (2), 77–86.
(157) Yujun, W.; Jian, X.; Guangsheng, L.; Youyuan, D. *Bioresour. Technol.* **2008**, *99* (7), 2299–2303.
(158) Zhu, X.-Y.; Chen, C.; Chen, P.-C.; Gao, Q.-L.; Fang, F.; Li, J.; Huang, X.-J. *RSC Adv.* **2016**, *6* (37), 30804–30812.
(159) Luo, J.; Marpani, F.; Brites, R.; Frederiksen, L.; Meyer, A. S.; Jonsson, G.; Pinelo, M. *J. Memb. Sci.* **2014**, *459*, 1–11.
(160) Luo, J.; Meyer, A. S.; Jonsson, G.; Pinelo, M. *Biochem. Eng. J.* **2014**, *83*, 79–89.
(161) Luo, J.; Meyer, A. S.; Mateiu, R. V; Kalyani, D.; Pinelo, M. *ACS Appl. Mater. Interfaces* **2014**, *6*, 22894–22904.
(162) Miller, D. J.; Dreyer, D. R.; Bielawski, C. W.; Paul, D. R.; Freeman, B. D. *Angew. Chemie - Int. Ed.* **2017**, *56* (17), 4662–4711.
(163) Brink, L. E. S.; Romijn, D. J. *Desalination* **1990**, *78* (2), 209–233.
(164) Hyun, J.; Jang, H.; Kim, K.; Na, K.; Tak, T. *J. Memb. Sci.* **2006**, *282* (1–2), 52–59.
(165) Ju, H.; McCloskey, B. D.; Sagle, A. C.; Kusuma, V. A.; Freeman, B. D. *J. Memb. Sci.* **2009**, *330* (1–2), 180–188.
(166) Lang, K.; Chowdhury, G.; Matsuura, T.; Sourirajan, S. *Journal of colloid and interface science*. 1994, pp 239–244.
(167) Gonawan, F. N.; Kamaruddin, A. H.; Abu Bakar, M. Z.; Abd Karim, K. *Ind. Eng. Chem.*

Res. **2016**, *55* (1), 21–29.
(168) Marpani, F.; Luo, J.; Mateiu, R. V.; Meyer, A. S.; Pinelo, M. *ACS Appl. Mater. Interfaces* **2015**, *7* (32), 17682–17691.
(169) Song, Y.-Q.; Sheng, J.; Wei, M.; Yuan, X.-B. *J. Appl. Polym. Sci.* **2000**, *78*, 979–985.
(170) Wavhal, D. S.; Fisher, E. R. *J. Memb. Sci.* **2002**, *209* (1), 255–269.
(171) Mahlicli, F. Y.; Şen, Y.; Mutlu, M.; Alsoy Altinkaya, S. *J. Memb. Sci.* **2015**, *479*, 175–189.
(172) Susanto, H.; Balakrishnan, M.; Ulbricht, M. *J. Memb. Sci.* **2007**, *288* (1–2), 157–167.
(173) Song, H.; Wu, G.; Liu, K. *J. Environ. Sci.* **2004**, *16* (3), 392–396.
(174) Higuchi, A.; Nakagawa, T. *J. Appl. Polym. Sci.* **1990**, *41* (9–10), 1973–1979.
(175) Higuchi, A.; Koga, H.; Nakagawa, T. *J. Appl. Polym. Sci.* **1992**, *46* (3), 449–457.
(176) Breitbach, L.; Hinke, E.; Staude, E. *Die Angew. Makromol. Chemie* **1991**, *184* (3134), 183–196.
(177) Guiver, M. D.; Croteau, S.; Hazlett, J. D.; Kutowy, O. *Br. Polym. J.* **1990**, *23* (1–2), 29–39.
(178) Guiver, M. D.; Black, P.; Tam, C. M.; Deslandes, Y. *J. Polym. Sci.* **1993**, *48*, 1597–1606.
(179) Qiu, J.; Zhang, Y.; Shen, Y.; Zhang, Y.; Zhang, H.; Liu, J. *Appl. Surf. Sci.* **2010**, *256* (10), 3274–3280.
(180) Kolb, H. C.; Finn, M. G.; Sharpless, K. B. *Angew. Chemie* **2001**, *40* (11), 2004–2021.
(181) Meng, J. Q.; Yuan, T.; Kurth, C. J.; Shi, Q.; Zhang, Y. F. *J. Memb. Sci.* **2012**, *401*, 109–117.
(182) Xiang, T.; Wang, R.; Zhao, W.-F.; Sun, S.-D.; Zhao, C.-S. *Langmuir* **2014**, *30* (18), 5115–5125.
(183) Holm, T. *Acta Chem. Scand. B* **1978**, *32*, 162–166.
(184) Guiver, M. D.; Robertson, G. P. *Macromolecules* **1995**, *28*, 294–301.
(185) Dimitrov, I.; Takamuku, S.; Jankova, K.; Jannasch, P.; Hvilsted, S. *Macromol. Chem. Phys.* **2012**, *33*, 1368–1374.
(186) Hoffmann, C.; Stuparu, M. C.; Daugaard, A.; Khan, A. *J. Polym. Sci. Part A Polym. Chem.* **2015**, *53* (6), 745–749.
(187) Tarducci, C.; Badyal, J. P. S.; Brewer, S. A.; Willis, C. *Chem. Commun.* **2005**, No. 3, 406–408.
(188) Gandini, A. *Prog. Polym. Sci.* **2013**, *38* (1), 1–29.
(189) Daugaard, A. E.; Hvilsted, S.; Hansen, T. S.; Larsen, N. B. *Macromolecules* **2008**, *41*, 4321–4327.
(190) Anderson, E. B.; Long, T. E. **2010**, *51*, 2447–2454.
(191) De Smidt, O.; Du Preez, J. C.; Albertyn, J. *FEMS Yeast Res.* **2008**, *8* (7), 967–978.
(192) Obert, R.; Dave, B. C. *J. Am. Chem. Soc.* **1999**, *121* (6), 12192–12193.
(193) Cochrane, F. C.; Petach, H. H.; Henderson, W. *Enzyme Microb. Technol.* **1996**, *18* (5), 373–378.
(194) Jadhav, S. B.; Bankar, S. B.; Granström, T.; Ojamo, H.; Singhal, R. S.; Survase, S. a. *Appl. Microbiol. Biotechnol.* **2014**, *98* (14), 6307–6316.
(195) Guldu, O. K.; Ece, S.; Evran, S.; Medine, E. I.; Demirkol, D. O.; Unak, P.; Timur, S. *J. Macromol. Sci. Part A* **2014**, *51* (9), 699–705.

Appendix 1

Development of a thiol-ene based screening platform for enzyme immobilization demonstrated using horseradish peroxidase

*Christian Hoffmann, Manuel Pinelo, John M. Woodley, Anders E. Daugaard**

published in Biotechnology Progress, 2017, DOI: 10.1002/btpr.2526

Appendix 1.1 – Publication

Development of a Thiol-Ene Based Screening Platform for Enzyme Immobilization Demonstrated Using Horseradish Peroxidase

Christian Hoffmann
Dept. of Chemical and Biochemical Engineering, Danish Polymer Centre, Technical University of Denmark, Søltofts Plads Building 229, 2800 Kgs, Lyngby, Denmark

Manuel Pinelo
Dept. of Chemical and Biochemical Engineering, Center for BioProcess Engineering, Technical University of Denmark, Søltofts Plads Building 229, 2800 Kgs, Lyngby, Denmark

John M. Woodley
Dept. of Chemical and Biochemical Engineering, Process and Systems Engineering Center (PROSYS), Technical University of Denmark, Søltofts Plads Building 229, 2800 Kgs., Lyngby, Denmark

Anders E. Daugaard
Dept. of Chemical and Biochemical Engineering, Danish Polymer Centre, Technical University of Denmark, Søltofts Plads Building 229, 2800 Kgs, Lyngby, Denmark

DOI 10.1002/btpr.2526
Published online 00 Month 2017 in Wiley Online Library (wileyonlinelibrary.com)

Efficient immobilization of enzymes on support surfaces requires an exact match between the surface chemistry and the specific enzyme. A successful match would normally be identified through time consuming screening of conventional resins in multiple experiments testing individual immobilization strategies. In this study we present a versatile strategy that largely expands the number of possible surface functionalities for enzyme immobilization in a single, generic platform. The combination of many individual surface chemistries and thus immobilization methods in one modular system permits faster and more efficient screening, which we believe will result in a higher chance of discovery of optimal surface/enzyme interactions. The proposed system consists of a thiol-functional microplate prepared through fast photochemical curing of an off-stoichiometric thiol-ene (OSTE) mixture. Surface functionalization by thiol-ene chemistry (TEC) resulted in the formation of a functional monolayer in each well, whereas, polymer surface grafts were introduced through surface chain transfer free radical polymerization (SCT-FRP). Enzyme immobilization on the modified surfaces was evaluated by using a rhodamine labeled horseradish peroxidase (Rho-HRP) as a model enzyme, and the amount of immobilized enzyme was qualitatively assessed by fluorescence intensity (FI) measurements. Subsequently, Rho-HRP activity was measured directly on the surface. The broad range of utilized surface chemistries permits direct correlation of enzymatic activity to the surface functionality and improves the determination of promising enzyme-surface candidates. The results underline the high potential of this system as a screening platform for synergistic immobilization of enzymes onto thiol-ene polymer surfaces. © 2017 American Institute of Chemical Engineers *Biotechnol. Prog.*, 000:000–000, 2017
Keywords: thiol-ene chemistry, surface functionalization, enzyme immobilization, enzyme-surface interaction

Introduction

Immobilized enzymes are widely used as biosensors, in drug delivery, as well as in dairy and food processes for the production of pharmaceuticals and cosmetics.[1,2] Their high substrate specificity, selectivity, and efficiency at mild reaction conditions, such as ambient temperature, physiological pH, and atmospheric pressure make them interesting alternatives to conventional catalysts. However, as functional biocatalysts, enzymes frequently demonstrate limited operational stability. Immobilization of enzymes has generally been demonstrated to have a stabilizing effect due to stronger confinement in enzyme rigidity, which leads to improved pH, organic solvent, and thermal stability.[3–5] However, increased stability and even improved selectivity or activity can only be achieved, when a favorable environment for the enzyme is obtained. Further advantages are the improved

Contract grant sponsor: Aage and Johanne Louis-Hansen Endowment.
Additional Supporting Information may be found in the online version of this article.
Correspondence concerning this article should be addressed to Anders E. Daugaard at adt@kt.dtu.dk.

recovery and purification from reaction media and potential recirculation of immobilized biocatalysts in the process.[6] Depending on the application and the particular enzyme of interest, many strategies are available for immobilization with, or without, a support matrix.[7,8] Cross-linking enzymes by either physical or covalent interactions, leads to the formation of enzyme aggregates, which can directly be used.[9] Entrapment or binding to a support matrix requires the use of a solid carrier material.[10] However, a general concern of most of these procedures is the potential reduction in biocatalytic activity upon immobilization due to a combination of various individual factors, such as changes in conformation and accessibility to the active site.[11] These factors are greatly influenced when confining structural freedom or even changing their structural conformation upon immobilization.[12] In some specific cases, strong attachment of enzymes to a surface, for instance by multibond attachment, might also have a beneficial effect for the activity in addition to improvements in stability due to conformational restrictions of the enzyme.[13]

For the attachment of enzymes to the surface of solid supports various factors for stabilization and destabilization have been identified and reviewed by Talbert and Goddard.[14] To prevent deactivation, the properties of the surface (hydrophilicity, hydrophobicity, charge, surface topology, and functionality) have to match structural and compositional characteristics of a particular enzyme and provide a favorable local environment for immobilized enzyme.[15]

Each enzyme or protein has a unique structure and generalizations about stabilization effects on specific surfaces are therefore not universal applicable. For this reason different approaches have been investigated to achieve surface modifications, which can lead to improved biocatalytic activity of immobilized enzymes. Surface functionalizations with charged,[16,17] hydrophilic,[18] or hydrophobic[19] moieties as well as functional groups, to which enzymes can bind covalently,[20] have been investigated. Direct attachment to the surface via covalent binding leads to structurally confined and rigid immobilized enzymes with strong interactions between the surface and the enzyme.[14] Polymers grafted to or from a surface[21–23] as well as surface bound tethers[24,25] can act as spacers between surface and enzyme, which offers higher mobility of the enzyme. This may either result in an improved enzyme activity, or this may negatively impact the stability due to higher mobility and reduced rigidity. Consequently, the final result on activity and stability will be a balance between several effects, which should be identified for each specific enzyme.

Different materials like glass, metals or polymers can serve as a solid support for enzyme immobilization. The easy processibility of polymers, adjustable mechanical properties, conductivity, and ease of post-functionalization make polymers an extensively used support material.[26] Recently, the development of stoichiometric thiol-ene (STE) and furthermore off-stoichiometric thiol-ene (OSTE) polymer thermosets with tunable mechanical properties was reported.[27–30] OSTE materials show high compatibility with many solvents, are thermally stable and can directly be surface functionalized after preparation. Here, thiol and alkene containing monomers undergo cross-linking by thiol-ene chemistry (TEC) under radical conditions. TEC is an efficient method providing high yields under relatively mild reaction conditions.[31] This highly modular system has allowed STE and OSTE materials to be applied for fabrication of microfluidics,[32,33] particles,[34] hydrogels,[35] or high internal phase emulsions (HIPE).[36] Variations in stoichiometry between the reagents lead to either unreacted thiol or alkene groups, which are present in the bulk OSTE material as well as on the surface. This excess of functional groups can be used further for surface modification via TEC.[37–40] Hence, surface hydrophilization, hydrophobization, as well as introduction of biological moieties has been reported.[41–43] Post preparation modification of the materials has even been shown to be possible by incorporation of glycidyl methacrylate into a photocurable TE material, which resulted in unreacted epoxide groups after curing. These residual functionalities were used for covalent immobilization of α-amylase for the preparation of a biocatalytic surface.[44]

However, due to the vast amount of existing enzyme support resins, the selection of a suitable candidate for specific enzymes is very difficult, as a beneficial match surface-enzyme cannot be generally predicted by just considering the chemistry of the support surface and its potential interaction with the enzyme. For instance, these interactions can be of hydrophilic or hydrophobic nature as well as formed hydrogen bonds, which show a different influence on different enzymes and thus, impact their biocatalytic performance. Therefore, the objective of this study was to develop a single, versatile platform that allows broader screening of different surface chemistries for enzyme immobilization. For this purpose the high modularity in preparation of TE materials and their possibility for facile surface modification was exploited to illustrate their potential as support for the immobilization of enzymes. An STE/OSTE microplate was fabricated, which enabled versatile surface functionalization via photochemical TEC or in a new approach through surface chain transfer free radical polymerization (SCT-FRP). Initial activity measurements of immobilized horseradish peroxidase as a model enzyme on those surfaces were conducted, which were used for evaluation of beneficial surface chemistries as enzyme support. Such a microplate permits screening of synergistic interactions between enzymes and surfaces in a time-saving, systematic approach, which should enable facile identification of efficient immobilization systems.

Materials and Methods

Materials

Pentaerythritol tetrakis(3-mercaptopropionate) (PETMP, >95%), 1,3,5-Triallyl-1,3,5-triazine-2,4,6(1H,3H,5H)-trione (TATATO, 98%), allyl pentafluorobenzene (APFB, >99%), allyltrifluoroacetate (ATFA, 98%), allyl alcohol (AA, 99%), allyl malonic acid (AMA, ≥98%), 1-vinyl imidazole (Vim, ≥99%), allylamine hydrochloride (Aam, 98%), [2-(Methacryloyloxy)ethyl]dimethyl-(3-sulfopropyl)ammonium hydroxide (97%) as a sulfobetaine methacrylate (SBMA), 2,2-dimethoxy-2-phenylacetophenone (DMPA, 99%), allyl glycidyl ether (AGE, >99%), horseradish peroxidase (HRP, lyophilized powder, 50–150 U mg^{-1}), 2,2′-Azino-bis(3-ethylbenzothiazoline-6-sulfonic acid) diammonium salt (ABTS, ≥98%) and hydrogen peroxide (H_2O_2, 3%) were obtained from Sigma Aldrich and used without further purification.

Methoxy poly(ethylene glycol) monomethacrylate (MPEGMA, M_n 500), glycidyl methacrylate (GMA, 97%) and 2,2,3,3,4,4,5,5 octafluoropentyl acrylate (OFPA, 97%) were purchased from Sigma Aldrich and passed through a

short plug flow column containing aluminum oxide (Sigma-Aldrich, activated, basic, Brockmann I, standard grade) prior to use. Ethanol was obtained from VWR Chemical. Lucirin TPO-L (ethyl-2, 4, 6-tri- methylbenzoylphenyl phosphinate) was obtained from IGM Resins. Sylgard 184 – poly(dimethylsiloxane) (PDMS) elastomer kit was purchased from Dow Corning.

Characterization

Fourier transform infrared (FT-IR) spectroscopy was performed using a Nicolet iS50 FT-IR fitted with a diamond crystal attenuated total reflection accessory (ATR), which operated at a resolution of 4 cm^{-1} and 32 scans per measurement and was used to identify chemical modifications made by surface functionalization. XPS experiments were conducted on a Thermo Fisher Scientific K-Alpha (East Grinstead, UK). Large area surface analysis used a 400 μm spot of monochromatized aluminum Kα radiation, following which survey (pass energy 200 eV) and high-resolution (pass energy 50 eV) spectra for relevant elements were acquired. Data analyses of the obtained XPS spectra were performed using the Avantage software package as provided by the manufacturer. Average values and standard deviations were conducted for each surface in technical replicates of three ($n = 3$). Static water contact angles (WCAs) of the virgin and functionalized OSTE surfaces were determined by using a Dataphysics Contact Angle System OCA20. Each surface was tested via the static sessile drop method at 23°C, the average value and standard deviations were determined from three technical replicates ($n = 3$).

The immobilization yield of rhodamine labeled HRP in the wells was determined using a POLARstar® Omega from BMG Labtech equipped with a fluorescence probe (gain of 1,000 as a general setting of the instrument) at 25°C. This value was subtracted by the fluorescence intensity result measured prior enzyme immobilization. The enzyme activity of immobilized Rho-HRP was determined by absorbance measurements (at 414 nm) using a POLARstar® Omega from BMG Labtech equipped with a UV-VIS probe (20 scans per measurement) at 25°C. For each surface, immobilization of Rho-HRP including FI and enzyme activity measurements, were performed in experimental replicates of three ($n = 3$), from which the average values and standard deviations were calculated.

Preparation of OSTE microtiter plate

In a stoichiometric ratio between thiol and ene groups, PETMP (24.44 g, 0.050 mol, 0.20 mol *thiol*), TATATO (16.64 g, 0.067 mol, 0.20 mol *ene*) and TPO-L (11.1 mg, 0.03 wt%) were mixed with a dual asymmetric centrifuge Speed-Mixer, High Wycombe, UK, DAC 150 FVZ-K at 2,500 to 3,500 r.p.m. for 2 min screened from ambient light. A previously prepared PDMS mold with the negative imprint of the top part of the microtiter plate was filled with this mixture, which was subsequently cured under UV light ($\lambda =$ 365 nm, 2.9 mW cm^{-2}) for 3 min. Then, PETMP (22.06 g, 0.045 mol, 0.18 mol *thiol*), TATATO (7.91 g, 0.032 mol, 0.095 mol *ene*) and TPO-L (8.1 mg, 0.03 wt%) were mixed in a Speed-mixer and a second PDMS mold for the bottom component was filled with this mixture. This mixture was left under sunlight for 7 min and then the previously top component was attached from the top. This assembly was again cured under UV light ($\lambda =$ 365 nm, 2.9 mW cm^{-2}) for 3 min resulting in the final microwell plate. A schematic drawing with measures of the top and bottom component of the microwell plate separately is shown in Supporting Information Figure S1.

IR (cm^{-1}): 2,961 (C-H), 2,571 (S-H), 1,731 (C = O), 1,678 (C = C_{alkene}), 1,459 (O-$CH_{2\ ester}$), 1,351, 1,141 (C-O-$C_{stretch\ vibr}$), 1,021 (C-O-C), 764(C-O-$C_{deformation}$), 528.

Surface functionalization via TEC with allyl pentafluorobenzene (OSTE-APFB)

In a general functionalization procedure, an ethanolic solution (10 mL) containing APFB (0.460 mL, 3.0 mmol) and TPO-L (9.9 mg, 1 mol%) was prepared screened from ambient light. 300 μL of this solution was added to a single well and subsequently irradiated with UV light ($\lambda =$ 365 nm, 2.9 mW cm^{-2}) for 5 min. Subsequently, the well was thoroughly rinsed with Ethanol and finally blow dried with air. Typically, five replicates of each modification were prepared.

IR (cm^{-1}): 2,959 (C-H), 2,567 (S-H), 1,730 (C = O), 1,678 (C = C_{alkene}), 1,459 (O-$CH_{2\ ester}$), 1,352, 1,140 (C-O-$C_{stretch\ vibr}$), 1,022 (C-O-C), 764 (C-O-$C_{deformation}$), 528.

Preparation of OSTE-ATFA

OSTE-ATFA was prepared in accordance with the general procedure, using 300 μL of an ethanolic solution (10 mL) of allyltrifluoroacetate (ATFA, 0.27 mL, 2.1 mmol) and TPO-L (9.0 mg, 0.7 mol%) as reagents.

IR (cm^{-1}): 2,961 (C-H), 2,571 (S-H), 1,731 (C = O), 1,678 (C = C_{alkene}), 1,459 (O-$CH_{2\ ester}$), 1,353, 1,141 (C-O-$C_{stretch\ vibr}$), 1,021 (C-O-C), 764 (C-O-$C_{deformation}$), 528.

Preparation of OSTE-OFPA. OSTE-OPFA was prepared in accordance with the general procedure, using 300 μL an ethanolic solution (10 mL) of 2,2,3,3,4,4,5,5 octafluoropentyl acrylate (OFPA, 0.58 mL, 3.0 mmol) and TPO-L (9.3 mg, 0.97 mol%) as reagent.

IR (cm^{-1}): 2,961 (C-H), 2,570 (S-H), 1,730 (C = O), 1,678 (C = C_{alkene}), 1,459 (O-$CH_{2\ ester}$), 1,353, 1,141 (C-O-$C_{stretch\ vibr}$), 1,021 (C-O-C), 764 (C-O-$C_{deformation}$), 528.

Preparation of OSTE-AA. OSTE-AA was prepared in accordance with the general procedure, using 300 μL of an ethanolic solution (10 mL) of allyl alcohol (AA, 0.20 mL, 3.0 mmol) and TPO-L (10.5 mg, 1.1 mol%) as reagent.

IR (cm^{-1}): 2,961 (C-H), 2,570 (S-H), 1,731 (C = O), 1,678 (C = C_{alkene}), 1,459 (O-$CH_{2\ ester}$), 1,353, 1,141 (C-O-$C_{stretch\ vibr}$), 1,020 (C-O-C), 764 (C-O-$C_{deformation}$), 528.

Preparation of OSTE-AMA. OSTE-AMA was prepared in accordance with the general procedure, using 300 μL of an ethanolic solution (10 mL) of allyl malonic acid (AMA, 0.433 g, 3.0 mmol) and TPO-L (10.4 mg, 1.1 mol%) as reagent.

IR (cm^{-1}): 2,961 (C-H), 2,571 (S-H), 1,731 (C = O), 1,678 (C = C_{alkene}), 1,459 (O-$CH_{2\ ester}$), 1,353, 1,141 (C-O-$C_{stretch\ vibr}$), 1,021 (C-O-C), 764 (C-O-$C_{deformation}$), 528.

Preparation of OSTE-Vim. OSTE-Vim was prepared in accordance with the general procedure, using 300 μL of an ethanolic solution (10 mL) of 1-vinyl imidazole (Vim, 0.30 mL, 3.0 mmol) and TPO-L (9.2 mg, 1.0 mol%) as reagent.

IR (cm^{-1}): 3,136 (N-H), 2,961 (C-H), 2,571 (S-H), 1,730 (C = O), 1,677 (C = C_{alkene}), 1,459 (O-$CH_{2\ ester}$), 1,352, 1,139 (C-O-$C_{stretch\ vibr}$), 1,024 (C-O-C), 763 (C-O-$C_{deformation}$), 528.

Preparation of OSTE-AGE. OSTE-AGE was prepared in accordance with the general procedure, using 300 μL of an ethanolic solution (10 mL) of allyl glycidyl ether (AGE, 0.36 mL, 3.0 mmol) and TPO-L (9.0 mg, 0.97 mol%) as reagent.

IR (cm^{-1}): 2,961 (C-H), 2,567 (S-H), 1,730 (C = O), 1,678 (C = C_{alkene}), 1,459 (O-$CH_{2\ ester}$), 1,353, 1,140 (C-O-$C_{stretch\ vibr}$), 1,021 (C-O-C), 764 (C-O-$C_{deformation}$), 527.

Preparation of OSTE-Aam hc. OSTE-Aam hc was prepared in accordance with the general procedure, using 300 μL of an ethanolic solution (10 mL) of allylamine hydrochloride (Aam hc, 0.281 g, 3.0 mmol) and TPO-L (10.1 mg, 1.1 mol%) as reagent.

IR (cm^{-1}): 2,962 (C-H), 2,571 (S-H), 1,731 (C = O), 1,678 (C = C_{alkene}), 1,459 (O-$CH_{2\ ester}$), 1,353, 1,141 (C-O-$C_{stretch\ vibr}$), 1,020 (C-O-C), 764 (C-O-$C_{deformation}$), 528.

Surface functionalization via surface chain transfer free radical polymerization (SCT FRP) with poly(ethylene glycol) methylether methacrylate (OSTE-g-pMPEGMA)

In a general procedure Methoxy poly(ethylene glycol) monomethacrylate (MPEGMA, 0.92 mL, 2.0 mmol) and 2,2-dimethoxy-2-phenylacetophenone (DMPA, 2.6 mg, 0.50 mol%) were dissolved in ethanol (1.85 mL) screened from ambient light. 300 μL of this solution was added to a single well and subsequently irradiated with UV light (λ= 365 nm, 2.9 mW cm^{-2}) for 30 min. Subsequently, the well was thoroughly rinsed with Ethanol and finally blow dried with air. Typically, five wells in the same well plates were functionalized.

IR (cm^{-1}): 2,871 (C-H), 1,733 (C = O), 1,684 (C = C_{alkene}), 1,461 (O-$CH_{2\ ester}$), 1,349, 1,101 (C-O-$C_{stretch\ vibr}$), 1,035 (C-O-C), 944, 852, 764 (C-O-$C_{deformation}$), 528.

Preparation of OSTE-g-pGMA. OSTE-g-pGMA was prepared in accordance with the general procedure, using 300 μL of a solution of glycidyl methacrylate (GMA, 0.453 mL, 3.3 mmol), DMPA (4.3 mg, 0.5 mol%) in ethanol (0.91 mL) as reagents.

IR (cm^{-1}): 2,999 (C-$H_{epoxide}$), 2,936 (C-H), 1,724 (C = O), 1,685 (C = C_{alkene}), 1,449 (O-$CH_{2\ ester}$), 1,129 (C-$O_{stretch\ vibr}$), 989 (C-O), 904 (epoxide ring vibr), 841 (C-C), 757 (C-O-$C_{deformation}$).

Preparation of OSTE-g-pSBMA. OSTE-g-pSBMA was prepared in accordance with the general procedure, using 300 μL of a solution of [2-(methacryloyloxy)ethyl]dimethyl-(3-sulfopropyl)ammonium hydroxide (SBMA, 0.846 g, 3.0 mmol), DMPA (3.9 mg, 0.5 mol%) in ethanol (1.28 mL) as reagents.

IR (cm^{-1}): 3,443 (N-H), 2,964 (C-H), 1,726 (C = O), 1,676 (C = C_{alkene}), 1,459 (O-$CH_{2\ ester}$), 1,143 (C-$O_{stretch\ vibr}$), 1,035, 901, 762 (C-O-$C_{deformation}$), 603, 524.

Preparation of OSTE-g-pOFPA. OSTE-g-pOFPA was prepared in accordance with the general procedure, using 300 μL of a solution of 2,2,3,3,4,4,5,5 octafluoropentyl acrylate (OFPA, 1.25 mL, 3.0 mmol), DMPA (3.1 mg, 0.4 mol%) in ethanol (0.93 mL) as reagents.

IR (cm^{-1}): 2,968 (C-H), 1,737 (C = O), 1,684 (C = C_{alkene}), 1,464 (O-$CH_{2\ ester}$), 1,163 (C-F), 1,124 (C-$O_{stretch\ vibr}$), 1,044, 805, 765 (C-O-$C_{deformation}$), 539 (C-F).

Labeling of horseradish peroxidase

Horseradish peroxidase (10.0 mg) was dissolved in sodium carbonate buffer (0.1M, pH 9.5, 1.0 mL) and 20 μL of sulforhodamine B acid chloride in DMF (10 mg mL^{-1}) was added dropwise under mild vortex mixing was added. This solution was incubated at 4°C overnight and subsequently purified by dialysis for 3 days against PBS buffer. The purified solution was stored at 4°C for further use.

Immobilization of horseradish peroxidase

The previously labeled Rho-HRP solution (0.455 mL) was diluted with PBS buffer (pH 7.3, 1.0 mL), and 300 μL of this solution was added to each well. To prevent evaporation of liquid the plate was covered with a PDMS cover and incubated at 4°C for 16 h. Then, the supernatant was removed and PBS buffer (300μL) was added to the well. The rinsing buffer was replaced four times while slowly shaking. The immobilization yield was determined via fluorescence intensity measurement of the surface.

Activity assay of bioactive surfaces

A phosphate buffer solution (0.1M, pH5, 300 μL) containing 2,2′-azino-bis(3-ethylbenzothiazoline-6-sulfonic acid) diammonium salt (ABTS, 1.0 mM) and hydrogen peroxide (10 mM) was added into a well with immobilized Rho-HRP. In the presence of H_2O_2, ABTS (absorbance maximum at 340 nm) is oxidized by HRP to $ABTS^{\bullet+}$, which shifts the absorbance maximum to 412 nm (ε_{412}=3.6 × $10^4 M^{-1}$ cm^{-1}).[45]

The absorbance at 412 nm corresponding to the absorbance maximum of the oxidized product ($ABTS^{\bullet+}$) was measured, which corresponds directly to the concentration of the product. The measurements were conducted every 20 s over 10 min directly through the well including shaking (10 s, 300 r.p.m.) between each measurement. The slope of the measurements was used as a measure for the activity of the immobilized Rho-HRP on the surface.

Results and Discussion

The preparation of STE/OSTE microplates was based on a 2-step curing process via photoinitiated TEC using pentaerythritol tetrakis(3-mercaptopropionate) (PETMP) and 1,3,5-triallyl-1,3,5-triazine-2,4,6(1H,3H,5H)-trione (TATATO) as shown in Figure 1A.

In a first stage, the top part of the microplate in a STE mixture of PETMP and TATATO was photochemically cured in the presence of TPO-L in a poly(dimethylsiloxane) (PDMS) mold, as shown in Figure 1A-1. The mold consisted of the outer geometries of the microplate (127.7 × 85.6 mm^2), pillars with the size of the round wells (diameter 15.1 mm) and a depth of 5 mm. A second mold with a depth of 1.5 mm and the outer diameters of the microtiter plate was then applied for the second curing step. Here, an OSTE composition of PETMP, TATATO, and TPO-L using a 90% excess of thiol was applied for the well bottom. The previously prepared STE top part was then placed on top of the uncured OSTE mixture and both parts were cured together

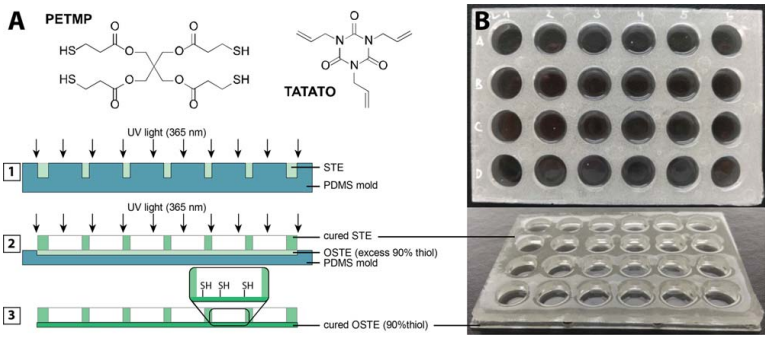

Figure 1. (A) schematic representation of the microplate preparation using a 2-step curing process, (1) curing by irradiation with UV light of the top part prepared from a stoichiometric thiol-ene (STE) mixture of PETMP and TATATO in a PDMS mold, (2) the prepared top part is placed on a OSTE mixture (excess 90% thiol) of PETMP and TATATO, where a second curing step by irradiation with UV light leads to the final microplate, (3) which contain excess thiol groups in the bottom and STE on the well walls, (B) Photographs of the final microwell plate.

(see Figure 1A-2). This preparation process resulted in a fully sealed microplate consisting of 24 wells with a depth of 5 mm, shown in Figure 1A-3 and Figure 1B. Due to the used compositions, excess thiol groups remained on the bottom of each well. The side walls of the wells, based on a STE composition, did not contain any residual thiols, as determined using Ellman's reagent, which is commonly used for quantification of thiol groups either on surfaces or in solution (see Supporting Information Figure S2).[46] From these results it could be seen that Ellman's reagent, which was added to a STE surface, exhibit a very low absorbance compared to the OSTE with 90% excess of thiols. Therefore, it was deduced that the number of thiols on the side walls was considered negligible and that modification of surface bound thiols occurred exclusively on the bottom surfaces. Furthermore, the transmittance of the OSTE material was measured to validate the possible application in colorimetric assays. The material demonstrated a strong absorbance in the UV range from 220 to 340 nm, as shown in Supporting Information Figure S3. Between 340 and 410 nm, the transmittance increased up to 36% (absorbance = 0.44) and at any wavelength above, the material was completely transparent (absorbance < 0.15). In general, the absorbance of the STE/OSTE microplate does not substantially differ from a commercial polystyrene microplate, as indicated in Supporting Information Figure S3. Therefore, the STE/OSTE plate is well suited for any application in which absorbance measurements of solutions or surface modifications are performed.

Excess thiol groups on the bottom surface originating from the OSTE mixture allow controlled surface functionalization via TEC and SCT-FRP. In this study, the surface modification using both methods has been attempted with a large range of monomers to introduce different types of functionalities as illustrated in Scheme 1.

With the aim to develop a platform for enzyme immobilization, which enables screening of various surface functionalities and their impact on the activity of surface bound enzymes, a variety of functional monomers were utilized under TEC conditions. Based on different types of possible interactions and immobilization mechanisms various reactive moieties were selected. Hydroxyl functional groups (AA) were introduced as well as fluorine groups (APFB, ATFA and OFPA). pH responsive modifications, with either acidic groups (AMA) or basic functionalities, such as amine (Aam hc) and imidazole (Vim) were used as well. This range of introduced surface chemistries offered possible immobilization mechanisms including hydrophilic (with OSTE-AA, -AMA), hydrophobic (OSTE-APFB, -ATFA, -OFPA) and ionic interactions (OSTE-Vim and -AMA). Furthermore, epoxides were introduced (AGE) allowing bioconjugation through covalent enzymes binding with amine, thiol, imidazole or phenolic moieties from the enzyme.[6] The application of such a broad range of reagents demonstrates the great versatility of this process and can extensively be expanded, since TEC offers a vast range of surface chemistries by reaction of any allyl, vinyl or acrylic compound onto the screening platform. Photochemical surface TEC was performed with low monomer concentrations (0.3 M) in ethanol solutions to prevent polymerization reactions. The IR spectrum of the starting material (OSTE) contains typical alkane (C-H, 2,968 cm^{-1}), carbonyl (C = O, 1,729 cm^{-1}), alkene (C = C, 1,683 cm^{-1}), and aliphatic ester (C-O-C, 1,141 cm^{-1}) elements. Comparison with TEC grafted surfaces did not exhibit significant differences, as illustrated in Supporting Information Figure S4. This could be explained by a low surface coverage due to a TE addition on the surface. Small structural changes as a result of monolayer formation can generally not be detected by attenuated total reflectance (ATR) FT-IR due to the domination of the bulk material in the spectrum, caused by the penetration depth of the IR signal. However, by using X-ray photoelectron spectroscopy (XPS) in combination with static water contact angle (WCA) measurements, the individual modifications were confirmed, as shown in Table 1 for the virgin (OSTE) and TEC modified surfaces.

In parenthesis, theoretical atom composition of the virgin surface (OSTE), results are based on three replicated measurements on the same surface ($n = 3$)

The atom composition of the unreacted OSTE surface estimated by XPS was in agreement with the theoretical values and therefore used for further comparisons with modified surfaces. Surface functionalization with fluorinated reagents such as APFB, ATFA, and OFPA was confirmed by the presence of fluorine atoms (F1s) in the XPS spectra, which was not detected on the native OSTE surface. APFB modified OSTE exhibited with 1.4 atom% the lowest fluorine

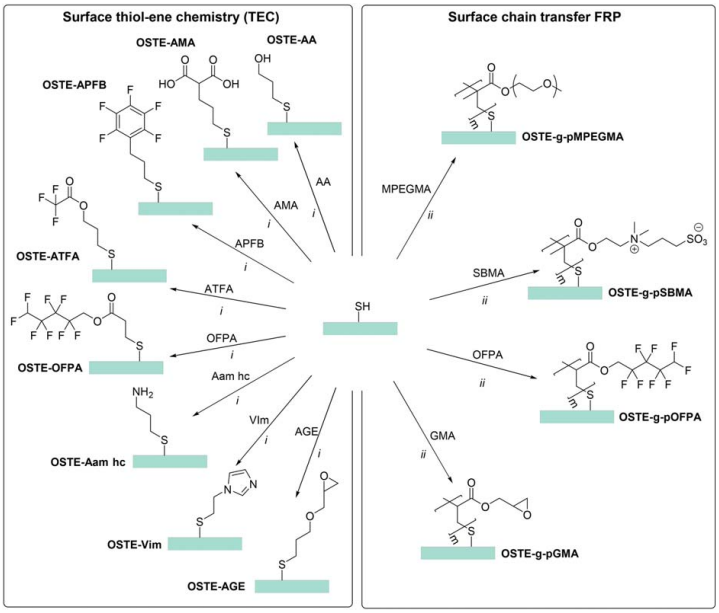

Sch 1. Surface functionalization of thiols from OSTE microwell surfaces via two different routes; left: surface thiol-ene chemistry (TEC) with allyl alcohol (AA), allyl malonic acid (AMA), allyl pentafluorobenzene (APFB), allyl trifluoroacetate (ATFA), 2,2,3,3,4,4,5,5 octafluoropentyl acrylate (OFPA), allyl amine hydrochloride (Aam hc), 1-vinyl imidazole (Vim) and allyl glycidyl ether (AGE) at low concentration (0.3 M) leading to a functional monolayer on the surface; right: SCT-FRP with methoxy poly(ethylene glycol) methacrylate (MPEGMA), zwitterionic sulfobetaine methacrylate (SBMA, via [2-(methacryloyloxy)ethyl]-dimethyl-(3-sulfopropyl)ammonium hydroxide), OFPA and glycidyl methacrylate (GMA) based monomers at high concentration (0.7 – 2.4 M), leading to a functional polymer grafted surface.

Table 1. XPS Data and Static Water Contact Angles (WCA) of Virgin and Functionalized OSTE Surfaces via TEC with a Variety of ene Compounds

	C1s [atom%]	O1s [atom%]	N1s [atom%]	S2p [atom%]	F1s [atom%]	WCA [°]
OSTE	61.1 ± 0.6 (60.6)	23.3 ± 0.2 (24.9)	4.5 ± 0.3 (4.1)	11.1 ± 0.3 (10.4)		67.0 ± 1.2
OSTE-APFB	58.8 ± 2.8	27.2 ± 2.0	2.7 ± 0.0	9.9 ± 0.5	1.4 ± 0.3	62.4 ± 2.1
OSTE-ATFA	55.3 ± 0.0	28.6 ± 0.1	5.2 ± 0.2	8.1 ± 0.2	2.8 ± 0.1	41.1 ± 2.4
OSTE-OPFA	53.4 ± 0.4	26.9 ± 0.1	4.5 ± 0.3	8.1 ± 0.0	7.1 ± 0.6	77.7 ± 4.1
OSTE-AA	60.4 ± 0.2	27.6 ± 0.7	4.5 ± 0.5	7.6 ± 0.4		35.0 ± 1.5
OSTE-AMA	61.3 ± 0.1	27.8 ± 0.1	4.2 ± 0.0	6.7 ± 0.1		25.1 ± 3.6
OSTE-Vim	63.3 ± 1.5	22.6 ± 0.8	7.3 ± 0.2	6.8 ± 0.5		38.5 ± 3.6
OSTE-AGE	58.7 ± 0.6	28.7 ± 0.3	4.2 ± 0.3	8.4 ± 0.2		55.9 ± 3.7
OSTE- Aam hc	59.3 ± 0.2	26.5 ± 0.1	5.5 ± 0.1	8.7 ± 0.1		55.4 ± 4.7

content, which suggested a low grafting efficiency. This could be improved by reaction with ATFA and OFPA (2.8 and 7.1 atom%). In contrast to the allylic reagents, OFPA being an acrylic monomer is prone to undergo polymerization under radical conditions. Here, the overall atom composition of OFPA modified surfaces under TEC conditions, showed additional to the increase in fluorine content a slight reduction in carbon, sulfur and nitrogen. This confirmed that under the applied low concentration TEC conditions, even for an acrylic monomer, like OFPA, the addition reaction dominated, leading to the formation of a monolayer (polymerization could then be suppressed). The atom composition after surface TEC with AMA, AA and AGE did not differ significantly from the reference OSTE surface. This could be attributed to similar theoretical atom composition of these reagents and the OSTE base material. In contrast, surface functionalization via TEC of Vim and Aam hc could be clearly confirmed by a significant increase in nitrogen (N1s) content, from 4.5 (OSTE) to 7.3 and 5.5 atom%, respectively. Vim is a reactive monomer and known to polymerize under radical condition, which could explain the relatively strong increase in nitrogen content using Vim.[47] Consequently, the high reactivity of Vim could have led to the formation of short polymer grafts on the surface, even at low concentrations and short reaction times.

In addition to XPS analysis, the impact of the different surface modifications was also investigated by water contact angle (WCA) measurements. The WCA of APFB reacted surface (62.4°) changed slightly compared to the reference surface (OSTE, 67.0°), which was assumed to be the result of the low reactivity, as already seen from the XPS data. A similar trend was observed for OSTE-ATFA, where the WCA was reduced more significantly to 41.1° upon modification. This was attributed to the polar nature of ATFA. As

expected, increased hydrophobicity of the surface was achieved via functionalization with OFPB, which was confirmed by a WCA of 77.0°. Reduced WCAs of 35.0° (OSTE-AA), 25.1° (OSTE-AMA) and 55.2° (OSTE-AGE) were observed due to the introduction of hydroxyl, carboxylic acid and epoxide groups via surface TEC with AMA, AA and AGE. Similarly, WCAs of 38.5° (OSTE-Vim) and 55.4° (OSTE-Aam hc) validated the functionalization with Vim and Aam hc. This illustrates the versatility of the system providing successful surface modification by TEC and that the surface properties of the microplate wells could be adjusted by the formation of a functional monolayer.

Additionally, thiol groups are known to serve as chain transfer agents in free radical polymerization reactions to reduce molecular weight of the polymers. Surface bound thiols can act in a similar way as reported earlier for other types of surfaces, where the surface could be grafted by termination of growing polymer chains.[48–50] In this study, we have expanded this SCT-FRP approach as an alternative method to TEC for controlled surface modification of OSTE materials. Different acrylic and methacrylic monomers containing polyethylene glycol (PEG) (via MPEGMA), a zwitterionic sulfobetaine (SBMA), fluorine (OFPA) and epoxide groups (GMA) were utilized. In this case, by running the photochemical reaction at a higher concentration, polymer grafting onto the well surfaces could be achieved by SCT-FRP in the presence of DMPA as radical photoinitiator, as shown in Scheme 1. Typically, the liquid monomers were used in a 1:2 volume ratio in ethanol, whereas SBMA, being a solid, was applied in a concentration of 2.4 M. In contrast to TEC, surface modification via SCT-FRP can be confirmed by IR spectroscopy, as illustrated in Figure 2.

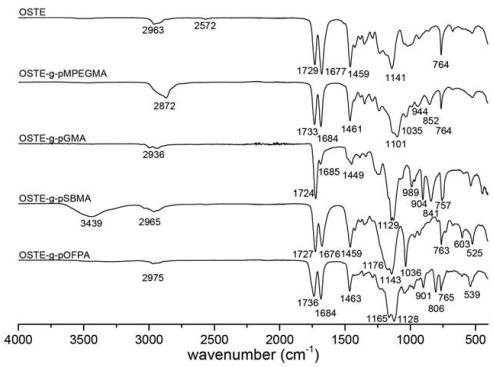

Figure 2. IR spectra of virgin OSTE surface and OSTE grafted via SCT FRP with various acrylate and methacrylate based polymer, such as MPEGMA, GMA, SBMA or OFPA.

A clear indication of the formation of a thick surface layer by SCT-FRP is the full disappearance of the S-H stretch band at 2,572 cm^{-1} upon surface polymerization of each monomer. The spectrum of OSTE-g-pMPEGMA showed a strong absorption at 1,100 cm^{-1}, which can be assigned to C-O-C stretch vibration originating from the PEG side chain. An additional band at 904 cm^{-1} for the OSTE-g-pGMA is observed, which is the epoxide ring vibration. In the IR spectrum of the OSTE surface upon grafting with pSBMA, a band at 3,439 cm^{-1} indicates the ammonium N-H stretch vibration. Furthermore a broadening of the C-O-C stretch absorption at 1,143 cm^{-1} as well as the strong band at 1,036 cm^{-1} confirms the presence of pSBMA. Surface grafting with pOFPA led to the appearance of carbon-fluorine bands at 1,163, 806, and 539 cm^{-1}. XPS and WCA analysis corroborated these results, which are presented in Table 2.

XPS analysis of a pMPEGMA grafted surface (OSTE-g-pMPEGMA) showed significantly increased carbon and oxygen contents, which is consistent with the theoretical value of MPEGMA. Combination with the simultaneous decrease in sulfur and nitrogen confirms the polymer grafting of the OSTE-g-pMPEGMA surface. Similar XPS results were achieved by polymer grafting with pGMA, where the oxygen and carbon content increased approaching the theoretical value of the monomer. The amount of nitrogen and sulfur was even lower compared to OSTE-g-pMPEGMA, indicating an even thicker pGMA layer. The theoretical atom composition of SBMA is more similar to that of the OSTE background, which leads to only minor changes in the atom composition as a result of grafting. However, the content of the individual atoms from the OSTE-g-pSBMA surface approximated the theoretical values of the SBMA monomer, substantiating the success of the grafting reaction. Compared to the aforementioned surface modification via TEC with OFPA, polymerization conditions (higher concentration, longer reaction time) lead here to the appearance of a much higher fluorine content of 44.0 atom% compared to the 7.1 atom% by TEC. Additionally, the total atom composition of the OSTE-g-pOFPA surface was found to be in good agreement with that of the pure monomer, which confirms the formation of a polymer layer on the surface under SCT-FRP conditions.

Table 2. XPS Data and Static Water Contact Angles (WCA) of Virgin and Grafted OSTE Surfaces Via SCT FRP with a Variety of Acrylate and Methacrylate Based Polymers*

	C1s [atom%]	O1s [atom%]	N1s [atom%]	S2p [atom%]	F1s [atom%]	WCA [°]
OSTE	61.1 (60.6)	23.3 ± 0.2 (24.9)	4.5 ± 0.3 (4.1)	11.1 ± 0.3 (10.4)		67.0 ± 1.2
OSTE-g-pMPEGMA	65.6 ± 0.6 (67.6)	30.1 ± 0.2 (32.4)	0.5 ± 0.4 (0.0)	3.9 ± 0.2 (0.0)		25.4 ± 3.6
OSTE-g-pGMA	70.7 ± 0.4 (70.0)	28.7 ± 0.4 (30.0)	0.5 ± 0.1 (0.0)			69.6 ± 7.5
OSTE-g-pSBMA	62.9 ± 0.0 (61.1)	25.2 ± 0.0 (27.8)	4.7 ± 0.1 (5.6)	7.2 ± 0.1 (5.6)		20.4 ± 4.8
OSTE-g-pOFPA	43.2 ± 0.6 (44.4)	11.1 ± 0.3 (11.1)	0.5 ± 0.1 (0.0)	1.3 ± 0.3 (0.0)	44.0 ± 1.3 (44.4)	118.1 ± 1.9

*In parenthesis, theoretical atom composition of the virgin surface (OSTE) and monomers used for SCT FRP, results are based on three replicated measurements on the same surface ($n = 3$).

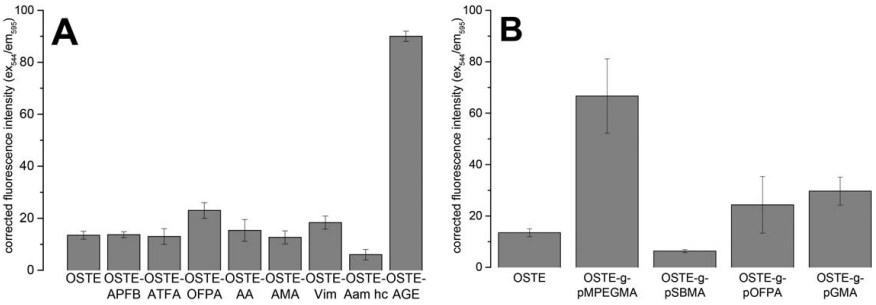

Figure 3. Reference corrected fluorescence intensity of virgin (OSTE) and functionalized surfaces via TEC (A) and SCT FRP (B) after immobilization of rhodamine labeled horseradish peroxidase (Rho-HRP), excitation at 544 nm and emission at 595 nm, standard deviations are based on three experimental replicates ($n = 3$).

These presented changes in atom composition, upon polymer grafting with the individual monomers, were corroborated by the variation in WCAs of the reacted surfaces. Grafting with pMPEGMA increased the hydrophilic character, which was shown by a reduction in WCA from 67° (OSTE) to 25.4°. Similarly, a substantial hydrophilization was achieved by grafting with pSBMA (20.4°) confirming the surface reaction. The WCA increased slightly upon SCT-FRP using GMA (69.6°). OSTE-g-pOFPA exhibits a very high WCA of 118.1° and demonstrates the drastically increased hydrophobicity of the surface upon polymer grafting, which is significantly higher than the one obtained from TEC using the same monomer (77.0°). These results, together with the earlier discussed XPS and IR data, illustrate the potential for altering surface properties through selection of reaction conditions. Low concentrations and short reaction times lead to addition of the acrylate to the thiol groups based on TEC. Increased concentrations and longer reaction times favor polymerization, which undergoes chain transfer or termination with surface thiols leading to a thicker surface coating. The application of either surface modification method, TEC or SCT-FRP, demonstrates the versatility of these grafting reactions to achieve high control over the surface functionality and properties.

The functionalized well bottom surfaces were subsequently used for enzyme immobilization. For this purpose, a rhodamine labeled horseradish peroxidase (Rho-HRP) dissolved in PBS buffer (pH7.3) was used as a model enzyme. Fluorescence intensity (FI) measurements were used to confirm the presence of immobilized enzyme on all surfaces. To evaluate qualitatively the amount of immobilized enzyme, FI measurements ($\lambda_{\text{excitation}} = 544$ nm, $\lambda_{\text{emission}} = 595$ nm) of the surfaces were conducted before (as reference) and after incubation with Rho-HRP. Figure 3 shows the reference corrected FI measurements of enzyme exposed TEC (A) and SCT-FRP modified surfaces (B).

It can be seen that the native OSTE surface exhibited a substantial FI upon exposure to Rho-HRP (Figure 3A, OSTE), which relates to significant loading of labeled enzyme on the surface. TEC functionalized surfaces, such as APFB, ATFA, AA, AMA, and Vim provided similar FI results and consequently comparable adsorption of Rho-HRP. Higher FI results are the consequence of OPFA modifications, which is an indication for increased enzyme loading. Accordingly the lower FI values of Aam hc compared to other functionalized surfaces suggest a lower enzyme coverage. Compared to all aforementioned surfaces, surface functionalization with epoxide groups due to the reaction with AGE leads to a drastic increase in FI upon exposure to enzyme, which is more than sixfold higher compared to that of the native OSTE surface. Amine groups from lysine or thiols from cysteine residues within the enzyme structure are expected to react covalently with epoxide groups on the surface and thus create a higher enzyme loading.[51]

Similar measurements were performed with surfaces functionalized by SCT-FRP, as shown in Figure 3B. The highest FI was observed for pMPEGMA modified surfaces. This result was unexpected, since PEG surface grafts were reported in the literature to exhibit anti-fouling properties and therefore reduced unspecific protein adsorption.[52,53] To explain this discrepancy, FI of Rho-HRP was measured in solution in the presence of different MPEGMA concentrations, as presented in Supporting Information Figure S5. These results show a direct correlation of FI with increasing amounts of MPEGMA. This effect of FI enhancement for Rho-HRP in the presence of MPEGMA could indicate an artificially high loading of enzyme on the OSTE-g-pMPEGMA surfaces. Good biocompatibility and anti-fouling properties have also been described for zwitterionic polymers, such as pSBMA.[54–56] Herein, pSBMA grafted surfaces with an increased hydrophilicity, show a very low FI after enzyme immobilization, which reinforces the hypothesis of low enzyme loading on these surfaces. Surface functionalization by pOFPA under SCT-FRP conditions shows slightly increased FI compared to the native OSTE surface, which is similar to that of TEC functionalized surface with OFPA (Figure 3A). Relatively similar enzyme loading based on comparable FI results were achieved by surface grafting with pGMA via SCT-FRP, even though the epoxide containing pGMA enables covalent immobilization.

A significant advantage of this platform is that biocatalytic activity of immobilized enzymes could be measured spectrophotometrically directly in a microplate reader by using a colorimetric assay. For immobilized Rho-HRP on the previously prepared surfaces by either TEC or SCT-FRP, 2,2′-azino-bis(3-ethylbenzothiazoline-6-sulfonic acid) diammonium salt (ABTS) was used as a colorimetric assay. The slope of absorbance, which correlated directly to the formed product, over time, was used to express the initial enzymatic activity of the particular surfaces, as shown in Figure 4A for TEC modified surfaces.

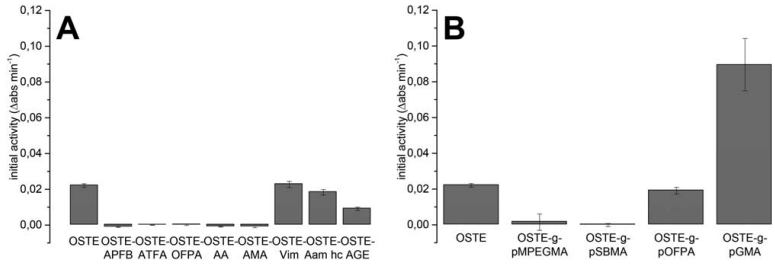

Figure 4. Initial enzyme activity of Rho-HRP immobilized on virgin (OSTE) and functionalized surfaces via TEC (A) with various ene compounds and SCT FRP (B) with various acrylate and methacrylate based polymers, standard deviations are based on three experimental replicates ($n = 3$).

From these results, a clear difference in Rho-HRP activity from the individual surface modification, upon enzyme immobilization, can be seen. In general, the displayed activities are caused by two factors, enzyme loading and biocatalytic activity, which both directly affected the overall activity. This directly reflects the influence of the individual surface chemistry. The native OSTE surface exhibited an activity of 0.022 Δabs min^{-1}. Even though TEC modified surfaces with fluorinated (APFB, ATFA and OFPA), hydroxyl (AA) and carboxylic acid containing compounds (AMA) expressed a substantial enzyme loading, these were not active at all (see Figure 4A), which suggested an unfavorable environment for the enzyme by these functional groups. On the contrary, imidazole (Vim) and amine (Aam hc) functional surfaces showed the highest initial activities for TEC modified surfaces of about 0.023 and 0.018 Δabs min^{-1}, respectively. These results indicate that amine, imidazole as well as thiol groups from the native OSTE surface provide a more beneficial local environment toward the enzyme and thus, activity was retained. FI indicated high enzyme coverage on surfaces, functionalized with epoxide groups (OSTE-AGE). However, the resulting initial activity was only 0.009 Δabs min^{-1}, which is significantly lower than that of OSTE, Vim and Aam hc surfaces. It was assumed that this is a result of unfavorable interaction of the surface with the enzyme, which is known to have a significant impact during the adsorption-covalent immobilization mechanism onto epoxy supports.[6] As a consequence, blocking of the active site or conformational changes of the enzyme could have resulted in the low activity.

Likewise, the initial enzyme activity was determined from surfaces grafted with polymer layers by SCT-FRP after Rho-HRP immobilization (see Figure 4B). Hydrophilic surfaces due to grafting with pMPEGMA and pSBMA tend to be enzymatically inactive. The low activity of OSTE-g-pSBMA correlates directly with the low enzyme loading, which was determined by FI measurements. The low activity of pMPEGMA grafted OSTE surfaces relates well with the anti-fouling nature of PEG grafted surfaces. Their tendency to FI enhancement indicates an artificially high enzyme loading. Surfaces which were grafted with hydrophobic pOFPA by SCT-FRP, exhibit a similar activity (0.019 Δabs min^{-1}) compared to the original OSTE surface, which correlates well with the results from the FI measurements. The activity was found to be substantially higher than those of surfaces with OFPA monolayer functionalization via TEC, even though both surfaces show comparable enzyme loadings. Thus, increased hydrophobic interactions between the enzyme and the surface created by a thicker surface layer seems to have a positive effect on the enzyme activity A high HRP activity (0.07 Δabs min^{-1}) can be seen from OSTE-g-pGMA surfaces prepared by SCT-FRP. GMA based polymers, bearing epoxide groups, allow covalent attachment of HRP and has already been used in various studies for enzyme immobilization.[57,58] Compared to the epoxide functional monolayer formed from AGE by TEC, the pGMA surface layer shows a decreased enzyme loading, but substantial improvement of enzymatic activity.

Conclusions

A single, versatile platform for testing a broad variety of surface chemistries as candidates for supports for enzyme immobilization is proposed in this study, with the main objective of making identification of suitable surface/enzyme combinations in a more facile and time saving manner. This strategy indeed permits a faster, easier and broader surface–enzyme screening compared to the traditional "trial and error" method generally involving resins. The results showed that the STE/OSTE microplate is suitable for colorimetric measurements above 340 nm and the thiol functional wells can be functionalized through either TEC or SCT-FRP providing a broad selection of functional surfaces. We have shown how TEC/SCT-FRP can be exploited to prepare functional monolayers (TEC) or thicker polymer layers (SCT-FRP). Thus, different surface functionalities, such as hydroxyl, carboxylic acid, amine, fluorine, imidazole, epoxide, PEG and zwitterionic groups could be introduced, which was confirmed by XPS analysis. Through immobilization of HRP as a model enzyme, the effects of surface/enzyme interactions were illustrated in the microplate, showing clear correlations between surface functionalities and enzymatic activities. HRP displayed improved activities when attached directly to imidazole, thiol and amine functional surfaces, compared to hydroxyl, fluorinated, carboxylic acid or epoxide containing surfaces. Immobilization of HRP on pOFPA modified surfaces demonstrated a significant activity, which might be caused by increased hydrophobic interactions between enzyme and surface. Based on the initial biocatalytic activities relative to the surface chemistry it is possible to identify candidates that should be tested in depth for enzyme immobilization. Thereby we have demonstrated the potential of this screening platform to be used for other enzymes, facilitating the identification of suitable surfaces for immobilization. Furthermore, by use of such a platform it would be possible to determine the influence of other

parameters, such as temperature, pH, and e.g., substrate concentration.

Acknowledgments

The authors wish to thank the Aage and Johanne Louis-Hansens Endowment for financial support.

Literature Cited

1. DiCosimo R, McAuliffe J, Poulose AJ, Bohlmann G. Industrial use of immobilized enzymes. *Chem Soc Rev*. 2013;42:6437–6474.
2. Cantone S, Ferrario V, Corici L, Ebert C, Fattor D, Spizzo P, Gardossi L. Efficient immobilisation of industrial biocatalysts: criteria and constraints for the selection of organic polymeric carriers and immobilisation methods. *Chem Soc Rev*. 2013;42:6262–6276.
3. Mateo C, Palomo JM, Fernandez-Lorente G, Guisan JM, Fernandez-Lafuente R. Improvement of enzyme activity, stability and selectivity via immobilization techniques. *Enzyme Microb Technol*. 2007;40:1451–1463.
4. Minteer SD. *Enzyme Stabilization and Immobilization*. 2nd ed. (Minteer SD, ed.). Springer Science+Business Media; 2010.
5. Balcão VM, Vila MMDC. Structural and functional stabilization of protein entities: State-of-the-art. *Adv Drug Deliv Rev*. 2015;93:25–41.
6. Mateo C, Grazú V, Pessela BCC, Montes T, Palomo JM, Torres R, López-Gallego F, Fernàndez-Lafuente R, Guisán JM. Advances in the design of new epoxy supports for enzyme immobilization–stabilization. *Biochem Soc Trans*. 2007;35:1593–1601.
7. Kallenberg AI, van Rantwijk F, Sheldon RA. Immobilization of Penicillin G acylase: The key to optimum performance. *Adv Synth Catal*. 2005;347:905–926.
8. Sheldon RA, van Pelt S. Enzyme immobilisation in biocatalysis: why, what and how. *Chem Soc Rev*. 2013;42:6223–6235.
9. Mateo C, Palomo JM, van Langen LM, van Rantwijk F, Sheldon RA. A new, mild cross-linking methodology to prepare cross-linked enzyme aggregates. *Biotechnol Bioeng*. 2004;86:273–276.
10. Mohamad NR, Marzuki NHC, Buang NA, Huyop F, Wahab RA. An overview of technologies for immobilization of enzymes and surface analysis techniques for immobilized enzymes. *Biotechnol Biotechnol Equip*. 2015;29:205–220.
11. Ying L, Kang ET, Neoh KG. Covalent immobilization of glucose oxidase on microporous membranes prepared from poly (vinylidene fluoride) with grafted poly(acrylic acid) side chains. *J Memb Sci*. 2002;208:361–374.
12. Secundo F. Conformational changes of enzymes upon immobilisation. *Chem Soc Rev*. 2013;42:6250–6261.
13. Rodrigues RC, Ortiz C, Berenguer-Murcia Á, Torres R, Fernández-Lafuente R. Modifying enzyme activity and selectivity by immobilization. *Chem Soc Rev*. 2013;42:6290–6307.
14. Talbert JN, Goddard JM. Enzymes on material surfaces. *Colloids Surfaces B Biointerfaces*. 2012;93:8–19.
15. Santos JCS, Dos, Barbosa O, Ortiz C, Berenguer-Murcia A, Rodrigues RC, Fernandez-Lafuente R. Importance of the support properties for immobilization or purification of enzymes. *ChemCatChem*. 2015;7:2413–2432.
16. Hamlin RE, Daytong TL, Johnson LE, Johal MS. A QCM study of the immobilization of b-galactosidase on polyelectrolyte surfaces: Effect of the terminal polyion on enzymatic surface activity. *Langmuir*. 2007;23:4432–4437.
17. Malinin AS, Rakhnyanskaya AA, Bacheva AV, Yaroslavov AA. Activity of an enzyme immobilized on polyelectrolyte multilayers. *Polym Sci Ser A*. 2011;53:52–56.
18. Cheng Z, Teoh S-H. Surface modification of ultra thin poly (ε-caprolactone) films using acrylic acid and collagen. *Biomaterials*. 2004;25:1991–2001.
19. Misson M, Dai S, Jin B, Chen BH, Zhang H. Manipulation of nanofiber-based β-galactosidase nanoenvironment for enhancement of galacto-oligosaccharide production. *J Biotechnol*. 2016;222:56–64.
20. Cao L. Covalent enzyme immobilization. In: *Carrier-Bound Immobilized Enzymes: Principles, Application and Design*. Wiley-VCH; 2006:169–316.
21. Huang J, Li X, Zheng Y, Zhang Y, Zhao R, Gao X, Yan H. Immobilization of penicillin G acylase on poly[(glycidyl methacrylate)-co-(glycerol monomethacrylate)]-grafted magnetic microspheres. *Macromol Biosci*. 2008;8:508–515.
22. Bayramoglu G, Karagoz B, Altintas B, Arica MY, Bicak N. Poly(styrene–divinylbenzene) beads surface functionalized with di-block polymer grafting and multi-modal ligand attachment: performance of reversibly immobilized lipase in ester synthesis. *Bioprocess Biosyst Eng*. 2011;34:735–746.
23. Chen H, Teramura Y, Iwata H. Co-immobilization of urokinase and thrombomodulin on islet surfaces by poly(ethylene glycol)-conjugated phospholipid. *J Control Release*. 2011;150:229–234.
24. Manta C, Ferraz N, Betancor L, Antunes G, Batista-Viera F, Carlsson J, Caldwell K. Polyethylene glycol as a spacer for solid-phase enzyme immobilization. *Enzyme Microb Technol*. 2003;33:890–898.
25. Mahoney KW, Talbert JN, Goddard JM. Effect of polyethylene glycol tether size and chemistry on the attachment of lactase to polyethylene films. *J Appl Polym Sci*. 2013;127:1203–1210.
26. Goddard JM, Hotchkiss JH. Polymer surface modification for the attachment of bioactive compounds. *Prog Polym Sci*. 2007;32:698–725.
27. Campos LM, Meinel I, Guino RG, Schierhorn M, Gupta N, Stucky GD, Hawker CJ. Highly versatile and robust materials for soft imprint lithography based on thiol-ene click chemistry. *Adv Mater*. 2008;20:3728–3733.
28. Khire VS, Yi Y, Clark NA, Bowman CN. Formation and surface modification of nanopatterned thiol-ene substrates using step and flash imprint lithography. *Adv Mater*. 2008;20:3308–3313.
29. Carlborg CF, Haraldsson T, Öberg K, Malkoch M, van der Wijngaart W. Beyond PDMS: off-stoichiometry thiol–ene (OSTE) based soft lithography for rapid prototyping of microfluidic devices. *Lab Chip*. 2011;11:3136.
30. Mongkhontreerat S, Öberg K, Erixon L, Löwenhielm P, Hult A, Malkoch M. UV initiated thiol–ene chemistry: a facile and modular synthetic methodology for the construction of functional 3D networks with tunable properties. *J Mater Chem A*. 2013;1:13732–13737.
31. Lowe AB. Thiol-ene "click" reactions and recent applications in polymer and materials synthesis. *Polym Chem*. 2010;1:17–36.
32. Tähkä SM, Bonabi A, Nordberg ME, Kanerva M, Jokinen VP, Sikanen TM. Thiol-ene microfluidic devices for microchip electrophoresis: Effects of curing conditions and monomer composition on surface properties. *J Chromatogr A* 2015;1426:233–240.
33. Mazurek P, Daugaard AE, Skolimowski M, Hvilsted S, Skov AL. Preparing mono-dispersed liquid core PDMS microcapsules from thiol–ene–epoxy-tailored flow-focusing microfluidic devices. *RSC Adv*. 2015;5:15379–15386.
34. Durham OZ, Norton HR, Shipp DA. Functional polymer particles via thiol–ene and thiol–yne suspension "click" polymerization. *RSC Adv*. 2015;5:66757–66766.
35. Aimetti AA, Machen AJ, Anseth KS. Poly(ethylene glycol) hydrogels formed by thiol-ene photopolymerization for enzyme-responsive protein delivery. *Biomaterials*. 2009;30:6048–6054.
36. Lovelady E, Kimmins SD, Wu J, Cameron NR. Preparation of emulsion-templated porous polymers using thiol–ene and thiol–yne chemistry. *Polym Chem*. 2011;2:559–562.
37. Zhang J, Chen Y, Brook MA. Facile functionalization of PDMS elastomer surfaces using thiol− ene click chemistry. *Langmuir*. 2013;29:12432–12442.
38. Wasserberg D, Steentjes T, Stopel MHW, Huskens J, Blum C, Subramaniam V, Jonkheijm P. Patterning perylenes on surfaces using thiol–ene chemistry. *J Mater Chem*. 2012;22:16606–16610.
39. Han X, Wu C, Sun S. Photochemical reactions of thiol-terminated self-assembled monolayers (SAMs) for micropatterning of gold nanoparticles and controlled surface functionality. *Appl Surf Sci*. 2012;258:5153–5156.

40. Tan KY, Ramstedt M, Colak B, Huck WTS, Gautrot JE. Study of thiol–ene chemistry on polymer brushes and application to surface patterning and protein adsorption. *Polym Chem.* 2016;7: 979–990.
41. Pardon G, Saharil F, Karlsson JM, Supekar O, Carlborg CF, van der Wijngaart W, Haraldsson T. Rapid mold-free manufacturing of microfluidic devices with robust and spatially directed surface modifications. *Microfluid Nanofluidics.* 2014;17:773–779.
42. Carlborg CF, Moraga F, Saharil F, van der Wijngaart W, Haraldsson T. Rapid permanent hydrophilic and hydrophobic patterning of polymer surfaces via off-stoichiometry thiol-ene (OSTE) photografting. In: *Proceedings Micro Total Analysis Systems*;2012:677–679.
43. Feidenhans'l NA, Lafleur JP, Jensen TG, Kutter JP. Surface functionalized thiol-ene waveguides for fluorescence biosensing in microfluidic devices. *Electrophoresis.* 2014;35:282–288.
44. Cakmakci E, Danis O, Demir S, Mulazim Y, Kahraman MV. Alpha-amylase immobilization on epoxy containing thiol-ene photocurable materials. *J Microbiol Biotechnol.* 2013;23:205–210.
45. Childs BRE, Bardsley WG. The steady-state kinetics of peroxidase with 2,2'-azino-di-(3-ethylbenzthiazoline- 6-sulphonic acid) as chromogen. *Biochem J.* 1975;145:93–103.
46. Hansson S, Antoni P, Bergenudd H, Malmström E. Selective cleavage of polymer grafts from solid surfaces: assessment of initiator content and polymer characteristics. *Polym Chem.* 2011;2:556–558.
47. Fodor C, Bozi J, Blazsó M, Iván B. Thermal behavior, stability, and decomposition mechanism of poly(N-vinylimidazole). *Macromolecules.* 2012;45:8953–8960.
48. Liu S, Zhou F, Di D, Jiang S. Surface-confined radical chain transfer. *Colloids Surfaces A Physicochem Eng Asp.* 2004;244: 87–93.
49. Wang S, Zhou Y, Guan W, Ding B. One-step copolymerization modified magnetic nanoparticles via surface chain transfer free radical polymerization. *Appl Surf Sci.* 2008;254:5170–5174.
50. Bertin A, Schlaad H. Mild and versatile (Bio-)functionalization of glass surfaces via thiol-ene photochemistry. *Chem Mater.* 2009;21:5698–5700.
51. Jiang H, Xu F-J. Biomolecule-functionalized polymer brushes. *Chem Soc Rev.* 2013;42:3394–3426.
52. Xu FJ, Neoh KG, Kang ET. Bioactive surfaces and biomaterials via atom transfer radical polymerization. *Prog Polym Sci.* 2009; 34:719–761.
53. Xiu KM, Cai Q, Li JS, Yang XP, Yang WT, Xu FJ. Anti-fouling surfaces by combined molecular self-assembly and surface-initiated ATRP for micropatterning active proteins. *Colloids Surf B Biointerfaces.* 2012; 90:177–183.
54. Fristrup CJ, Jankova K, Hvilsted S. Surface-initiated atom transfer radical polymerization—a technique to develop biofunctional coatings. *Soft Matter.* 2009;5:4623.
55. Yue W-W, Li H-J, Xiang T, Qin H, Sun S-D, Zhao C-S. Grafting of zwitterion from polysulfone membrane via surface-initiated ATRP with enhanced antifouling property and biocompatibility. *J Memb Sci.* 2013;446:79–91.
56. Xiang T, Zhang L-S, Wang R, Xia Y, Su B-H, Zhao C-S. Blood compatibility comparison for polysulfone membranes modified by grafting block and random zwitterionic copolymers via surface-initiated ATRP. *J Colloid Interface Sci.* 2014;432: 47–56.
57. Xu FJ, Cai QJ, Li YL, Kang ET, Neoh KG. Covalent immobilization of glucose oxidase on well-defined poly(glycidyl methacrylate)-Si(111) hybrids from surface-initiated atom-transfer radical polymerization. *Biomacromolecules.* 2005;6:1012–1020.
58. Shen Y, Guo W, Qi L, Qiao J, Wang F, Mao L. Immobilization of trypsin via reactive polymer grafting from magnetic nanoparticles for microwave-assisted digestion. *J Mater Chem B.* 2013; 1:2260–2267.

Manuscript received Apr. 25, 2017, and revision received July 7, 2017.

Appendix 1.2 – Supporting information

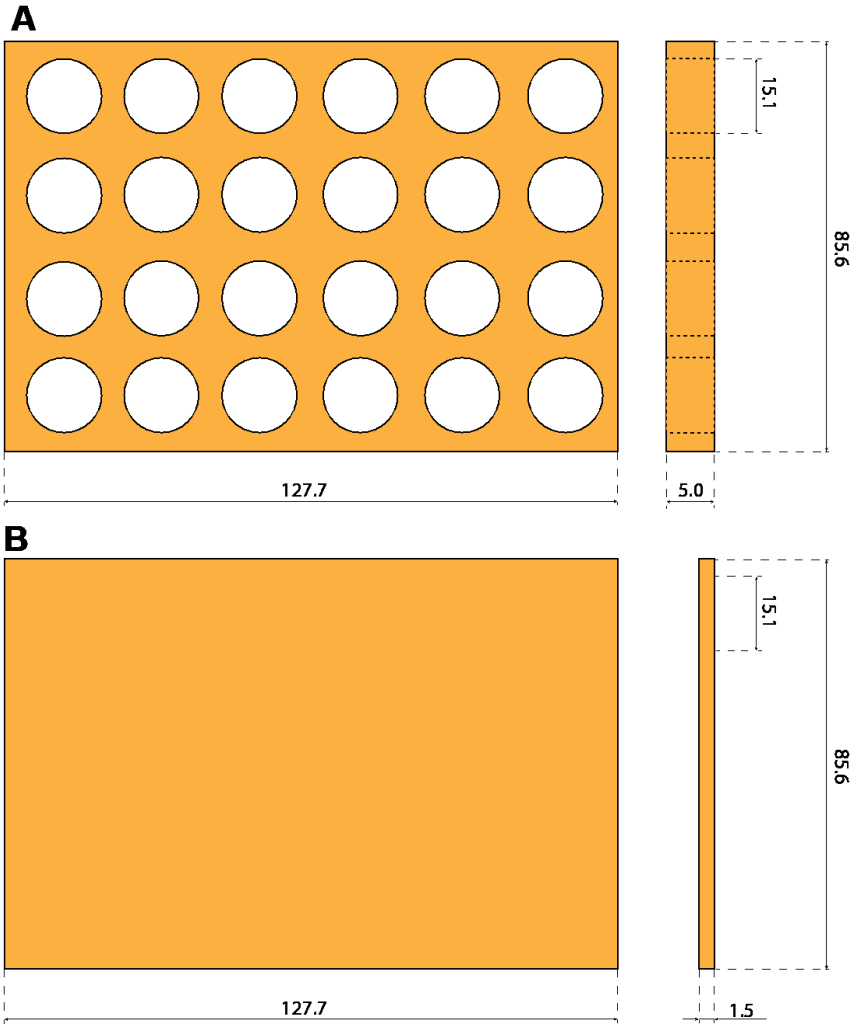

Figure S1. Schematic drawing with measures of the microwell plate; top part (A), which is during the preparation process attached to the bottom part (B)

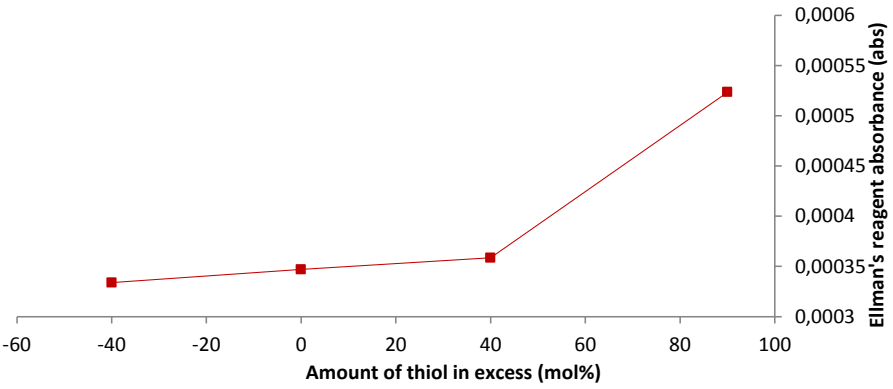

Figure S2. Ellman's test of thiol-ene (TE) surfaces with different TE ratio, absorbance measurements at 412 nm of the Ellman's reagent

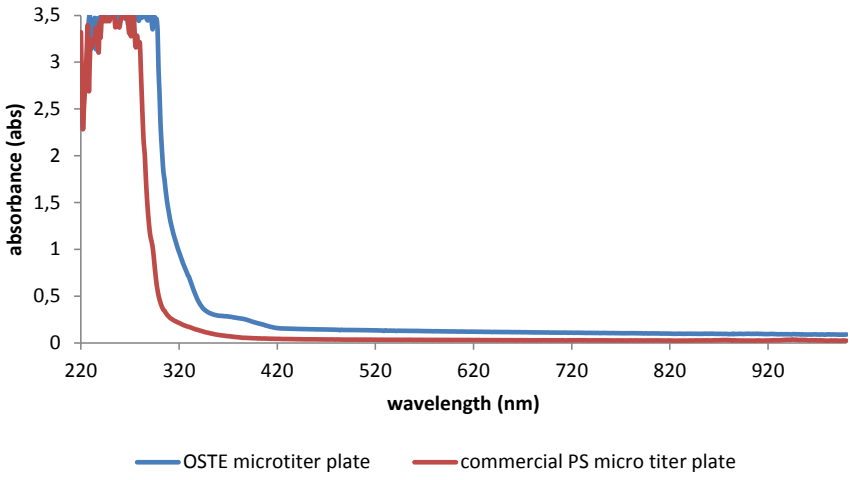

Figure S3. Absorbance measurement of OSTE microplate and a commercial PS microplate

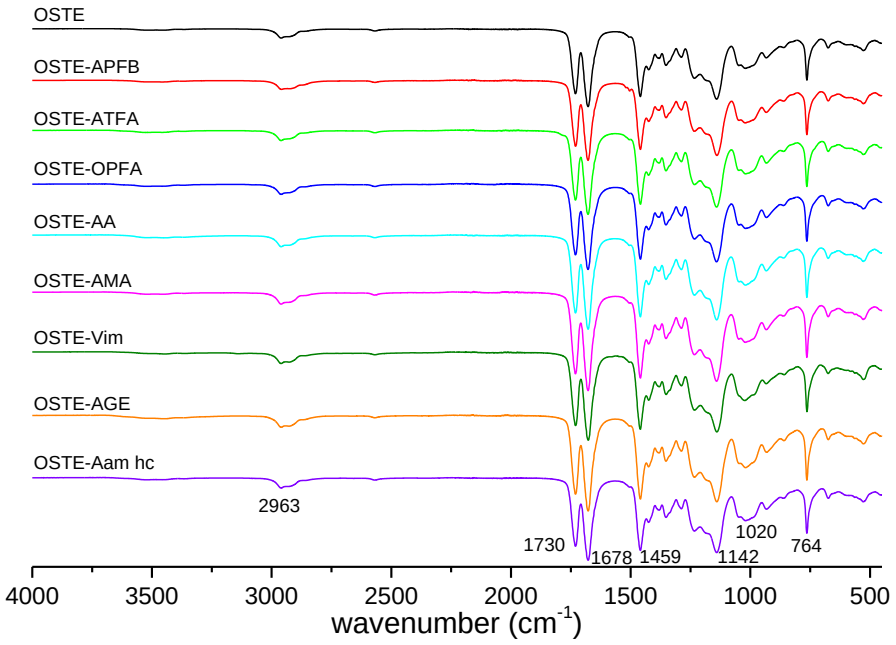

Figure S4. FT-IR spectra of TEC functionalized surfaces with various allyl, vinyl and acrylic monomers

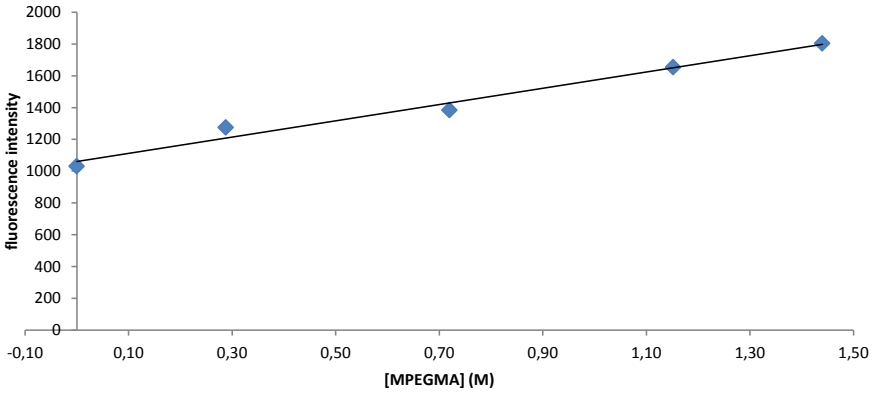

Figure S5. Fluorescence intensity measurements of Rho-HRP as a function of MPEGMA concentration

Appendix 2

Simple preparation of thiol-ene particles from glycerol and surface functionalization by thiol-ene chemistry (TEC) and surface chain transfer free radical polymerization (SCT-FRP)

*Christian Hoffmann, Manuel Pinelo, John M. Woodley, Anders E. Daugaard**

Submitted to Macromolecular Rapid Communications

Appendix 2.1 – Manuscript

Simple preparation of thiol-ene particles from glycerol and surface functionalization by thiol-ene chemistry (TEC) and surface chain transfer free radical polymerization (SCT-FRP)

Christian Hoffmann, Valeria Chiaula, Manuel Pinelo, John M. Woodley, Anders E. Daugaard*

Christian Hoffmann
Danish Polymer Centre, Department of Chemical and Biochemical Engineering, Technical University of Denmark, Søltofts Plads Building 229, 2800 Kgs. Lyngby, Denmark

Valeria Chiaula
Danish Polymer Centre, Department of Chemical and Biochemical Engineering, Technical University of Denmark, Søltofts Plads Building 229, 2800 Kgs. Lyngby, Denmark

Associate Prof. Manuel Pinelo
Center for BioProcess Engineering, Department of Chemical and Biochemical Engineering, Technical University of Denmark, Søltofts Plads Building 229, 2800 Kgs. Lyngby, Denmark

Prof. John M. Woodley
Process and Systems Engineering Center (PROSYS), Department of Chemical and Biochemical Engineering, Technical University of Denmark, Søltofts Plads Building 229, 2800 Kgs. Lyngby, Denmark

Associate Prof. Anders E. Daugaard
Danish Polymer Centre, Department of Chemical and Biochemical Engineering, Technical University of Denmark, Søltofts Plads Building 229, 2800 Kgs. Lyngby, Denmark
E-Mail: adt@kt.dtu.dk

Abstract

Thiol-ene (TE) based polymer particles have traditionally been prepared via emulsion polymerization in water (using surfactants, stabilizers and co-solvents). Here, we present a green and simple alternative with excellent control over particle size, while avoiding the addition of stabilizers. Glycerol is applied as a dispersing medium for the preparation of off-stoichiometric TE (OSTE) microparticles, where sizes in the range of 40 to 400 µm are obtained solely by changing the mixing speed of the emulsions prior to cross-linking. Control over surface chemistry is achieved by surface functionalization of excess thiol groups via photochemical thiol-ene chemistry (TEC) resulting in a

functional monolayer. In addition, surface chain transfer free radical polymerization (SCT-FRP) is used for the first time to introduce a thicker polymer layer on the particle surface.

The application potential of the system is demonstrated by using functional particles as a support for immobilized enzymes in a continuous plug-flow reactor.

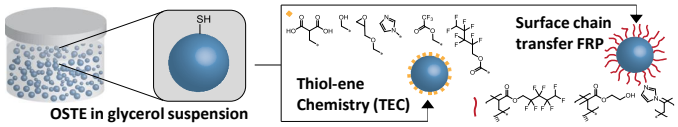

1. Introduction

During the past decades thiol-ene chemistry (TEC) has received increased attention for the preparation and modification of novel polymer systems.[1] Radical mediated TEC or thiol-Michael addition under basic conditions allows the reaction between a thiol group and a carbon-carbon double bond (so called "ene").[2] Radical TEC can be initiated in various ways, such as photochemically, thermally or even electrochemically. High yields can be achieved within short reaction times under mild reaction conditions, which make TEC very robust and efficient. By applying a large variety and combination of different reactive monomers, various polymer architectures, such as linear, branched and cross-linked systems can be prepared.[3] This versatility of network structures can be further increased by variations in monomer stoichiometry leading to excellent control over mechanical properties.[4] The potential of this modularity has been demonstrated by applying stoichiometric thiol-ene (STE) and furthermore off-stoichiometric thiol-ene (OSTE) materials for the preparation of microfluidic systems[5], hydrogels[6], and high internal phase emulsions (HIPE).[7] The stoichiometric imbalance between functional groups in the OSTE system results in unreacted thiol or ene groups within the polymer structure as well as on surfaces and can therefore directly be used for surface modification via TEC.[8] Thus, hydrophilic and hydrophobic functional groups [9] and biological moieties[10] can easily be introduced, as well as more specific groups, such as maleic anhydride[11] and cysteamine[12], which have been applied for immobilization of enzymes.

The high versatility and modularity of TEC has also allowed the preparation of well-defined polymer particles with controlled properties, such as surface functionality, particle size, and thermal and mechanical behavior. Polymer particles are attractive due to their large application spectrum, such as drug-delivery, paints and coatings, chromatography and catalyst supports.[13] TE particles are typically prepared by suspension polymerization in which the monomers, facilitated by the use of different stabilizers and co-solvents, form initially an emulsion in water. Following polymerization, well-defined particles are obtained, as shown by Durham et al., who investigated the effect of different monomer combinations, stabilizers and stabilizer concentrations,[14] as well as the effects of different modes of initiation, such as photochemical, thermal and redox initiation and their influence on particle size.[15] Similarly, porous TE and thiol-alkyne particles were prepared using different porogens.[16] Jasinski et al. used photoinitiated TEC for the preparation of nanoparticles from linear polymers.[17] Likewise thiol-Michael addition has been used for the formation of monodisperse particles at the micrometer scale.[18] It has also been demonstrated that the surface of OSTE particles, containing excess thiol or ene groups, can be functionalized with fluorescent moieties by thiol-Michael reaction under basic conditions, photochemical TEC or thiol-isocyanate reaction.[19]

However, surfactants as well as organic co-solvents are generally necessary for the formation of polymer particles via suspension polymerization. The objective of this

study was the development of a simple method for the controlled formation of OSTE particles without using surfactants or organic co-solvents by replacing water with glycerol as the dispersing medium. Post-preparation surface functionalization of the particles was demonstrated via photochemical TEC and by surface chain transfer free radical polymerization (SCT-FRP) in order to introduce well-defined functional groups on the surface. The obtained particles exhibited high control over size and surface chemistry, facilitating a broad range of application possibilities, which was demonstrated through the use of epoxide functional OSTE particles as support for the immobilization of enzymes in a biocatalytic plug-flow reactor.

2. Results and Discussion

2.1. Preparation of OSTE particles in glycerol

In a surfactant and organic co-solvent free process, off-stoichiometric thiol-ene (OSTE) particles were prepared by suspension polymerization in glycerol, which is a byproduct of biodiesel production and therefore a cheap, green and environmentally friendly alternative to water.[20] OSTE particles (90% thiol excess) were prepared by one-pot mixing of the monomers pentaerythritol tetrakis(3-mercaptopropionate) (PETMP) and 1,3,5-triallyl-1,3,5-triazine-2,4,6(1H,3H,5H)-trione (TATATO) and the photoinitiator TPO-L in glycerol in a high speed mixer, as shown in **Figure 1A**.

Mixing speeds in the range of 1000 to 3500 rpm were applied in order to obtain OSTE in glycerol emulsions, followed by photochemical cross-linking. The resulting microparticles were characterized by dynamic light scattering (DLS) and optical microscopy. As illustrated in Figure 1B, the applied mixing speed could be used to control the particle size. The particle size, depicted here as median of the volume distribution (Dv50) obtained from DLS, decreased with increasing mixing speeds from 402 ± 43 µm to 40.4 ± 3.6 µm. Additionally, the size distributions (span) of the formed particles (between 1.1 and 2.4) was very similar to those obtained from traditional processes in water, in which sodium dodecyl sulfate (SDS) or sodium dodecyl benzene sulfate (SDBS) as surfactants and water as a dispersion phase were used.[14b] Optical microscopy images (see **Figure 1B**) confirmed the spherical shape of the prepared particles as well as the decreasing size of particles as a function of mixing speed.

2.2. Surface functionalization of OSTE particles via TEC and SCT-FRP

Post-preparation surface functionalization was conducted by photoinitiated TEC using different vinyl, allyl or (meth-)acrylic monomers as well as by SCT-FRP, as a novel pathway for surface modification of OSTE particles. These approaches demonstrated the capacity of excess surface thiols for versatile surface functionalization with control over different surface chemistries, as illustrated in **Figure 2A**.

In the first approach, OSTE particles (prepared at a mixing speed of 1000 rpm) were surface functionalized via TEC introducing hydroxyl (AA), epoxide (AGE) and fluorinated groups (ATFA, OFPA). Additionally, pH responsive particle surfaces were

achieved by grafting with Vim and AMA. Photochemical TEC was conducted at low monomer concentrations (0.3 M) in order to suppress potential polymerization reactions to occur. The IR spectrum of the virgin OSTE particles was characterized by alkane (2960 cm^{-1}, C-H), thiol (2569 cm^{-1}, S-H) carbonyl (1730 cm^{-1}, C=O), alkene (1678, C=C) and ester (1020 cm^{-1}, C-O-C) stretches. TEC surface functionalized particles did not show any significant changes in their IR spectra, as shown in Figure S1. This was attributed to the penetration depth of the IR signal of several micrometers into the sample, which is known to result in very low intensity from thin surface layers.[21] Consequently, the OSTE background dominated the spectrum. However, analysis via surface sensitive x-ray photoelectron spectroscopy (XPS) confirmed the surface modification with the individual reagents (see **Table 1**).

The atom composition of the virgin OSTE particles determined by XPS was in good agreement with the theoretical values. Surface TEC with ATFA and OFPA showed fluorine (F1s) contents of 17.3 atom% and 9.0 atom%, which confirmed the functionalization since fluorine was unique for these types of particles. Modification using Vim led to an increase in nitrogen content (4.4 N1s atom%) compared to the original OSTE surfaces (3.0 N1s atom%). The atom composition after surface modification with AGE, AA and AMA was identical to the reference OSTE particles, which is a result of similar theoretical atom compositions of these monomers and the OSTE material. Overall, short reaction times (5 min) and low monomer concentrations (0.3 M) limited the thiol-ene reaction to a surface reaction forming a functional monolayer.

Conversely, by increasing the monomer concentration to classical polymerization conditions (1:2 v/v monomers to ethanol) and extending the reaction time to 30 min it was possible to promote polymerization and termination on the surface by SCT-FRP in order to achieve a thick and dense polymer layer on the particle surface. In this way, it is possible to control the type of grafting reaction by tuning the reaction conditions, which was demonstrated by SCT-FRP with Vim, OFPA and HEMA. The monomers were polymerized in proximity to the particles and IR analysis confirmed a significant polymer grafting (see **Figure S2**). The spectrum of OSTE-g-pVim exhibited a sharp alkene stretch at 662 cm^{-1}, which confirmed the introduced imidazole groups. The polymer grafting with pOFPA and pHEMA was confirmed through the presence of C-F stretches (806 cm^{-1}) typical for fluorinated compounds and hydroxyl stretches (3465 cm^{-1}, O-H), respectively. Additionally, increased intensity of the C-O band at 1129 and 1143 cm^{-1}, originating from the ester in the pendant group confirmed the polymer grafting. Furthermore, XPS analysis showed substantial changes in atom composition for SCT-FRP functionalized particles, which were significantly higher than the corresponding particles prepared by TEC (see Table 1). The substantial decrease in sulfur content (S1s) in each case (pVim, pOFPA, and pHEMA) illustrated the formation of a polymer surface layer. pHEMA grafted particles showed increased oxygen and carbon content, as well as a significant reduction in nitrogen content (2.2 atom% N1s), confirming the pHEMA grafting. Surface grafting with pVim and pOFPA resulted in

significant increases in nitrogen (9.0 atom% N1s) and fluorine (44.4 atom% F1s) content, respectively, compared to the reference OSTE surface. These results confirmed that the grafting density can be controlled by selecting TEC conditions for monolayer formation or polymer grafting via SCT-FRP.

Furthermore, a swelling study of the pristine and functionalized particles was conducted in ethanol and water in order to determine the swelling behavior as a function of the surface chemistry (see Figure 2 B). The pristine OSTE particles displayed a very similar median size (Dv50) in both ethanol (353 µm) and water (408 µm). Statistical ANOVA analysis using a significance level ≤ 0.05 revealed a minor reduction in particle size in both, ethanol and water, upon TEC functionalization. Compared to the pristine OSTE, Vim, ATFA and OFPA functional particles could be considered similar when swollen in ethanol, whereas AMA, AGE and AA showed further decrease in size. This general tendency was statistically more pronounced in water, where all functionalized particles, besides OSTE-Vim, decreased significantly in size compared to the pristine one. This general size reduction in both ethanol and water was attributed to the newly introduced functional moieties that prevented the penetration of solvent into the particle core and thereby limited the swelling of the particles.

Compared to functionalizations by TEC, SCT-FRP with Vim, OFPA or HEMA resulted in particles with a significant reduction in size when measured in ethanol (120 to 174 µm). A reference experiment without initiator and UV irradiation did not show any changes in particle size, which confirmed that the reduction in size was a result of functionalization and not abrasion from the agitator. The size of the particles was highly dependent on the type polymer graft, where pHEMA grafted particles had similar sizes in water and ethanol. In contrast, OSTE-pVim particles submerged in water exhibited a much higher degree of swelling (293 µm) compared to the swelling in ethanol (173 µm), which could be explained by protonation of imidazole moieties in water and the resultant repulsive interactions between the polymer grafts leading to an increased thickness of the grafting layer. Likewise pOFPA grafted particles were observed to exhibit significantly different sizes in water and ethanol with a particle size of 447 µm in water, almost 4-fold higher than the corresponding particle size in ethanol. The difference in size was attributed to a high degree of agglomeration as a result of the hydrophobic nature of the pOFPA, which was also observed visually.

2.3. Epoxide functional particles as support for horseradish peroxidase (HRP) in a plug-flow reactor

In order to demonstrate their application potential, particles were used as a support for enzyme immobilization in a biocatalytic plug-flow reactor. Epoxide groups are known to covalently bind enzymes through direct reaction with amine and thiol groups, which are found in the lysine and cysteine residues on the surface of the protein structure.[22] In this study, epoxide functional particles (OSTE-AGE), which were prepared by TEC modification by AGE of OSTE particles prepared at 1000 rpm mixing speed, were

incubated with horseradish peroxidase (HRP) serving as a model enzyme, as illustrated in **Figure 3A**.

After filling the reactor with HRP immobilized particles and thorough rinsing with PBS buffer, the enzymatic activity was continuously tested using a solution containing 2,2′-azino-bis(3-ethylbenzothiazoline-6-sulfonic acid) diammonium salt (ABTS, 1 mM) and hydrogen peroxide (H_2O_2, 10 mM) in phosphate buffer (pH 5, 0.1 M) as a colorimetric assay. ABTS (absorbance maximum at 340 nm) could be oxidized by HRP in the presence of H_2O_2 to $ABTS^{\bullet+}$, which resulted in a shift in absorbance maximum to 412 nm (ε_{412}=3.6 x $10^4 M^{-1}$ cm^{-1}).[23] Using a constant flowrate of 0.2 mL min^{-1} allowed sampling at regular time intervals. In **Figure 3B**, photographs of the reactor at 1, 10 and 60 minutes operation time are shown, where the substrate solution was continuously added at the top and samples were taken at the bottom. The green color, which is formed after 1 min only at the top and over the entire reactor at 10 and 60 min, corresponds to the formed product. The absorbance of the withdrawn samples corresponding to the formed $ABTS^{\bullet+}$ was determined and monitored over time, as shown in **Figure 3C** (full squares). Once the residence time within the plug-flow reactor of 6 min was reached, the absorbance from the product measured at the outlet increased significantly. After 15 minutes, steady state conditions were reached demonstrating stable enzymatic activity over the entire operation time. Reference particles (OSTE-AGE particles without HRP) were also tested, and are represented as empty squares in the Figure 3C, showing no enzymatic activity at any time. These results demonstrate the successful application of the prepared and surface functionalized OSTE particles in a biocatalytic application.

3. Conclusions

In this study, we have presented a novel, green and simple method for the preparation of OSTE particles in a controlled fashion via suspension polymerization in glycerol without using stabilizers, surfactants or co-solvents. Particle sizes were controlled by varying the mixing speed of the suspension prior to cross-linking via photoinitiated TEC. A variety of different surface chemistries were introduced in a post-preparation step via surface TEC or SCT-FRP. By TEC a functional monolayer was formed, which resulted in a minor decrease in particle size, when submerged in ethanol or water. However, thicker polymer grafts formed as a result of the SCT-FRP approach which showed substantially reduced swelling in ethanol and increased swelling and agglomeration tendencies in water. The complementary nature of the two approaches enables simple control over surface grafting and surface chemistries depending on the specific application of the particles. Finally, epoxide functional particles were successfully applied as support material for the immobilization of HRP, which was demonstrated in a biocatalytic plug-flow reactor. The ease of particle preparation and controlled surface functionalization opens up for a broad range of application possibilities.

Supporting Information

Supporting Information is available from the Wiley Online Library or from the author.

Acknowledgements: The authors wish to thank the Aage and Johanne Louis-Hansen Endowment for financial support.

Received: Month XX, XXXX; Revised: Month XX, XXXX; Published online:
((For PPP, use "Accepted: Month XX, XXXX" instead of "Published online")); DOI: 10.1002/marc.((insert number)) ((or ppap., mabi., macp., mame., mren., mats.))

Keywords:
Thiol-ene chemistry, polymer particles, suspension polymerization, surface functionalization, enzyme immobilization

[1] A. B. Lowe, *Polym. Chem.* **2010**, *1*, 17.
[2] C. E. Hoyle, C. N. Bowman, *Angew. Chemie* **2010**, *49*, 1540.
[3] A. B. Lowe, *Polym. Chem.* **2014**, *5*, 4820.
[4] C. F. Carlborg, A. Vastesson, Y. Liu, W. van der Wijngaart, M. Johansson, T. Haraldsson, *J. Polym. Sci. Part A Polym. Chem.* **2014**, *52*, 2604.
[5] a) C. F. Carlborg, T. Haraldsson, K. Öberg, M. Malkoch, W. van der Wijngaart, *Lab Chip* **2011**, *11*, 3136, b) P. Mazurek, A. E. Daugaard, M. Skolimowski, S. Hvilsted, A. L. Skov, *RSC Adv.* **2015**, *5*, 15379, c) S. M. Tähkä, A. Bonabi, M. E. Nordberg, M. Kanerva, V. P. Jokinen, T. M. Sikanen, *J. Chromatogr. A* **2015**, *1426*, 233.
[6] a) A. A. Aimetti, A. J. Machen, K. S. Anseth, *Biomaterials* **2009**, *30*, 6048, b) T. Yang, H. Long, M. Malkoch, E. K. Gamstedt, L. Berglund, A. Hult, *J. Polym. Sci. Part A Polym. Chem.* **2011**, *49*, 4044.
[7] E. Lovelady, S. D. Kimmins, J. Wu, N. R. Cameron, *Polym. Chem.* **2011**, *2*, 559.
[8] a) D. Wasserberg, T. Steentjes, M. H. W. Stopel, J. Huskens, C. Blum, V. Subramaniam, P. Jonkheijm, *J. Mater. Chem.* **2012**, *22*, 16606, b) J. Zhang, Y. Chen, M. A. Brook, *Langmuir* **2013**, *29*, 12432, c) K. Y. Tan, M. Ramstedt, B. Colak, W. T. S. Huck, J. E. Gautrot, *Polym. Chem.* **2016**, *7*, 979.
[9] a) G. Pardon, F. Saharil, J. M. Karlsson, O. Supekar, C. F. Carlborg, W. van der Wijngaart, T. Haraldsson, *Microfluid. Nanofluidics* **2014**, *17*, 773, b) C. F. Carlborg, F. Moraga, F. Saharil, W. van der Wijngaart, T. Haraldsson, *Proc. Micro Total Anal. Syst.* **2012**, 677.
[10] N. A. Feidenhans'l, J. P. Lafleur, T. G. Jensen, J. P. Kutter, *Electrophoresis* **2014**, *35*, 282.
[11] E. Çakmakçi, B. Yuce-Dursun, S. Demir, *React. Funct. Polym.* **2017**, *111*, 38.
[12] J. P. Lafleur, S. Senkbeil, J. Novotny, G. Nys, N. Bøgelund, K. D. Rand, F. Foret, J. P. Kutter, *Lab Chip* **2015**, *15*, 1.
[13] a) H. Kawaguchi, *Prog. Polym. Sci.* **2000**, *25*, 1171, b) J. A. Champion, Y. K. Katare, S. Mitragotri, *J. Control. Release* **2007**, *121*, 3.
[14] a) O. Z. Durham, S. Krishnan, D. A. Shipp, *ACS Macro Lett.* **2012**, *1*, 1134, b) O. Z.

Durham, D. A. Shipp, *Polymer* **2014**, *55*, 1674, c) O. Z. Durham, D. A. Shipp, *Colloid Polym. Sci.* **2015**, *293*, 2385.

[15] F. Alimohammadi, C. Wang, O. Z. Durham, H. R. Norton, C. N. Bowman, D. A. Shipp, *Polymer* **2016**, *105*, 180.

[16] a) J. Tan, C. Li, J. Zhou, C. Yin, B. Zhang, J. Gu, Q. Zhang, *Rsc Adv.* **2014**, *4*, 13334, b) S. Cai, Z. Wenig, Y. Zheng, B. Zhao, Z. Gao, C. Gao, *Polym. Chem.* **2016**, *7*, 7400.

[17] F. Jasinski, E. Lobry, B. Tarablsi, A. Chemtob, C. Croutxé-Barghorn, D. Le Nouen, A. Criqui, *ACS Macro Lett.* **2014**, *3*, 958.

[18] a) C. Wang, M. Podgórski, C. N. Bowman, *Mater. Horizons* **2014**, 1173, doi:10.1073/pnas.1201800109, b) C. Wang, X. Zhang, M. Podgórski, W. Xi, P. Shah, J. Stansbury, C. Bowman, *Macromolecules* **2015**, *48*, 8461.

[19] a) D. V. Amato, D. N. Amato, A. S. Flynt, D. L. Patton, *Polym. Chem.* **2014**, *6*, 5625, b) D. N. Amato, D. V. Amato, J. Narayyanan, B. R. Donovan, J. R. Douglas, S. E. Walley, A. S. Flynt, D. L. Patton, *Chem. Commun.* **2015**, *51*, 10910, c) O. Z. Durham, H. R. Norton, D. A. Shipp, *RSC Adv.* **2015**, *5*, 66757.

[20] C. A. G. Quispe, C. J. R. Coronado, J. A. Carvalho Jr, *Renew. Sustain. Energy Rev.* **2013**, *27*, 475.

[21] C. Y. Tang, Y. N. Kwon, J. O. Leckie, *J. Memb. Sci.* **2007**, *287*, 146.

[22] E. Cakmakci, O. Danis, S. Demir, Y. Mulazim, M. V. Kahraman, *J. Microbiol. Biotechnol.* **2013**, *23*, 205.

[23] B. R. E. Childs, W. G. Bardsley, *Biochem. J.* **1975**, *145*, 93.

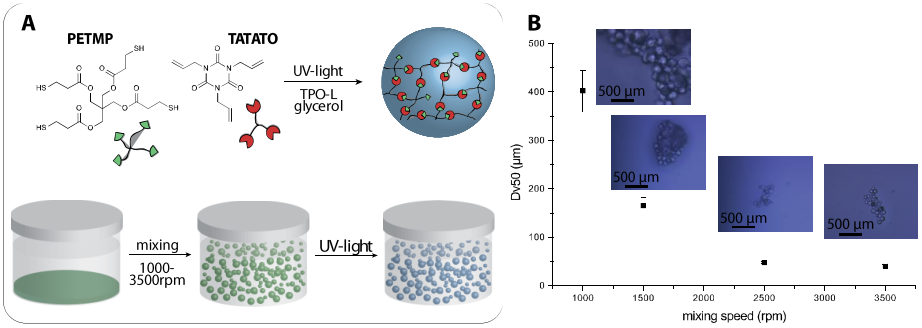

Figure 1. A) Preparation of OSTE microparticles via suspension in a speedmixer followed by subsequent photochemical cross-linking of PETMP and TATATO. B) Particle size (Dv50) as a function of mixing speed with optical microscopy images (50 x magnification) of the OSTE particles.

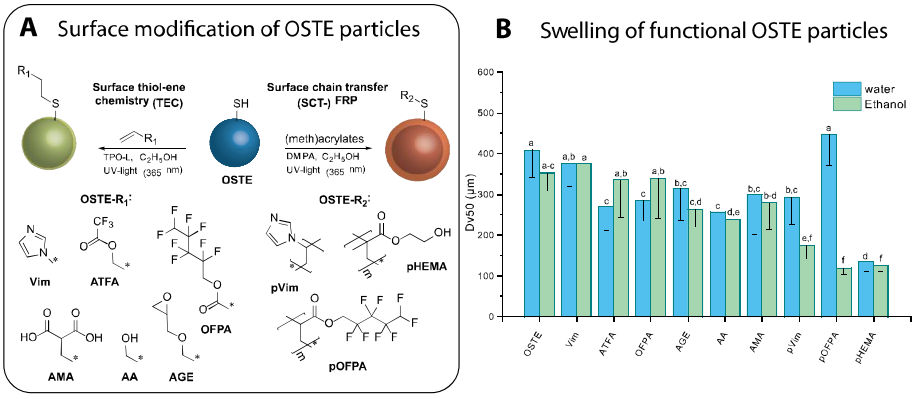

Figure 2. A) Surface functionalization of OSTE particles via two different routes, left: surface TEC with different reagents, such as 1-vinyl imidazole (Vim), allyl trifluoroacetate (ATFA), 2,2,3,3,4,4,5,5 octylfluoropentylacrylate (OFPA), allyl malonic acid (AMA), allyl alcohol (AA), and allyl glycidyl ether (AGE) at low concentration (0.3 M) leading to a functional monolayer on the surface; right: SCT-FRP with various monomers, such as Vim, 2-hydroxyethyl methacrylate (HEMA) and OFPA at high concentration (0.7 – 2.4 M), leading to a functional polymer grafted surface. B) Swelling study of OSTE particles containing various surface functionalities grouped by ANOVA analysis (letters above bars, p=0.05) in ethanol and water individually.

Table 1. XPS data of pristine and surface functionalized OSTE particles via TEC[a] and SCT-FRP[b]

particle type	**C1s [atom%]**	**O1s [atom%]**	**N1s [atom%]**	**S2p [atom%]**	**F1s [atom%]**
OSTE	60.1 ± 1.4	26.6 ± 0.9	3.0 ± 0.6	10.3 ± 0.3	-
OSTE-Vim[a]	60.8 ± 0.5	24.2 ± 0.8	4.4 ± 0.3	10.6 ± 0.8	-
OSTE-ATFA[a]	52.8 ± 0.4	21.5 ± 0.5	2.4 ± 0.4	6.0 ± 0.4	17.3 ± 0.7
OSTE-OFPA[a]	55.5 ± 1.0	22.4 ± 0.7	4.1 ± 0.5	9.0 ± 0.5	9.0 ± 1.7
OSTE-AGE[a]	62.3 ± 0.3	24.1 ± 0.5	3.5 ± 0.5	10.1 ± 0.3	-
OSTE-AA[a]	62.2 ± 0.9	23.6 ± 0.7	3.5 ± 0.4	10.7 ± 0.2	-
OSTE-AMA[a]	61.7 ± 0.3	24.4 ± 0.5	3.7 ± 0.0	10.2 ± 0.5	-
OSTE-pVim[b]	63.8 ± 0.9	19.0 ± 0.3	9.0 ± 0.3	8.2 ± 0.8	-
OSTE-pOFPA[b]	42.6 ± 0.2	11.1 ± 0.5	0.6 ± 0.6	1.4 ± 0.2	44.4 ± 1.0
OSTE-pHEMA[b]	62.9 ± 0.7	28.3 ± 0.5	2.2 ± 0.1	6.6 ± 0.1	-

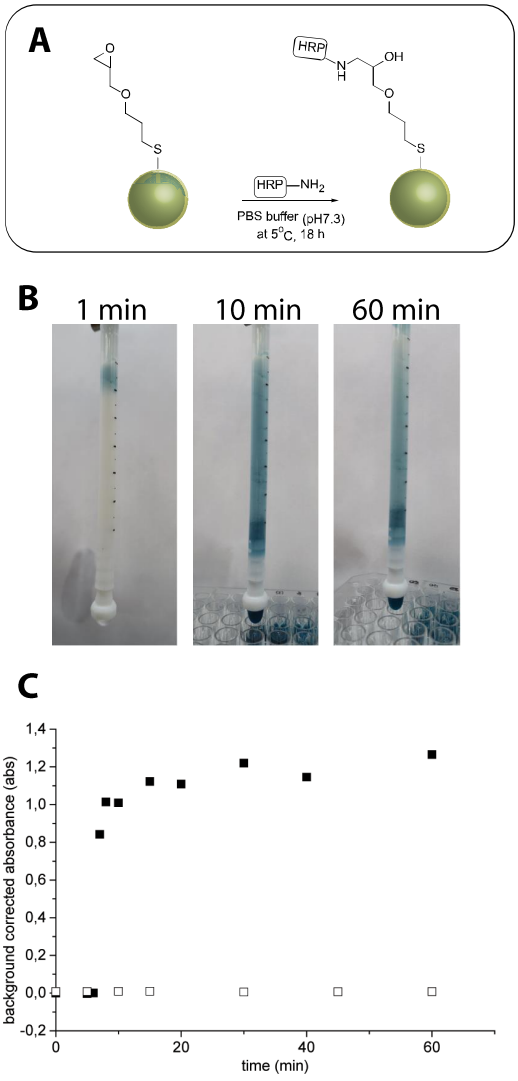

Figure 3. A) Immobilization of HRP on OSTE-AGE particles. B) Photographs of plug-flow reactor at 1 min, 10 min and 60 min of reaction time using a flow of 0.2 ml min^{-1} during a ABTS/H_2O_2 activity measurement of immobilized HRP on OSTE-AGE particles. C) Enzyme activity as background corrected absorbance at 412 nm over time of OSTE-AGE particles with immobilized enzyme (full squares) and a reference (without enzyme -empty squares)

Appendix 2.2 – Supporting information

1. Experimental Section

1.1. Materials

Pentaerythritol tetrakis(3-mercaptopropionate) (PETMP, >95%), 1,3,5-Triallyl-1,3,5-triazine-2,4,6(1H,3H,5H)-trione (TATATO, 98%), allyl pentafluorobenzene (APFB, >99%), allyltrifluoroacetate (ATFA , 98%), allyl alcohol (AA, 99%), allyl malonic acid (AMA, ≥98%), 1-vinyl imidazole (Vim, ≥99%), allyl glycidyl ether (AGE, >99%), 2,2-dimethoxy-2-phenylacetophenone (DMPA, 99%), horseradish peroxidase (HRP, lyophilized powder, 50-150 U mg-1), 2,2′-Azino-bis(3-ethylbenzothiazoline-6-sulfonic acid) diammonium salt (ABTS, ≥98%) and hydrogen peroxide (H_2O_2, 3%) were obtained from Sigma-Aldrich. 2-hydroxyethyl methacrylate (HEMA, 99%) and 2,2,3,3,4,4,5,5 octafluoropentyl acrylate (OFPA, 97%) were purchased from Sigma Aldrich and passed through a short plug-flow column containing aluminum oxide (Sigma-Aldrich, activated, basic, Brockmann I, standard grade) prior to use. Lucirin TPO-L (ethyl-2, 4, 6-tri- methylbenzoylphenyl phosphinate) was obtained from BASF. Ethanol absolute (99.97%) was purchased from VWR. Glycerol was kindly provided by Emmelev, Otterup A/S Denmark and was used as received.

1.2. Methods

Fourier transform infrared (FT-IR) spectroscopy was conducted using a Nicolet iS50 FT-IR fitted with a diamond crystal attenuated total reflection accessory (ATR), which operated at a resolution of 4 cm^{-1} and 32 scans per measurement. X-ray photoelectron spectroscopy (XPS) analysis was carried out on a Thermo Fisher Scientific K-Alpha (East Grinstead, UK). Large area surface analysis used a 400 μm spot of monochromatized aluminum Kα radiation. Survey (pass energy 200 eV) and high-resolution (pass energy 50 eV) spectra for relevant elements were acquired of the particles. Data analyses of the obtained XPS spectra were performed using the Avantage software package as provided by the manufacturer. The shape and size of the particles was assessed by optical microscopy using a Leica DM LB optical microscope. Particle size distributions were determined by Dynamic Light Scattering (DLS) measurements, performed on a Malvern Mastersizer 3000 using laser diffraction method. The particles, dispersed in a fluid, passing through a focused red (or blue) laser beam in a quartz measurement cell scattered light at various angles. Generally, the median for volume distribution (Dv50), which divides the whole population in two equal parts, and the span were determined from 5 measurements. The span is calculated according to the following equation:

$$\text{Span} = \frac{D_{v0.9} - D_{v0.1}}{D_{v0.5}}$$

Enzyme activity measurements were conducted in a PS 96 well microplate using a POLARstar® Omega from BMG Labtech equipped with an UV-VIS probe (20 scans per measurement) at 25 °C.

1.3. Preparation of off-stoichiometric thiol-ene (OSTE) particles in glycerol

PETMP (0.736 g, 0.0015 mol), TATATO (0.264 g, 0.0011 mol), TPO-L (1.0 mg, 0.1 wt%) and glycerol (10 mL) were added into a mixing cup under exclusion of light. Then, the mixture were homogenized by mixing in a Speedmixer at 1000 rpm (SpeedMixerTM DAC 150.1 FVZ) for 1.5 minutes. Subsequently, the mixture was exposed to UV light (λ= 365 nm, 1.4 mW cm^{-2}) for 10 minutes. Then, ethanol was added to the suspension, which was manually stirred and the resulting particles were filtered and thoroughly rinsed with ethanol. An aliquot of the particles was dried in vacuo for further characterization, whereas the main part was resuspended in ethanol for storage and further functionalization.

IR (cm^{-1}): 2960 (C-H), 2569 (S-H), 1730 (C=O), 1678 ($C=C_{alkene}$), 1459 ($O-CH_{2\ ester}$), 1140 ($C-O-C_{stretch\ vibr}$), 1020 (C-O-C), 763 ($C-O-C_{deformation}$)

1.4. General surface functionalization of OSTE particles via TEC using allyl malonic acid (OSTE-AMA)

In a general procedure, 1.0 g of OSTE microparticles (obtained at 1000 rpm) was suspended in 10 ml of ethanol. Under exclusion of light, allyl malonic acid (0.432 g, 3.0 mmol) and TPO-L (8.4 µL, 0.003 mmol) were added. Then, the suspension was stirred by magnetic stirring (300 rpm) for 5 min and irradiated with UV light (λ= 365 nm, 0.4 mW cm^{-2}). Subsequently, the particles were filtered and washed thoroughly with ethanol before resuspending them in ethanol (10 mL) for further use.

IR (cm^{-1}): 2961 (C-H), 2568 (S-H), 1730 (C=O), 1678 ($C=C_{alkene}$), 1460 ($O-CH_{2\ ester}$), 1141 ($C-O-C_{stretch\ vibr}$), 1020 (C-O-C), 763 ($C-O-C_{deformation}$)

1.4.1. Preparation of OSTE-AA

OSTE-AA was prepared in accordance to the general procedure, using 10 mL of an ethanolic solution of allyl alcohol (204 µL, 3.0 mmol) and TPO-L (8.4 µL, 0.003 mmol) as reagent.

IR (cm^{-1}): 2960 (C-H), 2566 (S-H), 1730 (C=O), 1678 ($C=C_{alkene}$), 1460 ($O-CH_{2\ ester}$), 1141 ($C-O-C_{stretch\ vibr}$), 1020 (C-O-C), 763 ($C-O-C_{deformation}$)

1.4.2. Preparation of OSTE-Vim

OSTE-Vim was prepared in accordance to the general procedure, using 10 mL of an ethanolic solution of 1-vinyl imidazole (Vim, 271 µL, 3.0 mmol) and TPO-L (8.4 µL, 0.003 mmol) as reagent.

IR (cm^{-1}): 2960 (C-H), 2567 (S-H), 1730 (C=O), 1678 ($C=C_{alkene}$), 1460 ($O-CH_{2\ ester}$), 1141 ($C-O-C_{stretch\ vibr}$), 1020 (C-O-C), 763 ($C-O-C_{deformation}$)

1.4.3. Preparation of OSTE-ATFA

OSTE-ATFA was prepared in accordance to the general procedure, using 10 mL of an ethanolic solution of allyl trifluoroacetate (ATFA, 391 µL, 3.0 mmol) and TPO-L (8.4 µL, 0.003 mmol) as reagent.

IR (cm^{-1}): 2960 (C-H), 2566 (S-H), 1730 (C=O), 1678 ($C=C_{alkene}$), 1460 ($O-CH_{2\ ester}$), 1140 ($C-O-C_{stretch\ vibr}$), 1020 (C-O-C), 763 ($C-O-C_{deformation}$)

1.4.4. Preparation of OSTE-OFPA

OSTE-OFPA was prepared in accordance to the general procedure, using 10 mL of an ethanolic solution of 2,2,3,3,4,4,5,5 octafluoropentyl acrylate (OFPA, 583 µL, 3.0 mmol) and TPO-L (8.4 µL, 0.003 mmol) as reagent.
IR (cm^{-1}): 2960 (C-H), 2568 (S-H), 1730 (C=O), 1678 ($C=C_{alkene}$), 1460 ($O-CH_{2\ ester}$), 1141 ($C-O-C_{stretch\ vibr}$), 1020 (C-O-C), 763 ($C-O-C_{deformation}$)

1.4.5. Preparation of OSTE-AGE

OSTE-AGE was prepared in accordance to the general procedure, using 10 mL of an ethanolic solution of allyl glycidylether (AGE, 360 µL, 3.0 mmol) and TPO-L (8.4 µL, 0.003 mmol) as reagent.
IR (cm^{-1}): 2960 (C-H), 2567 (S-H), 1730 (C=O), 1678 ($C=C_{alkene}$), 1460 ($O-CH_{2\ ester}$), 1140 ($C-O-C_{stretch\ vibr}$), 1021 (C-O-C), 763 ($C-O-C_{deformation}$)

1.5. General surface functionalization of OSTE particles via surface chain transfer free radical polymerization (SCT FRP) with 1-vinyl imidazole (OSTE-g-pVim)

In a general procedure, 1 g of previously prepared OSTE particles were submerged in a solution containing 1-vinyl imidazole (Vim, 3.3 mL, 27.5 mmol), 2,2-dimethoxy-2-phenylacetophenone (DMPA, 47.2 mg, 0.50 mol%) and ethanol (6.7 mL), which was screened from ambient light. Under magnetic stirring, this mixture was subsequently irradiated with UV light (λ= 365 nm, 0.4 mW cm^{-2}) for 30 min. Then, the particles were filtered and thoroughly rinsed with ethanol before storing them in 10 mL of ethanol until further use.
IR (cm^{-1}): 2955 (C-H), 1729 (C=O), 1676 ($C=C_{alkene}$), 1461 ($O-CH_{2\ ester}$), 1350, 1229 (N-H), 1138, 1101 ($C-O-C_{stretch\ vibr}$), 764 ($C-O-C_{deformation}$), 662 ($imidazole\ ring_{deformation}$).

1.5.1. Preparation of OSTE-g-pOFPA

OSTE-g-pOFPA was prepared in accordance with the general procedure, using a solution containing OFPA (3.3 mL, 17.3 mmol), DMPA (22.2 mg, 0.5 mol%) and ethanol (6.7 mL).
IR (cm^{-1}): 2961 (C-H), 1733 (C=O), 1681 ($C=C_{alkene}$), 1461 ($O-CH_{2\ ester}$), 1129 ($C-O_{stretch\ vibr}$), 989 (C-O), 902, 806 (C-F), 764 ($C-O-C_{deformation}$)

1.5.2. Preparation of OSTE-g-pHEMA

OSTE-g-pHEMA was prepared in accordance with the general procedure, using a solution containing 2-hydroxylethyl methacrylate (HEMA, 3.3 mL, 27.5 mmol), DMPA (35.2 mg, 0.5 mol%) and ethanol (6.7 mL).

IR (cm^{-1}): 3465 (O-H), 2948 (C-H), 1728 (C=O), 1678 ($C=C_{alkene}$), 1460 ($O-CH_{2\ ester}$), 1143 ($C-O_{stretch\ vibr}$), 1021, 764 ($C-O-C_{deformation}$)

1.6. Preparation and testing of a plug-flow reactor with enzymatically active OSTE-AGE particles

A batch of previously prepared OSTE-AGE particles was dried in vacuo. 0.8 g of these particles was redispersed in ethanol, which was solvent exchanged with PBS buffer (pH 7.3). The final amount of PBS buffer was 3.2 mL and 3.5 mg of horseradish peroxidase (HRP) was subsequently added. This mixture was incubated under shaking at 22°C for 20 h. Then, 1 mL of the supernatant was removed for further analysis and the particles were added into a tubular reactor with an inner diameter of 5.0 mm. The filled reactor was rinsed with PBS buffer; first manually with 10 mL and then with a flow rate of 0.2 mL min^{-1} for 30 min using a NE-1000 single syringe pump. While washing with PBS buffer, a phosphate buffer solution (0.1M, pH5) containing ABTS (1.0 mM) and hydrogen peroxide (H_2O_2, 10 mM) was added to the eluent at the outlet and after 20 min of flushing with 0.2 mL min^{-1} no enzyme activity in the eluent was observed. After flushing with PBS buffer a phosphate buffer solution (0.1 M, pH5) containing ABTS (1.0 mM) and hydrogen peroxide (H_2O_2, 10 mM) was passed through the reactor with a flow rate of 0.2 mL min^{-1}. At distinct time intervals, aliquots of the solution at the outlet were collected. 50 as well 100 µL of these samples were transferred into a polystyrene (PS) 96 microplate and the absorbance was measured at 412 nm corresponding to the absorbance maximum of the oxidized product ($ABTS^{\bullet+}$).

2. Supporting Figures

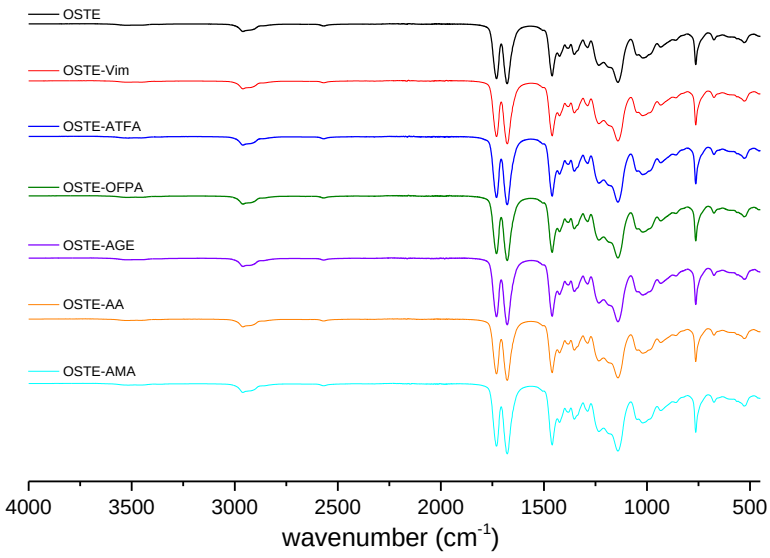

Figure S1 IR spectra of surface functionalized OSTE particles via TEC using various allylic and vinylic reagents

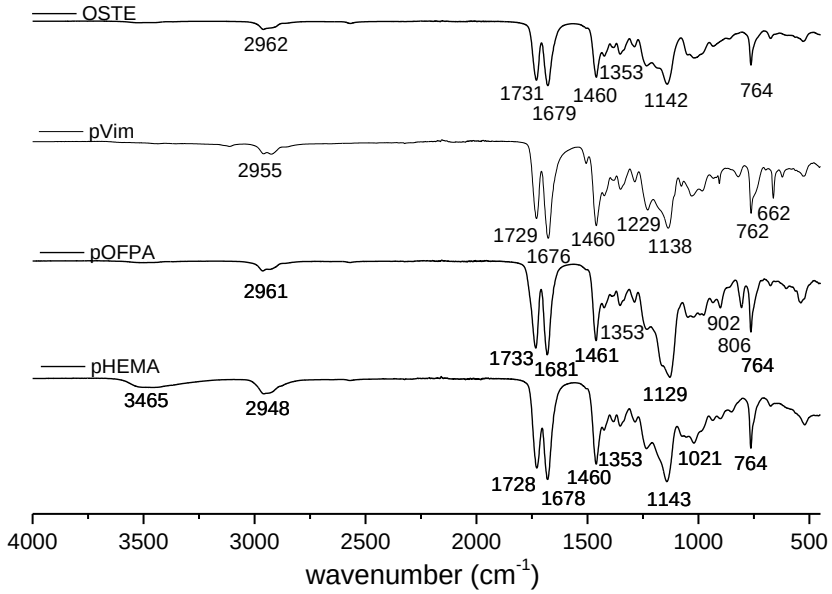

Figure S2 IR spectra of surface functionalized OSTE particles via SCT-FRP using vinylic, acrylic and methacrylic reagents

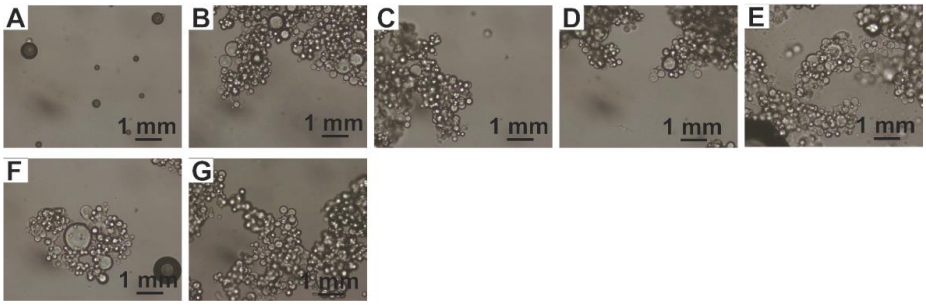

Figure S3 Optical microscopy images of surface functionalized OSTE-1000 particles via TEC using different allyl and vinyl monomers, A) OSTE-AMA, B) OSTE-AA, C) OSTE-Vim, D) OSTE-Aam, E) OSTE.APFB, F) OSTE-ATFA, G) OSTE-AGE

Appendix 3

Improved alkyl glycoside synthesis by trans-glycosylation through tailored micro-environment of immobilized β-glucosidase

Christian Hoffmann[†], Carl Grey[‡], Manuel Pinelo[†], John M. Woodley[†], Anders E. Daugaard[†,],Patrick Adlercreutz[‡]*

Manuscript draft, submission after successful publication of *manuscript 2*

Appendix 3.1 – Manuscript

Improved alkyl glycoside synthesis by trans-glycosylation through tailored micro-environment of immobilized β-glucosidase

Christian Hoffmann[†], *Carl Grey*[‡], *Manuel Pinelo*[†], *John M. Woodley*[†], *Anders E. Daugaard*[†,*], *Patrick Adlercreutz*[‡]

[†]Department of Chemical and Biochemical Engineering, Technical University of Denmark, Søltofts Plads Building 229, 2800 Kgs. Lyngby, Denmark

[‡]Department of Chemistry, Division of Biotechnology, Lund University, P.O. Box 124, 221 00 Lund, Sweden

ABSTRACT

Here, we present for the first time how the micro-environment can directly improve biocatalytic selectivity of immobilized β-glucosidase. β-Glucosidase from *Thermotoga neapolitana* was immobilized on a variety of functionalized off-stoichiometric thiol-ene (OSTE) particles, and highest activities were observed for thiol and imidazole functional particles. Compared to the soluble enzyme, the selectivity (r_s/r_h) between trans-glycosylation of p-nitrophenyl β-D-glucopyranoside (pNPG) with 1-propanol over hydrolysis was substantially promoted by a factor of 2 and 3 using particles containing imidazole and carboxylic acid moieties, respectively. These results demonstrate clearly that enzyme selectivity depends directly on the local environment of the enzyme with the support.

KEYWORDS

Trans-glycosylation, hydrolase, alkyl glycoside, enzyme immobilization, surface functionalization

Alkyl glycosides are amphiphilic molecules, in which a hydrophilic sugar moiety is covalently linked through a glycosidic bond to a hydrophobic alkyl chain. Due to their structure alkyl glycosides are industrially useful as non-ionic surfactants in detergents and cosmetics.[1,2] Compared to the traditional method of chemical preparation, enzymatically catalyzed synthesis of alkyl glycosides using glycoside hydrolases (EC 3.2.1) has lately received increased attention due to mild reaction conditions and high selectivity.[3,4] Enzymatic glycosylation involves the reaction of an alcohol directly with a monosaccharide in reverse hydrolysis (thermodynamic control), or with a glycoside as a donor undergoing a trans-glycosylation (kinetic control). The developments within this field have been the subject of a recent mini review, which summarized different approaches in order to increase the catalytic activity, selectivity and yields.[5] Especially the selectivity between synthesis (s) (in this case trans-glycosylation) and hydrolysis (h) is an important parameter that can be described as a ratio of the individual reaction rates r_s/r_h or as a selectivity, S_c taking the nucleophile concentrations (or activities) into account.[6,7] For the synthesis of alkyl glycosides, water-miscible[8] as well as water-immiscible alcohols, as glycoside acceptors have been studied. It has been shown that the enzyme activity and selectivity are highly dependent on the water activity[7,9–11] and the alcohol concentrations and can be exploited in 2-phase systems.[12,13] Protein engineering of β-glucosidases[14] as well as the choice of other glycoside hydrolases[15–17] were also considered in order to improve the selectivity and activity. In addition, immobilization of β-glucosidases on commercial resins was investigated for trans-glycosylation reactions, resulting in improved activity and selectivity at low water activities compared to freeze-dried enzymes.[18] Increased stability and reusability was obtained from immobilization on zinc oxide (ZnO) as solid support.[19] In general, many different materials, such as chitosan, calcium alginate and polymer materials have already been applied for glycoside hydrolase immobilization.[20] Recently, off-stoichiometric thiol-ene (OSTE) materials, being a thermosetting polymer, prepared by photochemically cross-linking of thiol and an alkene (termed “ene”) containing compounds, have also been used as an enzyme support.[21–23] We demonstrated the development of an OSTE microtiter plate as a screening platform for a large range of surface chemistries as promising supports for the immobilization of enzymes. [REF] This type of platform allows the fast and versatile investigation of micro-environmental effects on enzyme activity, as verified by the use of horseradish peroxidase (HRP). This approach was further extended by a new method for the preparation of OSTE particles followed by versatile surface functionalization, which was successfully applied as a support for immobilization of HRP in a continuous plug-flow reactor.[REF] Changes in the environmental properties at the interface between the enzyme and support surface have already been shown to be an important factor for the performance of immobilized enzymes.[24] For immobilized β-galactosidases and lipases for instance, it has been found that a favorable environment can improve both, the stability and activity.[25–29]

The objective of this study was to exploit micro-environmental influences in order to promote biocatalytic activity, and more importantly selectivity, of an immobilized β-glucosidase. The goal was to increase the selectivity between trans-glycosylation (s) with 1-propanol compared to the hydrolysis (h) of p-nitrophenyl glucopyranoside (pNPG) by changing the surface chemistry of the support material and thus, the environmental properties between enzyme and support. Therefore, *Thermotoga neapolitana* β-glucosidase 3B (belonging to glycoside hydrolase family 3) was immobilized onto functional OSTE particles, which were initially prepared by suspension polymerization in glycerol using the monomers pentaerythritol tetrakis(3-mercaptopropionate) (PETMP) and 1,3,5-triallyl-1,3,5-triazine-2,4,6(1H,3H,5H)-trione (TATATO) and TPO-L as a photoinitiator. This simple method allowed the formation of micrometer-sized monomer droplets in glycerol by rapid mixing, followed by photochemical cross-linking. The off-stoichiometric ratio between the monomers (90% thiol in excess) resulted in thiol functional OSTE particles, which were subsequently subjected for further surface functionalization. Photochemical thiol-ene chemistry (TEC) and surface chain transfer free radical polymerization (SCT-FRP) were previously described to be efficient methods for the introduction of distinct functionalities as a functional monolayer or thicker polymer grafts. As illustrated in **Scheme 1**, TEC was applied with a variety of monomers, such as allyl alcohol (AA), allyl malonic acid (AMA), 2,2,3,3,4,4,5,5-octafluoropentyl acrylate (OFPA) and 1-vinyl imidazole (Vim) in order to introduce different functional groups on the particle surface. Thus, hydroxyl, carboxylic acid, fluorine and imidazole functional particles were obtained. In contrast to this monolayer functionalization achieved by TEC, SCT-FRP was applied using Vim in order to create a thicker poly(1-vinyl imidazole) (pVim) layer on the particle surface.

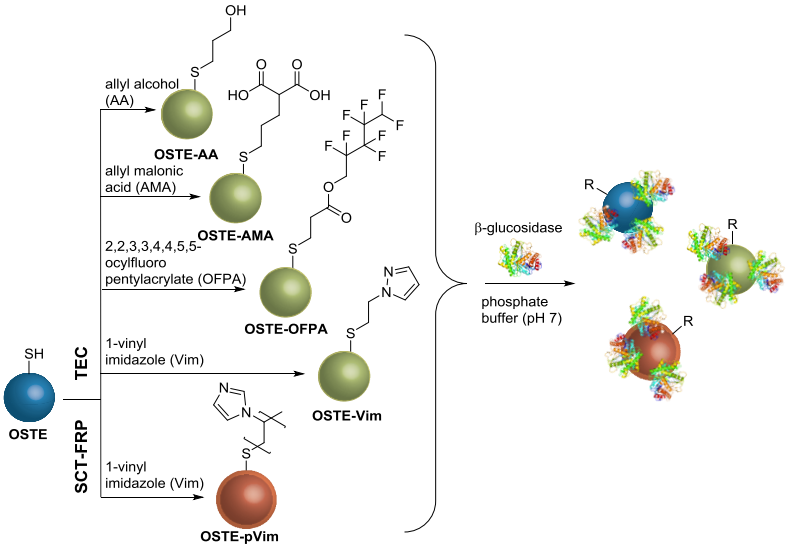

Scheme 1. Surface functionalization of OSTE particles via thiol-ene chemistry (TEC) using Vim, AA, AMA, and OFPA to introduce a functional monolayer; and via surface chain transfer free radical polymerization (SCT-FRP) using Vim to graft the surface with a dense polymer layer (pVim) followed by immobilization of β-glucosidase on pristine and functional OSTE particles

The chemical changes on the surface following TEC and SCT-FRP were confirmed by FT- IR and x-ray photoelectron spectroscopy (XPS).[REF] The different functionalities in this study were selected in order to create various surface environments for the immobilization of β-glucosidase, and thus impact the enzyme performance in terms of activity and selectivity. Hydroxyl or carboxylic acid functional particles were intended to form hydrophilic interactions or hydrogen bonds, whereas fluorinated particles have the potential of creating hydrophobic interactions between the surface and the immobilized enzymes. Imidazole groups and their derivatives are known for their biological importance and have already demonstrated beneficial effects for immobilized horseradish peroxidase.[REF]

As a model system, the β-glucosidase catalyzed competition reaction between trans-glycosylation and hydrolysis of p-nitrophenyl glucopyranoside (pNPG) was selected, as illustrated in **Scheme 2**.

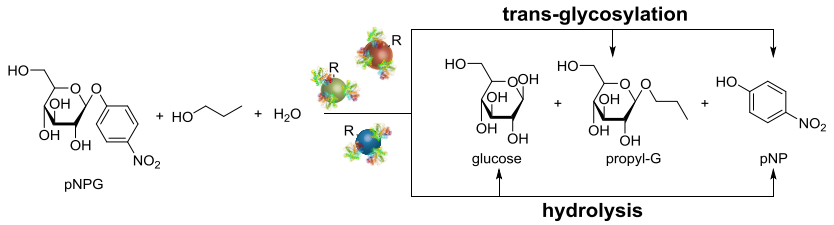

Scheme 2. Enzymatic conversion of p-nitrophenyl β-D-glucopyranoside (pNPG) to propyl-glucoside (propyl-G), p-nitrophenol (pNP) and glucose catalyzed by β-glucosidase immobilized on pristine and functional OSTE particles

1-Propanol was used as a water soluble glycosyl acceptor in order to obtain a one-phase reaction system with different volume ratios between alcohol and acetate buffer (0.1 M, pH 5.0). β-Glucosidase from *Thermotoga neapolitana*, which already demonstrated its potential as a catalyst for the trans-glycosylation of pNPG with 1-hexanol in a 2-phase system (r_s/r_h = 4.0), was immobilized on pristine and functional OSTE particles (see Scheme 1).[12] Initial experiments with free β-glucosidase, in which the 1-propanol content was varied from 75 to 5 vol%, demonstrated high preference of β-glucosidase for trans-glycosylation over hydrolysis at high water contents (see **Figure S1**). Under these conditions, the ratio between trans-glycosylation and hydrolysis r_s/r_h ranged between 28.3 and 2.6 (see **Table S1**). However, it is particularly interesting to improve the selectivity even further at lower alcohol contents. In order to study the effects of the micro-environment on the enzyme selectivity with high precision, a regime with significant reaction rates for both trans-glycosylation and hydrolysis was chosen, which was achieved using 1-propanol contents of 5, 2, and 1 vol% and 95, 98, 99 vol% acetate buffer, respectively. In these experiments, the pristine and functional OSTE particles with immobilized β-glucosidase (≈ 0.6 g particles) were submerged in acetate buffer/1-propanol solutions containing pNPG (28 mM) as the substrate. The resulting enzyme activity, as combined initial reaction rate of trans-glycosylation and hydrolysis was evaluated according to the particle functionality as well as the amount of 1-propanol, which is presented in **Figure 1**.

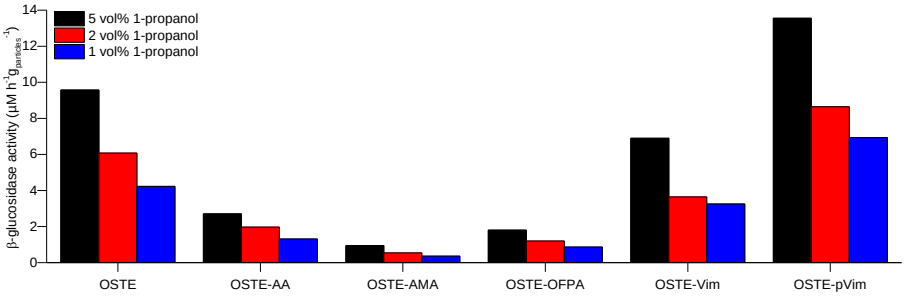

Figure 1. Activity (combined initial reaction rates of trans-glycosylation and hydrolysis) of β-glucosidase immobilized on pristine (OSTE) and functional OSTE particles OSTE-AA, OSTE-AMA, OSTE-OFPA, OSTE-Vim and OSTE-pVim in solutions with different 1-propanol contents, such as 5, 2 and 1 vol%

From these results a general increase in overall enzyme activity with increasing alcohol content was observed, indicating that the enzyme has a high preference for 1-propanol as acceptor substrate. Furthermore, the activity varied substantially between the individual functional particles due to micro-environmental differences around the enzyme. Depending on the amount of 1-propanol, the reference OSTE particles containing β-glucosidase showed a high activity of 4.2 to 9.7 μM h^{-1} $g_{particles}^{-1}$, whereas a considerably reduced activity by 3 to 12-fold was observed for hydroxyl (OSTE-AA), carboxylic acid (OSTE-AMA) and fluorine (OSTE-OFPA) functional particles. Immobilization of β-glucosidase on imidazole functional particles (OSTE-Vim) resulted in activities of about 3.2 to 6.9 μM h^{-1} $g_{particles}^{-1}$, which was even further increased by polymer grafting (OSTE-pVim) (6.9 - 13.6 μM h^{-1} $g_{particles}^{-1}$) corresponding to a factor of 1.4 compared to the pristine particles. Reactions ran in total for 23 hours and the conversion was monitored in time course plots as shown in **Figure 2A-C**.

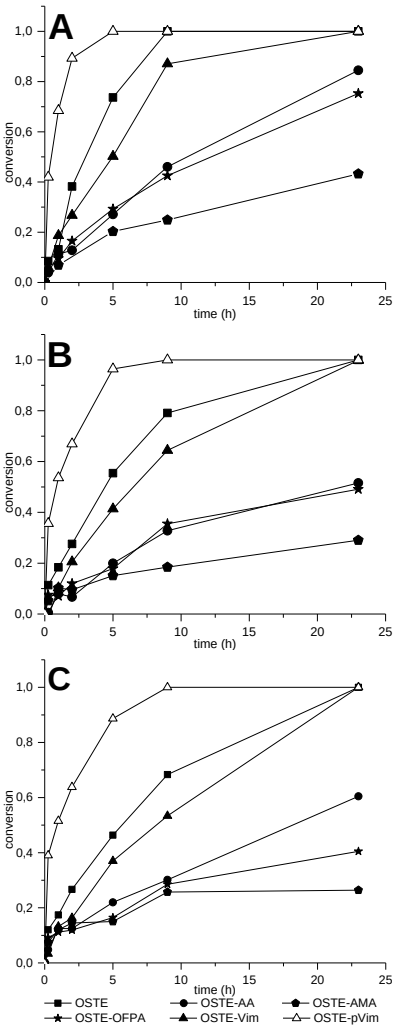

Figure 2. Time course of fractional pNPG conversion catalyzed by β-glucosidase immobilized on pristine (OSTE) and functionalized OSTE particles OSTE-AA, OSTE-AMA, OSTE-OFPA, OSTE-Vim and OSTE-pVim in reaction solution, containing (A) 5 vol% , (B) 2 vol% and (C) 1 vol% 1-propanol

The reaction reached 100 % conversion for OSTE-pVim and OSTE-Vim particles as well as pristine OSTE particles after 23 hours at any alcohol concentration. For the remaining particle types OSTE-AA (84-52%), OSTE-AMA (43-26%) and OSTE-OFPA (75-40%) conversions below 100% were observed.

The previously obtained activities (combined initial reaction rates) were split into the individual rates for trans-glycosylation and hydrolysis (see **Table S2**) in order to

calculate the reactivity ratios r_s/r_h for the individual particles. The ratios r_s/r_h as a measure for the selectivity is presented in **Figure 3** for the three different 1-propanol contents and the different particles.

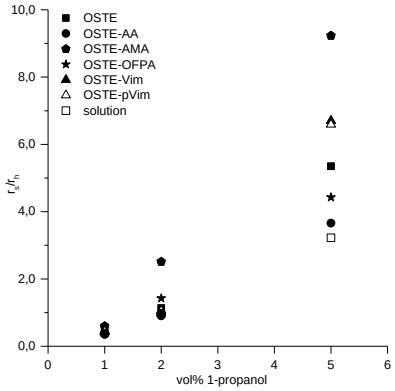

Figure 3. Selectivity (r_s/r_h) between trans-glycosylation (s) and hydrolysis (h) of pNPG catalyzed by β-glucosidase immobilized on pristine (OSTE) and functionalized OSTE particles OSTE-AA, OSTE-AMA, OSTE-OFPA, OSTE-Vim and OSTE-pVim at different 1-propanol contents

The selectivity (r_s/r_h) improved with increasing alcohol concentration. Furthermore, the results demonstrated that the immobilization has a considerable impact on selectivity, especially at higher alcohol contents. Using 1 vol% 1-propanol, r_s/r_h ratios below 1 (0.35 to 0.60) were obtained, implying substantial preference for the hydrolysis for all types of particles as well as in solution. An increase of 1-propanol content to 2 vol% resulted in similar trans-glycosylation and hydrolysis rates and therefore r_s/r_h values of about 1 were obtained for immobilized and free enzyme. An exception being OSTE-AMA particles consisting of carboxylic acid surface moieties, which generated a preference for trans-glycosylation (r_s/r_h = 2.3) already at this low alcohol content. This tendency was even more pronounced at higher alcohol concentration (5 vol%) with a r_s/r_h of 9.2. The high preference for trans-glycosylation of OSTE-AMA was also seen for Vim and pVim functional (6.6/6.7), pristine OSTE (5.4), OSTE-OFPA (4.4) and OSTE-AA (3.7) particles. At this 1-propanol content, immobilization of β-glucosidase improved in each case the formation of propyl-G compared to the reaction in solution (with r_s/r_h of 3.2). As assumed, the differences in selectivity were ascribed to the variations in surface chemistry and consequently in the generation of different enzyme-surface environments. Despite significant differences in overall activity, identical selectivity was achieved for OSTE-Vim and OSTE-pVim particles both containing imidazole functional groups underlining a high dependency of the selectivity on the surface chemistry and micro-environment.

In this study, we present a new method to improve the selectivity between trans-glycosylation over hydrolysis of β-glucosidases by changing the microenvironment through immobilization on OSTE particles containing various surface chemistries. OSTE particles were prepared by suspension polymerization in glycerol. Subsequent surface functionalization via TEC and SCT-FRP allowed the introduction of various surface chemistries, such as hydroxyl (AA), carboxylic acid (AMA), fluorine-containing (OFPA) and imidazole (Vim and pVim) groups. β-glucosidase from *Thermotoga neapolitana* was immobilized via physical adsorption and all particles exhibited significant activity for the reaction of pNPG depending on the surface functionality. Especially, pristine OSTE (containing surface thiols) as well as imidazole (OSTE-Vim and OSTE-pVim) functional particles demonstrated high activities between 6.9 and 13.6 $\mu M\ h^{-1}\ g_{particles}^{-1}$. Furthermore, in each case an increase in overall activity was observed with increased 1-propanol contents from 1 to 5 vol%. Similarly, the trans-glycosylation over hydrolysis ratio increased with increasing alcohol concentration. Compared to free β-glucosidase, trans-glycosylation could be further promoted by immobilization on OSTE particles. Especially at 5 vol% alcohol, the selectivity r_s/r_h increased almost 3 fold from 3.2 up to 9.2 for carboxylic acid functional particles (OSTE-AMA), which was attributed to the individual surface functionalities. These results demonstrated clearly that variations in surface chemistry and thus, changes in surface environment have a significant impact on the selectivity of immobilized enzymes and therefore can be used in order to tailor biocatalytic reactions as demonstrated with β-glucosidase in this case.

ASSOCIATED CONTENT

Supporting Information. Materials and analytical methods, experimental procedures. Initial reaction rates and selectivity of free β-glucosidase, trans-glycosylation and hydrolysis rates of immobilized β-glucosidase, selectivity S_c of immobilized β-glucosidase

AUTHOR INFORMATION

Corresponding Author

*E-mail for A.E.D.: adt@kt.dtu.dk

ORCID

Anders E. Daugaard: 0000-0002-0627-6310

Notes

The authors declare no competing financial interest.

ACKNOWLEDGMENT

Financial support from the Aage and Johanne Louis-Hansen Endowment is gratefully acknowledged.

ABBREVIATIONS

AA: allyl alcohol, AMA allyl malonic acid, HRP: horseradish peroxidase, pNP: p-nitrophenol, pNPG: p-nitrophenyl β-D-glucopyranoside, pVim: poly(1-vinyl imidazole), OFPA: 2,2,3,3,4,4,5,5-octafluoropentyl acrylate, OSTE: off-stoichiometric thiol-ene, PETMP: pentaerythritol tetrakis(3-mercaptopropionate), propyl-G: propyl-glucoside, SCT-FRP: surface chain transfer free radical polymerization, TATATO: 1,3,5-triallyl-1,3,5-triazine-2,4,6(1H,3H,5H)-trione, TEC: thiol-ene chemistry, Vim: 1-vinyl imidazole

REFERENCES

(1) Andree, H.; Hessel, J. F.; Krings, P.; Meine, G.; Middelhauve, B.; Schmid, K. In *Alkyl Polyglycosides: Technology, Properties, Applications*; Hill, K., von Rybinski, W., Stoll, G., Eds.; John Wiley & Sons, Inc., 2008; pp 99–130.
(2) Tesmann, H.; Kahre, J.; Hensen, H.; Salka, B. A. In *Alkyl Polyglycosides: Technology, Properties, Applications*; Hill, K., von Rybinski, W., Stoll, G., Eds.; John Wiley & Sons, Inc., 2008; pp 71–98.
(3) De Roode, B. M.; Franssen, M. C. R.; Van Der Padt, A.; Boom, R. M. *Biotechnol. Prog.* **2003**, *19* (5), 1391–1402.
(4) Rather, M.; Mishra, S. *Sustain. Chem. Process.* **2013**, *1* (1), 7.
(5) Adlercreutz, P. *Appl. Microbiol. Biotechnol.* **2017**, *101* (2), 513–519.
(6) Van Rantwijk, F.; Woudenberg-Van Oosterom, M.; Sheldon, R. A. *J. Mol. Catal. - B Enzym.* **1999**, *6* (6), 511–532.
(7) Hansson, T.; Andersson, M.; Wehtje, E.; Adlercreutz, P. *Enzyme Microb. Technol.* **2001**, *29* (8–9), 527–534.
(8) Parry, N. J.; Beever, D. E.; Owen, E.; Vandenberghe, I.; Van Beeumen, J.; Bhat, Mm. K. *Biochem. J.* **2001**, *353*, 117–127.
(9) Ljunger, G.; Adlercreutz, P.; Mattiasson, B. *Enzyme Microb. Technol.* **1994**, *16*, 751–755.
(10) Hansson, T.; Adlercreutz, P. *Biotechnol. Bioeng.* **2001**, *75* (6), 656–665.
(11) Mladenoska, I. *Food Technol. Biotechnol.* **2016**, *54* (2), 211–216.
(12) Turner, P.; Svensson, D.; Adlercreutz, P.; Karlsson, E. N. *J. Biotechnol.* **2007**, *130* (1), 67–74.
(13) Guo, D. H.; Xu, Y. S.; Kang, Y. J.; Han, S. Y.; Zheng, S. P. *Enzyme Microb. Technol.* **2016**, *85*, 90–97.
(14) Lundemo, P.; Adlercreutz, P.; Karlsson, E. N. *Appl. Environ. Microbiol.* **2013**, *79* (11), 3400–3405.
(15) Martearena, M. R.; Blanco, S.; Ellenrieder, G. *Bioresour. Technol.* **2003**, *90* (3), 297–303.
(16) Larsson, J.; Svensson, D.; Adlercreutz, P. *J. Mol. Catal. B Enzym.* **2005**, *37* (1–6), 84–

87.
(17) Svensson, D.; Ulvenlund, S.; Adlercreutz, P. *Biotechnol. Bioeng.* **2009**, *104* (5), 854–861.
(18) Lundemo, P.; Karlsson, E. N.; Adlercreutz, P. *J. Mol. Catal. B Enzym.* **2014**, *108*, 1–6.
(19) Kumar, P.; Ryan, B.; Henehan, G. T. M. *Protein Expr. Purif.* **2017**, *132*, 164–170.
(20) Graebin, N. G.; Schöffer, J. D. N.; De Andrades, D.; Hertz, P. F.; Ayub, M. A. Z.; Rodrigues, R. C. *Immobilization of glycoside hydrolase families GH1, GH13, and GH70: State of the art and perspectives*; 2016; Vol. 21.
(21) Cakmakci, E.; Danis, O.; Demir, S.; Mulazim, Y.; Kahraman, M. V. *J. Microbiol. Biotechnol.* **2013**, *23*, 205–210.
(22) Lafleur, J. P.; Senkbeil, S.; Novotny, J.; Nys, G.; Bøgelund, N.; Rand, K. D.; Foret, F.; Kutter, J. P. J. P. *Lab Chip* **2015**, *15* (10), 1–2.
(23) Çakmakçi, E.; Yuce-Dursun, B.; Demir, S. *React. Funct. Polym.* **2017**, *111*, 38–43.
(24) Santos, J. C. S. Dos; Barbosa, O.; Ortiz, C.; Berenguer-Murcia, A.; Rodrigues, R. C.; Fernandez-Lafuente, R. *ChemCatChem* **2015**, *7* (16), 2413–2432.
(25) Giacomini, C.; Irazoqui, G.; Batista-Viera, F.; Brena, B. M. *J. Mol. Catal. - B Enzym.* **2001**, *11* (4–6), 597–606.
(26) Irazoqui, G.; Villarino, A.; Batista-Viera, F.; Brena, B. M. *Biotechnol. Bioeng.* **2002**, *77* (4), 430–434.
(27) Liu, J.; Bai, S.; Jin, Q.; Zhong, H.; Li, C.; Yang, Q. *Langmuir* **2012**, *28* (25), 9788–9796.
(28) Barbosa, O.; Torres, R.; Ortiz, C.; Berenguer-Murcia, Á.; Rodrigues, R. C.; Fernandez-Lafuente, R. *Biomacromolecules* **2013**, *14* (8), 2433–2462.

Appendix 3.2 – Supporting information

MATERIALS AND METHODS

Materials. Pentaerythritol tetrakis(3-mercaptopropionate) (PETMP, >95%), 1,3,5-Triallyl-1,3,5-triazine-2,4,6(1H,3H,5H)-trione (TATATO, 98%), allyl alcohol (AA, 99%), allyl malonic acid (AMA, ≥98%), 1-vinyl imidazole (Vim, ≥99%), 2,2,3,3,4,4,5,5-octafluoropentyl acrylate (OFPA, 97%), 2,2-dimethoxy-2-phenylacetophenone (DMPA, 99%), p-nitrophenyl β-D-glucopyranoside (pNPG, ≥98%), p-nitrophenol (pNP, ≥98%), n-Amyl β-D-glucopyranoside (AG, 98%), D-(+)-glucose (≥99%) were obtained from Sigma-Aldrich. Ethyl-2, 4, 6-tri-methylbenzoylphenyl phosphinate (Lucirin TPO-L) was obtained from BASF. Ethanol absolute (99.97%) was purchased from VWR. Glycerol was kindly provided by Emmelev, Otterup A/S Denmark and was used as received. *Thermotoga neapolitana* β-glucosidase 3B (EC 3.2.1.21) was obtained from *Escherichia coli* batch cultivations. It was purified using a two-step protocol, including heat treatment of the cell extract (70 ◦C, 30 min), which was followed by immobilized metal ion affinity chromatography using the supernatant from the heat treatment step as described by Pozzo et al. The enzyme was stored at 4 °C until use.[30]

Methods. β-glucosidase reactions were followed using HPLC (LaChrom; pump L-7100, interface L-7000, autosampler L- 7250 with a 20 ml injection loop, UV-detector L7400, Hitachi Ltd. Tokyo, Japan) equipped with an evaporative light scattering detector (Alltech 500 ELSD, Alltech Associates Inc., Deer-field, USA) with evaporator temperature 78 °C, a nebulizer gas flow of 2.0 standard liters per minute and a Kromasil 100-5-NH2 column (4.6 μm × 250 mm, Kromasil). Isokratic conditions with 85 % acetonitrile and 15 % MQ water under a constant flow rate of 1.0 ml min^{-1} were used. pNP has a retention time of 4.1 and was monitored at 405 nm using the UV detector. pNPG elutes after 4.9 min and was followed at 405 nm as well as with ELSD. PG eluted after 6.2 min and glucose after 13.8 min, both were detected by ELSD. Concentrations were determined by use of 8 point external standard curves. For PG no standard was available, therefore the calibration was prepared using n-amyl β-D-glucopyranoside. Combined initial reaction rates taking both, trans-glycosylation and hydrolysis into consideration, were estimated from the initial changes in molar concentration of pNPG over time. Similarly, the individual initial reaction rates for trans-glycosilation and hydrolysis were estimated using the initial changes molar concentrations over time of propyl-G and glucose, respectively.

Preparation off-stoichiometric thiol-ene (OSTE) particles. TPO-L (3.0 mg, 0.1 wt%), PETMP (2.217 g, 0.0012 mol), TATATO (0.794 g, 0.0016 mol), and glycerol (30 mL) were added into a mixing cup under exclusion of light. Then, the mixture was mixed in a Speedmixer at 1000 rpm (SpeedMixerTM DAC 150.1 FVZ) for 1.5 minutes before the formed emulsion was exposed to UV light (λ= 365 nm, 1.4 mW cm^{-2}) for 10

minutes. Subsequently, ethanol was added to the formed particles in glycerol, which was homogenized by brief manual stirring and the resulting particles were filtered and thoroughly rinsed with ethanol.

Surface functionalization of OSTE particles via thiol-ene chemistry (TEC). In a general procedure, the full batch of previously prepared OSTE particles was directly submerged in a solution containing 1-vinyl imidazole (0.824 mL, 0.009 mol), TPO-L (28.6 mg) and 20 mL ethanol. After magnetically stirring for 5 min under light exclusion, the stirring mixture was exposed to UV-light (λ= 365 nm, 1.4 mW cm^{-2}) for 5 minutes. Thereafter, the particles were filtered and thoroughly rinsed with ethanol before drying in vacuo overnight, which led to a white material (2.1459 g, yield 71 %).

Surface functionalization via allyl alcohol (AA) by TEC. OSTE-AA was prepared in accordance to the general procedure, using 20 mL of an ethanolic solution of allyl alcohol (AA, 408 µL, 6.0 mmol) and TPO-L (28.6 mg) as reagent.

Surface functionalization via allyl malonic acid (AMA) by TEC. OSTE-AMA was prepared in accordance to the general procedure, using 20 mL of an ethanolic solution of allyl malonic acid (AMA, 0.864 g, 6.0 mmol) and TPO-L (28.6 mg) as reagent.

Surface functionalization via 2,2,3,3,4,4,5,5 octafluoropentyl acrylate (OFPA) by TEC. OSTE-OFPA was prepared in accordance to the general procedure, using 20 mL of an ethanolic solution of 2,2,3,3,4,4,5,5 octafluoropentyl acrylate (OFPA, 1.36 mL, 6.0 mmol) and TPO-L (28.4 mg) as reagent.

Surface functionalization of OSTE particles via surface chain transfer free radical polymerization (SCT FRP) with 1-vinyl imidazole (OSTE-pVim). In a general procedure, the full batch of previously prepared OSTE particles was submerged in a solution containing 1-vinyl imidazole (Vim, 10.4 mL, 0.115 mol), 2,2-dimethoxy-2-phenylacetophenone (DMPA, 142.8 mg, 0.50 mol%) and ethanol (20 mL), which was screened from ambient light. Under magnetic stirring, this mixture was subsequently irradiated with UV light (λ= 365 nm, 0.4 mW cm^{-2}) for 30 min. Thereafter, the particles were filtered and thoroughly rinsed with ethanol before drying in vacuo overnight, which led to a light yellow material.

Immobilization of β-glucosidase. 1.5 g of the previously functionalized particles was resuspended in ethanol, which was subsequently 4 times solvent exchanged by phosphate buffer (0.1 M, pH 7.2). The final amount of buffer was 7.5 mL and β-glucosidase (7.5 mg, 1.0 mg mL^{-1}) was added to this mixture. The suspension was incubated under shaking at 4 °C. After 17 h the particles were filtered under suction and thoroughly washed with phosphate buffer (0.1 M, pH 7.2). An aliquot of 100 µL was directly withdrawn and the suspension was incubated under shaking at 4 °C. After 17 h

an aliquot of the supernatant was withdrawn and the particles were filtered under suction and thoroughly washed with phosphate buffer (0.1 M, pH 7.2).

Selectivity study of immobilized β-glucosidase. The particles used for immobilization of β-glucosidase were directly after filtration divided into three equal sized portions. To portion 1 (0.6724 g), 4 mL of a mixture of acetate buffer (0.1 M, pH 5.0) and 1-propanol in a volume ratio of 95 : 5 containing pNPG (28 mM) was added. Similarly, to portion 2 (0.6570 g) and portion 3 (0.6872 g), 4 mL of an acetate buffer/1-propanol mixture in a volume ratio of 98 : 2, and 99 : 1 vol% containing each pNPG (28 mM) was added. These suspensions were vortex mixed for 10 s and subsequently incubated under shaking (750 rpm) at 37 °C. Samples of the supernatant (100 µL) were withdrawn after 0, 0.25, 0.5, 1, 2, 5, 9 and 23 h. To each aliquot, 100 µL of a NaOH solution (2 mM) and 500 µL of acetonitrile were added, and the final samples were analyzed by HPLC.

Selectivity study of free β-glucosidase. To 2.0 mL of a 95 : 5 vol% acetate buffer (0.1 M, pH 5.0)/1-propanol solution containing pNPG (28 mM), 5 µL of dissolved β-glucosidase (in phosphate buffer, 0.1 M, pH 7.3, 3.95 mg mL^{-1}) was added resulting in a final enzyme concentration of 9.85 µg mL^{-1}. In the same way, a 98 : 2 vol% acetate buffer (0.1 M, pH 5.0)/1-propanol solution containing pNPG (28 mM) and a 99 : 1 vol% acetate buffer (0.1 M, pH 5.0)/1-propanol solution containing pNPG (28 mM) were used. These reaction mixtures were incubated at 37 °C under shaking (750 rpm) and samples (100 µL) were withdrawn after 0, 0.25, 0.5, 1, 2, 5, 9 and 23 h. To each aliquot, 100 µL of a NaOH solution (2 mM) and 500 µL of acetonitrile were added, and the final samples were analyzed by HPLC.

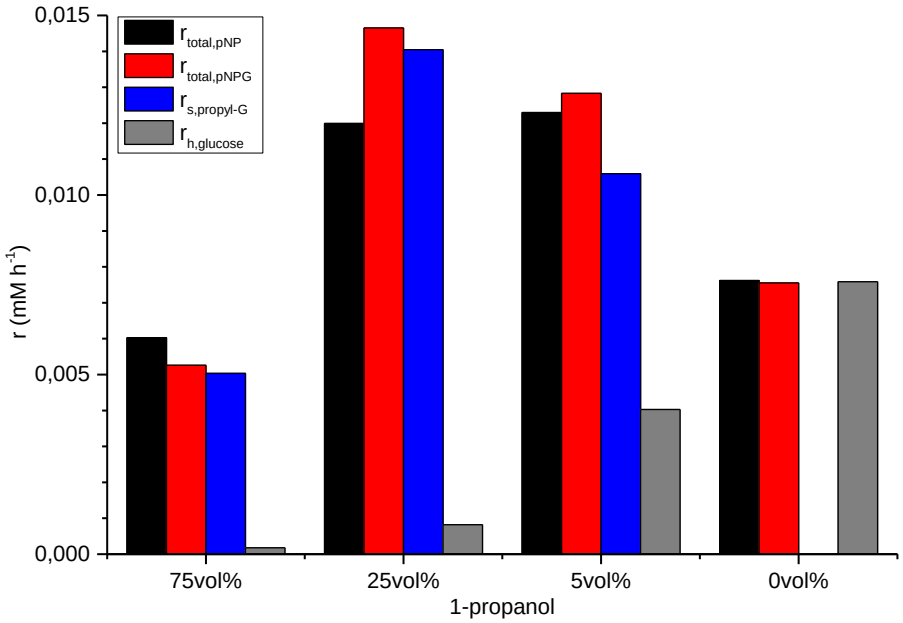

Figure S1. Overall initial reaction rates for the conversion of pNPG ($r_{total,pNPG}$) and the formation of pNP ($r_{total,pNP}$), as well as for the individual trans-glycosylation ($r_{s,propyl\text{-}G}$) and hydrolysis ($r_{h,glucose}$) reactions between pNPG, water and 1-propanol by β-glucosidase from *Thermotoga neapolitana* in solution

Table S1 Selectivity determination between trans-glycosylation (s) and hydrolysis (h), represented as by ratio of the reaction rates r_s/r_h of β-glucosidase from *Thermotoga neapolitana* in solution at different 1-propanol contents

r_s/r_h	$vol\%_{1\text{-propanol}}$
28.3	75
17.1	25
2.6	5
0,0	0

Table S2 rates of trans-glycosylation and hydrolysis of immobilized β-glucosidase depending on the surface chemistry of the particles and solvent ratio between water and 1-propanol

Particle type	Particle size	5 vol% 1-propanol		2 vol% 1-propanol		1 vol% 1-propanol	
		r_s	r_h	r_s	r_h	r_s	r_h
OSTE	396	7,38	1,38	2,41	2,13	1,00	2,28
OSTE-Vim	141	5,16	0,77	0,95	0,97	0,54	1,25
OSTE-AA	83	1,69	0,46	0,50	0,55	0,22	0,61
OSTE-AMA	110	0,85	0,09	0,22	0,09	0,08	0,13
OSTE-OFPA	131	1,66	0,38	0,61	0,43	0,25	0,45
OSTE-pVim	173	12,4	1,9	3,4	3,3	1,6	3,7

[a]reaction rates in [μM h^{-1} $g_{particle}^{-1}$], particle size as Dv50 (median) in [μm]

Table S3 Selectivity results between trans-glycosilation and hydrolysis of immobilized β-glucosidase depending on the surface chemistry of the applied particles and solvent ratio between water and 1-propanol, S_c values were calculated according as described in literature using the concentration of aqueous and alcohol phase: $S_c = \frac{r_s}{r_h}\frac{[water]}{[1-propanol]}$ [7]

type of particles	S_c		
	5vol% 1-propanol	2vol% 1-propanol	1vol% 1-propanol
OSTE	422	231	180
OSTE-AA	289	184	146
OSTE-AMA	728	511	246
OSTE-OFPA	349	290	222
OSTE-Vim	529	198	177
OSTE-pVim	520	213	182

Appendix 4

Area selective enzyme immobilization and its effect on biocatalytic activity experimentally and by CFD

*Christian Hoffmann[a], Inês P. Rosinha Grundtvig[b], Joachim Thrane[b], Nipun Garg[a], Krist V. Gernaey[b], Manuel Pinelo[c], John M. Woodley[b], Ulrich Krühne[b], Anders E. Daugaard[a,]**

Submitted to Chemical Engineering Journal

Appendix 4.1 – Manuscript

Experimental and computational evaluation of area selectively immobilized horseradish peroxidase in a microfluidic device

Christian Hoffmann[a], Inês P. Rosinha Grundtvig[b], Joachim Thrane[b], Nipun Garg[a], Krist V. Gernaey[b], Manuel Pinelo[c], John M. Woodley[b], Ulrich Krühne[b], Anders E. Daugaard[a,]*

[a]Danish Polymer Centre, Department of Chemical and Biochemical Engineering, Technical University of Denmark, Søltofts Plads Building 229, 2800 Kgs. Lyngby, Denmark

[b]Process and Systems Engineering Center (PROSYS), Department of Chemical and Biochemical Engineering, Technical University of Denmark, Søltofts Plads Building 229, 2800 Kgs. Lyngby, Denmark

[c]Center for BioProcess Engineering, Department of Chemical and Biochemical Engineering, Technical University of Denmark, Søltofts Plads Building 229, 2800 Kgs. Lyngby, Denmark

*Corresponding author, adt@kt.dtu.dk

Abstract

A microreactor with a square shaped reactor chamber was developed with the aim to correlate enzyme positioning with biocatalytic activity. The enzyme position as an important parameter to improve the contribution of the individual enzymes towards the overall reactor efficacy was therefore evaluated experimentally and by computational fluid dynamics (CFD) simulations. Ultimately, such a correlation would lead to faster development through computational pre-screening and optimized experimental design.

In this proof-of-concept study, microreactors were prepared in a 2-step curing process of an off-stoichiometric thiol-ene-epoxy (OSTE+) mixture employing both a thiol-ene (TEC) and a thiol-epoxy curing reaction. Subsequent surface functionalization of the remaining thiol groups on the reactor surface through stenciled photoinitiated TEC enabled the preparation of specific surface patterns in the reactor. Patterns were visualized using an allyl-functional disperse red dye, illustrating the successful preparation of a fully reacted surface, a half covered surface and 2 checkerboard patterns. Similarly, allyl glycidyl ether was exploited to functionalize the microreactor surface with epoxide groups, which were used for covalent immobilization of horseradish peroxidase (HRP) in the same patterns. Biocatalytic activity measurements confirmed a clear dependency of the overall reactor performance depending on the spatial distribution of the immobilized enzymes, where specifically the two checkerboard motifs were identified as being particularly effective compared to enzymes covering homogeneously the entire reactor surface. The performance of the same configurations was additionally determined by 3-dimensional CFD simulations. The computational model predicted the same tendencies for

the overall reactor performance as obtained from experimental determination. This good agreement between the obtained experimental and computational results confirmed the high potential of CFD models for predicting and optimizing the biocatalytic performance of such a reactor.

Keywords
Microfluidics; thiol-ene chemistry; enzyme immobilization; surface functionalization; computational fluid dynamic simulation (CFD)

1. Introduction

The application of enzymes as biocatalysts in industrial processes has attracted increased attention in recent years due to several major advantages of enzymes compared to conventional catalysts. Enzymes originate from renewable resources and take part in green processes with a high catalytic selectivity under mild reaction conditions [1]. These advantageous properties make them attractive for specific applications like synthesis of targeted enantiomerically-pure chiral compounds relevant for pharmaceuticals. However, the disadvantage of enzymes for application at large scale and in continuous processes is their low long-term stability. In order to increase the attractiveness of enzymes for industrial processes, improving their long-term biocatalytic efficiency is a key target. It is well known that an increase in enzyme stability, and consequently biocatalytic productivity, can be achieved through immobilization on solid supports [2–4]. In particular, polymers have shown high potential as enzyme carriers generating biocatalytic systems with an improved stability to external conditions, such as temperature, pH and reaction media [5]. The binding of enzymes on support surfaces can generally be established by adsorption, ionic or covalent bond formation. However, the positive effect in terms of stability is frequently offset by a loss in biocatalytic activity. One explanation is the decreased accessibility to the enzyme's active site by the substrate due to conformational restrictions by attaching the protein to the support material. In order to overcome this, the preservation of the natural environment for a specific enzyme has been identified to be of high importance [6]. This can be realized by chemical modification of the surface, such as by increasing the hydrophilicity of the surface. Functionalization with poly(ethylene glycol) (PEG) for instance shows an improvement in enzymatic activity [7]. Developments in reactor design and reaction conditions play an additional role in order to optimize enzyme efficiency and consequently entire biocatalytic processes. We recently reported that biocatalytic reactors with immobilized enzymes can exhibit differences in their overall productivity, depending on the local position of the enzymes within the flow field of the reactor [8]. Changing the surface pattern of a given amount of enzyme resulted in a different productivity. It was shown that optimization of the spatial distribution of the immobilized enzymes could thus lead to an improved reactor efficiency.

In order to test the influence of such modifications in continuous flow systems, microfluidic devices have been proven to be suitable due to their small size, low consumption of reagents and limited reaction volumes as well as high throughput combined with a high degree of reproducibility [9,10]. Additionally, good heat and mass transfer in combination with laminar flow provide good control over reaction conditions [11]. Laminar flow restricts mixing to occur exclusively by diffusion, unless this is circumvented by specific microchannel configurations.

Heterogeneous reactions take place solely on the surface of the catalyst or on the surface that the catalyst is bound to. In these systems, diffusion shows a great impact on the overall reaction, which is influenced by many different parameters, such as flow rate, concentration, dimensions of the reactor geometry and reaction rate [12]. Microfluidic systems are traditionally fabricated in glass or polymeric materials such as poly(methyl methacrylate) (PMMA) or poly(dimethylsiloxane) (PDMS) [13–15]. Especially PDMS has been used extensively for microfluidics due to the ease of fabrication and relatively low cost [16]. Mold casting enables the preparation of different reactor designs and has been applied for the development of biocatalytic microreactors. Hence, enzymes were immobilized on polymer microbeads [17,18] or onto the reactor walls [19]. Alternatively, the formation of a surface patterned phospholipid bi-layer or an adsorbed protein layer [20] enabled the attachment of enzymes on the PDMS surfaces.

Direct protein and enzyme immobilization onto polymer surfaces in microfluidic devices in off-stoichiometric thiol-ene (OSTE) material is an interesting alternative to the currently used PDMS systems. OSTE thermosets have recently evolved into a very versatile platform, which have been successfully applied for fabrication of microfluidic devices [21]. Generally, OSTE systems consist of a multifunctional thiol and a multifunctional alkene (ene) reacting through thiol-ene chemistry (TEC) either under photochemical or thermal conditions [22]. OSTE networks are compatible with many organic solvents, are thermally stable and can be directly surface functionalized. Material properties can be controlled by selecting from a large variety of reagents, which makes this system very versatile. The OSTE approach has recently been updated in order to improve mechanical properties as well as surface bonding, which is essential for the fabrication of microfluidics. In this OSTE+ system, Bisphenol A diglycidyl ether (BADGE) undergoes a thiol-epoxy reaction in an additional, orthogonal curing step. This enables covalent sealing between interfaces of the precured material in order to prevent leaking under operating conditions, which is a well-known challenge in microfluidics [23,24]. Mechanical properties of the thermoset can be controlled by stoichiometric variations between thiol and ene groups. Furthermore, off-stoichiometric ratios result in excess of unreacted functional groups, either thiol or ene [25]. These functional groups are well suited for further surface functionalization via photochemical TEC, which has been applied for tailoring surface properties [26,27] or introducing different functional molecules [28]. Additionally, photochemical TEC on the surface offers a possible pathway for surface modification in various patterns by application of a stencil [29,30].

So far, OSTE(+) thermosets have been rarely used for the immobilization of enzymes. Lafleur and coworkers utilized OSTE monoliths for the immobilization of galactose oxidase and peptide-N-glycosidase F after surface activation by means of L-ascorbic acid linking groups [31].

Recently, Schäpper et al. developed a theoretical topology optimization of immobilization of yeast cells, which resulted in an 8-10 fold improvement in theoretical production rate [32]. Inspired by this approach and by applying isolated enzymes instead of whole cells, we demonstrated using computational fluid dynamic (CFD) simulations that in a laminar flow field of a square reactor with a distributed flow pattern, the biocatalytic reactor efficacy considerably depends on the positioning of the immobilized enzyme [8]. By varying computationally the topology of immobilized enzymes inside the microreactor, simulated reactor configurations with substantially improved productivities were obtained. To the best of our knowledge, reactor

optimization based on the positioning of the immobilized biocatalyst within the reactor, either computationally or experimentally, has not yet been done.
The objective of this proof-of-concept study was the methodological development of a biocatalytic reactor, which enabled experimental and computational investigation of the effect of the local distribution of immobilized enzymes towards the overall reactor efficacy. The correlation between experimental and computational results should demonstrate the potential of CFD simulations to predict the biocatalytic performance of such reactors, and would thus open up for the use of CFD for optimization of the microfluidic reactor configuration. In order to achieve this, an enzymatic microreactor containing immobilized horseradish peroxidase as a model enzyme in distinct surface patterns was developed. A square reactor geometry was selected in order to achieve a specific flow pattern characterized by a velocity distribution across the reactor. The laminar flow within the reactor made it possible to assess the impact of selectively distributing the immobilized enzyme on the overall reactor productivity. The impact of the spatial distribution of surface immobilized HRP towards the biocatalytic performance was determined and the results were correlated to those obtained from CFD simulations. This strategy offers a possibility for reactor development and can facilitate the optimization process of new catalytic reactors.

2. Experimental

2.1. Materials

Pentaerythritol tetrakis(3-mercaptopropionate) (PETMP, >95%), 1,3,5-Triallyl-1,3,5-triazine-2,4,6(1H,3H,5H)-trione (TATATO, 98%), bisphenol A diglycidyl ether (BADGE, >95%), 1,5-Diazabicyclo[4.3.0]non-5-ene (DBN), allyl bromide (97%), disperse red 1 (95%), potassium hydroxide, 18-crown-6-ether, allyl glycidyl ether (>99%), horseradish peroxidase (HRP, lyophilized powder, 50-150 U mg^{-1}), 2,2′-Azino-bis(3-ethylbenzothiazoline-6-sulfonic acid) diammonium salt (ABTS, ≥98%), hydrogen peroxide (3%), toluene and THF were obtained from Sigma Aldrich and used without further purification. Lucirin TPO-L (ethyl-2, 4, 6-tri-methylbenzoylphenyl phosphinate) was purchased from BASF. Sylgard 184 – poly(dimethylsiloxane) (PDMS) elastomer kit was purchased from Dow Corning.

2.2. Characterization

NMR spectroscopy was carried out on a Bruker Avance 300 MHz spectrometer. Chemical shifts are given in ppm.

2.3. Microchip preparation

Master molds for the top and bottom part of the microfluidic device fabricated in poly(methyl methacrylate) (PMMA) were micro-milled in order to use them for the preparation of negative molds. Those were prepared from PDMS (Sylgard 184 elastomer kit) by curing at 80 °C and casting from the master molds. The PDMS molds were utilized for all further microchip preparation procedures. For this in brief, PETMP, TATATO and BADGE were mixed in a functionality ratio of 2.0 : 1.0 : 0.25. Lucirin (1.0 wt%) and DBN (1.0 wt%) were added and the solution was homogenized by mixing in a Speedmixer (SpeedMixer™ DAC 150.1 FVZ) for 2 min at 3000 rpm and subsequently poured into the PDMS molds and covered with a PMMA slide (thickness 2 mm) in order to ensure uniform thickness. In the subsequent light induced

curing step, this mixture was irradiated with UV light (□= 365 nm, 2.9 mW cm^{-2} without and 1.6 mW cm^{-2} with PMMA slide on top of the thiol-ene mixture) for 10 min. The obtained upper and lower layer of the microchip were aligned and properly attached to each other. Two thin PMMA plates, one on top and one at the bottom, were fixed at the microchip and by employing several clamps; the system was mechanically sealed in order to provide best contact. Subsequently, the microchip was thermally cured at 80 °C under vacuum for 2 h. The resulting sealed microchips were used without further treatment.

2.4. Synthesis of allyl disperse red 1

18-crown-6-ether (12.9 mg, 0.048 mmol), THF/water (10 mL, 99.5:0.5 vol%), potassium hydroxide (0.693 g, 12.1 mmol) and disperse red 1 (1.00 g, 3.03 mmol) were added into a round bottom flask and stirred at room temperature for 1 h. Allyl bromide (0.81 mL, 9.08 mmol) was subsequently added at room temperature. The solution was stirred for 21 h until the substrate was fully converted, which was determined by thin layer chromatography in heptane/ethyl acetate (60:40). After addition of ammonium chloride solution (NH_4Cl, 20 mL, 2 M), the reaction solution was extracted with dichloromethane (5x20 mL). The organic phase was dried over $MgSO_4$, filtrated and subsequently concentrated in vacuo leading to a dark red solid powder as the final product (1.18 g, 86 % yield).

2.5. Microchip surface modification with allyl disperse red 1

An allyl disperse red 1 (83.8 mg, 0.30 M) solution was prepared in toluene (0.8 mL) containing benzotriazole (0.69 mM) and Lucirin (33 mM). During the entire procedure light exposure of the reaction solution was minimized by covering vials and syringes with aluminum foil. Before filling the microchip with the reactive solution, a stencil mask (with specific pattern) made of a black polypropylene (PP) sheet was attached on top of it and a black PP sheet on the bottom of the chip. Then, an aliquot of the light sensitive solution was added into the cavity of the microchip using a syringe. The microchip was then irradiated with UV light (λ= 365 nm, 1.0 mW cm^{-2}) from the top for 3 min and subsequently covered with aluminum foil and flushed continuously with 80 mL of toluene for 240 min.

2.6. Microchip surface modification for enzyme immobilization

For the surface modification, 174 µL allyl glycidyl ether (1.47 mmol, 0.29 mM) and 4.83 mL toluene (containing 0.78 mM benzotriazole) were added into a vial. During the entire procedure light exposure of the reaction solution was minimized by covering vials and syringes with aluminum foil. Subsequently, 51.6 mg of Lucirin (0.163 mmol, 33 mM) were added and the solution was homogenized by mixing using a Vortex mixer. Before filling the microchip with the reactive solution, a black polypropylene (PP) stencil mask (with specific pattern) was attached on top of it. Additionally, the bottom of the chip was also covered with a black PP mask. Then, an aliquot of the light sensitive solution was added into the cavity of the microchip using a syringe. The microchip was then irradiated with UV light (λ= 365 nm, 1.0 mW cm^{-2}) from the top for 3 min and subsequently covered with aluminum foil and flushed continuously with 50 mL of toluene for 180 min. The solvent was evaporated in a vacuum oven at room temperature.

2.7. Horseradish peroxidase immobilization

The surface modified microchips were filled with HRP solution (1.0 mg mL^{-1} in PBS buffer pH 7.2) and incubated for 15 h at 4 °C. Then, the supernatant immobilization solution was removed and the microchip was flushed with 25 mL of PBS buffer (pH 7.2) within 1 h.

2.8. Activity study

The microchip was filled with phosphate buffer (0.1 M, pH 5). Subsequently the inlet of the microchip was attached to a syringe pump and the outlet to a UV-Vis detector for online absorbance measurements [33]. The microchip was continuously flushed with phosphate buffer solution (0.1M, pH5) containing ABTS (1.0 mM) and hydrogen peroxide (2.0 mM) at a flow rate of 225 µL min^{-1}.using a syringe pump (500µL, Tecan Cavro XLP6000) The outlet of the microreactor was connected to an 8-port injection valve (VICIE45-230-CR2 head) which was programmed to collect samples every 16s. The UV-Vis detector (Agilent G1315AR) recorded the absorbance at wavelengths of 340 and 414 nm corresponding to the absorbance maxima of the substrate (ABTS) and its oxidized product ($ABTS^{\bullet+}$), respectively. After reaching steady state conditions, the measurements were constantly recorded for a further 30 min. Afterwards the microchips were rinsed with phosphate (0.1 M, pH 5) and PBS buffer (pH 7.4). A schematic drawing of the setup can be found in the supporting information (SI-Fig. 1).

2.9. Computational fluid dynamic simulation

Each microreactor geometry was designed and discretized in calculation elements using the software ICEM CFD® 16.0. The number of elements for the four simulated structures varied between 850000 and 900000 elements. The setup of the system as well as the 3-dimensional simulations were performed with help of the commercial software ANSYS CFX (16.0). The flow inside was simulated as a steady state laminar flow, with a constant flow rate of 225 µL min^{-1} matching the experimental conditions. The diffusion coefficients used in the computational investigation have been previously reported in the scientific literature [34]. The diffusion coefficients for both the substrate and the product were assumed to be the same, $2.4 \cdot 10^{-10}$ m^2 s^{-1}, since there are no significant structural changes for the molecules. The kinetic parameters K_M and k_{cat} were experimentally determined by maintaining the hydrogen peroxide concentration constant, which simplifies the Ping Pong Bi Bi kinetic mechanism to the Michaelis-Menten mechanism. The apparent kinetic parameters were determined from this mechanism. The Michaelis-Menten constant (K_M) and the maximum reaction rate (V_{max}) were calculated using the Hanes-Wolf method and the turnover number (k_{cat}) was obtained through the linear relation between the V_{max} values and the enzyme concentration. The experimentally determined reaction kinetic parameters are: k_{cat} = 732 s^{-1} and K_M = 0.76 mM. The immobilized enzyme is defined as a wall on which the reaction occurs. The enzyme concentration on the surface was determined considering that the diameter of an enzyme molecule is assumed to be roughly 10 nm. From the area of a molecule ($7.85 \cdot 10^{-17}$ m^2), the maximum concentration of enzyme that can be immobilized in a monolayer is calculated as $2.12 \cdot 10^{-8}$ $mol \cdot m^{-2}$ [35]. The dimensions of the immobilization areas in the CFD simulation are the same as the areas of the experimental work.

The performance of each structure was evaluated by considering the average product concentration at the outlet at steady state as the performance indicator.

3. Results and discussion

In Figure 1 the fabrication process of the thiol-ene-epoxy based microreactors is illustrated, including the used monomers (A), the photochemical (B) and the subsequent thermal (C) curing step. As base compounds PETMP, TATATO and BADGE (see Figure 1A) were used in a ratio of 2.0:1.0:0.25.

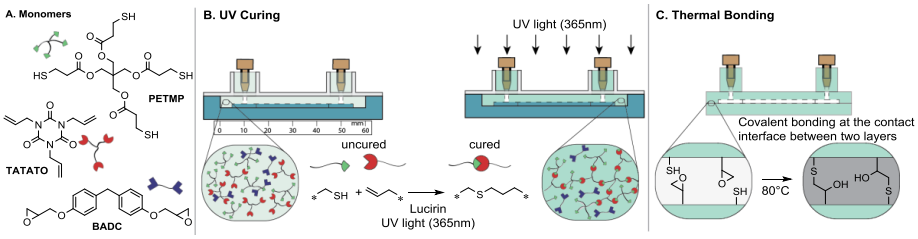

Figure 1. Schematic representation of the preparation of OSTE+ microchips with subsequent surface modification. A) Monomers for OSTE+ preparation tetra functional thiol PETMP, trifunctional allyl TATATO and bifunctional BADGE, B) First UV curing of the OSTE+ mixture via thiol-ene reaction followed by C) a second curing that seals the system "leakage free"

The liquid mixture was cured in a PDMS mold using lucirin as a photoinitiator and UV light (λ=365 nm), as illustrated in Figure 1B. After crosslinking, the upper and lower part of the microchip were assembled and residual epoxide and thiol groups were utilized in a thermal bonding reaction at the interface, which resulted in a stable and leakage-free microreactor (see Figure 1C). The geometry of the microreactor is based on a square shape with a length and width of 30 mm and a thickness of 0.25 mm with an inlet and outlet channel of 10 mm in length and width located at the two opposite ends of the reactor, as can be seen in Figure 2A.

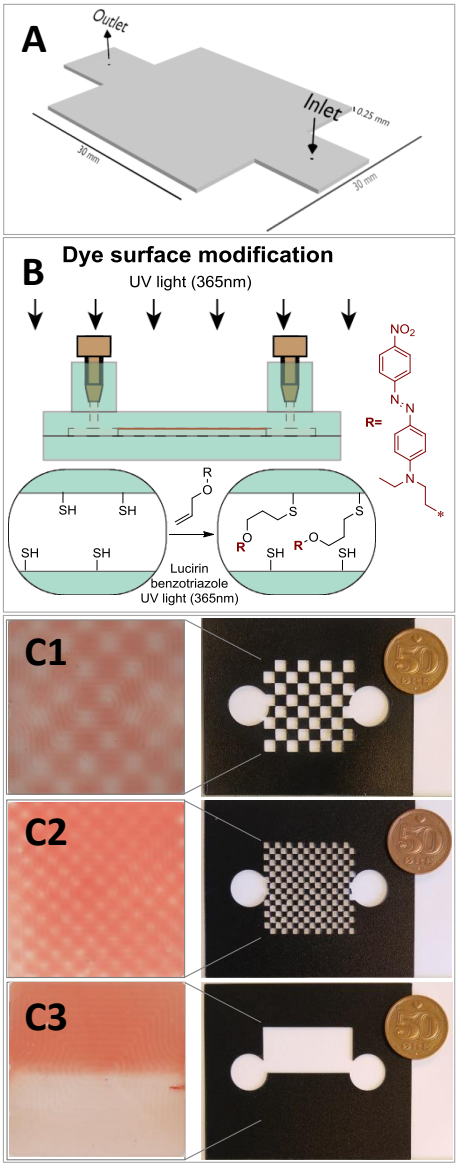

Figure 2. A) Microreactor geometry, B) Microreactor surface modification via TEC using allyl disperse red, C1-3) Images of surface functionalized microchips using allyl disperse red and different stencil masks: C1 – coarse checkerboard, C2 – fine checkerboard, C3 - half reacted surface

The reactor was prepared using a thiol-ene mixture with excess of PETMP, which leads to residual unreacted thiol groups within the bulk material and on the reactor surface. These free thiol groups on the microreactor surface permit functionalization of the surface after assembly of the microfluidic system. Application of stencil masks combined with UV initiated surface grafting enabled preparation of various patterns in the reactor. In order to test the enzymatic activity of immobilized enzymes in various configurations, four different geometric patterns were selected. A full surface (30 x 30 mm^2), a half surface (15 x 30 mm^2) and two checkerboard patterns with either a fine (256 squares of 1.7 x 1.7 mm^2 each of which 128 were modified) or a coarse (64 squares of 3.55 x 3.55 mm^2 each of which 32 were modified) were prepared. In order to test and visualize the surface patterning, an allyl functional disperse red dye was used as shown schematically in Figure 2B. The high selectivity of the reaction permits direct and accurate replication of the applied stencils as shown in the photographs of the final surfaces in Figure 2C. Additionally, due to the use of benzotriazole as UV-absorber, significant reaction selectivity for the irradiated surface was obtained. In fact, by irradiation from the top, exclusively the upper surface of the reactor cavity was modified with the allyl disperse red leaving the bottom surface unreacted. An image of the upper and lower surface after photochemical reaction with the red dye can be found in the supporting information (SI-Fig. 2). The surface modification procedure offers a controlled area functionalization with high selectivity for the irradiated surface by UV initiated TEC. Replacement of the dye with allyl glycidyl ether undergoing the same TEC leads to surface patterned epoxides, which are known to covalently bind enzymes via ring-opening with free amine residues from the enzyme structure [36]. The reaction scheme from surface modification with allyl glycidyl ether and subsequent covalent immobilization of horseradish peroxidase (HRP, EC 1.11.1.7) can be seen in Figure 3.

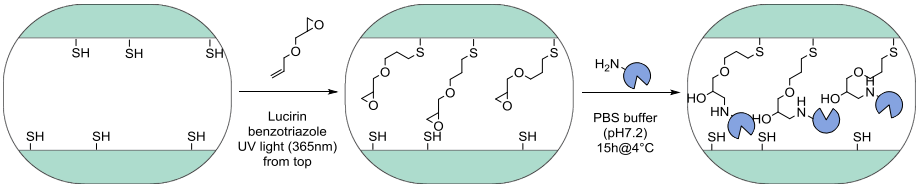

Figure 3. Microchip functionalization of remaining surface thiol groups using allyl glycidyl ether via UV initiated thiol-ene reaction and subsequent covalent HRP immobilization with introduced epoxide groups on the microreactor surface

HRP dissolved in PBS buffer was immobilized on the epoxy patterned reactors by overnight incubation. HRP is a well-studied enzyme, which oxidizes a wide range of aromatic compounds in the presence of hydrogen peroxide (H_2O_2). It can be widely applied in bio-sensing, medical diagnostics and other biomedical applications [37,38]. The quantification of the immobilized amount of HRP was attempted using the Bradford assay [39] and the bicinchoninic acid (BCA) assay, which were in both cases inconclusive due to the low concentration of enzyme and interference with residual thiol groups on the surface, respectively [40]. Quantification using fluorescently labeled enzymes on thiol-ene surfaces confirmed the presence of immobilized enzymes on the surface, but could not be used to determine the amount of attached enzyme due to background fluorescence from the material (see SI-Fig. 3). Therefore, the exact quantification of the enzyme concentration on the surfaces is not possible.

In the presence of H_2O_2, HRP catalyzes a one-electron oxidation of 2,2′-azino-bis(3-ethylbenzothiazoline-6-sulfonate) (ABTS) to a radical cationic product ($ABTS^{\bullet+}$). The absorbance maximum of ABTS at 340 nm (ε_{340}=3.6 x 10^4 M^{-1} cm^{-1}) is shifted to 414 nm (ε_{414}=3.6 x 10^4 M^{-1} cm^{-1}) for its oxidized product $ABTS^{\bullet+}$, from which the activity of immobilized HRP can be determined [41]. Kinetic parameters of immobilized HRP have been studied previously in a microfluidic packed bed reactor [18], monolith structures [42] or on planar surfaces [43]. It has been shown that apparent enzyme kinetics vary greatly depending on the applied configuration, flow rate and type of immobilization compared to that of enzymes free in solution. In this study, HRP was uniformly immobilized via covalent bonding on the same support, which resulted in the same individual activity for all immobilized enzymes. However, their contribution to the overall reactor activity is a function of many parameters, including flow rate mass transfer, diffusion but also the spatial distribution of the immobilized enzymes in the microreactor. The used concentrations of ABTS and H_2O_2 were significantly higher than required for the applied conditions in order to ensure large excess of substrates. The overall reactor performance of the individual configurations was constantly measured over time as shown in SI-Figure 4. An average of the absorbance measured under steady state conditions between 350 and 850 s, which was in agreement with CFD, correlated directly to the formed product at the outlet of the reactor, as presented in Figure 4.

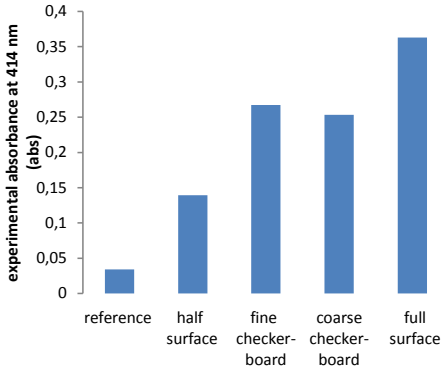

Figure 4. Overall reactor performance of the different reactor configurations illustrated as absorbance measurements at 414 nm corresponding to the formed product at the reactor outlet

A reference measurement was performed, in order to eliminate the potential contribution of adsorbed enzymes to the measured activities. This native surface, undergoing the same enzyme incubation procedure, did not show any activity (Figure 4, reference). Therefore the absence of unspecific adsorption of HRP on the selected surfaces could be confirmed, which makes this surface well suited for immobilization of HRP. These results of the four different configurations show clearly that the fully modified microreactor, containing the largest activated surface and thus the highest amount of immobilized HRP, was the most active one. The two checkerboard structures had a reduced performance by 26 and 30 % of that of the fully immobilized surface. Furthermore, the overall reactor activity was reduced even further when only half of the reactor surface was modified.

The main focus of this study was the determination of the effect of enzyme distribution over the reactor surface and the specific system was therefore designed only to illustrate the impact of

different surface patterns. Therefore, the product absorbance for the individual patterns is additionally shown relative to the respective modified surface area, which allows direct comparison of the reactor efficiency between the selected patterns (see Figure 5A). The areas of the individual activated surface patterns were calculated from the applied photomasks (see SI-Table 1).

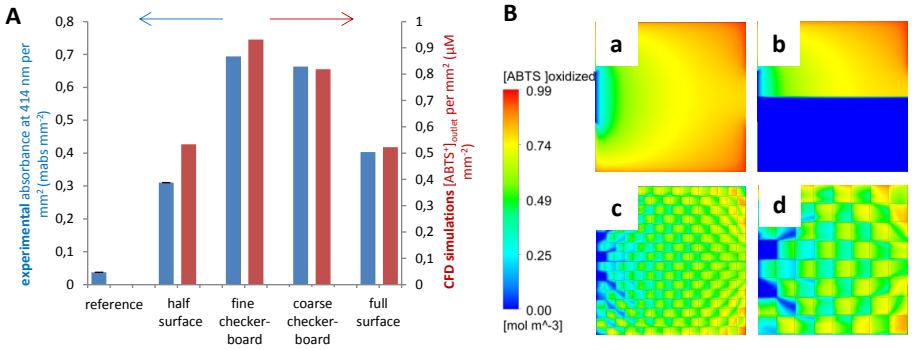

Figure 5. Comparison of experimentally determined $ABTS^{\bullet+}$ absorbance at 414 nm per mm^2 modified area at the reactor outlet in steady state condition (blue) and $ABTS^{\bullet+}$ outlet concentration obtained from CFD simulations in mM mm^{-2} (red) of various surface patterns, reference (HRP adsorption on non-modified surface, empty squares), half modified surface, coarse checkerboard, fine checkerboard, fully modified surface; and B) Illustration of product concentration on the top surface in the microreactor (in steady state simulations) dimensions using fully modified surface (a), half modified surface (b), fine checkerboard structure (c), coarse checkerboard structure (d), where red surfaces illustrate a high and blue surfaces a low product concentration.

Investigating the impact of different patterns demonstrated a slightly reduced absorbance per enzyme area (by 23%) for the microreactor with half of the area covered compared to the fully modified surface, which was not entirely plausible due to symmetry of the pattern, but was finally attributed to experimental inaccuracy. However, the fine and the coarse checkerboard structures exhibited an increased efficiency with 81 and 56 % higher absorbance per active area than the fully modified surface, which demonstrates a significant improvement in product concentration relative to the functionalized surface area or in other words, amount of immobilized enzyme. In fact, it is clearly demonstrated here that the enzyme distribution over the surface affects the overall activity of the microreactor. This improvement of the reactor productivity is influenced by a series of other factors such as flow conditions, substrate diffusion rates and local substrate concentrations. The flow within this reactor geometry is characterized by a gradient, in which the highest velocity is present in the center of the reactor and a reduced velocity at the sides. The difference in velocities across the reactor can consequently influence the mass transport and mixing of the fluid. Therefore, the accessibility of substrate for the enzyme near the surface depends on the position and the local conditions. The selection of this particular reactor design was used in order to generate this complexity of overlapping phenomena.

Computational fluid dynamic (CFD) simulations were conducted in order to validate the experimentally determined performance of the microreactors as a function of the different enzyme immobilization patterns, the impact of the laminar flow conditions, geometry and material transport limitations (diffusion). The product concentrations at the outlet of the reactor for each modified surface area were determined, as presented in Figure 5A (red) and visualized in different patterns, as shown in Figure 5B.

In the flow simulations under steady-state condition all parameters were selected to reflect the experimental setup, such as dimensions of the microreactor, outlet, inlet and immobilization patterns, flow rates, substrate concentrations and theoretical diffusivity. Therefore, it is not possible to compare the results from the experimental and the computational results directly, but merely the trends. Using the same surface patterns, the CFD simulations exhibit the same trend in terms of reactor efficiency as seen in the experimental setup (see Figure 5A, red). The simulation of the full and half modified surface show very similar product concentrations relative to the activated surface area. Similarly for the experimental results, the product concentration obtained from CFD simulations showed an increase of 78 and 57 % for the fine and the coarse checkerboard structure compared to the fully modified surface. The experimental results and computational findings correlate well and demonstrate a clear dependence of the overall product formation relative to the distribution pattern of enzymes on the modified surface area.

4. Conclusions

In order to demonstrate how the position of immobilized enzymes influences the biocatalytic efficacy of a reactor and thus, how reactor performance can be predicted; we have developed a method that correlates experimental results with microreactors containing patterned immobilized enzyme surfaces to CFD simulations as a proof-of-concept study. Initially, an experimental setup was prepared in which HRP could be selectively immobilized in specific patterns onto the surface of an OSTE+ microfluidic reactor. OSTE+ based microfluidic devices were surface modified with allyl disperse red, illustrating the effect of applied stencil masks, and with allyl glycidyl ether enabling the covalent immobilization of HRP. High selectivity of the stencils and exclusive functionalization of the directly irradiated surface was achieved by use of a UV absorber. The performance of the microreactors was significantly influenced by patterning of the enzyme on the surface and two checkerboard structures (fine and coarse patterns) showed an increased efficiency compared to a half area covered reactor, even though the total area of immobilized enzyme was similar. These results correlated very well with CFD simulations of the same reactor designs, illustrating that the configuration pattern plays a significant role in explaining the outstanding performance of the two checkerboard structures. The good agreement between experimental and computational results demonstrates the potential of computational models in order to predict and optimize the performance of such reactors. Further reactor optimization using computational simulations in combination with experimental reactor preparation is the subject of ongoing research.

Acknowledgements

The authors wish to thank the Aage and Johanne Louis-Hansen Endowment for financial support. Additionally, it is gratefully thanked for funding from the European Union FP7

(FP7/2007-2013) Project BIOINTENSE – Mastering Bioprocess integration and intensification across scales (Grant Agreement number 312148). Furthermore, Rolf Hoffmeyer Ringborg is acknowledged for support with the continuous enzyme activity measurements.

References

[1] R. DiCosimo, J. McAuliffe, A.J. Poulose, G. Bohlmann, Industrial use of immobilized enzymes, Chem. Soc. Rev. 42 (2013) 6437–74. doi:10.1039/c3cs35506c.

[2] R.A. Sheldon, S. van Pelt, Enzyme immobilisation in biocatalysis: why, what and how, Chem. Soc. Rev. 42 (2013) 6223–35. doi:10.1039/c3cs60075k.

[3] R.C. Rodrigues, C. Ortiz, Á. Berenguer-Murcia, R. Torres, R. Fernández-Lafuente, Modifying enzyme activity and selectivity by immobilization, Chem. Soc. Rev. 42 (2013) 6290–307. doi:10.1039/c2cs35231a.

[4] J.M. Goddard, J.H. Hotchkiss, Polymer surface modification for the attachment of bioactive compounds, Prog. Polym. Sci. 32 (2007) 698–725. doi:10.1016/j.progpolymsci.2007.04.002.

[5] S. Cantone, V. Ferrario, L. Corici, C. Ebert, D. Fattor, P. Spizzo, L. Gardossi, Efficient immobilisation of industrial biocatalysts: criteria and constraints for the selection of organic polymeric carriers and immobilisation methods, Chem. Soc. Rev. 42 (2013) 6262–76. doi:10.1039/c3cs35464d.

[6] J.N. Talbert, J.M. Goddard, Enzymes on material surfaces., Colloids Surfaces B Biointerfaces. 93 (2012) 8–19. doi:10.1016/j.colsurfb.2012.01.003.

[7] C.Z. Dinu, G. Zhu, S.S. Bale, G. Anand, P.J. Reeder, K. Sanford, G. Whited, R.S. Kane, J.S. Dordick, Enzyme-Based Nanoscale Composites for Use as Active Decontamination Surfaces, Adv. Funct. Mater. 20 (2010) 392–398. doi:10.1002/adfm.200901388.

[8] I.P. Rosinha Grundtvig, J.M. Woodley, K. V. Gernaey, A.E. Daugaard, U. Krühne, Shape and topology optimization of enzymatic microreactors, Technical University of Denmark, 2015.

[9] J. Krenková, F. Foret, Immobilized microfluidic enzymatic reactors, Electrophoresis. 25 (2004) 3550–3563. doi:10.1002/elps.200406096.

[10] H. Yamaguchi, T. Honda, M. Miyazaki, Application of enzyme-immobilization technique for microflow reactor, J. Flow Chem. (2016) 1–5. doi:10.1556/1846.2015.00039.

[11] K.F. Jensen, Microchemical systems: Status, challenges, and opportunities, AIChE J. 45 (1999) 2051–2054. doi:10.1002/aic.690451003.

[12] J.W. Swarts, R.C. Kolfschoten, M.C.A.A. Jansen, A.E.M. Janssen, R.M. Boom, Effect of diffusion on enzyme activity in a microreactor, Chem. Eng. J. 162 (2010) 301–306. doi:10.1016/j.cej.2010.04.040.

[13] W. Zhang, S. Lin, C. Wang, J. Hu, C. Li, Z. Zhuang, Y. Zhou, R.A. Mathies, C.J. Yang, PMMA/PDMS valves and pumps for disposable microfluidics., Lab Chip. 9 (2009) 3088–94. doi:10.1039/b907254c.

[14] S.H. Lee, D.H. Kang, H.N. Kim, K.Y. Suh, Use of directly molded poly(methyl methacrylate) channels for microfluidic applications., Lab Chip. 10 (2010) 3300–3306. doi:10.1039/c0lc00127a.

[15] B. Farshchian, S. Park, J. Choi, A. Amirsadeghi, J. Lee, S. Park, 3D nanomolding for

lab-on-a-chip applications, Lab Chip. 12 (2012) 4764. doi:10.1039/c2lc40572e.
[16] J.C. McDonald, G.M. Whitesides, Poly(dimethylsiloxane) as a Material for Fabricating Microfluidic Devices, Acc. Chem. Res. 35 (2002) 491–499. doi:10.1021/ac001132d.
[17] G.H. Seong, R.M. Crooks, Efficient mixing and reactions within microfluidic channels using microbead-supported catalysts, J. Am. Chem. Soc. 124 (2002) 13360–13361. doi:10.1021/ja020932y.
[18] G.H. Seong, J. Heo, R.M. Crooks, Measurement of Enzyme Kinetics Using a Continuous-Flow Microfluidic System Measurement of Enzyme Kinetics Using a Continuous-Flow Microfluidic System, Anal. Chem. 75 (2003) 5206–5212. doi:10.1021/ac034155b.
[19] H. Mao, T. Yang, P.S. Cremer, Design and characterization of immobilized enzymes in microfluidic systems, Anal. Chem. 74 (2002) 379–385. doi:10.1021/ac010822u.
[20] M.A. Holden, S.Y. Jung, P.S. Cremer, Patterning Enzymes Inside Microfluidic Channels via Photoattachment Chemistry, Anal. Chem. 76 (2004) 1838–1843. doi:10.1021/ac035234q.
[21] C.F. Carlborg, T. Haraldsson, K. Öberg, M. Malkoch, W. van der Wijngaart, Beyond PDMS: off-stoichiometry thiol–ene (OSTE) based soft lithography for rapid prototyping of microfluidic devices, Lab Chip. 11 (2011) 3136. doi:10.1039/c1lc20388f.
[22] C.E. Hoyle, C.N. Bowman, Thiol-ene click chemistry., Angew. Chemie. 49 (2010) 1540–1573. doi:10.1002/anie.200903924.
[23] C.F. Carlborg, A. Vastesson, Y. Liu, W. van der Wijngaart, M. Johansson, T. Haraldsson, Functional off-stoichiometry thiol-ene-epoxy thermosets featuring temporally controlled curing stages via an UV/UV dual cure process, J. Polym. Sci. Part A Polym. Chem. 52 (2014) 2604–2615. doi:10.1002/pola.27276.
[24] P. Mazurek, A.E. Daugaard, M. Skolimowski, S. Hvilsted, A.L. Skov, Preparing mono-dispersed liquid core PDMS microcapsules from thiol–ene–epoxy-tailored flow-focusing microfluidic devices, RSC Adv. 5 (2015) 15379–15386. doi:10.1039/C4RA16255B.
[25] T. Haraldsson, C.F. Carlborg, W. van der Wijngaart, OSTE: a novel polymer system developed for Lab-on-Chip, in: Microfluid. BioMEMS, Med. Microsystems XII, 2014. doi:10.1117/12.2041918.
[26] G. Pardon, T. Haraldsson, W. Van Der Wijngaart, Surface energy micropattern inheritance from mold to replica, in: Micro Electro Mech. Syst., 2014: pp. 96–99. doi:10.1109/MEMSYS.2014.6765582.
[27] C.F. Carlborg, F. Moraga, F. Saharil, W. van der Wijngaart, T. Haraldsson, Rapid Permanent Hydrophilic and Hydrophobic Patterning of Polymer Surfaces Via Off-Stoichiometry Thiol-Ene (OSTE) Phtografting, in: Proc. Micro Total Anal. Syst., 2012: pp. 677–679. http://www.rsc.org/images/loc/2012/pdf/M.5.137.pdf.
[28] N.A. Feidenhans'l, J.P. Lafleur, T.G. Jensen, J.P. Kutter, Surface functionalized thiol-ene waveguides for fluorescence biosensing in microfluidic devices, Electrophoresis. 35 (2014) 282–288. doi:10.1002/elps.201300271.
[29] P. Jonkheijm, D. Weinrich, M. Köhn, H. Engelkamp, P.C.M. Christianen, J. Kuhlmann, J.C. Maan, D. Nüsse, H. Schroeder, R. Wacker, R. Breinbauer, C.M. Niemeyer, H. Waldmann, Photochemical Surface Patterning by the Thiol-Ene Reaction, Angew. Chemie. 120 (2008) 4493–4496. doi:10.1002/ange.200800101.
[30] D. Wasserberg, T. Steentjes, M.H.W. Stopel, J. Huskens, C. Blum, V. Subramaniam, P. Jonkheijm, Patterning perylenes on surfaces using thiol–ene chemistry, J. Mater. Chem.

22 (2012) 16606–16610. doi:10.1039/c2jm32610h.
[31] J.P. Lafleur, S. Senkbeil, J. Novotny, G. Nys, N. Bøgelund, K.D. Rand, F. Foret, J.P.J.P. Kutter, Rapid and simple preparation of thiol-ene emulsion-templated monoliths and their application as enzymatic microreactors., Lab Chip. 15 (2015) 1381–1388. doi:10.1039/C4LC01038H.
[32] D. Schäpper, R. Lencastre Fernandes, A.E. Lantz, F. Okkels, H. Bruus, K. V. Gernaey, Topology optimized microbioreactors, Biotechnol. Bioeng. 108 (2011) 786–796. doi:10.1002/bit.23001.
[33] R.H. Ringborg, J.M. Woodley, K. V. Gernaey, U. Krühne, Application of a Microfluidic Tool for the Determination of Enzyme Kinetics, Technical University of Denmark, 2015.
[34] M. Di Fusco, G. Favero, F. Mazzei, Polyazetidine-coated microelectrodes: Electrochemical and diffusion characterization of different redox substrates, J. Phys. Chem. B. 115 (2011) 972–979. doi:10.1021/jp107153c.
[35] M.F. Chaplin, C. Bucke, Enzyme Technology, Cambridge University Press, 1990.
[36] E. Cakmakci, O. Danis, S. Demir, Y. Mulazim, M.V. Kahraman, Alpha-amylase immobilization on epoxy containing thiol-ene photocurable materials, J. Microbiol. Biotechnol. 23 (2013) 205–210. doi:10.4014/jmb.1209.09017.
[37] N. Mogharrab, H. Ghourchian, M. Amininasab, Structural stabilization and functional improvement of horseradish peroxidase upon modification of accessible lysines: experiments and simulation, Biophys. J. 92 (2007) 1192–1203. doi:10.1529/biophysj.106.092858.
[38] N.C. Veitch, Horseradish peroxidase: A modern view of a classic enzyme, Phytochemistry. 65 (2004) 249–259. doi:10.1016/j.phytochem.2003.10.022.
[39] M.M. Bradford, A rapid and sensitive method for the quantitation of microgram quantities of protein utilizing the principle of protein-dye binding, Anal. Biochem. 72 (1976) 248–254. doi:10.1016/0003-2697(76)90527-3.
[40] K.J. Wiechelman, R.D. Braun, J.D. Fitzpatrick, Investigation of the Bicinchoninic Acid Protein Assay: Identification of the Groups Responsible for Color Formation, Anal. Biochem. 237 (1988) 231–237.
[41] B.R.E. Childs, W.G. Bardsley, The Steady-State Kinetics of Peroxidase with 2,2'-Azino-di-(3-ethylbenzthiazoline- 6-sulphonic acid) as Chromogen, Biochem. J. 145 (1975) 93–103. doi:10.1042/bj1450093.
[42] T.C. Logan, D.S. Clark, T.B. Stachowiak, F. Svec, J.M.J. Fréchet, Photopatterning enzymes on polymer monoliths in microfluidic devices for steady-state kinetic analysis and spatially separated multi-enzyme reactions, Anal. Chem. 79 (2007) 6592–6598. doi:10.1021/ac070705k.
[43] Z. Wang, T.L. King, S.P. Branagan, P.W. Bohn, Enzymatic activity of surface-immobilized horseradish peroxidase confined to micrometer- to nanometer-scale structures in nanocapillary array membranes., Analyst. 134 (2009) 851–859. doi:10.1039/b815590a.

Appendix 4.2 – Supporting information

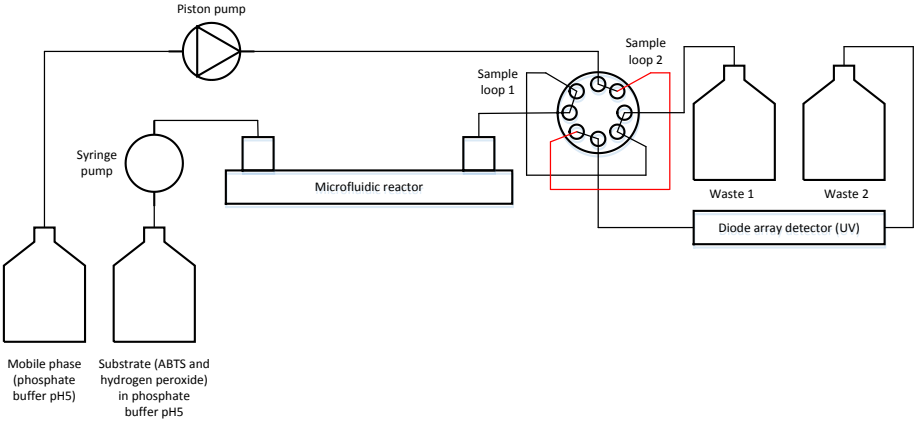

Figure 1 Schematic of the experimental setup used for activity measurement

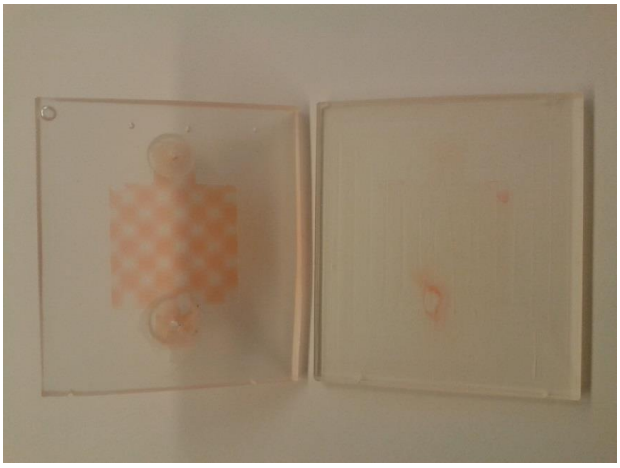

Figure 2 Photograph of disassembled microreactor after thiol-ene surface reaction with allyl disperse red, left: functionalized top part of microreactor, right: not functionalized bottom part of microreactor

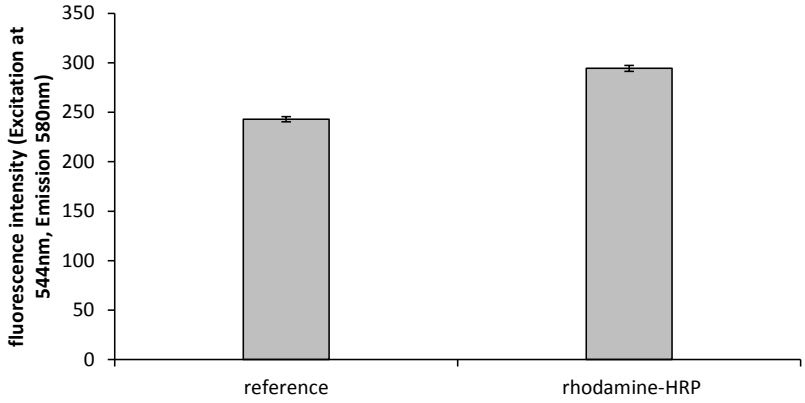

Figure 3 Fluorescence intensity measurements of a plane thiol-ene surface compared to a thiol-ene surface activated with epoxides (with allyl glycidyl ether) and covalently immobilized rhodamine labeled horseradish peroxidase (HRP)

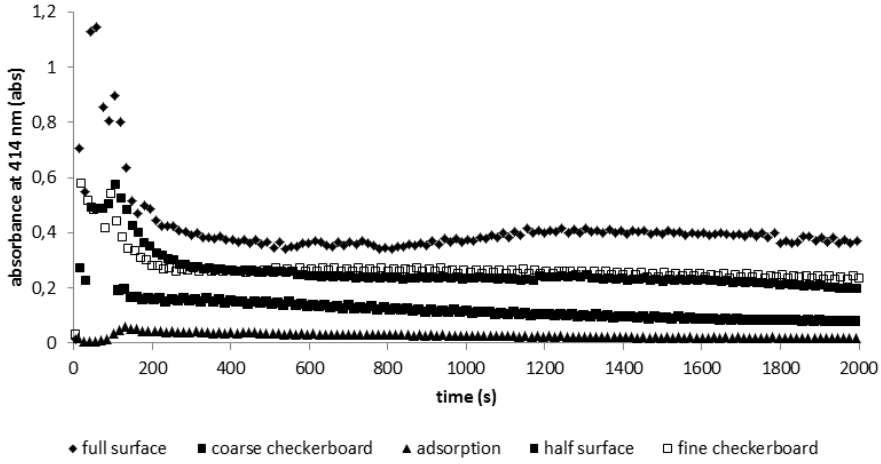

Figure 4 Experimentally obtained absorbance values at 414 nm during continuous product formation in the microreactor

Table 1 Concentration of $ABTS^{\bullet+}$ at the outlet for the different configurations of immobilized enzyme and immobilization surface area obtained from CFD model

Structure	**$[ABTS^{\bullet+}]$outlet (mM)**	**Enzyme area[a] (mm^2)**
Full surface	0.47	900
Coarse checkerboard	0.33	403
Fine checkerboard	0.34	370
Half surface	0.24	450

[a]area determined directly from the applied photomasks

Appendix 5

Supporting information to Chapter 7

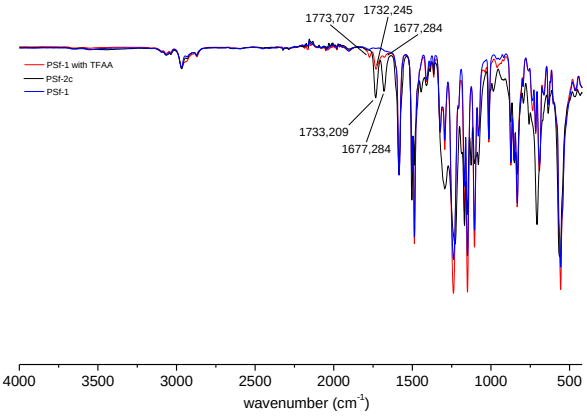

Figure S1 IR spectra of virgin membrane (PSf-1), reacted membrane with trifluoroacetic anhydride (TFAA, PSf-1 with TFAA) and as comparison the IR spectrum of PSf-2c (membrane reacted with acid chloride after lithiation)

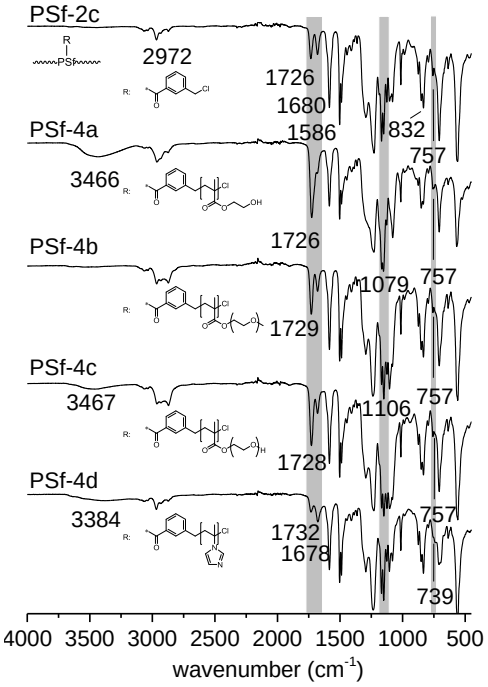

Figure S2 IR spectra of polymer grafted PSf membranes post functionalization, top: via SI-ATRP including activated 3-(chloromethyl)benzoyl PSf membrane, grafted with polyHEMA (PSf-4a), polyMPEGMA (PSf-4b), polyPEGMA (PSf-4c) and polyVim (PSf-4d)

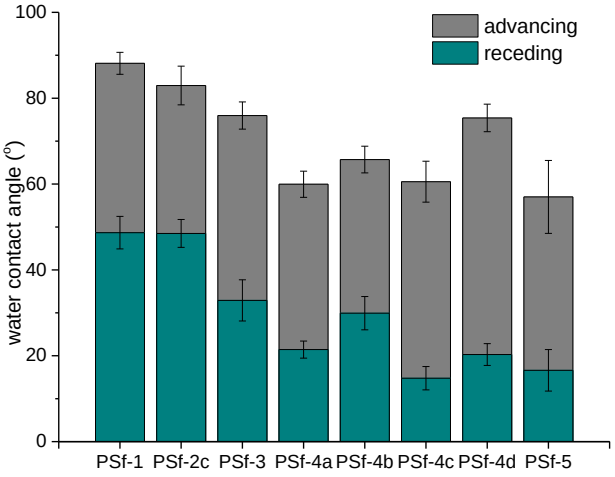

Figure S3 Dynamic WCA measurements of PSf membranes activated via acylation and azidation, post-functionalization, via SI-ATRP and CuAAC

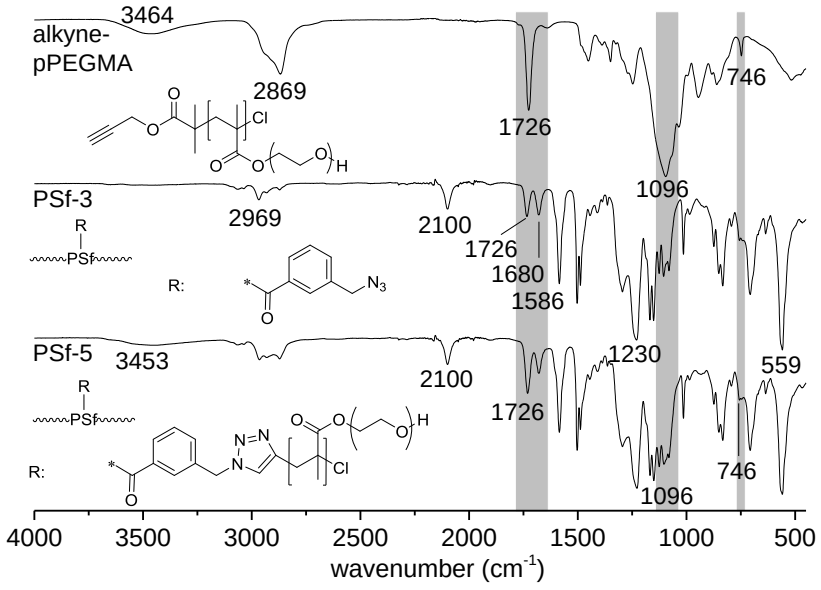

Figure S4 IR spectra of polymer grafted PSf membranes post functionalization via azidation (PSf-3) and subsequent CuAAC with alkyne-pPEGMA (PSf-5)

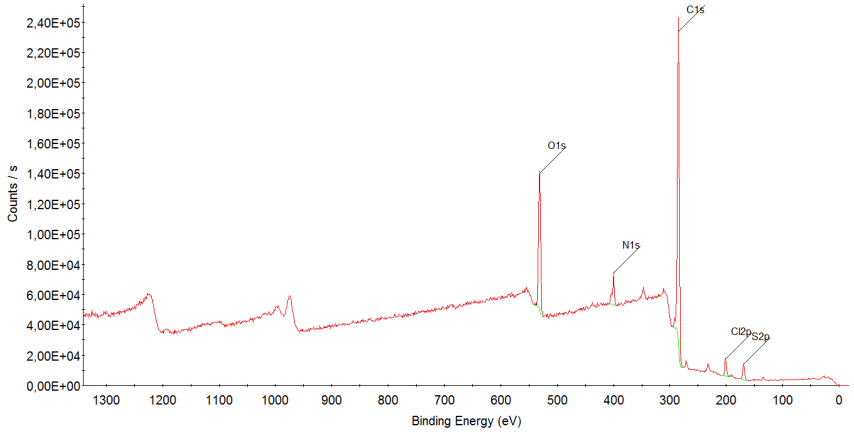

Figure S5 XPS spectrum of PSf membrane surface modified with azide groups (PSf-3)

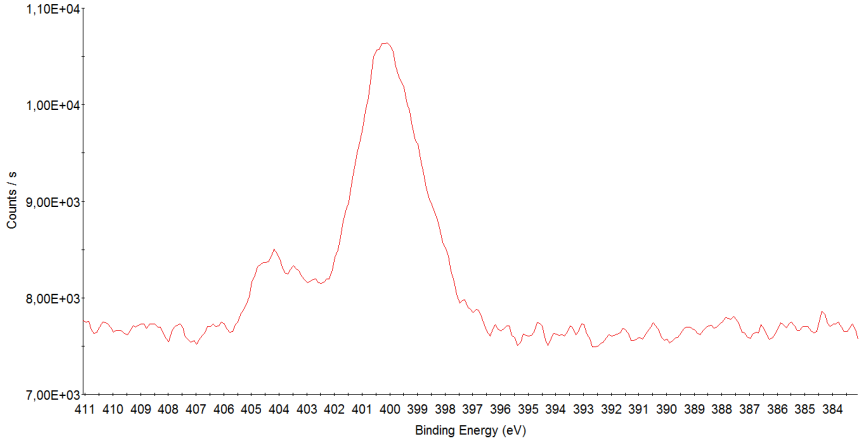

Figure S6 High resolution nitrogen N1s XPS spectrum of PSf membrane surface modified with azide groups (PSf-3)

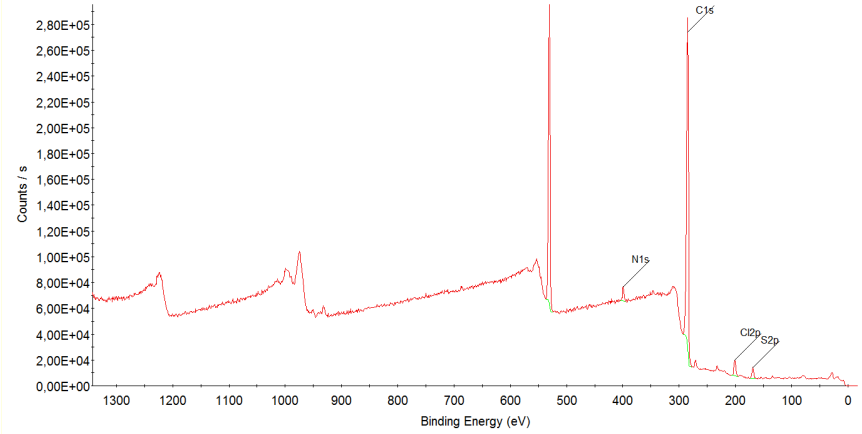

Figure S7 XPS spectrum of PSf membrane surface grafted by CuAAC with alkyne-pPEGMA (PSf-5)

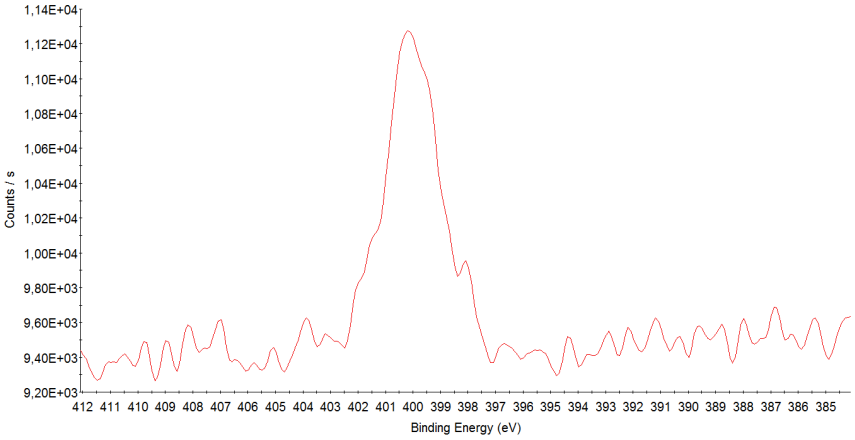

Figure S8 High resolution nitrogen N1s XPS spectrum of PSf membrane surface grafted by CuAAC with alkyne-pPEGMA (PSf-5)

Table S1 Dynamic WCAs (advancing and receding) and permeability results of PSf membranes activated via acylation and azidation, post-functionalization, via SI-ATRP and CuAAC

#	$\theta_{advancing}$ (°)	$\theta_{receding}$ (°)	Permeability (L m^{-2} h^{-1} bar^{-1})
PSf-1	88.1 ± 0.9	48.7 ± 1.2	42.8 ± 1.6
PSf-2c	83.0 ± 1.5	48.5 ± 1.0	35.1 ± 4.4
PSf-3	76.0 ± 1.0	32.9 ± 1.6	25.6 ± 2.6
PSf-4a	60.0 ± 1.0	21.4 ± 0.7	7.0 ± 1.0
PSf-4b	65.7 ± 1.0	29.9 ± 1.3	6.9 ± 0.3
PSf-4c	60.6 ± 1.6	14.8 ± 0.9	4.8 ± 0.2
PSf-4d	75.4 ± 3.2	20.3 ± 2.5	13.6 ± 1.0
PSf-5	57.0 ± 2.8	16.6 ± 1.5	8.4 ± 0.4

Danish Polymer Centre
Department of Chemical and Biochemical Engineering
Technical University of Denmark
Søltofts Plads, building 227
2800 Kgs. Lyngby
Denmark

Phone: +45 45 25 28 00
Web: www.kt.dtu.dk